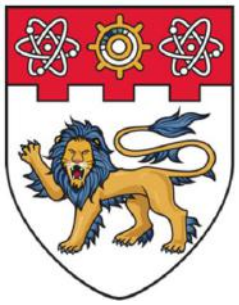

NANYANG TECHNOLOGICAL UNIVERSITY
SINGAPORE

VISIBLE LIGHT COMMUNICATION SYSTEMS SUPPORTING WIRELESS DATA ACCESS AND INDOOR POSITIONING APPLICATIONS

YANG HELIN

School of Electrical & Electronic Engineering

2020

VISIBLE LIGHT COMMUNICATION SYSTEMS SUPPORTING WIRELESS DATA ACCESS AND INDOOR POSITIONING APPLICATIONS

YANG HELIN

School of Electrical & Electronic Engineering

Nanyang Technological University

A thesis submitted to the Nanyang Technological University
in partial fulfillment of the requirement for the degree of
Doctor of Philosophy

2020

Statement of Originality

I hereby certify that the work embodied in this thesis is the result of original research, is free of plagiarised materials, and has not been submitted for a higher degree to any other University or Institution.

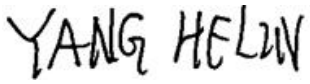

20/02/2020	YANG HELIN
. . . . .	. . . . .
Date	Student's Name Here

Supervisor Declaration Statement

I have reviewed the content and presentation style of this thesis and declare it is free of plagiarism and of sufficient grammatical clarity to be examined. To the best of my knowledge, the research and writing are those of the candidate except as acknowledged in the Author Attribution Statement. I confirm that the investigations were conducted in accord with the ethics policies and integrity standards of Nanyang Technological University and that the research data are presented honestly and without prejudice.

24/02/2019	Arokiaswami Alphones
. . . . .	. . . . .
Date	Supervisor's Name

Authorship Attribution Statement

This thesis contains materials from 10 papers published in the following peer-reviewed journals/conferences and 1 papers were under review in the following peer-reviewed journals in which I am listed as an author.

1. H. L. Yang, C. Chen, W. D Zhong, A. Alphones, S. Zhang and P. F. Du, “Demonstration of a quasi-gapless integrated visible light communication and positioning system,” *IEEE Photonic Technology Letters*, vol. 30, no. 23, pp. 2001-2004, Dec. 2018. DOI: 10.1109/LPT.2018.2874311. (related to Chapter 3)

The contributions of the co-authors are as follows:

- I prepared the manuscript draft, carried out experiment and simulation, and performed analysis of experiment and simulation results.
- C. Chen and Prof Zhong gave initial project and research direction of the work, and provided comments for the paper.
- Prof. Alphones provided comments and revised the paper.
- S. Zhang and Dr Du assisted me to do the experiment and provided comments for the paper.

2. H. L. Yang, C. Chen, W. D. Zhong, S. Zhang and P. F. Du, “An integrated indoor visible light communication and positioning system based on FBMC-SCM,” *2017 IEEE Photonics Conference (IPC)*, pp. 129-130, 2017. DOI: 10.1109/IPCon.2017.8116035. (related to Chapter 3)

The contributions of the co-authors are as follows:

- I prepared the manuscript draft, provided the simulation results and analysis.
- C. Chen and Prof. Zhong analyzed the simulation results and provided comments for the paper.
- S. Zhang and P. F. Du provided comments and assisted in revising the paper.

3. H. L. Yang, P. F. Du, W. D. Zhong, C. Chen, A. Alphones, and S. Zhang, “Reinforcement learning based intelligent resource allocation for integrated VLCP systems,” *IEEE Wireless Communications Letters*., vol. 8, no. 4, pp.

1204-1207, Aug. 2019. DOI: 10.1109/LWC.2019.2911682. (related to Chapter 4)

The contributions of the co-authors are as follows:

- I wrote the draft of the manuscript, derived all the theoretical equations, and analyzed the performance results.
- P. F. Du and Prof. Zhong suggested the performance optimization area, provided resource allocation aspect and edited the manuscript draft.
- C. Chen and Prof. Alphones provided comments and revised the manuscript based on the feedback comments of the journal.
- S. Zhang conducted some positioning simulation result analysis of the manuscript.

4. H. L. Yang, C. Chen, W. D. Zhong, A. Alphones, P. F. Du and S. Zhang, "Resource allocation for multi-user integrated visible light communication and positioning systems," in *IEEE International Conference Communications (ICC)*, pp. 1–6, Shanghai, China, May 2019. DOI: 10.1109/ICC.2019.8761953. (related to Chapter 4)

The contributions of the co-authors are as follows:

- I proposed a resource allocation approach to support communication and positioning services and I also conducted simulations.
- C. Chen, Prof. Zhong and Prof. Alphones provided some positioning simulation result analysis of the manuscript, and gave comments for the paper.
- P. F. Du and S. Zhang gave comments and helped me to revise the paper.

5. H. L. Yang, W. D. Zhong, A. Alphones, C. Chen, and P. F. Du, "QoS-driven optimized design based integrated visible light communication and positioning for indoor IoT," *IEEE Internet of Things Journal,* vol. 7, no. 1, pp. 269-283, Jan. 2020. DOI: 10.1109/JIOT.2019.2951396. (related to Chapter 4)

The contributions of the co-authors are as follows:

- I proposed the QoS-driven optimized design to provide high-speed data rate and high-accuracy positioning services, and conducted analysis and simulation. In addition, I also completed the draft of the manuscript.

- Prof. Zhong and Prof. Alphones conducted some simulation analysis of the manuscripts, and gave comments for the paper.
- C. Chen, and P. F. Du gave comments and revised the manuscript.

6. H. L. Yang, A. Alphones, W. D. Zhong, C. Chen, P. F. Du and S. Zhang, "QoS-driven optimized design in a new integrated visible light communication and positioning system," in *IEEE International Conference on Communications (ICC)*, 2020. (Accepted) (related to Chapter 4)

The contributions of the co-authors are as follows:

- I proposed the QoS-driven optimized design to provide both communication and positioning services. In addition, I also completed the draft of the manuscript.
- Prof. Alphones, Prof. Zhong, and C. Chen conducted some simulation analysis of the manuscripts, and gave comments for the paper.
- P. F. Du and S. Zhang revised the manuscript.

7. H. L. Yang, C. Chen, W. D. Zhong and A. Alphones, "Joint precoder and equalizer design for multi-user multi-cell MIMO VLC systems," *IEEE Transactions on Vehicular* Technology, vol. 67, no. 12, pp. 11354-11364, Dec. 2018. DOI: 10.1109/TVT.2018.2876788. (related to Chapter 5)

The contributions of the co-authors are as follows:

- I wrote the draft of the manuscript. In addition, I performed all the theoretical analysis, investigated multi-cell interference mitigation designs. I also analyzed the results.
- C. Chen and Prof. Zhong gave comments and revised the paper.
- Prof. Alphones revised the manuscript and analyzed the simulation results.

8. H. L. Yang, C. Chen and W. D. Zhong, "Cognitive multi-cell visible light communication with hybrid underlay/overlay resource allocation," *IEEE Photonic Technology Letters*, vol. 30, no. 12, pp. 1135-1138, Jun. 2018. DOI: 10.1109/LPT.2018.2834903. (related to Chapter 6)

The contributions of the co-authors are as follows:

- I investigated the effect of multi-cell interference on the performance degradation in visible light communication. In addition, I proposed a cognitive system architecture to mitigate the multi-cell interference.
- C. Chen proofread the paper and provided suggestions on the resource allocation scheme.
- Prof. Zhong gave comments and assisted me to revise the paper.

9. H. L. Yang, A. Alphones, C. Chen, W. D. Zhong, and X. Z. Xie, “Learning-based energy-efficient resource management by heterogeneous RF/VLC for ultra-reliable low-latency industrial IoT networks,” Accepted for publication in *IEEE Transactions on Industrial Informatics*. DOI: 10.1109/TII.2019.2933867. (related to Chapter 6)

The contributions of the co-authors are as follows:

- I completed the draft of the manuscript, provided the specific review of the 5G technologies, evaluated the performance of the presented network architecture and analyzed the simulation results.
- Prof. Alphones and C. Chen highlighted new current research areas of 5G technologies and suggested me to integrate visible light communication into 5G networks to improve the performance.
- Prof. Zhong gave some key comments and revised the manuscript.
- Prof. Xie gave comments and revised the manuscript.

10. H. L. Yang, W. D. Zhong, C. Chen and A. Alphones, “Integration of visible light communication and positioning within 5G networks for Internet of Things”, *IEEE Network.* (Accepted) (related to Chapter 2)

The contributions of the co-authors are as follows:

- I reviewed relevant literatures, concluded the contributions of the literatures and prepared the manuscript draft.
- Prof. Zhong and C. Chen directed the research work, and helped me to list the main works which I need to consider in the paper.
- Prof. Alphones helped me to revise the paper, and gave comments for the paper.

11. H. L. Yang, W. D. Zhong, A. Alphones, C. Chen, S. Zhang, P. F. Du, and X. Z. Xie, “Coordinated resource allocation-based integrated visible light

communication and positioning systems for indoor IoT," Revision was submitted to *IEEE Transactions on Wireless Communications.* (related to Chapter 3)

The contributions of the co-authors are as follows:

- I prepared the manuscript draft. In addition, I programmed and optimized the algorithm and conducted simulations.
- Prof. Zhong and Prof. Alphones directed the research work, and helped choose a resource allocation scheme to address resource optimization problem, and provided comments for the paper.
- C. Chen, S. Zhang and P. F. Du helped me to analyze the data in simulations, and gave comments for the paper.
- Prof. Xie assisted me to revise the paper, and gave comments for the paper.

21/02/2020	YANG HELIN
. . . . .	. . . . .
Date	Student's Name Here

Acknowledgement

First of all, I would like to thank my supervisor Prof. Zhong Wen-De, from Nanyang Technological University, for his great guidance and continuous encouragement over the four years. His excellent academic resource and research styles have lighted me to become a qualified PhD student. In addition, I want to thank my co-supervisor Prof. Arokiaswami Alphones, from Nanyang Technological University, for his great help and tireless advice during my PhD study. Thank you for Prof. Zhong Wen-De and Prof. Arokiaswami Alphones' kind help and advice, I have completed my PhD thesis.

My deepest gratitude goes to my family members, my father, my mother, and my girl friend Jiang Yifu, for their kind love and encouragement, so I have a nice atmosphere to study well during my PhD study.

I would also like to thank the colleagues and friends in Nanyang Technological University, who help me in both my study and life, including Dr. Chen Chen, Dr. Du Pengfei, Mr. Zhang Sheng, Ms. Zhang Ran, and many other dear staffs. With their presence, I have the wonderful time in Singapore.

Abstract

White light emitting diodes (LEDs) have attracted much attention recently in the lighting market for their long lifetime, low power consumption, fast switching time and reliability. Besides illumination, LEDs are also used for visible light communications (VLC) and visible light positioning (VLP). On the one hand, VLC has been emerging as a promising candidate for indoor wireless communications due to its supporting high-speed data rate, economic, electro-magnetic interference free and high security, compared with traditional radio-frequency (RF) systems. On the other hand, VLP can provide high-accuracy positioning performance compared with RF based indoor positioning systems. However, the development and deployment of indoor VLC and VLP systems face some key challenges, such as integration of VLC and VLP to provide simultaneous communication and positioning services, inter-cell interference (ICI) in indoor multi-cell VLC systems, negative effect of line-of-sight (LoS) blockages on the performance, and guaranteeing different quality of services (QoS) of various indoor devices. The goals of this thesis are to address the above mentioned challenges, and propose integrated system, robust optimized design, ICI mitigation scheme and resource management strategy to improve the system performance.

The combination of orthogonal frequency division multiplexing (OFDM) and positioning algorithm can provide simultaneous communication and positioning for indoor devices, but the performance is degraded due to the high out-of-band interference (OOBI) generated from OFDM signals on adjacent subcarriers. This thesis first

proposes a quasi-gapless integrated VLC and VLP (called VLCP) system based on filter bank multicarrier-based subcarrier multiplexing (FBMC-SCM). Compared with OFDM-based SCM (OFDM-SCM), FBMC-SCM is capable of mitigating OOBI and therefore requires much smaller guard band (GB) spacing. Simulations and experimental results verify that our proposed FBMC-SCM can improve the effective bandwidth utilization ratio and enhance the positioning accuracy in the integrated VLCP system, compared with OFDM-SCM.

The FBMC-SCM needs extra computational complexity of signal processing compared with OFDM. An OFDM-SCM-interleaving based integrated VLCP system is further proposed, where the sinusoidal positioning signals can be placed into the idle subcarriers (called frequency holes) which have the negligible OOBI from OFDM communication signal. In order to maximize the system data rate while guaranteeing the minimum data rate and high positioning accuracy requirements, a QoS-driven optimized design with joint adaptive modulation, subcarrier allocation and weighted pre-equalization is proposed to improve the system performance. The LoS blockage issue is investigated in this thesis, and robust communication and positioning schemes are presented to maintain the system performance. Furthermore, this thesis also extends the system model into multi-cell integrated VLCP networks, where a joint VLC access point section, bandwidth allocation, adaptive modulation and power allocation approach is proposed to maximize the network data rate while guaranteeing different QoS requirements of indoor devices. The experimental results and simulations show that the presented integrated VLCP system model and solutions effectively enhance the data rate, improve the positioning accuracy and guarantee devices' QoS requirements.

In indoor multi-user multi-cell multiple-input multiple-output (MIMO) VLC systems, ICI and inter-user interference (IUI) are the two key factors that could severely degrade the system performance. In this thesis, a novel joint precoder and equalizer design based on interference alignment (IA) is proposed to mitigate both IUI and ICI

in multi-user multi-cell MIMO VLC systems under both perfect and imperfect channel state information (CSI). The proposed design aims to choose proper precoder and receiving equalizer to minimize the mean square error (MSE) under unique optical power constraints. Furthermore, this thesis considers optical channel estimation errors in the formulated joint optimization problem. Numerical results show that the proposed design achieves better performance under different users' locations, channel estimation errors and transmitter/receiver spacing, compared to the existing designs.

In wireless indoor networks, Internet of Things (IoT) devices and industrial IoT devices may have different QoS requirements, ranging from high reliability and low-latency to high transmission data rate, leading to high complex and heterogeneous network environments. Hence, this thesis presents a heterogeneous RF/VLC network architecture to guarantee the different QoS requirements, where RF is capable of offering seamless coverage and VLC has the ability to provide high transmission data rate. Then, a joint uplink and downlink energy-efficient resource management decision-making problem (network selection, subchannel assignment and power management) is formulated as a Markov decision process. After that, a new deep post-decision state (PDS) based experience replay and transfer (PDS-ERT) reinforcement learning (RL) algorithm is proposed to learn the optimal policy. Simulation results corroborate the superiority in performance of the presented heterogeneous network, and verify that the proposed PDS-ERT learning algorithm outperforms other existing algorithms in terms of meeting energy efficiency and QoS requirements.

Keywords

Visible Light Communication, Visible Light Positioning, Integrated System, Interference Mitigation, Robust Designs, Resource Management.

List of Main Abbreviations

AP	Access Point
AWGN	Additive White Gaussian Noise
BER	Bit Error Rate
CSI	Channel State Information
EE	Energy Efficiency
ERT	Experience Replay and Transfer
FBMC	Filter Bank Multi-Carrier
FFT	Fast Fourier Transform
FOV	Field-of-View
GB	Guard Band
IA	Interference Alignment
ICI	Inter-Cell Interference
IFFT	Inverse Fast Fourier Transform
IoT	Internet of Thighs
ISI	Inter-Symbol Interference
IUI	Inter-User Interference
LEDs	Light Emitting Diodes
LoS	Line-of-Sight
MIMO	Multiple-Input Multiple-Output
MMSE	Minimum Mean Square Error

MSE	Mean Square Error
NLoS	None Line-of-Sight
OOBI	Out-of-Band Interference
OFDM	Orthogonal Frequency Division Multiplexing
OFDMA	Orthogonal Frequency Division Multiple Access
OOK	On-Off Keying
PDOA	Phase Difference of Arrival
PDs	Photodetectors
PLC	Power Line Communications
PDR	Pedestrian Dead Reckoning
PDS	Post-Decision State
QAM	Quadrature Amplitude Modulation
QoS	Quality of Services
RF	Radio Frequency
RL	Reinforcement Learning
RSS	Received Signal Strength
SCM	Subcarrier Multiplexing
SINR	Signal-to-Interference-and-Noise Ratio
SNR	Signal-to-Noise Ratio
TDOA	Time Difference of Arrival
UWB	Ultra Wide Band
VLC	Visible Light Communication
VLP	Visible Light Positioning
Wi-Fi	Wireless-Fidelity

Contents

List of Figures

List of Tables

Chapter 1

Introduction

1.1 Background

1.1.1 Background of VLC

In the last several decades, demands for mobile data traffic to support various services, devices in both indoor and outdoor environments are rapidly ever growing, such as various Internet access, video/voice conferencing, high-definition television, and so on [1-3]. In addition, with widespread developments of wireless communication technologies, more and more devices are involved in wireless networks, the fourth generation (4G) or the fifth generation (5G) wireless network needs to support various communication connectivity and diverse services of massive number of devices [4, 5]. Devices will require massive connectivity, high reliability, high data rate, high positioning accuracy, low latency, low power consumption and improved security. Under ever increasing demands for bandwidth, it is difficult for current radio frequency (RF)-based wireless networks (such as 4G, 5G etc.) to support massive connectivity due to limited RF bandwidths, guarantee high-accuracy positioning because of severe multipath reflections, and satisfy colorful quality of services (QoS) requirements of devices [4-6].

Light emitting diodes (LEDs) have achieved much attention recently in the lighting market and will replace traditional light sources due to its long lifetime, low power

consumption and reliability [7]. The lifetime of LEDs ranges from about 30, 000 to 50, 000 hours, which is higher than that of fluorescent lamps which is just only about 10 000 hours [8]. In addition, the luminous efficacy of commercial LEDs can achieve about 200 lumens/watt by the year 2020 [8], which is much higher than conventional light bulbs.

In addition to the above benefits, LEDs are also used to serve as emitters for visible light communications (VLC, also known as Li-Fi,) due to fast switching capability of LEDs [7]. The visible light spectrum in VLC systems ranges from 375 nm to 780 nm, resulting in the abundant unlicensed bandwidth, much greater than that RF spectrum. This enables VLC systems to provide high-speed wireless data transmission for indoor communications. Hence, LEDs can provide both the simultaneous illumination and high-speed data rate communication services in indoor environments. The first work on VLC was presented by Tanaka, *et al.*, from Japan in 2000 [9], where white LEDs were adopted to set up visible light links, and amplitude modulation was used at visible light frequencies to offer a data channel without affecting LEDs' illumination function. The literature [10] reported a fundamental analysis on VLC systems based on white LEDs, where the basic system model, influence of reflection and inter-symbol interference (ISI) were discussed in detail. Since then, the development of VLC systems based on white LEDs has attracted much attention from both academia and industry. In 2007, two standards, VLC System Standard and Visible Light ID System Standard, were reported by VLC Consortium in Japan [11]. In 2011, the first IEEE standard (IEEE 802.15.7) for VLC was adopted [12].

VLC has been identified as a promising candidate technology for 4G or 5G networks to support different QoS requirements of devices [4-6]. VLC is capable of serving devices in indoor environments because of the following main advantages [4-6]: 1) low cost due to the use of the existing lighting infrastructure; 2) high-speed transmission with the abundant license-free visible light spectrum; 3) guaranteed communication secu-

Table 1.1: Three PHY Modes in IEEE 802.15.7 Standard

PHY Types	Modulation	Clock Rates	Data Rates
PHY-I	OOK & VPPM	200/400 kHz	11.67–266.6 kb/s
PHY-II	OOK & VPPM	120 MHz	1.25–96 Mb/s
PHY-III	CSK	12/24 MHz	12–96 Mb/s

rity, since visible light signals cannot penetrate walls; 4) high-accuracy localization via visible light positioning (VLP) for object tracking and navigation; 5) no interference between RF communications due to the different spectrum, and an absence of electromagnetic interference which is suitable in the electromagnetic interference-sensitive environments (e.g. hospitals, airports, and gas stations); 6) energy harvesting from visible light for power-constrained devices to extend their battery life. Thanks to the above benefits of VLC, densely deployed light emitting diodes (LEDs) points can be employed into access points (APs) to support high density of indoor devices and satisfy diverse services, since many studies have reported that wireless devices will spend about 80% of their time indoors[4-6].

Specifically, as listed in Table 1.1, IEEE 802.15.7 defines three physical layer (PHY) modes with adopting a combination of different modulation schemes (e.g., On-off keying (OOK), variable pulse position modulation (VPPM) and colour shift keying (CSK)) [12, 13]. The supported data rates defined in PHY II and PHY III are up to about 96 Mbit/s [12, 13], much higher data rate that has been achieved in laboratory experiments. For example, the data rate of 500 Mbit/s over a 2 m distance was achieved in prototype VLC systems based on high-quality LEDs [14]. The data rates of 1.3 and 1 Gbit/s over the distances of 3 and 10m were implemented in [15]. Moreover, in [16], D. Tsonev, *et al.*, utilized gallium nitride (GaN) LEDs to achieve about a 3 Gbit/s VLC link over a distance of 5 cm. In addition, several new VLC related standardization activities, such as the IEEE 802.11bb and ITUT G.9991 for the highspeed indoor VLC, etc [17].

Fig. 1.1 indicates the relationship between the data rate and the link distance

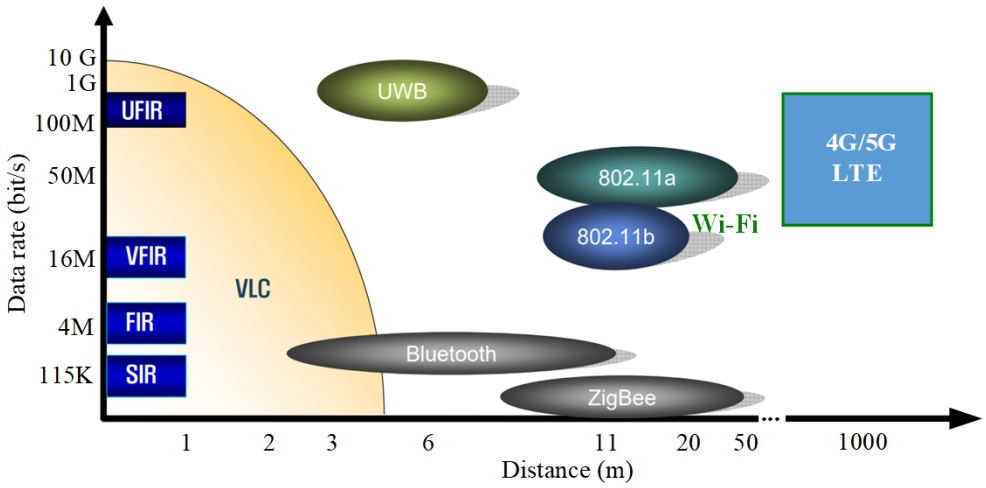

Figure 1.1: Different common technologies for short-range wireless communications [17].

for some common used technologies and standards in short-range wireless communication networks [17]. We can observe that even though wireless-fidelity (Wi-Fi) achieves longer transmission distance than VLC, VLC can get much higher transmission data rate (up to several Gbit/s) than the current Wi-Fi technology (about 350 Mbit/s for IEEE 802.11n) [17]. In addition, other technologies (ZigBee, Bluetooth, etc.) have quite lower data rates, which may fail to support high-speed transmission demands. Compared with RF based indoor communication systems, VLC systems based on LEDs have some attractive advantages, such as low-cost front-ends, low power consumption, no electromagnetic interference radiation, abundant unregulated bandwidth and high security [5, 7, 10, 18-21]. According to the above discussions, VLC has the potential to be an integral part of 5G networks to guarantee the diverse QoS requirements of devices.

1.1.2 Background of VLP

In addition to supporting illumination and communication functions, white LEDs are also adopted for indoor visible light positioning (called VLP) [22-25], where receivers equipped with photodetectors (PDs) can perform positioning function by using the

received optical signals from LED transmitters at known locations. In recent years, VLP has become an attractive research topic for indoor positioning and tracking, because it provides high positioning accuracy and guaranteed security compared with RF-based indoor positioning systems [22-25].

As a matter of fact, researchers have attempted to develop indoor localization or positioning systems with high positioning accuracy. For localization systems, the global positioning system (GPS) has been most widely used for outdoor localization [26], but it has poor localization accuracy in indoor environments due to link blockages and multipath effects. In addition, RF-based positioning systems, infrared-based systems and ultrasonic-based systems also have been widely applied for indoor positioning [27]-[32]. However, the RF-based positioning systems (such as Wi-Fi, Bluetooth etc.) are not safe to be used in hospitals and airplanes [28-30], and the negative effects of multipath reflections and shadowing on the positioning performance degradation are significant. Ultra wide band (UWB) and ultrasonic positioning systems have good positioning accuracy, but they are costly [31, 32]. Hence, among these indoor RF-based positioning systems, VLP is considered as a promising technique for indoor positioning, navigation, tracking and location-aware services, due to its high positioning accuracy, low cost and guaranteed security [22-25].

Currently, many algorithms have been adopted for VLP systems, such as received signal strength (RSS), time of arrival (TOA), angle of arrival (AOA), time difference of arrival (TDOA), and phase difference of arrival (PDOA) [22-25, 33-42]. Among these algorithms, RSS has low estimation accuracy when the receiver is located at the edges of a room [34, 35, 41]; TOA requires synchronization between transmitters and receiver [40]; AOA can achieve a high positioning accuracy, but needs a highly complicated image sensor arrays [36, 37]. Compared with RSS, TOA and AOA, the accuracy of TDOA and PDOA is related to the sampling rate at receivers. These two approaches have high positioning accuracy, but TDOA requires high time resolution

Table 1.2: Summary of indoor positioning technologies (Sakpere Adeyeye, 2015 and [43]).

Technology	Technique	Algorithm	Accuracy	Cost	Complexity	Scalability	Privacy / security	Real-time
Infrared	Trilateration	TOA, TDOA	Medium	Low	High	Medium	Low	Yes
Magnetic	Triangulation	AOA, TOA	High	High	High	Low	Low	Yes
Optical/vision	Scene analysis & proximity	RSSI	Low	Medium	Medium	Low	Low	Yes
Audible sound	Trilateration	TOA	Medium	Medium	Medium	Medium	Low	Yes
Ultrasound/ultrasonic								
Active bat	Trilateration	TOA, TDOA	Medium	Medium	Medium	Medium	Low	Yes
Cricket	Triangulation	AOA	Medium	Low	Medium	Medium	High	No
CricketNav	Triangulation	AOA, TOA	Medium	Medium	Medium	Medium	Medium	Yes
Dolphin	Trilateration	TOA, TDOA	Medium	Low	Medium	Medium	Low	Yes
Radio frequency								
Bluetooth	Trilateration, fingerprinting	TDOA, RSSI	Low	Medium	Medium	Medium	Medium	Yes
UWB	Trilateration	TOA, TDOA	High	Medium	Medium	Medium	Low	Yes
WSN	Fingerprinting	RSSI	Medium	Medium	Medium	Medium	Low	Yes
WLAN	Trilateration, fingerprinting	TDOA, RSSI	Low	Medium	High	Medium	Low	Yes
RFID	Fingerprinting	RSSI	Low	Medium	Medium	High	Low	Yes
NFC	Proximity	RSSI	High	Low	Low	High	High	No
Visible light	Triangulation, trilateration	AOA, TDOA, RSSI	High	Medium	Medium	Medium	High	Yes
PDR/INS	DR	EKF, PF	Medium	Low	Low	Medium	High	Yes
Hybrid	–	–	High	Medium	High	High	Medium	Yes

due to the short distance between transmitters and receivers in indoor environments, so that PDOA is more appropriate in indoor VLP systems [38, 39, 42]. Table 1.2 summarizes and compares the common indoor positioning systems and positioning algorithms in terms of positioning accuracy, cost, complexity, scalability and secure levels [4]-[6]. From Table 1.2, we can conclude that VLP systems achieve the high positioning accuracy with the medium complexity, low cost and high secure level.

Generally speaking, VLP systems mainly adopt two kinds of optical receiver to perform indoor positioning: PD and camera [44, 45]. Camera based VLP does not need the additional hardware equipment when mobile terminals are equipped with cameras, but it is expensive and has low transmission data rate, while PDs have the ability to achieve a high data rate. For these two different types of receivers, the AOA positioning algorithm is adopted in camera based VLP systems while the RSS, TOA,

TDOA and PDOA algorithms are mainly used in PD based VLP systems. This thesis employs the PD based VLP systems to provide both the high-speed data rate and the high-accuracy positioning services.

1.2 Challenges, Motivations and Objectives

1.2.1 Challenges

Despite the above-mentioned benefits or advantages of VLC and VLP systems, the capacity of VLC systems is greatly limited by the limited modulation bandwidth of white LEDs and the positioning performance needs to be improved in VLP systems. On the one hand, so far, many techniques have been proposed to increase the capacity of VLC systems, such as multiple-input multiple-output (MIMO) transmission [46, 47], frequency domain equalization [48. 49], orthogonal frequency division multiplexing (OFDM) using high-order constellations [50, 51], non-orthogonal multiple access (NOMA) [52, 53], and so on. More specifically, OFDM has also been widely applied in VLC systems to overcome multipath-induced ISI and inter-carrier interference [54]. On the other hand, machine learning techniques have been applied for VLP systems to correct the positioning errors caused by transmitters or receiver hardware [39, 55], and the high precision positioning algorithms based on Bayesian model were presented to improve the positioning capability based on the historical information [56, 57].

However, the developments of both VLC and VLP systems still face some key challenges, which can be summarized as follows:

- Most researchers only focused on VLC [10-21, 46-54] or VLP independently [22-25, 33-42, 55-57]. In practical indoor environments (such as supermarket, hospital, robotic industry, etc.), both communication and positioning might be expected in the same system. Hence, how to integrate both VLC and VLP in the same

system to provide both high-speed transmission data rate and the high-accuracy positioning accuracy still remains a significant challenge.

- Since each VLC cell associated with some LEDs generates an optical attocell and it provides a small illuminated coverage area, a practical VLC system or network usually consists of multiple attocells to support both the brightness and communication requirements [58-60]. Such a cellular indoor VLC system is referred to as a multi-cell VLC system [58-60], and the respective illumination areas of the adjacent cells inevitably overlapp with each other. When the users are located in the overlapped area, their performance may be greatly degraded due to the severe inter-cell interference (ICI) from adjacent cells.

- RF based communication systems can cover the entire indoor room with a few transmitters and it still maintains good performance under the non-line-of-sight (NLOS) when the RF signal is blocked by walls or obstacles, while VLC or systems strongly depend on line-of-sight (LoS) links to satisfy the good communication and positioning performance. In this case, the performance degradation is significant when LoS links are blocked by obstacles or human beings due to the mobility of devices.

- In indoor environments, different devices (such as phones, computers, sensors, actuators, machines and robots) may have different QoS requirements, ranging from high reliability and low-latency, high positioning accuracy to high transmission data rates. The varying requirements expect to search an efficient resource management strategy or network architecture to guarantee different QoS requirements and enhance the network data rate performance.

1.2.2 Motivations and Objectives

As mentioned in Section 1.1, the advantages of potential VLC and VLP systems using white LEDs have motivated the author to investigate them and present novel techniques to improve both the communication and positioning capabilities of VLC and VLP systems to satisfy the ever increasing high data rate and high positioning accuracy requirements. In addition, although lots of potential techniques have been studied to overcome the challenges of VLC and VLP, there still exist some key problems in developing high performance in VLC and VLP systems. Hence, the thesis aims to address the existing challenges and problems of VLC and VLP by proposing advanced schemes and designs. The major objectives are summarized below.

- The combination of modulation or multiple access techniques and positioning algorithm is an effective way for the integration of VLC and VLP. For example, the literatures [61-63] presented the combination of OFDM modulation and RSS algorithm to provide both communication and positioning services in the same system. However, the performance of the integrated system is degraded due to the high out-of-band interference (OOBI) generated from OFDM signals on adjacent subcarriers [61-63]. Hence, it is important to develop new integrated systems for the communication and positioning performance improvement.

- Traditional frequency division schemes have the ability to effectively eliminate ICI in multi-cell VLC systems by partitioning visible light spectrum [64-66], but the achievable capacity of each cell is greatly decreased due to the spectrum partitioning. As an effective way to eliminate ICI, precoding or equalizer has also been applied in multi-cell VLC systems, such as zero forcing (ZF) [67] and minimum mean square error (MMSE) [68, 69], but the interference is still not mitigated effectively in the systems. Therefore, it would be interesting if ICI

can be mitigated without spectrum partitioning. By adopting interference alignment technique based on advanced precoding or equalizer, the capacity can be significantly improved in indoor multi-cell VLC systems.

- The co-deployment of RF and VLC technologies is straightforward way to improve the network performance and satisfy specific QoS constraints in indoor environments [70-74], where RF is capable of offering reliable connectivity and VLC has the ability to provide high transmission data rate. For example, when the VLC links are blocked, devices can switch the transmission mode from VLC to RF to continue their services. However, different devices may have different QoS requirements, ranging from low-latency, high positioning accuracy to high transmission data rates, leading to highly complex and heterogeneous network architectures. The conventional hybrid RF/VLC network and resource management strategy may fail to guarantee these devices' QoS requirements. Hence, it is of practical meaning to explore a new heterogeneous network architecture and resource management approach to enhance the network performance.

- When VLC LoS links are blocked, the devices can change the link from VLC to RF to maintain the communication connection, but the positioning accuracy will reduce when it is switched to RF-based positioning systems. Utilizing devices' mobility behavior and historical location information is a very natural way to estimate or predict device' locations under blockages, such as pedestrian dead reckoning (PDR) [75 , 76] and Bayesian perspective [57]. However, the positioning error will increase during PDR over time and Bayesian perspective has the high computational complexity at receivers. As a result, under LoS blockages, developing a new positioning scheme with low complexity to maintain high-accuracy positioning services by utilizing device' historical location information is important for indoor VLP systems.

1.3 Major Contributions

In order to address the above-mentioned challenges and problems, novel advanced system architecture, interference mitigation scheme, resource management approach and robust design are explored and presented in this thesis. The major contributions of the thesis are summarized as follows

- This thesis first proposes a quasi-gapless integrated VLC and VLP (called VLCP) system based on filter bank multicarrier-based subcarrier multiplexing (FBMC-SCM). Compared with OFDM-based SCM (OFDM-SCM), FBMC-SCM has lower OOBI and therefore requires much smaller guard band (GB) spacing. PDOA is applied for positioning. Simulations and experimental results verify that our proposed FBMC-SCM can improve the effective bandwidth utilization ratio and enhance the positioning accuracy in the integrated VLCP system, compared with OFDM-SCM. (Chapter 3)

- This thesis proposes OFDM-SCM-interleaving based integrated VLCP system, where the sinusoidal positioning signals can be put into the idle subcarriers (called frequency holes) which have the negligible OOBI from OFDM signal. In order to maximize the system data rate while guaranteeing the minimum data rate and high positioning accuracy requirements, a QoS-driven optimized design with joint adaptive modulation, subcarrier allocation and weighted pre-equalization is proposed to improve the system performance. The LoS blockage issue is investigated in networks, and the robust communication and positioning schemes are presented to maintain the systems performance. The experimental results show that the presented solutions can effectively enhance the data rate, improve the positioning accuracy and guarantee devices' QoS requirements. Furthermore, this chapter also extends the system model into multi-cell integrated VLCP networks, where a joint AP section, bandwidth allocation, adaptive modulation and

power allocation approach is proposed to maximize the network data rate while guaranteeing the different QoS requirements of indoor devices. The simulation results corroborate the superiority in performance of the presented integrated VLCP system and the proposed solutions. (Chapter 4)

- In multi-user multi-cell MIMO VLC systems, ICI and inter-user interference (IUI) are the two key factors that could severely degrade the system performance. In this thesis, for the first time, a novel joint precoder and equalizer design based on interference alignment (IA) is proposed to mitigate both IUI and ICI in multi-user multi-cell MIMO VLC systems under both perfect and imperfect channel state information (CSI). The proposed design aims to choose proper precoder and receiving equalizer to minimize the mean square error (MSE) under the unique optical power constraints. Furthermore, this thesis considers optical channel estimation error in our formulated joint optimization problem. Numerical results show that the proposed design achieves a better performance under different users' locations, channel estimation errors and transmitter/receiver spacing, compared to the existing MMSE and max-rate designs. (Chapter 5)

- In wireless indoor networks, IoT devices and industrial IoT devices have different QoS requirements, ranging from high reliability and low-latency to high transmission data rates. These indoor networks will be highly complex and heterogeneous, as well as the spectrum and energy resources are severely limited. Hence, this thesis presents a heterogeneous RF/VLC network architecture to guarantee the different QoS requirements, where RF is capable of offering reliable connectivity and VLC has the ability to provide high transmission data rate. A joint uplink and downlink energy-efficient resource management decision-making problem (network selection, subchannel assignment and power management) is formulated as a Markov decision process. Then, a new deep post-decision state (PDS) based

experience replay and transfer (PDS-ERT) reinforcement learning (RL) algorithm is proposed to learn the optimal policy. Simulation results corroborate the superiority in performance of the presented heterogeneous network, and verify that the proposed PDS-ERT learning algorithm outperforms other existing algorithms in terms of meeting energy efficiency and QoS requirements. (Chapter 6)

1.4 Thesis Organization

This thesis comprises seven chapters, which is organized as follows

Chapter 1 briefly introduces the background, challenges and motivations of VLC and VLP systems, and the summary of the major contributions is provided in this chapter, too.

Chapter 2 provides an overview of VLC, VLP and integrated VLCP systems. The comprehensive literature review of VLC and VLP techniques is offered in this chapter. Moreover, the review on the interference mitigation in multi-cell VLC systems and resource allocation in RF/VLC networks is presented. The potential applications of VLC are also introduced.

Chapter 3 proposes a quasi-gapless integrated VLCP system based on FBMC-SCM to support both the communication and positioning services. The principle of FBMC-SCM is first introduced and the comparisons between FBMC-SCM and OFDM-SCM are presented. The performance of FBMC-SCM and OFDM-SCM is discussed and compared by both simulations and experiments.

In Chapter 4, the principle of the new integrated VLCP system based on OFDM-SCM-interleaving with the low signal processing complexity is presented. Then, the QoS-driven optimized design with joint adaptive modulation, subcarrier allocation and weighted pre-equalization is proposed in details. The robust designs for both communication and positioning are presented under LoS blockages. Furthermore, this chapter also extends the system model into multi-cell integrated VLCP networks. Finally, the

experimental results and simulations are provided to evaluate the system performance and analyze the comparisons between the proposed design and other existing designs.

Chapter 5 investigates the ICI and IUI mitigation in multi-user multi-cell MIMO VLC systems. The system model is first discussed. After that, the joint precoder and equalizer design based on IA and the solution to the optimization problem are provided. Then, the analysis in terms of the behavior of the proposed design is presented. Finally, numerical results are provided to verify the effectiveness of the proposed design in different scenarios.

Chapter 6 studies the energy-efficient resource management based on heterogeneous RF/VLC architecture for industrial IoT networks. The heterogeneous RF/VLC network architecture, communication models and services' requirements are first presented, and then optimization problem is formulated. The deep reinforcement learning algorithm is provided, and simulations are provided to evaluate the performance of the proposed solutions.

In Chapter 7, the conclusions of the thesis and the recommendations of the future works are provided.

Chapter 2

Literature Review

In this chapter, the system models of VLC and VLP are first introduced, and the advanced technologies for the performance improvements in VLC and VLP systems are also discussed. Then, the related works in multi-cell VLC systems and hybrid RF/VLC networks are reviewed. After that, a review of existing integration models of VLC and VLP is provided. The corresponding applications of VLC are also introduced.

2.1 Introduction of VLC

Due to the rapid development of LEDs, white LEDs have been widely adopted as optical transmitters for VLC systems [5, 18], where the signal or data can be transmitted at the visible light spectrum. In practical indoor environments, a number of LED lamps are usually installed to set up a VLC system to support lighting requirements, as well as to provide data communications and to estimate the locations of indoor devices. VLC systems generally use intensity modulation with direct detection (IM/DD), where the intensity of each LED lamp is modulated with the real-valued, non-negative transmitted signal [10, 21], PDs are used as receivers to convert the light into electrical signals.

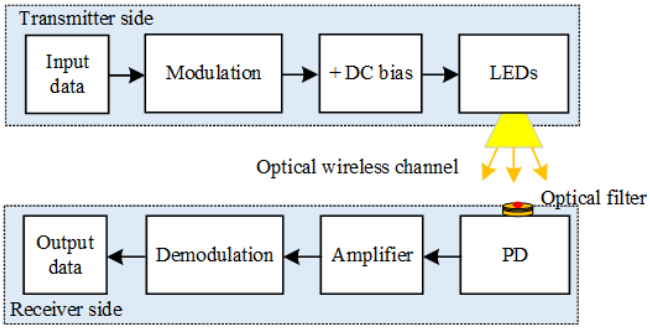

Figure 2.1: Block diagram of a typical VLC system.

2.1.1 System Model

Fig. 2.1 shows the basic block diagram of a typical VLC system. At the transmitter side, the input data stream is first modulated to achieve a real-valued signal and then a direct current (DC) bias is added to ensure that the modulated signal is non-negative. After that, the resultant electrical signal drives the LED lamps before passing through the wireless optical free-space channel. At the receiver side, the received signal is detected by the PD before converting it back to the digital signals. The signal can be achieved when the received signal pass through the optical filter, and the demodulation scheme is applied to demodulate the signal into the output data.

In VLC systems, white LEDs are used to support both the illumination and communication requirements, so LED lights consists of two properties, i.e., luminous intensity and transmitted optical power, where the first one is adopted for brightness and the second one is used for optical communications [10].

For LEDs, the luminous intensity can be written by

$$I = d\Theta/d\Omega \tag{2.1}$$

where Ω denotes the spatial angle, and Θ is the luminous flux, which can be expressed as a function of the energy flux Θ_e [18]

$$\Theta = \varpi \int_{380}^{780} V(\lambda)\Theta_e(\lambda)d\lambda \tag{2.2}$$

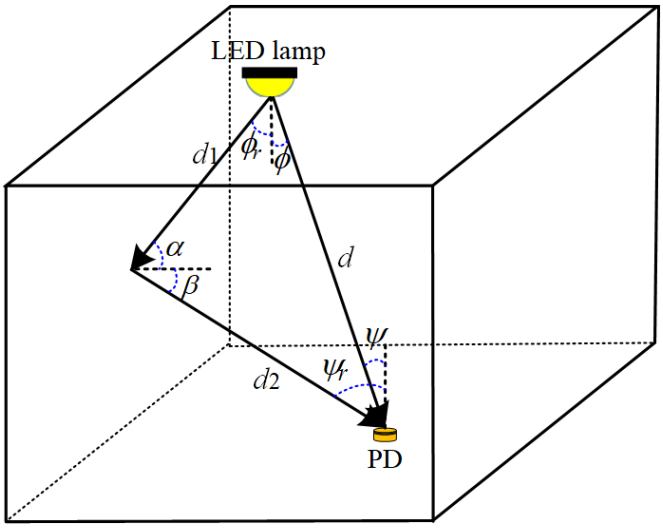

Figure 2.2: Propagation model of wireless optical channel links.

where ϖ is the maximum visibility $\varpi = 683$ lm/W at the wavelength $\lambda = 555$ nm. $V(\lambda)$ denotes the luminosity curve.

Let P_t denotes the transmit optical power and it is the integral of Θ_e in all directions, which can be written by

$$P_t = \varpi \int_{\varsigma_{\min}}^{\varsigma_{\max}} \int_0^{2\pi} \Theta_e d\theta d\lambda \tag{2.3}$$

where $\varsigma_{\min}$ and $\varsigma_{\max}$ are the constants determined by the sensitivity of PDs [18].

For the optical wireless channel, the channel response consists of the directed-LoS links and the reflected path [10, 77], as shown in Fig. 2.2. For the directed-LoS links, the optical channel gain between the LED lamp and the PD is expressed as [10, 18]

$$G = \begin{cases} \frac{(m+1)A_r}{2\pi d^2} \cos^m(\phi) T_s(\psi) g(\psi) cos\psi, & 0 \le \psi \le \psi_c \\ 0 & \psi > \psi_c \end{cases} \tag{2.4}$$

where A_r is the active area of the PD, ϕ is the angle of irradiance from the LED lamp to the receiver. m denotes the order of Lambertian emission. d and ψ denote the distance and the angle of incidence between the LED lamp and the receiver, respectively. ψ_c stands for the semi-angle field of view (FOV) of the receiver. $T_s(\psi)$ is the optical filter

gain. $g(\psi)$ is the optical concentrator gain, which can be given by

$$g(\psi) = \begin{cases} \eta/\sin^2\psi_c, 0 \leq \psi \leq \psi_c \\ 0 \qquad\qquad \psi > \psi_c \end{cases} \tag{2.5}$$

where η is the refractive index. In (2.4) and (2.5), the LoS channel link gain is zero (G=0) when ψ is outside of the FOV of the PD.

In addition, the optical channel gain of the first reflection (also called the diffuse component) can be given by [10, 77]

$$G_{first,ref} = \begin{cases} \frac{(m+1)A_r}{2\pi^2 d_1^2 d_2^2}\kappa A_{wall}\cos^m(\phi_r)\cos(\alpha)\cos(\beta)T_s(\psi_r)g(\psi_r)cos\psi_r,\ 0 \leq \psi_r \leq \psi_c \\ 0 \qquad\qquad\qquad\qquad\qquad\qquad\qquad\qquad \psi_r > \psi_c \end{cases} \tag{2.6}$$

where d_1 denotes the distance from the LED lamp to the reflection point, d_2 is the distance between the reflection point and the PD. κ is the reflectance parameter, A_{wall} is a small reflection area of the wall, ϕ_r is the angle of irradiance from the LED lamp. α and β denote the angle of incidence to the reflection point and the angle of irradiance from the reflection point to the PD, respectively, and ψ_r denotes the angle of incidence between the reflection point and the PD.

At the receiver side, the total received optical power of the PD from the LED lamp can be expressed as

$$P_{rec} = P_t G + \int_{walls} P_t \mathrm{d}G_{first,ref} \tag{2.7}$$

Generally, the weakest LOS component is less than 7dB higher in electrical power than the strongest diffuse component in general indoor environment [78]. Hence, the diffuse components are negligible and lots of literatures [46-54, 22-25, 33-42, 78] only consider the LOS component in the optical channel models.

In addition to the received optical power at the PD, the additive noise is also at the PD which is the sum of the contributions of both shot noise (denoted by δ^2_{shot}) and

the thermal noise (denoted by $\delta^2_{\text{thermal}}$). Then, the total additive noise is expressed by [10]

$$\delta^2_{\text{total}}=\delta^2_{\text{shot}}+\delta^2_{\text{thermal}} \tag{2.8}$$

with

$$\begin{cases} \delta^2_{\text{shot}} = 2q\mu P_{rec}B + 2qI_{bg}I_1B \\ \delta^2_{\text{thermal}} = \frac{8\pi kT_K}{a}\Xi A_r I_1 B^2 + \frac{16\pi^2 bT_K\Gamma}{\chi}\Xi^2 A_r^2 I_2 B^3 \end{cases}$$

respectively, where q is the electronic charge, μ is the photo detectors responsivity, B is the equivalent noise bandwidth, I_{bg} is the background current caused by ambient light and I_1 is an experimentally determined constant. In addition, b is Boltzmanns constant, T_K is the absolute temperature, a is the open-loop voltage gain, Ξ is the fixed capacitance of the PD per unit area, Γ is the FETs channel noise factor, χ is FET transconductance and I_2 is also a constant experimental value.

Then, the received signal-to-noise-ratio (SNR) at the PD can be calculated by

$$SNR = (\mu G\xi P_t)^2 \Big/ \delta^2_{\text{total}} \tag{2.9}$$

where ξ is the modulation index at the LED lamp. From (2.9), we can observe that SNR is determined by the transmit power level, the channel gain, the modulation index, the responsivity of the PD and the background noise at the PD.

2.1.2 Advanced Techniques for VLC

So far, a lot of advanced techniques or designs have been presented to improve the capacity of VLC systems, such as high-quality micro LEDs, frequency domain equalization, OFDM, and MIMO, which are briefly reviewed as follows.

1) High-quality micro LEDs: Considering the fact that the capacity of VLC systems is greatly limited by the limited modulation bandwidth of white LEDs, researchers have examined gallium nitride (GaN), AlInGaN, or InGaN based micro LEDs (also called μLED), which could achieve a 3-dB modulation bandwidth of more than 100 MHz [15,

16, 79, 80]. For example, in [16], D. Tsonev, *et al*., utilized GaN LEDs to achieve about a 3 Gbit/s VLC link over a distance of 5 cm.

2) Frequency domain equalization (FDE): FDE techniques can significantly enhance the 3-dB modulation bandwidth of commercially white LEDs, which can be performed either at transmitters or at receivers [48, 49, 81, 82]. The authors in [48] experimentally investigated weighted pre-equalization designs to optimize the system performance by compensating the frequency attenuation of LEDs. Li, *et al*. experimentally demonstrated a hybrid time-frequency domain equalization design to overcome the nonlinearity and frequency attenuation of LEDs [82].

3) OFDM VLC: The OFDM technique has the ability to reduce ISI by transmitting parallel data streams on the orthogonal subcarriers, and it can achieve the high spectral efficiency by combining high-order quadrature amplitude modulation (QAM) constellations, which has been widely adopted in VLC systems [50, 51]. Moreover, OFDM based multiple access technique i.e., orthogonal frequency-division multiple access (OFDMA) [83, 84] can provide flexible subcarrier allocation to guarantee each device' QoS requirements.

4) MIMO VLC: MIMO transmission is an effective way to enhance the capacity of VLC, where the indoor system consists of multiple transmitters (LED lamps) as inputs and multiple receiver elements (PDs) as outputs. Spatial multiplexing is a popular design for MIMO VLC systems, where different signals are transmitted by different LED lamps [85], as shown in Fig. 2.3 (a). Considering that the inter-channel-interference exists in spatial multiplexing based MIMO VLC systems, the techniques, i.e., precoding [46, 47, 86], power imbalance [87] and improved receiver design [88] have been presented to mitigate it. In addition, a spatial modulation technique was proposed to avoid inter-channel interference by using only one LED lamp to transmit signal at any point of time [89, 90], as shown in Fig. 2.3 (b).

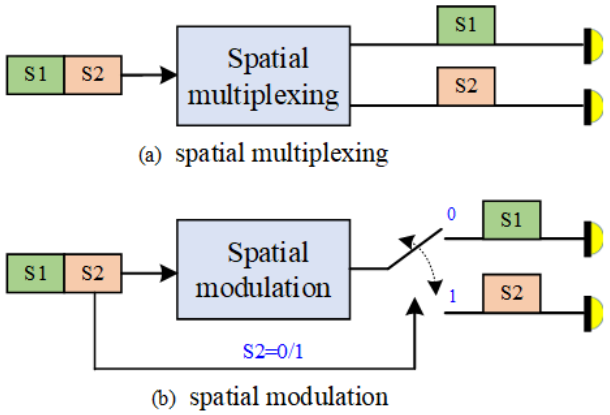

Figure 2.3: Illustration of two MIMO transmission designs

2.1.3 Applications of VLC

LEDs have achieved much attention recently in the lighting market and will replace traditional light sources for indoor environments due to its long lifetime, low power consumption, faster switching time and reliability [5]. At the same time, VLC based on white LEDs has been emerging as a promising candidate for indoor wireless communication systems due to its many attractive characteristics, such as economic, abundant unregulated bandwidth and high security [5, 6, 23]. Hence, VLC has gained much attention for applications in homes, supermarkets, hospitals, airplanes and industries [5-7]. It has been proved that VLC systems have the ability to achieve data rates up to several Gb/s, much higher than that of RF based systems (Wi-Fi) [5, 12]. Hence, in addition to provide illumination, VLC based LEDs systems can be directly employed to support high-speed Internet access in indoor environments, such as offices, classrooms, factories, homes and so on. In addition to the high-speed wireless communication, VLC based on LEDs also has other potential applications, which are discussed as follows.

1) Hospitals and healthcare: As we know, RF-based communication systems are undesirable in certain parts of hospitals or healthcare due to the electromagnetic interference, especially near magnetic resonance imaging scanners and in operating theatres.

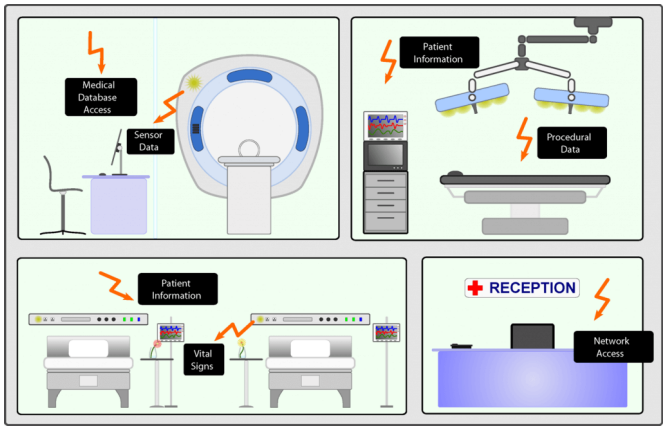

Figure 2.4: Illustration of VLC based hospitals and healthcare [92].

Hence, VLC is a promising technique for the electromagnetic interference -sensitive environments [91, 92]. Fig. 2.4 indicates the deployment of VLC systems for hospitals and healthcare.

2) Vehicular communication: Vehicle-to-vehicle (V2V), vehicle-to-infrastructure (V2I) and vehicle-to-everything (V2X) involve the wireless exchange of massages in vehicular communications. Vehicular networks have traffic light and street light, which enable VLC to provide wireless exchanges of data by acting lights as transmitters and employing PDs or image sensors as receivers to generate communication links [93, 94]. Fig. 2.5 shows the applications of VLC systems for vehicular communication.

3) Underwater communication: Underwater communication is important for underwater observation and sea monitoring [95]. However, in underwater environments, conventional RF-based systems do not effectively work due to the high attenuation of RF signals [95], and acoustic (sonar) wave cannot provide the high transmission data rate even though it has low attenuation. By contrast, visible light is capable of supporting the high-speed data rate over short distances in seawater, this could enable divers and underwater vehicles effectively communicate with each other [95-97]. Fig. 2.6 shows the application of VLC for underwater communication.

4) Indoor positioning: VLC has become an attractive research topic for indoor po-

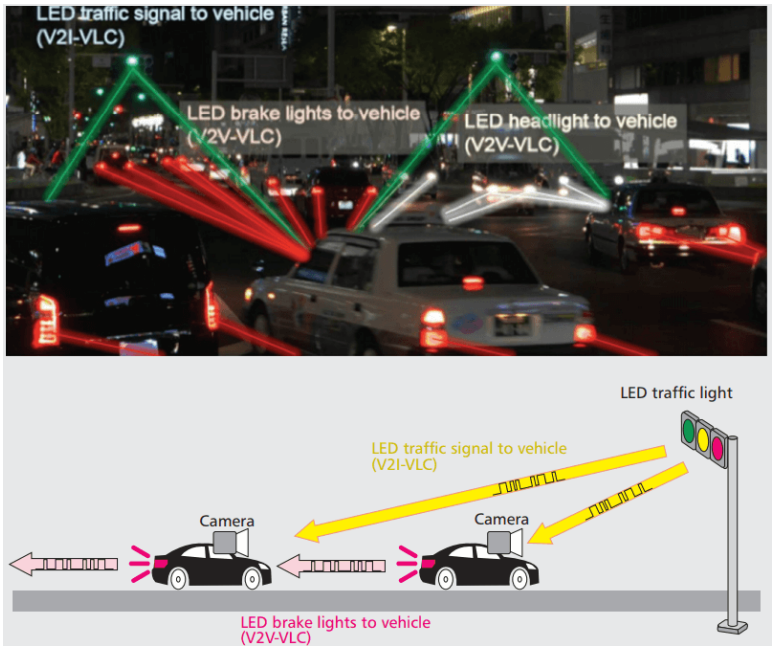

Figure 2.5: Illustration of VLC based vehicular communication [93].

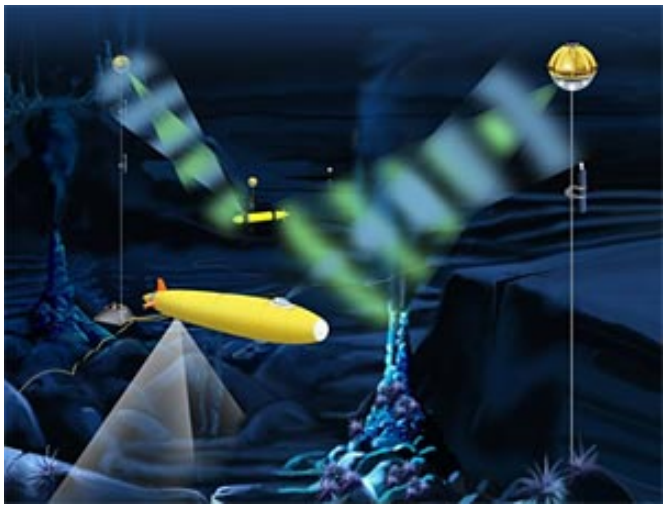

Figure 2.6: Illustration of VLC based underwater communication [97].

sitioning and tracking, because it provides the high positioning accuracy and guarantee security compared with the RF-based indoor positioning systems [22-25, 33-42, 98]. In VLC enabled positioning systems, the mobile device performs receiver side positioning by receiving the optical signal from LED lamps, where each LED lamps has its corre-

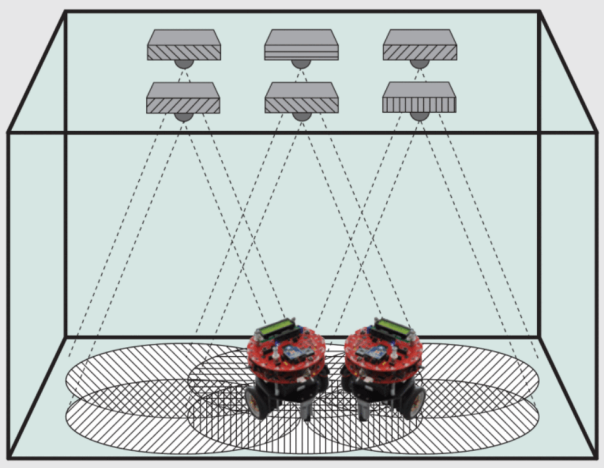

Figure 2.7: Illustrates the deployment of VLC based indoor positioning [98].

sponding identify indicator. Based on the received identify indicators, each device can perform positioning.

In addition to the above mentioned applications, VLC can be also applied for ranging, detection, monitoring, and sensing.

2.2 Introduction of VLP

2.2.1 System Model

Apart from the illumination and communication functions we have introduced in Section 2.1, visible light LEDs can also provide the indoor positioning services, called indoor VLP. Nowadays, indoor positioning is an important technology that could benefit both industries and consumers. Fig. 2.8 shows VLP for indoor environments. It adopts the received optical signals transmitted from different LED lamps referring to the locations of the LED lamps to perform location estimation of devices. Generally speaking, each LED lamp has its corresponding ID and it is transmitted via the VLC link, while the receiver is equipped a PD or camera to receive the different IDs. Finally, the device can adopt different positioning algorithms to perform the location

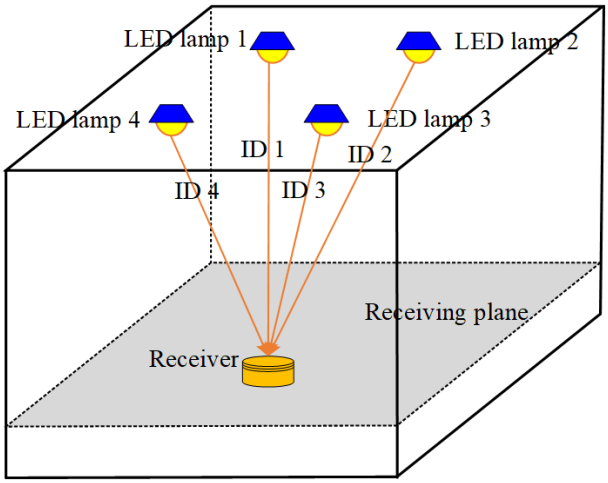

Figure 2.8: Illustration of VLP based on LEDs for indoor environments.

estimation, where the major positioning algorithms are RSS, AOA, TOA, TDOA and PDOA.

2.2.2 Positioning Algorithms for Indoor VLP Systems

An overview of the positioning algorithms for indoor VLP systems are presented herein. The measurements can be summarized as processing the received optical signals to achieve either distances or angles between the LED transmitters and the receiver. We investigate different types of positioning algorithms employed in VLP systems.

1) RSS: In RSS based VLP systems, the receiver evaluates the distances from a number of LED lamps (transmitters) to its equipped PD by measuring the received optical signal strength. After that, the location of the receiver can be estimated by using triangulation or the centroid method [23, 24, 34, 35]. Fig. 2.9 illustrates the positioning based on RSS for indoor VLP system. Here, a typical example for employing three LED lamp is introduced for 2-dimensional (2D) positioning. Once the receiver measures received optical signal strengths, each distance can be calculated by using the Lambertian model in VLP systems [35]

$$d_i = \sqrt[m_i+3]{P_i^{\text{tran}} A_r T_s(\psi_i) g(\psi_i)(m_i+1) h^{m_i+1} / (2\pi P_i^{\text{rec}})} \tag{2.10}$$

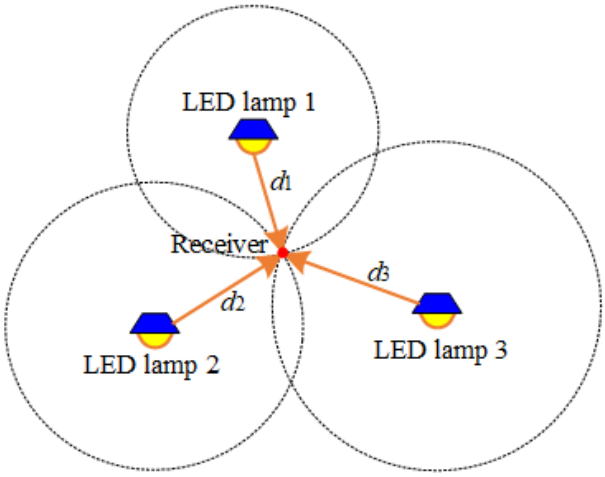

Figure 2.9: Positioning using RSS from different LED lamps.

where P_i^{tran} is the transmit power at the i-th LED lamp, and P_i^{rec} is the received power at the device from the i-th LED lamp, other parameter definitions can be seen in (2.6).

Forming three circles of at calculated distances, the location of the receiver can be estimated by calculating the intersection point of these circles, as shown in Fig. 2.9. In practical VLP systems, quantization and measurement errors exist, so the circles do not intersect perfectly, and other methods (such as least square estimation) can be used to estimate the location of devices [35].

So far, researchers have presented their studies in RSS based VLP systems [24, 34, 35, 39, 41, 55, 56, 57, 99]. In [99], a full analysis of VLP system based on RSS measurements are provided and the system achieves about sub-meter accuracy. Yang *et al.* in [41] utilized a single LED lamp to implement location estimation based RSS measurements, where the receiver is equipped with multiple PDs. The study in [24] experimentally demonstrated a carrier allocation RSS based VLC system, and the results illustrated that the system achieves the centimeter level positioning accuracy. In addition, The authors in [34, 35] derived the theoretical positioning accuracy by applying RSS in VLP systems under indoor multipath reflections, and the estimation accuracy can be improved by considering the multipath interference mitigation in the room. On

the other hand, machine learning techniques have been applied for VLP systems to correct the positioning errors caused by the transmitter or receiver hardware [39, 55, 100], and the high precision positioning algorithms based Bayesian model were presented to improve the positioning capability based on the historical location information [56, 57].

2) AOA: AOA realizes positioning based on the angles from the LED lamps to the receiver. Once the direction line of each angle is found, the location of the device can be estimated. Generally, AOA can be measured by using a number of PDs or a camera at the receiver side, leading to the two approaches: image transformation and modeling [101].

Image transformation adopts a camera to take photos of the light, and then uses the trigonometric relationship between the locations of the light beacons and the positions of the image on the photo to calculate the angles [36, 37, 102]. For example, Zhang *et al*. experimentally evaluated a high positioning accuracy scheme based on AOA by using image sensors at the receiver [37], but it needs a highly complicated sensor arrays. While the modeling approach uses the optical channel model to calculate the radiation angle. After measuring the light intensity at a certain receiver gesture, the angle can be calculated by using the channel radiation model [103, 104]. The receiver can use an array of PDs to determine the direction of arrival of the LED lamps by measuring the differences in RSS at the PDs [105, 106].

3) TOA: Similar to RSS, TOA calculates the distances to different LED lamps from the signal arrival time. The distances can be calculated by multiplying the light speed to the propagation times between LED lamps and the receiver. Then, the location of the receiver can be calculated via the distances to different LED lamps. The TOA based VLP systems requires that clocks of the LED lamps and the receiver should be synchronized [107].

Many researchers have presented their works in the TOA based VLP systems [40, 107-109], where TOA can achieve the higher positioning accuracy compared with other

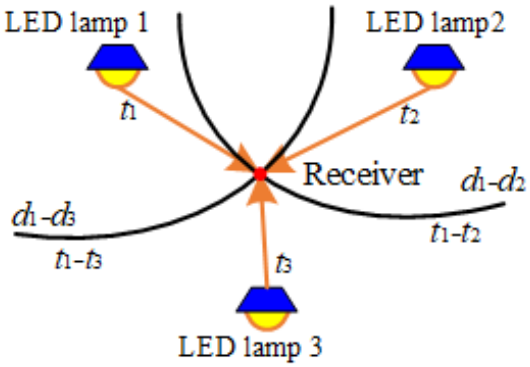

Figure 2.10: TDOA based VLP system.

positioning algorithms under the theoretical analysis. Moreover, the Cramer-Rao lower bound (CRLB) was presented for the distance calculation in TOA based VLP systems [40, 108, 109], and they also proved that the positioning performance mainly depends on the transmit power, center frequency and LED/PD quality. However, due to the strict time synchronization requirement, the cost of implementation associated with clock synchronization is high, which limits its application.

4) TDOA: Compared with TOA, TDOA only needs the time synchronization between the LED lamps that participate in positioning instead of requiring time-critical synchronization between the LED lamps and the receiver. TDOA measures the propagation time differences between the LED lamps and the receiver.

As shown in Fig. 2.10, the time differences and distance differences between any two LED lamps to the receiver are $t_i - t_j$ and $d_i - d_j$, respectively, where d_i and t_i are the distance and the propagation time between the i-th LED lamp and the receiver, respectively. Then, hyperbolas can be drawn based on the above mentioned distance differences on the map. The intersection of these two hyperbolas is the position of the receiver.

The fundamental analysis for TDOA based VLP systems using LEDs was presented in [22], and the literature also proved that no synchronization is needed between the

LED lamps and the receiver. The work in [110] utilized TDOA of the pilot signals to calculate the location of the receiver. In [111], a TDOA based VLP system adopting IM/DD with only two LED lamps was proposed. In addition, the works in [112] and [113] reported large positioning errors under background noise and the noise caused by the light reflections from the floors. Moreover, a low complexity TDOA based VLP approach was proposed in [38], and the experimental results demonstrated the effectiveness of the approach.

5) PDOA: The principle of PDOA is similar to TDOA, where PDOA calculates the phase differences between LED lamps to the receiver which is to utilize different carrier frequencies for the transmit optical signals belonging to different LED lamps [39, 42, 114, 115]. Then, the phase differences between the different received signals are converted to distance differences [22]. Similar to TDOA, PDOA requires the synchronization between the LED lamps.

So far, several works [39, 42, 114, 115, 116] of the positioning performance analysis were presented in PDOA based VLP systems, where the phase differences calculation was derived and the positioning accuracy was discussed in their studies. In [39], the authors presented a new differential PDOA scheme without using local oscillators and experimental results indicated that the high positioning accuracy was achieved by using the scheme. Moreover, a hybrid RSS/PDOA based VLP system was proposed to improve the robustness under various levels of intensity variations [116].

2.3 Multi-Cell VLC Systems

In practical indoor environments, each VLC cell associated with LEDs generates an optical attocell and it provides a small illuminated coverage area. In a practical VLC system or network usually consists of multiple attocells to support both the brightness and communication requirements [58-60]. Such a cellular indoor VLC system is referred to a multi-cell VLC system [58-60]. This section introduces the model of the multi-cell

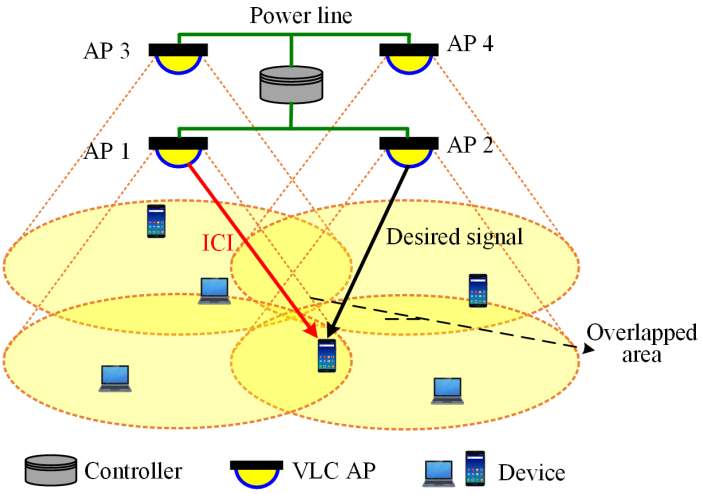

Figure 2.11: Illustration of an indoor multi-cell VLC broadcast system.

VLC system, and provides an overview of advanced technologies for ICI mitigation in multi-cell VLC systems.

2.3.1 System Model

Fig. 2.11 shows a typical indoor multi-cell VLC broadcast system model, where each VLC access point (AP) generates one small optical cell and the respective illumination areas of the adjacent cells are inevitably overlapped with each other. When the device locates in the overlapped area, it will detect the light intensity from LED fixtures in the overlapped areas, so the performance may be greatly degraded due to the severe ICI from adjacent cells.

2.3.2 Advanced Technologies for ICI Mitigation

Considering that ICI greatly degrades the system capacity and reduces the satisfied QoS levels of devices in multi-cell VLC systems, various technologies have been proposed to mitigate ICI, including frequency division, precoding, using an optical differential detection as a VLC receiver (called angle diversity receiver) and resource management

based on multiple access. Here, we provide an overview of the main ICI mitigation techniques in multi-cell VLC systems as follows.

1) Frequency division and subcarrier allocation: Frequency division has the ability to effectively mitigate ICI in multi-cell VLC systems by partitioning visible light spectrum and allocating the limited spectrum resource to each cell to accordingly avoid ICI [117-127]. The ICI coordination schemes, i.e, fractional frequency reuse (FFR) and soft frequency reuse (SFR), have been reported to improve the spectral efficiency by enabling each cell to reuse the spectrum [117, 118, 119]. An improved carrier allocation scheme by adopting filter bank multicarrier (FBMC) was studied to suppress the spectrum leakage interference in [120], where the guard band is greatly reduced. In [121], a user-centric cluster formation based on the VLC scheduler was proposed to mitigate ICI. In [122], the ICI mitigation through dynamic subcarrier allocation and power allocation was investigated. Moreover, in [123] and [124], the cell planning and ICI coordination approaches were proposed to avoid ICI in multi-cell VLC systems, which can significantly improve signal-to-interference-plus-noise ratio (SINR) for the cell-edge users.

Even though the ICI can be effectively mitigated according to the above mentioned works [117-124], the achievable spectral efficiency within each cell is obviously decreased due to spectrum division, as well as the use of a large guard band.

2) Precoding: Precoding is one of the advanced signal processing techniques that can be employed at the VLC APs (transmitters) to alleviate the impact of ICI. This technique also combines neighboring cells to perform the precoding strategy. For example, in [125], a coordinated precoding approach based on the weighted MMSE was proposed to mitigate ICI in multi-user multi-cell VLC systems, where the each AP can particularly or fully coordinate with adjacent APs to share its information (such as CSI).

In addition, the first study which concerned the multi-cell configuration and the cooperative precoding scheme was presented in [126-128], and the literature [128] also derived the lower and upper bounds on the system capacity under the non-negativity and amplitude-limited constraints. In order to reduce the overhead cost of information exchanges, a blind interference alignment (BIA) scheme based on a user-centric design was proposed to suppress ICI [129]. Moreover, the work in [130] aimed to maximize the network harvested energy under the individual harvested energy and data rate requirements of devices, before adopting the ZF precoding approach to mitigate ICI in multi-cell VLC systems.

3) Angle diversity receiver or transmitter: Recently, angle diversity receiver (ADR) was introduced for enhancing the performance of indoor multi-cell VLC systems [132-135], where an ADR consists of multiple narrow FOV PDs with different orientations. In this case, ADR can efficiently decorrelate the visible light channel gain and hence get the high rank of channel matrix. The authors in [131] provided an experimental demonstration of an indoor ADR optical system, and the data rate of 1.25 Gb/s was achieved in their presented system. In [132] and [133], Cheng *et al*. employed ADR to mitigate ICI in multi-cell VLC systems, where all the PDs of each ADR are attached to the fixed semi-sphere base. In addition, the equal gain combining, maximum ratio combining, and optimum combining were investigated in details in [134].

The optimized ADR approach was presented to optimize the system parameters to reduce the SINR fluctuation and improve the system capacity in indoor multi-cell VLC systems [135]. Moreover, an optical space division multiple access (SDMA) approach based on angle diversity transmitters for multi-cell VLC systems was proposed to mitigate ICI [136], and Tran *et al*., adopted the angle diversity transmitters into the hybrid RF/ VLC ultra-small cell network to maximize the communication QoS levels by mitigating ICI [137].

4) Resource management based on multiple access: Resource management (such

as power allocation, subcarrier allocation and VLC AP selection) based on multiple access technologies are effective ways to minimize ICI in multi-cell VLC systems and guarantee the QoS requirements of devices. In [122], an effective subcarrier and power allocation design was presented to maximize the system capacity under interference and power constraints. The literatures [138-140] investigated the dynamic throughput and energy efficiency maximization of user-centric multi-cell VLC systems, where the joint AP association and power allocation algorithms were presented in their works. In [141], a load balancing and power control approach for interference management was proposed for cell-free multi-cell VLC networks, and a dual projected gradient algorithm was adopted to solve the optimization problem with the low complexity. In addition, the rate adaptive radio resource allocation approach was presented to maximize the total system data rate under LoS blockages [142], and the authors in [143] proposed a careful subcarrier assignment design to mitigate the ICI with considering the user mobility and handover requirements in each cell.

The above mentioned works in [122, 138-143] paid attention to the interference mitigation in orthogonal multiple access (MA) systems. The studies in [143-146] employed an efficient MA scheme in multi-cell VLC networks, called the non-orthogonal multiple access (NOMA), which multiplexes a small number users in the power domain over the same band and it can greatly improve the spectral efficiency compared with orthogonal MA. The novel overlapped clustering approaches relying on a hybrid NOMA and orthogonal MA was presented to reduce the severe ICI [143, 144]. The authors in [145] optimized the power allocation within each cell to enhance the data rate under QoS constraints.

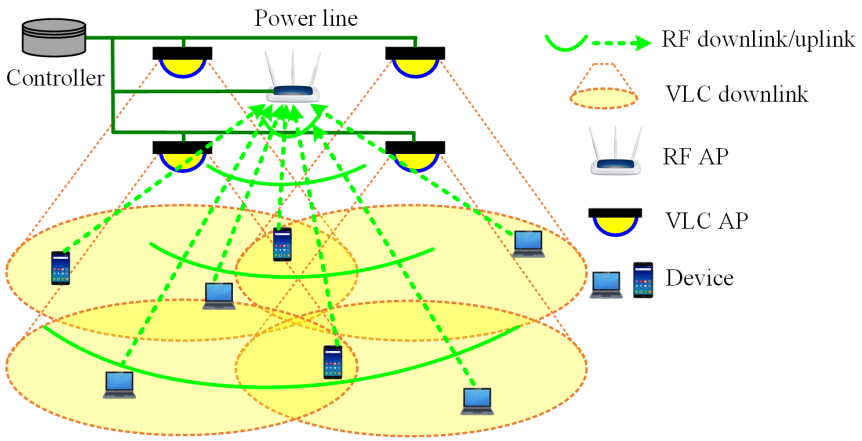

Figure 2.12: Illustration of an indoor hybrid RF/VLC network.

2.4 Heterogeneous or Hybrid RF/VLC Networks

2.4.1 System Model

Although VLC is capable of supporting the high-speed transmission data rate, it has the following two key shortcomings [147]: *1)* providing a wireless uplink in VLC systems is challenging, because it is impractical to equip energy-constrained devices with power-hungry light sources, and the device motion and orientation may frequently stop communication; *2)* VLC systems strongly depend on LoS links to satisfy the good communication performance, so the performance degradation is significant when LoS links are blocked by obstacles or human being due to the mobility of devices.

Hence, the co-deployment of RF and VLC technologies is straightforward way to overcome the above mentioned shortcomings, where RF has the ability to provide the uplink communication services and it is capable of offering reliable connectivity although its direct LoS link is blocked by walls [149-152]. Fig. 2.12 illustrates a typical hybrid RF/VLC network model.

As shown in Fig. 2.12, a number of VLC APs (refer to as a femtocell) are uniformly attached on the room ceiling and one RF AP (refers to as a microcell) is placed in the center. Each VLC AP contains one LED lamp based luminaries device offering both

lighting and communications services, and every VLC AP covers a confined area to generate a small optical cell. By contrast, the RF AP provides the coverage for the entire room. Both the VLC and RF APs connect the central controller to support the communication services, where VLC APs broadcast information to devices through visible light signals and the RF AP provides communication services by the RF signals. Considering the unpractical components and challenges of the wireless VLC uplink [149], and VLC only offers the downlink data streams while RF provides both the uplink and downlink data streams. When the VLC links are blocked, the device can switch the transmission mode from VLC links to RF links to continue their services.

2.4.2 Related Works in Hybrid RF/VLC Networks

Various heterogeneous or hybrid RF/VLC networking techniques and applications have be proposed for indoor communications [149-169]. The investigations can be summarized in terms of effective handover mechanism, energy efficiency maximization, energy harvesting, secrecy guaranteeing and so on. Here, we review the major related works as follows.

1) Handover mechanism: Due to the mobility behavior of devices in dynamic hybrid RF/VLC networks, vertical handover and horizontal handover need to be operated to maintain the good mobile connectivity and guarantee devices' QoS requirements [149-154]. The efficient vertical handover mechanisms based on Markov decision process were presented to reduce the handover cost and delay while satisfying devices' delay requirements [149, 150]. The literatures in [151] and [152] proposed dynamic load balancing schemes to maximize the systems throughput with considering the device mobility and handover overheads. Moreover, the received signal strength indicator - based handover approaches were proposed to reduce the handover rate and the spectrum access delay [153, 154].

2) Energy efficiency maximization: The energy-efficient resource allocation and transmission protocol designs were presented for the hybrid RF/VLC networks [155-160], in order to maximize the network energy efficiency (EE) while satisfying different QoS requirements of indoor devices. The studied in [155-157] proposed their energy efficient resource allocation approaches for hybrid indoor RF/VLC networks, where the problem under multiple constraints was formulated as a non-convex optimization problem in these works and the iterative algorithm was adopted to converge to the optimal point.

Also, the works in [158] and [159] formulated the problem of minimizing the energy consumption of the hybrid RF/VLC network while considering the outage probability or minimum data rate constrains. Furthermore, a coordinated beamforming design for hybrid RF/VLC networks was investigated in [160], where the objective is to maximize EE under both the perfect and imperfect CSI conditions.

3) Energy harvesting: Recently, the paradigm of energy harvesting was investigated in hybrid RF/VLC networks to prolong life time of indoor devices [161-165], where devices equipped with VLC receivers are designed to harvest the energy from the visible light. In indoor scenarios, the devices, like sensor nodes, can directly harvest the energy from the light transmitted from LED lamps over the downlink, which is used for the data transmission over the uplink [161, 162]. The authors in [163, 164] investigated the energy harvesting in dual-hop heterogeneous RF/VLC networks, where the relay harvests energy from the first-hop VLC link, and uses it to support the communication services over the second-hop RF link. Moreover, Sharma *et al*. proposed a novel energy harvesting model for IoT by integrating of energy harvesting and hybrid RF/VLC communication techniques [165].

4) Secrecy guaranteeing: Many works [166-169] have considered physical layer security (PLS) into hybrid RF/VLC networks to secure the communication and avoid eavesdropping and jamming attacks. The authors in [166] studied PLS aspects of hybrid

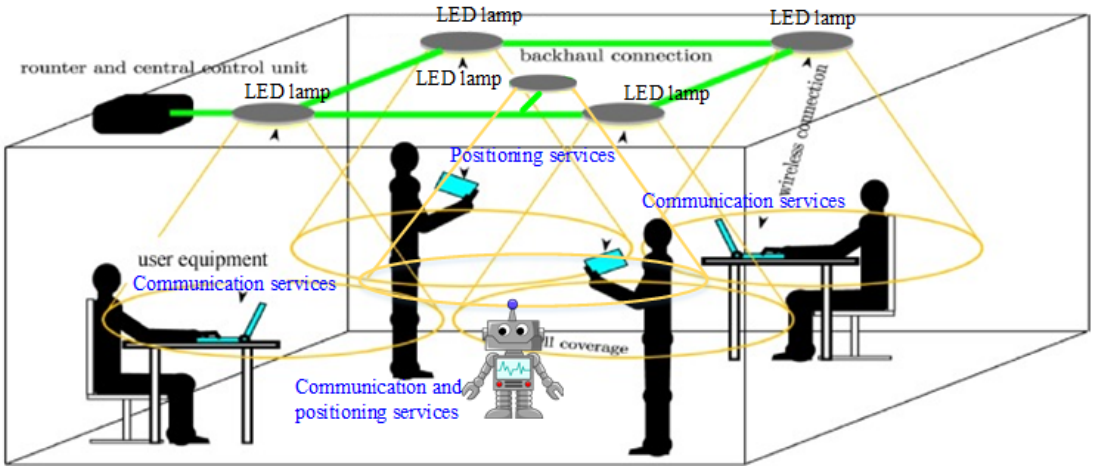

Figure 2.13: The integration of VLC and VLP system applied in indoor environments [170].

RF/VLC networks, and a novel joint relay-jammer selection approach was presented to guarantee the communication secrecy. In addition, the secure outage probability and secrecy data rate expressions were derived in [167-169], and the simulations were provided to evaluate the secrecy performance.

2.5 Introduction of Integrated VLCP Systems

2.5.1 System Model

In practical indoor environments, high-speed communication and high-accuracy positioning might be expected at the same time in certain scenarios (such as supermarket, hospital, robotic industry, etc.), and therefore the integration of VLC and VLP can be performed to provide simultaneous communication and positioning for indoor devices. Fig. 2.13 illustrates the integration of VLC and VLP in indoor environments, where some devices need the communication services, some devices require the positioning services and other devices may need both the communication and positioning services.

2.5.2 Related Works in Integrated VLCP Systems

Effective integration of VLC and VLP have not yet be adequately investigated and only several works [172-176] have reported integrated configurations for both communication and positioning purposes.

An integrated transmitter was firstly designed in [171] to flexibly achieve both communication and positioning applications. In [172], an integrated visible light network (VLN) architecture was proposed to achieve continuous communication as well as location tracking for indoor mobile devices. The integrated system was also applied in underwater environments [173]. Moreover, in order to mitigate the multipath reflections and realize a high data rate, OFDM VLC systems based on RSS were applied for both indoor positioning and communication [174-176]. The authors in [175] applied the OFDMA technique to allocate subcarriers for indoor positioning and data broadcasting. Moreover, the power allocation scheme was further adopted to reduce the positioning error in VLP system [176]. Thus, by combining communication and positioning capabilities, the integrated system can enable a new line of applications in indoor environments.

Fig. 2.14 illustrates two integrated VLCP system models of the existing works. In [175], as shown in Fig. 2.14 (a), three subcarriers with the three corresponding LED transmitters (Tx1, Tx2 and Tx3) are used for 2D positioning, while the other subcarriers are adopted for communication. In [176], as shown in Fig. 2.14 (b), the system has N LED transmitters and the whole bandwidth is divided into $2N$ subcarriers with each LED being allocated with two subcarrier blocks. At each LED transmitter, one available subcarrier is used for both the communication and positioning services. Hence, both the communication and positioning purposes can be achieved in the two works [175, 176]. Nevertheless, OFDM signals usually have relatively high out-of-band interference (OOBI), which might also degrade the performance of the integrated system.

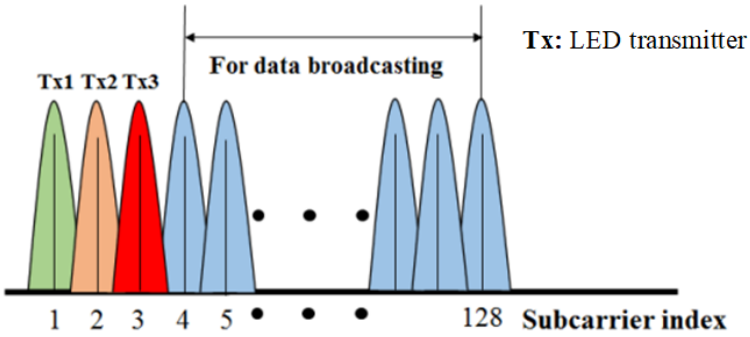

(a) Subcarrier allocation for positioning and data brocasting [175].

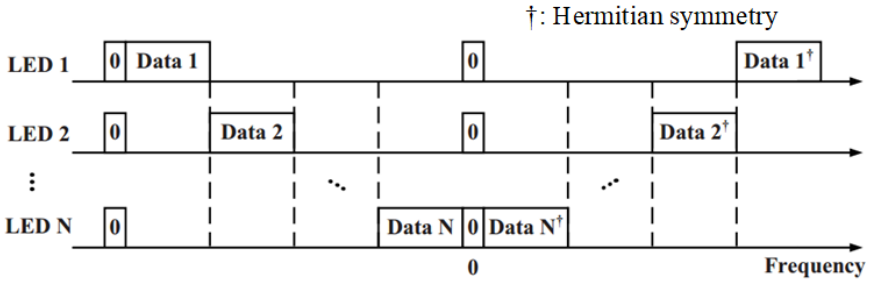

(b) Spectrum allocation of VLP system using OFDMA [176].

Figure 2.14: Illustrations of the existing integrated VLCP system models.

2.6 Summary

This chapter presented a brief review of the research progress in VLC systems, VLP systems, multi-cell VLC systems, RF/VLC networks and integrated VLCP systems. The advanced techniques for the capacity improvement for VLC systems, positioning algorithms for indoor VLP systems, ICI mitigation designs for multi-cell VLC systems, resource management for hybrid RF/VLC networks, and the integration of VLC and VLP have also been briefly reviewed. At the same time, some main practical applications of VLC have also been discussed.

Chapter 3

Quasi-Gapless Integrated VLCP System Using FBMC-SCM

3.1 Introduction

As discussed in Chapter 1 and Chapter 2, practical indoor environments may expect to have both the high-speed communication and high-accuracy positioning at the same time in one system instead of only offering VLC [10-21, 46-54] or VLP [22-25, 33-42, 55-57] independently.

So far, the combination of OFDM modulation and the RSS algorithm has been proposed for the integration of VLC and VLP in [174-176]. Specifically, in [175], three subcarriers with the maximum received signal strength with respect to three LED lamps were selected for RSS-based positioning, and the experimental demonstration was provided to evaluated the effectiveness of the presented system. In addition, the authors in [176] applied the OFDMA technique to allocate subcarriers for indoor positioning and data broadcasting.

Even though the integration of VLC and VLP using the OFDM modulation could improve both positioning accuracy and error vector magnitude (EVM) performance [174-176], the high OOBI of OFDM signal results in severe interference between ad-

jacent subcarriers, leading to the communication performance degradation [120]. In order to reduce the OOBI, GBs between two adjacent subbands are usually adopted [120]. The use of GBs can substantially mitigate the OOBI, but the overall spectral efficiency of the integrated system is inevitably reduced. In order to reduce the OOBI, an alternative technique called filter bank based multicarrier (FBMC) [177] has been applied for optical access networks and VLC systems [120, 178-180]. In FBMC-based systems, each subcarrier is filtered by a filter such that low OOBI can be achieved and hence the interference is effectively suppressed [120], which reduces the required GBs and thus improves the overall spectral efficiency.

To address the above issues, this chapter proposes an integrated VLCP system using FBMC-SCM and PDOA [181-183]. Compared with OFDM-SCM based VLCP systems, the proposed FBMC-SCM-based VLCP system can effectively suppress the OOBI and hence improve the performance of positioning accuracy. Simulation results versify that the VLCP system using FBMC-SCM requires much reduced GBs in comparison to that using OFDM-SCM, and therefore achieves a higher spectral efficiency and improved positioning accuracy. In addition, the experimental results show that, in a coverage area of 1.2×1.2 m^2 with a height of 2.1 m, the mean position errors using OFDM-SCM and FBMC-SCM for a GB of 0.7 MHz are 10.91 and 6.08 cm, respectively. Moreover, a comparable BER performance can be achieved for both OFDM-SCM and FBMC-SCM. Due to the negligible GBs when using FBMC-SCM, the effective bandwidth utilization ratio of the integrated VLCP system is improved from 72% to 98% when OFDM-SCM is replaced by FBMC-SCM.

The rest of this chapter is organized as follows. Section 3.2 describes the model of the integrated VLCP system and also present the detailed architecture of the proposed FBMC-SCM-based integrated VLCP system. Section 3.3 shows the simulation results where the performances of the FBMC-SCM-based and OFDM-SCM-based integrated VLCP systems are evaluated and compared under different operation conditions. The

experimental results are provided in Section 3.4. Finally, Section 3.5 summarizes the chapter. The content of this chapter is related to the author's work provided in [181-183].

3.2 Integrated VLCP Systems

In practical indoor environments, a number of LED lamps are usually installed to set up a VLC system to satisfy lighting requirements, as well as provide data communications and estimate the location of user-equipment (UE) in the room. The LED lamps generally use intensity modulation with IM/DD, where the intensity of each LED lamp is modulated with the transmitted data and PDs are used as receivers to convert the light into electrical signals. In the proposed integrated VLCP system, we apply the improved 2D PDOA localization algorithm without using local oscillators (LOs) at the receiver to estimate the location of the UE [39].

3.2.1 Improved PDOA Algorithm

In this subsection, we introduce the principle of the improved PDOA algorithm for the proposed integrated VLCP system. As discussed in [13], three LED lamps are used in the PDOA algorithm with four different positioning frequencies. As shown in Fig. 3.1, f_1 and f_4 are modulated onto LED 1 together, while f_2 to f_3 are modulated onto LED 2 to LED 3, respectively. All the LED lamps are synchronized. The frequency gap between two adjacent frequencies is equal to $\triangle f$. Hence, these LED lamps can be distinguished by their respective frequencies.

Note that the frequency band used for positioning is from 8.0 MHz to 8.6 MHz in our proposed integrated VLCP system [22, 39]. Because the frequency is inversely proportional to phase resolution, it is directly related to the positioning error [22, 39]. On one hand, if the positioning frequencies are selected at the low frequency region, the location errors are increased due to low phase resolution. On the other hand, even

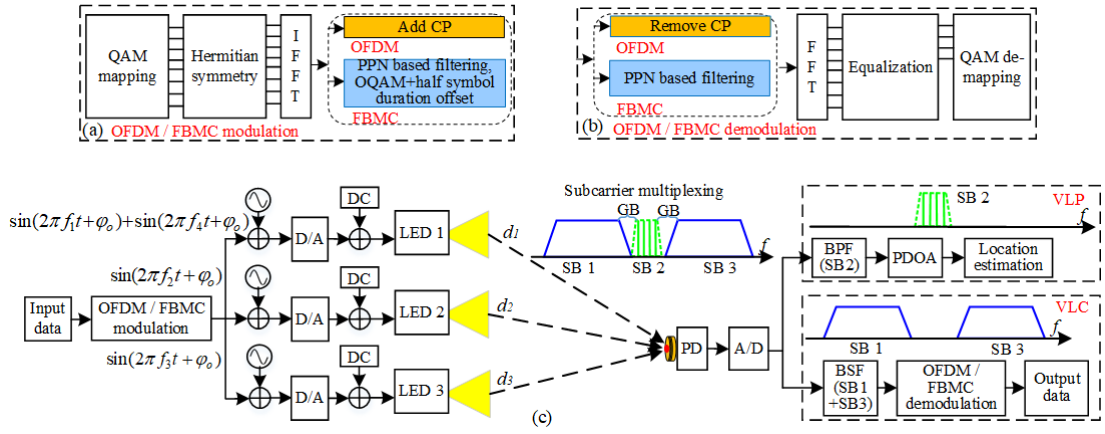

Figure 3.1: Block diagram of the proposed integrated VLCP system. Insets: principle of OFDM/FBMC.

though high positioning frequency for positioning can achieve good phase resolution, the severe power attenuation of the high frequency components will reduce the positioning accuracy performance [22, 39]. Hence, as a trade-off between phase resolution and power attenuation, we use this range of frequency for positioning.

At the receiver, after separating the received signals with four band pass filters (BPFs), signals with frequencies of f_1 to f_4 are distinguished from each other. The position of the UE is calculated using the improved PDOA algorithm (refer to [22, 39] for the more details).

The distance between the i-th LED lamp and the PD of the UE is give as

$$d_i = \sqrt{(x_i - x_o)^2 + (y_i - y_o)^2 + (z_i - z_o)^2} \tag{3.1}$$

where x_i, y_i and z_i, $(i = 1, 2, 3)$ are the coordinates of the i-th LED lamp, and the estimated position of the UE is (x_o, y_o, z_o). Given the location of the three LED lamps, the location of the UE can be successfully estimated [22, 39].

3.2.2 FBMC-SCM-Based Integrated VLCP Systems

In this subsection, we describe the principle of FBMC and compare it with the widely used cyclic prefix-based OFDM, and apply these two modulation schemes based SCM

techniques for the integrated VLCP system.

Insets (a) and (b) in Fig. 3.1 present the modulation and demodulation of OFDM /FBMC. In order to reduce the large OOBI, FBMC applies a prototype filter to filter each subcarrier. The basic structures of the two modulation schemes are the same, except the CP insertion in OFDM is replaced by the polyphaser network (PPN) based on the well-designed prototype filter [177] in FBMC. Before performing the inverse fast Fourier transform (IFFT), Hermitian symmetry is imposed to generate a real-valued signal. The goal of employing PPN in FBMC is to guarantee that FBMC has the same FFT size and similar complexity with OFDM. Even though FBMC could significantly reduce the sidelobes through filtering each subcarrier, it may break the pulse-shape orthogonality between adjacent subcarriers. Hence, the offset OQAM modulation is applied to guarantee the orthogonality [177].

The OFDM-SCM-based integrated VLCP system applies a low-pass linear phase finite impulse response (FIR) filter to filter the input data, called the Sinc-filter [177], the frequency response of the filter can be expressed as

$$H(f) = \frac{\sin(\pi f M)}{M \sin(\pi f)} \tag{3.2}$$

where M is the FFT size.

For the generation of FBMC signals in the FBMC-SCM- based integrated VLCP system, there are many FIR filters that can be used [120, 177], and we apply a prototype filter based on Mirabbasi-Martin filter (MM-filter) in our work since this filter function can effectively suppress the sidelobe with the low complexity [177]. In the frequency domain, the filter function of the MM-filter can be given by

$$H(f) = \sum_{k=-(K-1)}^{K-1} H_k \frac{\sin\left(\pi(f - k/MK)MK\right)}{MK \sin\left(\pi(f - k/MK)\right)} \tag{3.3}$$

where k is the overlapping factor and the coefficient H_k is used to control the out-of-band filter frequency response [177]. In this work, we choose $K = 4$ [120], [177].

The block diagram of the proposed integrated VLCP system based on OFDM-SCM/FBMC-SCM schemes is depicted in Fig. 3.1 (c). The total bandwidth is divided into three subbands and two GBs, where subband 2 is used for 2D PDOA positioning and the remaining two subbands are reserved for VLC. All the three LEDs transmit the same communication data. The data stream is then encoded to an OFDM or FBMC signal, while a sinusoidal signal for VLP is added with the OFDM/FBMC signal at each LED lamp after being converted the digital-to-analogue (D/A) process. All the sinusoidal signals for VLP are synchronized at the transmitter side. After adding a DC bias, each resultant signal is modulated to LED lamps. The four positioning frequencies from f_1 to f_4 are all in the subband 2. In addition, the bandwidth of each GB is equal in the system.

At the receiver, the received signal is detected by the PD before converting it back to digital signals. On one hand, the positioning data can be obtained after the received digital signals pass through the band pass filters (BPFs), and the position of the receiver is calculated through using the improved PDOA algorithm [39]. On the other hand, the communication signal can be achieved when the received signal passes through the band stop filter (BSF), and the OFDM or FBMC demodulation scheme is applied to demodulate the communication signal. Hence, both the communications and positioning purposes can be achieved in the proposed integrated VLCP system.

The spectra of the communication and positioning signals in OFDM-SCM-based and FBMC-SCM-based integrated VLCP systems are shown in Figs. 3.2 (a) and (b), respectively. Compared with OFDM, the OOBI of FBMC spectrum is effectively suppressed, which has low interference leakage to the positioning signal. In the OFDM-SCM-based integrated VLCP system, the high OOBI results in severe interference between adjacent subbands, leading to the reduced positioning accuracy.

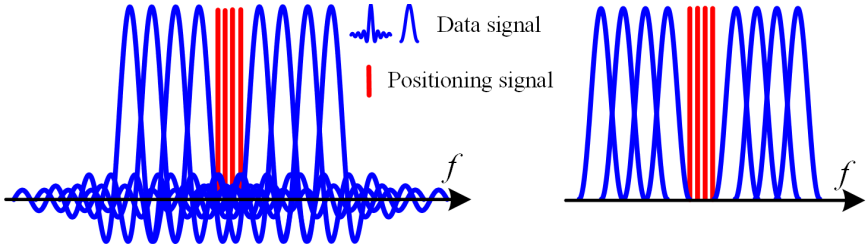

(a) OFDM-SCM-based integrated VLCP system (b) FBMC-SCM-based integrated VLCP system

Figure 3.2: Illustration of the spectra the integrated VLCP signal.

Table 3.1: Simulation Parameters

Parameters	Values
Rome size (length × width × height)	5m × 5m × 3m
Number of LED lamps	3
Location of LED lamp 1	[0, -0.175, 3]
Location of LED lamp 2	[0.25, 0.075, 3]
Location of LED lamp 3	[-0.25, 0.075, 3]
Transmitter semi-angle	60°
LED Lambertian emission order	1
PD concentrator refractive index	1.5
PD active area	1 cm^2
Gain of optical filter	1
PD responsivity	0.5 A/W
FOV of the PD	120^0
System bandwidth	30 MHz

3.3 Simulation Results and Comparisons

In this section, we evaluate the performance of the proposed FBMC-SCM-based integrated VLCP system and compare it with that of the OFDM-SCM-based integrated VLCP system. In a typical 5m×5m×3m room, three LED lamps are mounted in the ceiling. The receiving plane is 0.85 m above the floor.

The simulation parameters of the integrated VLCP system are listed in Table 1. The LED lamp semi-angle at half power is 60^o. The active area, the FOV and the responsivity of the PD are 1 cm^2, 120^o and 0.5 A/W, respectively. The gain of the

Table 3.2: Parameters of OFDM and FBMC

	OFDM	FBMC
IFFT/FFT size	256 (Hermitian symmetry)	
Modulation	4QAM, 16QAM and 64QAM	
Filtering	Rectangular	Mirabbasi-Martin filter (K=4)
Cyclic prefix	1/20	0

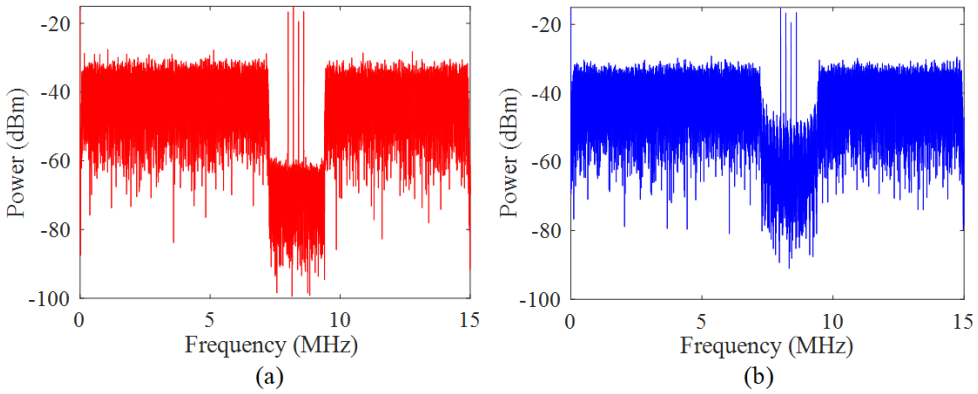

Figure 3.3: Received spectra of the integrated signal.

optical filter is 1. We use a modulation bandwidth of 30 MHz and different QAM mappings in the integrated VLCP system. The frequency gap between two adjacent positioning frequencies is 0.2 MHz.

For both OFDM and FBMC, the IFFT/FFT size is 256 and the other parameters are shown in Table 2.

3.3.1 Received Signal Spectrum

Figs. 3.3 (a) and (b) show the received electrical spectra of the OFDM-SCM signal and the FBMC-SCM signal, respectively. It can be observed that the OOBI of the OFDM-SCM signal is much stronger than that of the FBMC-SCM signal. The OOBI level of the OFDM-SCM signal at the positioning frequency is about -49dBm, while the OOBI level of the FBMC-SCM signal is almost -61dBm, indicating an OOBI reduction of about 12dB. The high OOBI in the OFDM-SCM-based integrated VLCP system will

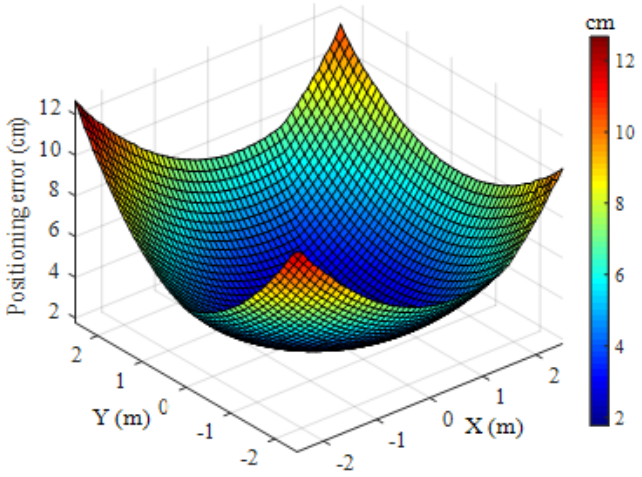

(a) FBMC-SCM-based integrated VLCP system

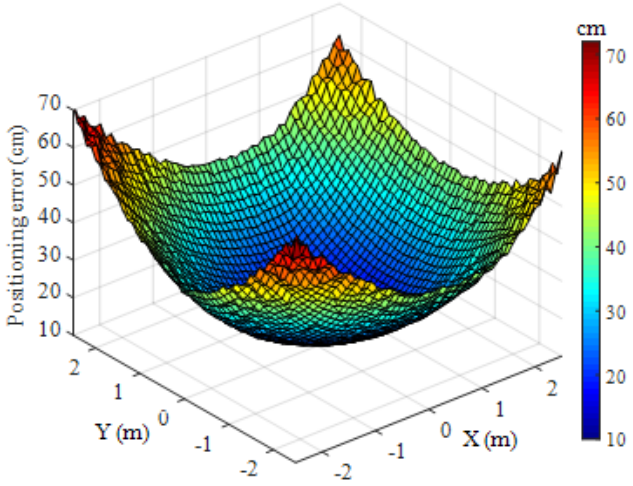

(b) OFDM-SCM-based integrated VLCP system

Figure 3.4: Positioning error distribution of the integrated VLCP systems.

lead to severe interference to adjacent subbands, which could degrades the positioning accuracy performance.

3.3.2 Positioning Accuracy

Figs. 3.4 (a) and (b) show the positioning error distribution over the receiving plane in the integrated VLCP system based on FBMC-SCM and OFDM-SCM, respectively. The frequency spacing of the GBs is set to 0.8 MHz. As we can see, the positioning

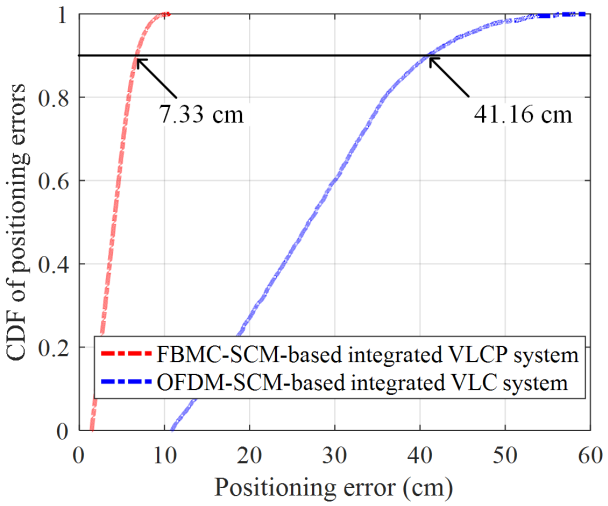

Figure 3.5: Comparison of the CDF of positioning errors.

error is low at the center, but is high at the corners. This is because the received power decreases when the receiver moves away from center to corners. As shown in Fig. 3.4 (a) and (b), most of the positioning errors in the OFDM-SCM-based integrated VLCP system are much high than those of the FBMC-SCM-based integrated VLCP system. This is because the high OOBI of OFDM data signal will lead to serious interference to positioning signals, therefore the positioning accuracy decreases dramatically.

Fig. 3.5 shows the cumulative distribution function (CDF) of the positioning errors. It can be observed that the 90% confidence interval is at 41.16 cm for the OFDM-SCM-based integrated VLCP system, while the FBMC-SCM-based integrated VLCP system improves it to about 7.33 cm, showing a significant improvement of positioning accuracy by using FBMC-SCM. In comparison, in the FBMC-SCM- based integrated VLCP system, most of the positioning errors in the room are below 5cm, and only a few locations at edge areas are just over 10cm.

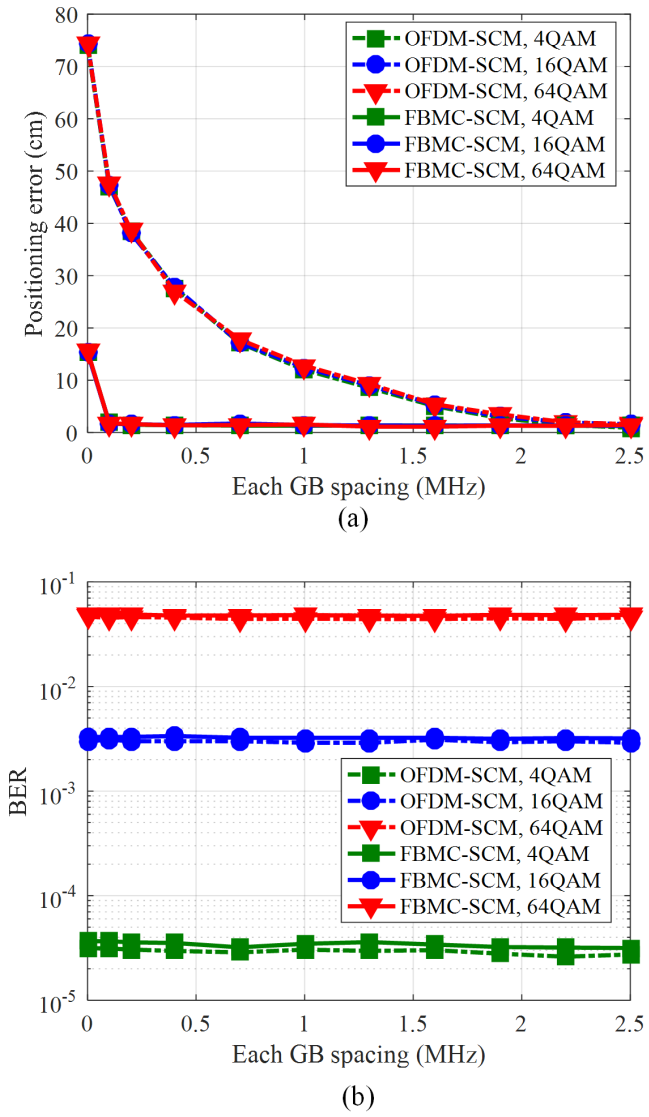

Figure 3.6: Comparison of (a) positioning error and (b) BER performance versus each GB frequency spacing in the integrated VLCP system.

3.3.3 Impact of Guard Bands

Figs. 3.6 (a) and (b) present the positioning errors and the average BER versus the frequency spacing of each GB, respectively. As can be seen in Fig. 3.6 (a), the positioning of the FBMC-SCM-based integrated VLCP system outperform that of the OFDM-SCM-based integrated VLCP system, especially when the frequency spacing

of each GB is relatively small. The FBMC-SCM-based integrated VLCP system does not need large GBs to mitigate the OOBI for the adjacent subbands. However, the positioning accuracy is much sensitive to the frequency spacing of each GB in the OFDM-SCM-based integrated VLCP system. We can observe that the OFDM-SCM-based integrated VLCP system achieves nearly the same positioning accuracy as the FBMC-SCM-based integrated VLCP system only when the frequency spacing of each GB is more than 2.4 MHz. Since the positioning accuracy of the FBMC-SCM-based integrated VLCP system become stable when the frequency spacing of each GB is about 0.15MHz, which is much smaller than that of OFDM-SCM. In addition, we find that both OFDM-SCM and FBMC-SCM integrated VLCP systems almost maintain at a same horizontal BER level over the whole GB frequency spacing [177], and the BER performance of the FBMC-SCM scheme is slightly worse than that of the OFDM-SCM scheme.

We define the effective bandwidth utilization ratio as the ratio of the bandwidth occupied by the subbands for communication and positioning to the total bandwidth. When both OFDM-SCM and FBMC-SCM integrated VLCP systems achieve at a target positioning accuracy, the FBMC- SCM scheme improves the effective bandwidth utilization ratio from 68% to 98% compared with the OFDM-SCM scheme.

3.4 Experimental Demonstration of the Integrated VLCP System

3.4.1 Experimental Setup

In this section, we present the experimental results to verify the feasibility of the integrated VLCP system within a practical indoor environment. The experimental setup of the integrated VLCP system is depicted in Fig. 3.7. Both the OFDM/FBMC signal for VLC and the sinusoidal signals for VLP are generated offline using MALTAB, AND

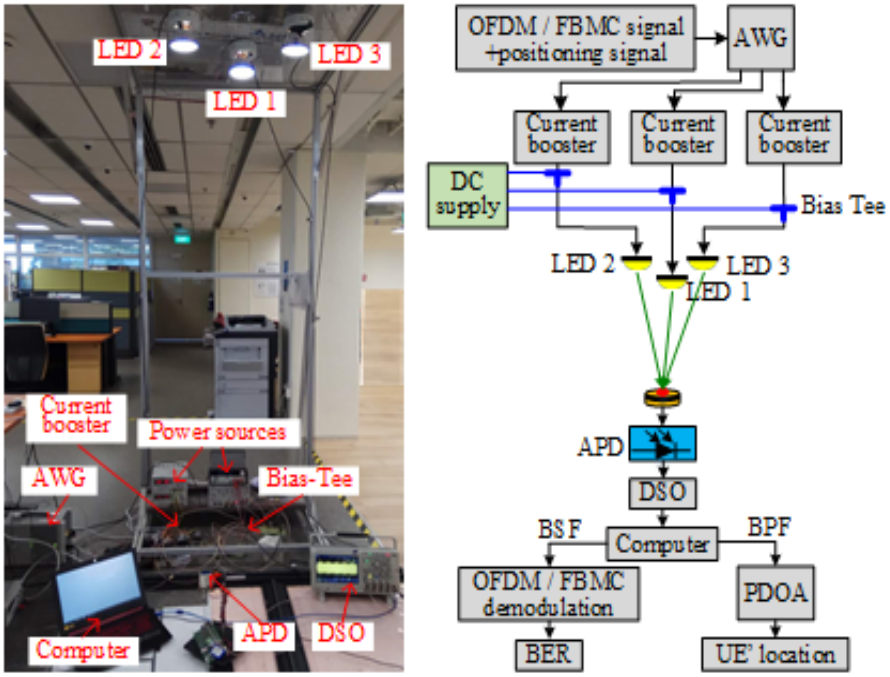

Figure 3.7: Experimental setup of the integrated VLCP system.

then uploaded to a multi- channel arbitrary waveform generator (AWG) with a sampling rate of 100 MSa/s. After amplifying and adding DC biases, the obtained signals are used to drive three LED lamps (Lumileds LXML-PWCI). After free-space propagation, the light is captured by an avalanche PD (APD, Hamamatsu S8664-50K) after passing by a blue filter (BF). The detected signal is recorded by a digital storage oscilloscope (Tektronix MDO3104) with a sampling rate of 100 MSa/s. The specifications of the amplifier is 811AR-16F amp (BUF634) buffer power gain 24 dB, the bias tee is made by our group with 2KHz to 500MHz, the driving current of each LED is 100 mA, and the illumination level at the receiving plane under the cell unit was 380 lux which has reached the standard of indoor illumination. Subsequently, the demodulation of the communication signal and the estimation of the users location are executed offline using MALTAB. To extend the modulation bandwidth, digital pre-frequency domain equalization is used in the system [49].

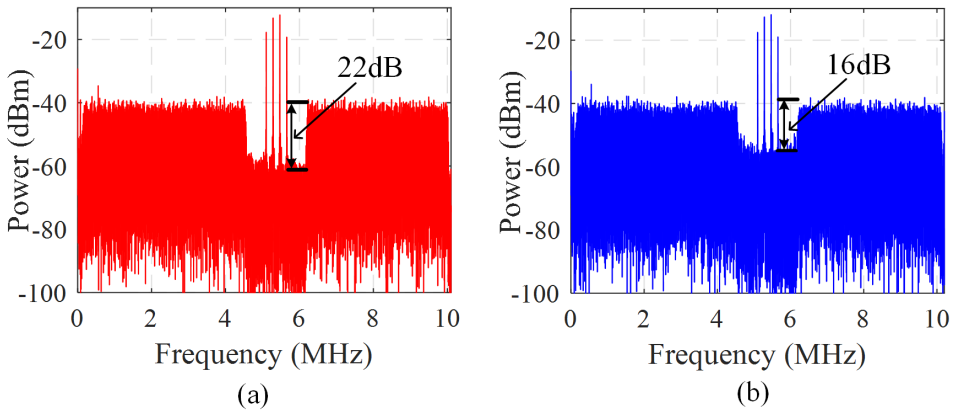

Figure 3.8: Received spectra of (a) FBMC-SCM signal and (b) OFDM-SCM signal.

We test the performance of the integrated VLCP system in a quarter area of 1.2m×1.2m and the vertical distance between the LED lamps and the PD is 2.1 m. The locations of three LED lamps are (0, -0.175, 2.1), (0.25, 0.075, 2.1) and (-0.25, 0.075, 2.1) with the origin (0, 0, 0), where the units are all meters. The APD has an active area of 19.6 mm^2 and a responsivity of 15 A/W at the wavelength of 450 nm. The system modulation bandwidth is extended to 10 MHz and 4-QAM mapping is used for communication. For both OFDM and FBMC, the IFFT/FFT size is 512, and the number of data subcarriers is 51. The overlapping factor in FBMC is set to K=4. The frequencies of the four sinusoidal signals for positioning are in the range between 5.1 to 5.7 MHz with a frequency gap of 0.2 MHz.

3.4.2 Experimental Results and Analysis

Figs. 3.8 (a) and (b) show the received electrical spectra of the OFDM-SCM signal and the FBMC-SCM signal, respectively, where the GB spacing is 0.7 MHz. We can see that, compared with OFDM, the OOBI of FBMC is effectively suppressed, resulting in much reduced power leakage at the positioning frequency subband. A significant 6-dB OOBI reduction can be achieved by using FBMC-SCM in comparison to OFDM-SCM.

Figs. 3.9 (a) and (b) demonstrate the positioning results over the testing area in

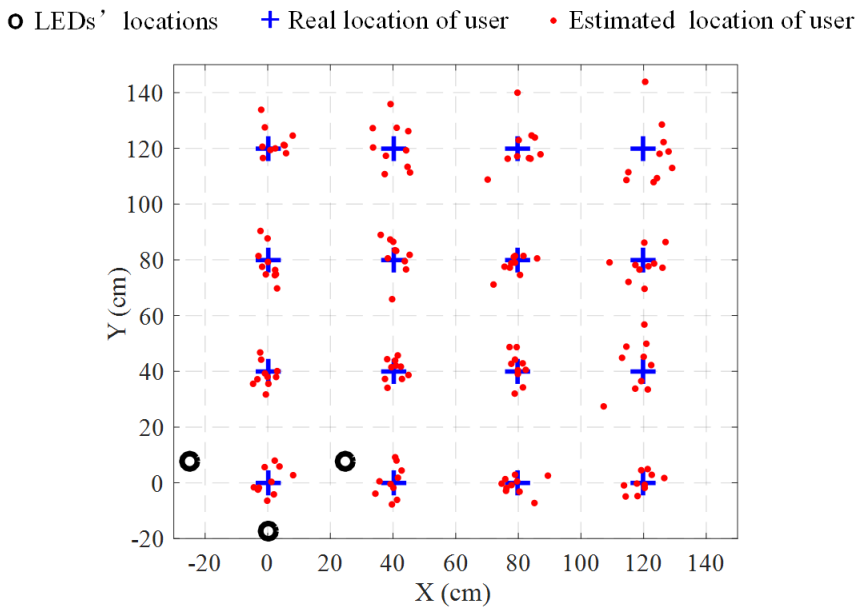

(a) FBMC-SCM-based integrated VLCP system

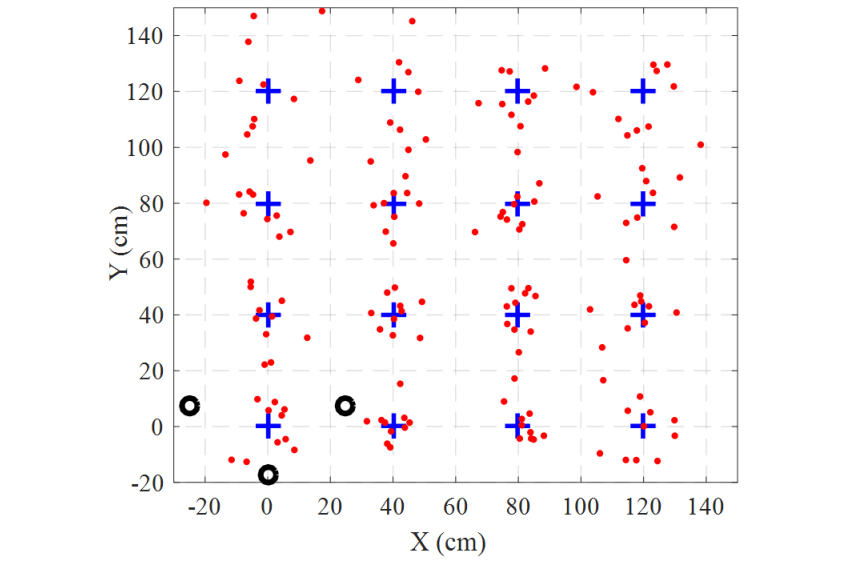

(b) OFDM-SCM-based integrated VLCP system

Figure 3.9: Positioning results based on (a) FBMC-SCM and (b) OFDM-SCM.

the integrated VLCP system using FBMC-SCM and OFDM-SCM, respectively. The frequency spacing of GB is set to 0.7 MHz. As we can see, when the user is moving

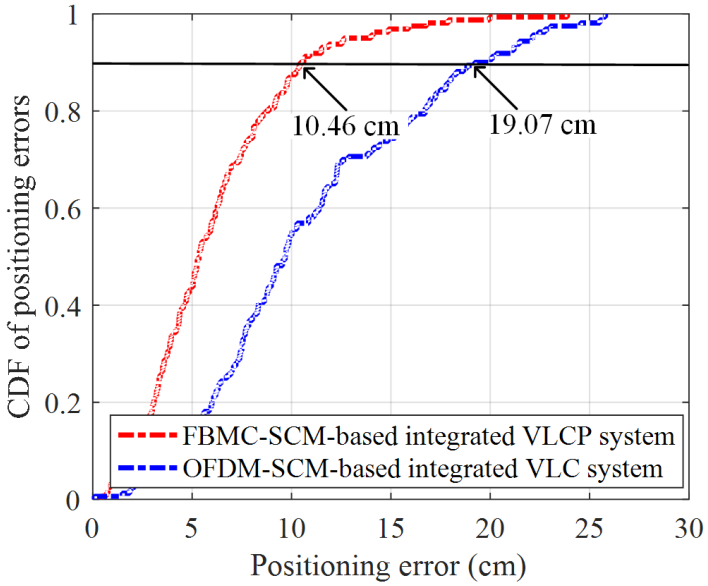

Figure 3.10: CDF of positioning errors using OFDM-SCM and FBMC-SCM.

away from the LED lamps, the positioning accuracy is gradually deceased for both FBMC-SCM and OFDM-SCM. It can be clearly observed from Fig. 3.9 that a higher positioning accuracy is achieved by using FBMC-SCM compared with OFDM-SCM over the 1.2 m 1.2 m coverage area. For FBMC-SCM, most of the positioning errors are less than 8 cm and only a few of them are more than 10 cm when the user is at edge of the coverage area, and the mean position error is 6.08 cm. However, for OFDM-SCM, the positioning errors are mainly ranging from 7 to 20 cm, and only a few of them are below 5 cm when the user is at center of the coverage area, and the mean positioning error is as high as 10.91 cm.

Fig. 3.10 shows the cumulative distribution functions (CDFs) of the positioning errors using OFDM-SCM and FBMC-SCM. As can be seen, the positioning errors at 90% confidence for OFDM-SCM and FBMC-SCM are 19.07 and 10.46 cm, respectively, which indicates a positioning accuracy improvement of up to 8.4 cm.

Fig. 3.11 shows the BER distribution over the testing area using OFDM-SCM and FBMC-SCM. It can be seen that the BER values over the testing area for both

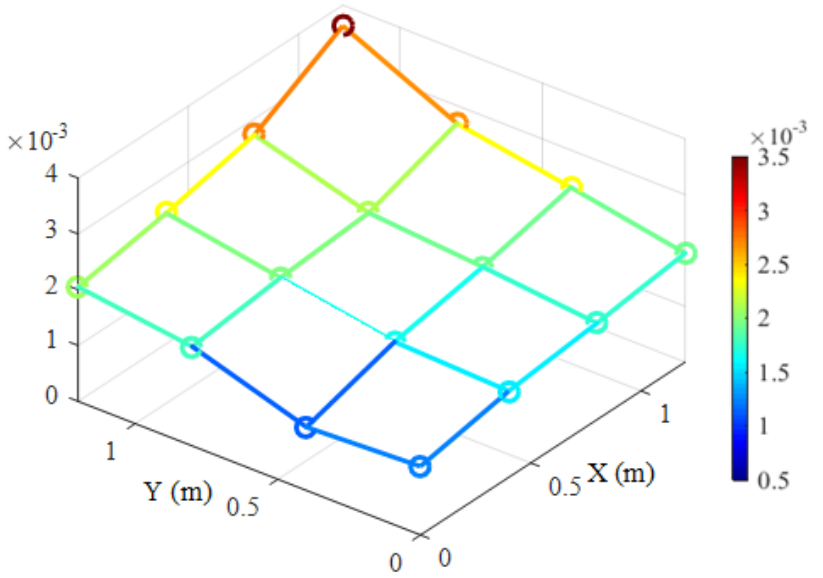

(a) FBMC-SCM-based integrated VLCP system

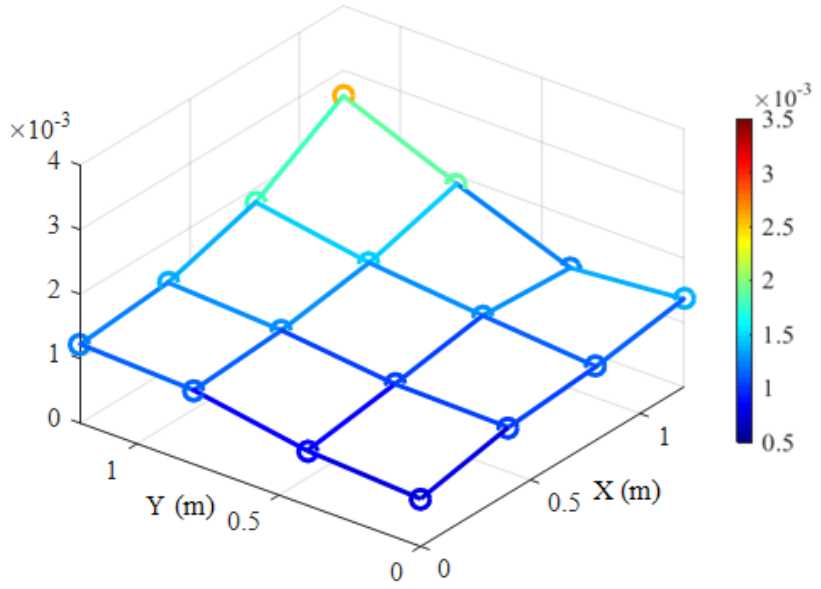

(b) OFDM-SCM-based integrated VLCP system

Figure 3.11: BER distribution of (a) FBMC-SCM and (b) OFDM-SCM.

OFDM-SCM and FBMC- SCM are all less than 3.8×10^{-3}. More specifically, due to the adverse effect of subcarrier filtering in FBMC [16], the BER performance of FBMC-

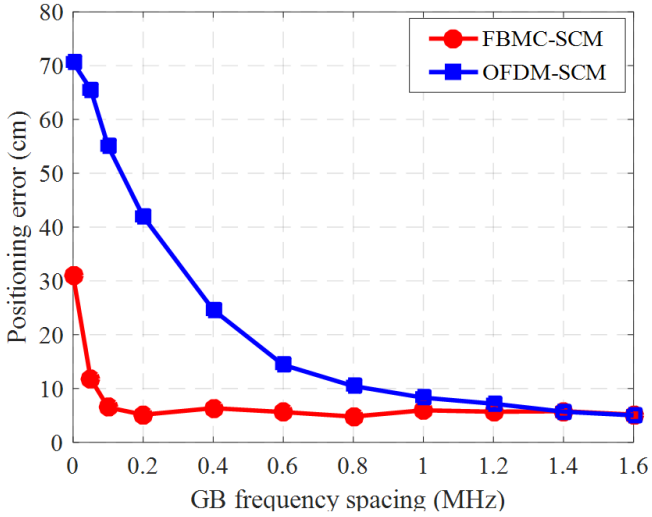

Figure 3.12: Positioning error versus GB frequency spacing.

SCM is slightly worse than that of OFDM-SCM, but still remains at a comparable level.

Fig. 3.12 presents the positioning error versus the GB frequency spacing. For OFDM-SCM, the positioning error is gradually reduced as the GB frequency spacing is increased from 0 to 1.4 MHz. However, a rapid reduction of positioning error is shown for FBMC-SCM when the GB frequency spacing is increased from 0 to 0.1 MHz. We can observe that OFDM-SCM achieves nearly the same positioning accuracy as the FBMC-SCM only when the GB frequency spacing is larger than 1.4 MHz. To achieve the best positioning accuracy, OFDM-SCM requires a minimum GB frequency spacing of 1.4 MHz; however, FBMC- SCM only requires a negligible GB frequency spacing of 0.1 MHz. Defining the effective bandwidth utilization ratio (EBUR) as the ratio of the bandwidth occupied by the communication and positioning signals to the total modulation bandwidth, the EBURs using OFDM-SCM and FBMC-SCM to achieve the same positioning accuracy are 72% and 98%, respectively.

In addition, I need to provide a discussion that the extra computation complexity of the FBMC-SCM based integrated VLCP system, compared with the OFDM-SCM

based integrated VLCP system.

Complexity of OFDM: We assume that the total of N subcarriers are available out of which N_f are occupied with symbols. We will consider first the number of real valued multiplications to transmit one block of N_f symbols. Starting with the fast Fourier transform (FFT), the number of real multiplications of a -point FFT/ inverse FFT (IFFT) using a split-radix algorithm is given by $N(\log_2 N - 3) + 4$.

Since the transmitter (Tx) of a CP-OFDM system is basic built with one single IFFT and by including the windowing operation, we get the computation complexity of OFDM: $O\left(N(\log_2 N - 3) + 4 + 4(N_f + L_{\text{cp}})\right)$ where L_{cp} denotes the length of CP.

Complexity of FBMC: Assuming an FBMC-OQAM system where the prototype filter has length KM, where K overlapping factor of FBMC. The FBMC-SCM based VLCP system needs the extra signal processing at transmitters compared with OFDM based VLCP via RSS. We get the computation complexity of FBMC: $O\left(2N(\log_2 N - 3) + 4NK + 4N_f\right)$

Obviously, we can find that the complexity of FBMC is slightly higher than that of OFDM.

3.5 Conclusion

This chapter proposed and investigated an integrated VLCP system based on the FBMC-SCM technique, which can provide both indoor communication and positioning functions. Compared with the conventional OFDM-SCM technique, FBMC-SCM can greatly reduced OOBI, which avoids the need of large GBs spacing and hence improves SE. Simulation results and Experimental results show that, the positioning accuracy performance is very sensitive to the frequency spacing of the GBs in the OFDM-SCM-based integrated VLCP system. However, the positioning accuracy performance of the FBMC-SCM-based VLCP system is much less dependent on the frequency spacing of the GBs.

The VLP function will have negative impacts to the VLC functionality because the positioning will occupy 1 sub-band of the total bandwidth. The VLC will suffer from short of bandwidth for the communication. Hence, there has tradeoff between their performances in terms of VLC and VLP, such as tradeoff between sum data rate (achieved by VLC) and positioning accuracy (achieved by VLP).

Transmission power allocation is a key issue that affects the tradeoff performances between them. As we know, the more transmission power allocated on the communication subcarriers, the higher received desired power archives, leading to the higher data rate in the system. In addition, the more transmission power allocated on the positioning signals, the higher received desired power archives, leading to the higher positioning accuracy in the system to some degree. However, since the transmission power at LED lamps is limited or fixed, allocating power for one metric with larger value will lead to the less power value allocated to another metric. In this case, the performance of the one metric improves while the performance of another metric decreases. For instance, if the system allocates more power to VLC and VLP will achieve less power, so the sum data rate of VLC improves while the positioning accuracy of VLP decreases.

Hence, I will consider the tradeoff between VLC and VLP in the integrated VLCP systems, and efficient power allocation approaches were proposed to optimize both the sum data rate of VLC and the positioning accuracy of VLP, please see them in Section 4.6.

Chapter 4

QoS-Driven Optimized Design in A New Integrated VLCP System

4.1 Introduction

In order to mitigate the OOBI in integrated VLCP systems, Chapter 3 proposed the FBMC-SCM based integrated VLCP system [181-183] to effectively minimize the negative effect of OOBI on the positioning frequency and improve the positioning accuracy, compared with OFDM-SCM based integrated VLCP system [174, 175]. However, the FBMC-SCM based VLCP system needs the extra signal processing at transmitters compared with OFDMA based VLCP via RSS.

In addition, considering the fact that the signals modulated on the high-frequency subcarriers are seriously attenuated in VLC systems, adaptive transmission or frequency domain equalization techniques have been proposed to optimize the transmission parameters to enhance the system capacity [49, 82, 184-186, 187-189]. In [184-186], adaptive modulation designs combined with OFDM based on the signal-to-noise-ratio (SNR) difference were studied in VLC systems to improve the system data rate, where lower frequency subcarriers use high-order modulation levels with good SNR while the higher-frequency subcarriers employ lower order modulation levels with poor SNR. To

compensate the frequency attenuation, some pre-equalization schemes were proposed to establish high-speed VLC systems [49, 82, 187-189]. Li *et al*. experimentally demonstrated a hybrid time-frequency domain equalization design to overcome the nonlinearity and frequency attenuation of LEDs [82]. In [187] and [188], bit and power loading approaches were presented to combat the channel frequency selectivity. The authors in [49] and [189] experimentally investigated weighted pre-equalization designs to optimize the system performance by compensating the frequency attenuation of LEDs. Moreover, Yang, *et al*. investigated the resource allocation for multi-user integrated VLCP systems under the minimum data rate and positioning accuracy requirements [190].

It is worth noticing that both the high-speed data rate and high positioning accuracy strongly depend on the LoS in VLC and VLP systems, while the LoS link is often partially or completely blocked due to the mobility of devices and human beings in practical indoor environments [191]. In this case, the system performance is notably affected and the QoS level is decreased. To the best of our knowledge, almost all of the above mentioned works did not investigate how to satisfy the minimum data rate requirements of devices and maintain the high positioning accuracy performance under blockages in dynamic indoor environments.

Moreover, an indoor VLC system consists of multiple VLC APs, so the AP selection has not been investigated in integrated VLCP systems or networks. Although the literatures [59, 66, 73, 141, 193, 194] investigated efficient AP selection schemes in multi-cell VLC networks to maximize the network transmission data rate and satisfy QoS requirements of devices with considering the ICI mitigation, the assumption of perfect location information of devices may be not practical.

Motivated by the above observations, this chapter proposes and experimentally demonstrates a new integrated VLCP system model to improve both the communication and positioning performance [195]. After that, a QoS-driven optimized design with

the adaptive modulation, subcarrier allocation and adaptive weighted pre-equalization is proposed to maximize the system transmission data rate while guaranteeing the different QoS requirements (the minimum data rate and positioning accuracy requirements of devices). The LoS blockage issue is investigated in the system, and the robust optimized schemes are presented to maintain the system performance. The experimental results corroborate the superiority in performance of the presented integrated VLCP system model, and verify that the proposed design outperforms other existing adaptive transmission designs in terms of effectively enhancing the data rate, improving the positioning accuracy and guaranteeing devices QoS requirements.

Moreover, this chapter also extends the system model into multi-cell integrated VLCP networks [196], where a joint AP selection, bandwidth allocation and power allocation approach is proposed to maximize the network data rate while guaranteeing the different QoS requirements of indoor devices. The LoS blockage issue is investigated in networks, and the robust optimized schemes are presented to maintain the network performance. The simulation results corroborate the superiority in performance of the presented integrated VLCP network and the proposed solutions.

The rest of this chapter is organized as follows.The new integrated VLCP system model in a single cell is presented in Section 4.2. Section 4.3 provides the principle of the proposed QoS-driven optimized design under devices' QoS requirements. The effect of LoS blockages and robust schemes are provided in Section 4.4.The experimental results and analysis are shown in Section 4.5. Furthermore, the extension of the system model for multi-cell systems and the problem formulation are presented in Section 4.6. Section 4.7 provides the solution to the optimization problem. Simulations are shown in Section 4.8. Finally, Section 4.9 concludes the chapter. The content of this chapter is related to the author's work provided in [195, 196].

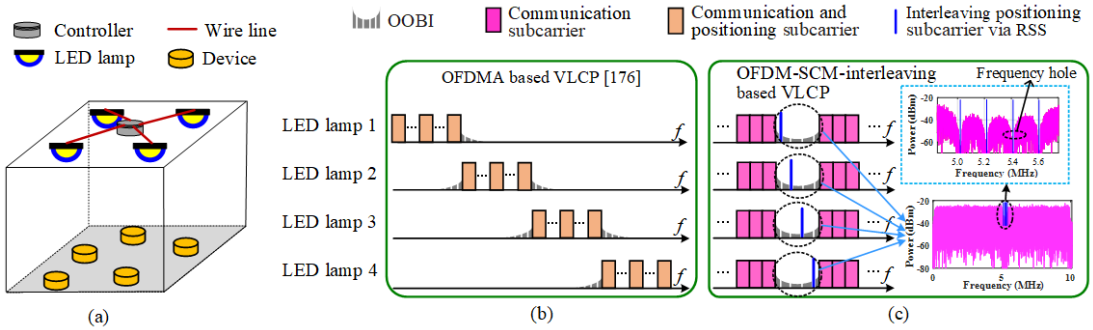

Figure 4.1: Block diagram of the proposed integrated VLCP system.

4.2 Principle of A New Integrated VLCP System

4.2.1 New Integrated VLCP System Model

In indoor environments, a number of LED lamps (L LED lamps) are attached on the ceiling to support the illumination requirements, as shown in Fig. 4.1(a). In addition to offer the lighting requirements, an integrated VLCP system is set up to provide both the communication and positioning services for indoor devices. In the system, the communication and positioning signals are modulated into the LED lamps before passing through the wireless optical channel, and the device is equipped with a PD to convert the received light into electrical signals.

In the system, a number of devices (K devices) are randomly located in the lighting coverage area. There exists a central controller in the system, which connects all LED lamps to broadcast information to multiple devices, and the uplink feedback is offered by Wi-Fi links. After receiving the feedback information, the central controller can tackle the transmission scheduling task. The total bandwidth is equally divided into N subcarriers and a number of subcarriers are used for positioning and the remaining subcarriers are served for communication. The communication subcarriers are divided into K groups (subcarrier group, called SG) and the $(K+1)$-th SG being the subcarriers used for RSS positioning. In addition, a transmission diversity method is applied, where

all LED lamps transmit the same communication signal if the communication subcarrier is allocated to a device.

In this section, we describe the existing and proposed integrated VLCP system models, the communication model and the RSS-based positioning model.

1) OFDMA based VLCP via RSS [176]: The design directly combines the OFDM modulation and 2D RSS positioning algorithm for the integrated VLCP system, as shown in Fig. 4.1(b), where the total available subcarriers are equally divided into four subbands and allocated to four LED lamps. Then, each subband with respect to its corresponding LED lamp is used for indoor positioning. The detailed procedures to implement OFDMA based VLCP via RSS can be seen in [176]. However, as shown in Fig. 4.1(b), OFDM signals usually leak relatively high OOBI to adjacent subbands or subcarriers, which degrades the communication and positioning performance of the integrated VLCP system. In addition, we can observe that the bandwidth utilization ratio of this system is not effective, because each LED lamp only uses a part of the bandwidth.

2) Proposed OFDM-SCM-interleaving based VLCP via RSS: As shown in Fig. 4.1(c), we can observe that there exist several specific frequencies (called frequency holes) having the negligible OOBI from OFDM signal when the number of subcarriers are not used to transmit the OFDM signal (idle subcarriers). In this case, the RSS sinusoidal positioning signals (blue color) can be put into the frequency holes, which is capable of avoiding the OOBI on the positioning frequencies from the adjacent communication subcarriers and achieves higher positioning accuracy performance compared with OFDMA based VLCP. In addition, it has the higher effective bandwidth utilization than OFDMA based VLCP.

4.2.2 Communication Model

At the receiver, the received SNR for the k-th device on the n-th communication subcarrier is given by

$$\gamma_{k,n}^{\text{co}} = \mu^2 \sum\nolimits_{n=l}^{L} P_{n,l}(G_{k,n,l})^2 \Big/ \delta^2 \tag{4.1}$$

where μ is the PD's responsivity. $P_{n,l}$ is the allocated electrical power on the n-th subcarrier at the l-th LED lamp. $G_{k,n,l}$ represents the optical channel gain from the l-th LED lamp to device k on the n-th subcarrier. δ^2 is the additive white Gaussian noise (AWGN) power including the shot noise and the thermal noise.

At the k-th device (receiver), if it assigns the n-th subcarrier and the OFDM signal is modulated by M_n-QAM with the modulation order M_n, the BER can be approximated by [197],

$$BER_{k,n} = \frac{\sqrt{M_n}-1}{\sqrt{M_n}\log_2(\sqrt{M_n})} erfc\left(\sqrt{\frac{3\gamma_{k,n}^{\text{co}}}{2(M_n-1)}}\right) \tag{4.2}$$

The sum transmission data rate of all devices across all the subcarriers can be expressed as [197]

$$R_{\text{sum}} = B_{sub} \sum\nolimits_{n=1}^{N/2-1} \log_2 M_n \tag{4.3}$$

where B_{sub} is the subcarrier bandwidth $B_{sub} = B/N$ with B being the system transmission bandwidth. In (4.3), for both OFDM and FBMC modulation schemes, the IFFT/FFT size is N, and the number of available data subcarriers is $N/2$-1 due to the Hermitian symmetry [184, 197].

4.2.3 RSS-based Positioning Model

For the k-th device, the received electrical power on the i-th positioning subcarrier from the l-th LED lamp can be expressed as $P_{k,i,l}^{\text{rec}} = G_{k,l}P_{i,l}$ [35, 176]. In addition, the PD axis and the LED lamp axis are perpendicular to the ceiling, we have $\cos(\phi_{k,l}) =$

$cos\psi_{k,l} = h/d_{k,l}$ with h being the height from LED lamps to the receiver plane [35, 176]. Consequently, $G_{k,l}$ in (2.4) can be rewritten as

$$G_{k,l} = \frac{h^{m_l+1}(m_l+1)A_r}{2\pi d_{k,l}^{m_l+3}} T_s(\psi_{k,l}) g(\psi_{k,l}) = C(m_l+1)\frac{h^{m_l+1}}{d_{k,l}^{m_l+3}} \tag{4.4}$$

where A_r denotes the PD' active area. $d_{k,l}$, ϕ and $\psi_{k,l}$ are the distance, the angle of irradiance and the angle of incidence between the l-th LED lamp LED and the k-th device, respectively. m_l denotes the order of Lambertian emission of the l-th LED lamp, which can be measured in the experimental preparation [198]. $T_s(\psi_{k,l})$ and $g(\psi_{k,l})$ are the gain of the optical filter and the optical concentrator gain at the PD, respectively. $C = A_r T_s(\psi_{k,l}) g(\psi_{k,l})/2\pi$ is a constant value which depends on the characteristic of LEDs and PDs.

Then, the received electrical power $P_{k,i,l}^{\text{rec}}$ is rewritten as

$$P_{k,i,l}^{\text{rec}} = P_{i,l} C(m_l+1) h^{m_l+1}/d_{k,l}^{m_l+3} \tag{4.5}$$

From (4.5), we can derive the distance $d_{k,l}$ as follows

$$d_{k,l} = \sqrt[m_l+3]{P_{i,l} C(m_l+1) h^{m_l+1}/P_{k,i,l}^{\text{rec}}} \tag{4.6}$$

In fact, in practical indoor systems, it is quite hard to find the accurate relationship between estimated distance and the received positioning power like (4.6). However, the estimated distance can be polyfit by a function, such as the formulated polyfit function shown in Eq. (10) in [175]. Hence, the final estimated distance $d_{k,l}$ can be expressed as a function with respect to the received positioning power $P_{k,i,l}^{\text{rec}}$, which is

$$d_{k,l} = Q_l(P_{k,i,l}^{\text{rec}}) \tag{4.7}$$

We would like to mention that each LED lamp has its corresponding function $Q_l(\cdot)$, because the order of Lambertian emission (m_l) of each LED lamp and the attenuation of its corresponding positioning frequency is different from each other [175, 198]. As

mentioned, it is difficult to find the accurate relationship between the estimated distance and the measured received positioning power (i.e, Eq. (4.7)). Hence, we take measurements at a number of points during the offline preparation in the integrated VLCP system to obtain (4.7) before estimating the positions of devices, more details can be found in [175].

When the received power $P_{k,i,l}^{\text{rec}}$ is measured at the k-th device, the distance $d_{k,l}$ can be calculated by (4.7). Finally, the estimated location of the device can be calculated by using the RSS-based trilateration algorithm [175, 198], the detailed procedures to experimentally implement RSS-based positioning can be seen in [175, 198].

4.3 Adaptive Transmission for Integrated VLCP Systems

4.3.1 QoS Requirements in Integrated VLCP Systems

In integrated VLCP systems, some certain QoS requirements of devices should be considered in the optimized design, which are discussed and analyzed as follows.

1) Minimum data rate requirements of VLC: The minimum data rate requirements of devices should be considered in the performance optimization design. Thus, the resulting constraint is expressed by

$$R_k = B_{sub} \sum\nolimits_{n=1}^{N/2-1} (\rho_{k,n} \log_2 M_n) \geq R_k^{\min} \tag{4.8}$$

where R_k and $R_k^{\min}$ are the current achievable data rate and the minimum data rate threshold of the k-th device, respectively; $\rho_{k,n}$ is a binary variable, $\rho_{k,n} \in \{0, 1\}$, and $\rho_{k,n} = 1$ indicates the n-th communication subcarrier is allocated to the k-device; otherwise, it takes the value 0.

2) Positioning accuracy requirements of VLP: In addition to the requirement in (4.8) of VLC, integrated VLCP systems should guarantee the positioning accuracy requirement of the devices who need positioning services.

Let $\mathbf{\Theta}_k = (x_k, y_k)$ and $\mathbf{\Theta}_k^{\mathrm{e}} = (x_{k,\mathrm{e}}, y_{k,\mathrm{e}})$ denote the true location and the estimated location of the k-th device, respectively. The positioning error (root square error (RSE)) of the k-th device is given by

$$RSE_k = \sqrt{(x_{k,\mathrm{e}} - x_k)^2 + (y_{k,\mathrm{e}} - y_k)^2} \tag{4.9}$$

The positioning accuracy constraint of the k-th device who needs the positioning service can be expressed as

$$RSE_k \leq RSE_k^{\max} \tag{4.10}$$

where $RSE_k^{\max}$ is the tolerant positioning error threshold of the k-th device. Without loss of generality, when other parameters (such as the positioning frequencies, PD responsibility and so on) are fixed, the positioning error is determined by the transmit power level (or received SNR values) [199, 200]. Hence, the transmit power allocated on positioning subcarriers need to be carefully considered in the integrated VLCP system, where we adopt the water-filling algorithm to gradually allocate transmit power on the positioning subcarriers to improve the positioning accuracy in the experiment [187, 188], which will be shown at the end of the Section 4.3.2.

4.3.2 Adaptive Transmission Design

The block diagram of the proposed QoS-driven optimized design for integrated VLCP systems is depicted in Fig. 4.2 (we take the system model shown in Fig. 4.1(c) as an example), where the joint adaptive modulation, subcarrier allocation and adaptive weighted pre-equalization is presented to guarantee the QoS requirements shown in (4.8) and (4.10). The details to implement it are shown in the following analysis.

At the transmitters, the sinusoidal signals for VLP are added with the OFDM signal at each LED lamp after allocating the SGs to devices, where the four positioning frequencies from f_1 to f_4 are all in the $(K+1)$-th SG and the communication data for

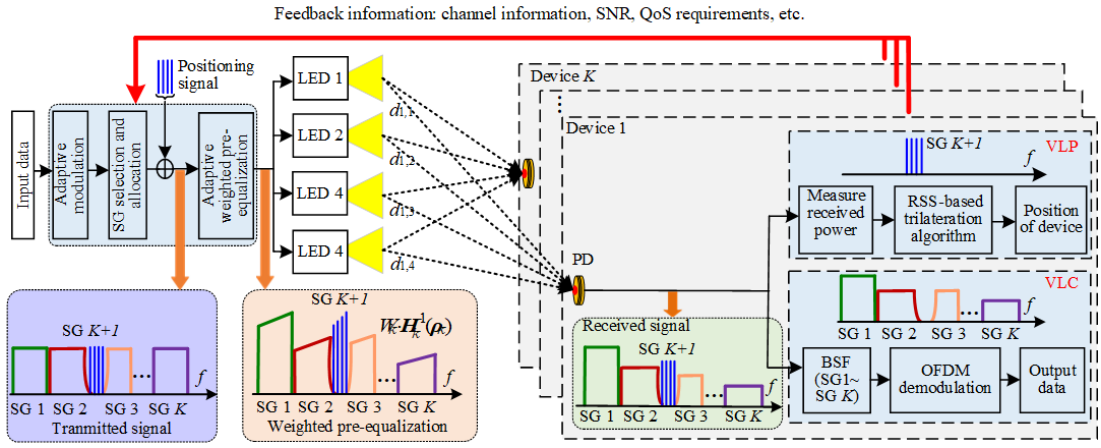

Figure 4.2: Block diagram of the proposed adaptive transmission design.

the devices are all in the K SGs. After collecting the feedback information (channel information, SNR, QoS requirements, etc.) from the devices by the Wi-Fi uplink, the communication data stream is then encoded to the OFDM signal with the adaptive M-QAM mapping based on the users' different minimum data requirements and the users' received SNR values. When the BER target is BER_{max}, the modulation thresholds can be expressed as [184, 197]

$$\begin{aligned} &\gamma_j^{\text{th}} = (\gamma_{k,n}^{\text{co}})_{M_n} \\ &= \frac{3(M_n-1)}{2} erfc^{-1}\left(BER_{\max}\frac{\sqrt{M_n}\log_2(\sqrt{M_n})}{\sqrt{M_n}-1}\right) \\ &M_n = 2^j,\ j = 1, ..., J \end{aligned} \tag{4.11}$$

where $erfc^{-1}(\cdot)$ is the inverse $erfc$-function, and $\gamma_1^{\text{th}} \leq \gamma_2^{\text{th}} \leq .... \leq \gamma_J^{\text{th}}$. Then, the system can select the modulation order according to the SNR value $\gamma_{k,n}^{\text{co}}$, which is

$$M_n = \begin{cases} 0, & \gamma_{k,n}^{\text{co}} < \gamma_1^{\text{th}} \\ 2^j, & \gamma_j^{\text{th}} \leq \gamma_{k,n}^{\text{co}} \leq \gamma_{j+1}^{\text{th}},\ j = 1, ..., J-1 \\ 2^J, & \gamma_J^{\text{th}} \leq \gamma_{k,n}^{\text{co}}. \end{cases} \tag{4.12}$$

The above analysis from (4.11) and (4.12) shows the selection of the modulation order according to the feedback SNR values from devices. The adaptive modulation scheme can effectively improve the transmission data rate and guarantee the devices' minimum data rate requirements.

Due to the severe attenuation of LED lamps in high frequency domains in integrated VLCP systems, the pre-equalization design is applied to compensate the frequency attenuation at transmitters. Considering the conventional pre-equalization scheme is not optimal due to the attenuation of high frequency domains is balanced at the cost of the SNR reduction of low frequency domains, the authors in [49] presented a weighted pre-equalization design to improve the communication performance of all subbands. However, weighted pre-equalization in [49] was still not the optimal approach in terms of the system throughput improvement due to the fixed-order modulation format and fixed bandwidth of each sub-band. Moreover, the weighted pre-equalization factor for the positioning SG should be carefully set to satisfy the positioning accuracy requirements, because the weighted pre-equalization factors of the two adjacent communication SGs near the positioning SG should not be too large to generate the high OOBI on the positioning SG, which directly degrades the positioning performance. Hence, the adaptive modulation, subcarrier allocation and weighted pre-equalization can be adaptively updated to optimize the system capacity while considering the QoS requirements of devices.

Let M_k denotes the modulation order in the k-th SG. Let $\boldsymbol{\rho}_k$ denotes the subcarrier allocation indicator vector for k-th device in the k-th SG and we set that these subcarriers are continuous. Then, the k-th SG signal in the frequency domain after the joint adaptive modulation, subcarrier allocation and weighted pre-equalization can be given by

$$\mathbf{S}'_k(M_k, \boldsymbol{\rho}_k) = W_k \cdot \mathbf{H}_k^{-1}(\boldsymbol{\rho}_k) \cdot \mathbf{S}_k(M_k, \boldsymbol{\rho}_k) \tag{4.13}$$

where $\mathbf{S}'_k(M_k, \boldsymbol{\rho}_k)$ and $\mathbf{S}_k(M_k, \boldsymbol{\rho}_k)$ are the k-th SG signal vector in the frequency domain before and after pre-equalization, respectively. W_k and $\mathbf{H}_k$ are the weighted pre-equalization coefficient and the transfer function matrix of the k-th SG, respectively, where $\mathbf{H}_k$ is also a diagonal matrix. $\mathbf{H}_k$ can be firstly measured in the integrated VLCP

system. After that, the pre-equalized signals are converted to the time domain before being modulated on the LED lamps.

At the receiver, on the one hand, the received power values on the four positioning frequencies from different LED lamps can be measured in OFDM-SCM-interleaving based VLCP. After measuring the four received positioning power values, the position of the device can be estimated by using the RSS positioning algorithm, which has been analyzed in Section 4.2.3. On the other hand, the communication signal can be obtained when the received signal passes through the band stop filter (BSF), and the OFDM demodulation method is applied to demodulate the communication signal.

In practical indoor environments, different devices have different QoS requirements, ranging from the positioning accuracy constraints to the transmission data rate requirements. The system aims to maximize the transmission data rate while satisfying the QoS requirements shown in (4.8) and (4.10), the detailed procedures to implement it are shown as follows:

Step 1: The central controller collects the feedback information from devices by the WiFi uplink, which mainly refers to channel information, SNR values, QoS requirements, etc.;

Step 2: The central controller iteratively optimizes the subcarrier allocation indicators $\{\boldsymbol{\rho}_k\}$, the weighted pre-equalization coefficients $\{W_k\}$ and the modulation orders $\{M_k\}$ to the satisfy the minimum data rate requirements in (4.8) and the positioning accuracy constraints in (4.10) first, by using the iteration algorithm [187, 188];

Step 3: After satisfying the QoS requirements of devices, the extra power and subcarriers are allocated to the devices with highest channel quality to maximize the system data rate by updating $\{\boldsymbol{\rho}_k\}$, $\{W_k\}$ and $\{M_k\}$.

The pseudocode of the designed scheme In Section 4.3.2 is shown in **Algorithm 1**.

Here, I provide a brief evaluation of the complexity of the presented design scheme. Let I denotes the number of iterations required for convergence in **Algorithm 1**.

Let J denote the total number of modulation level candidates. It is obvious to see that the subcarrier group (SG) allocation step takes $K \times K$ comparison operations (K communication SGs and K devices). Moreover, we know from [72] and [193] that the power allocation step can be solved in $(K+1)\log_2(K+1)$ operations by using the iterative algorithm over $K+1$ SGs. In addition, for adaptive modulation, the complexity of modulation order selection for K devices is $K \times J$. Since the total number of iterations is I, the complexity of the proposed adaptive transmission scheme is $O\left(I(K \times K + (K+1)\log_2(K+1) + K \times J)\right)$, which is not very high so that it can be implemented in real-time systems.

Algorithm 1 Adaptive transmission design for integrated VLCP systems

1: **Initialize:** Set the iteration $i = 0$, set $R_{\text{sum}}(0)$, subcarrier allocation indicator $\boldsymbol{\rho}_k(0)$, weighted pre-equalization coefficients $W_k(0)$ and the modulation order $M_k(0)$ of each device. Set the maximum tolerance $\varsigma \geq 0$.
2: **Repeat**
3: Update the weighted pre-equalization coefficients $W_{K+1}(0)$ on the *(K+1)*-th positioning SG to guarantee positioning accuracy constraints in (4.10) first;
4: Update subcarrier allocation indicator $\boldsymbol{\rho}_k(i+1)$, weighted pre-equalization coefficients $W_k(i+1)$ and modulation order $M_k(i+1)$ to the satisfy the minimum data rate requirement in (4.8);
5: After satisfying the QoS requirements of devices, the extra power and subcarriers are allocated to the devices with highest channel quality to maximize $R_{\text{sum}}(i+1)$ by updating $\boldsymbol{\rho}_k(i+1)$, $W_k(i+1)$, and $M_k(i+1)$;
6: $i = i+1$;
7: Update the sum data rate $R_{\text{sum}}(i)$;
8: Until $|R_{\text{sum}}(i)-R_{\text{sum}}(i-1)| \leq \varsigma$;
9: **End**
10: **Output:** $\boldsymbol{\rho}_k(i)$, $W_k(i)$ and $M_k(i)$.

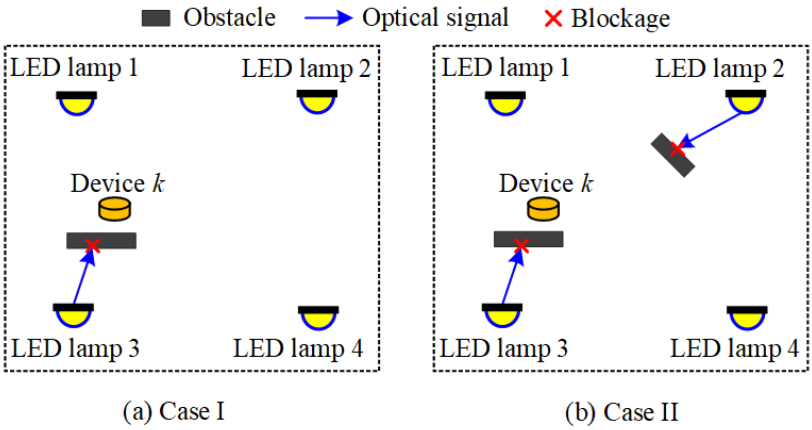

Figure 4.3: Two cases of LoS blockages in integrated VLCP IoT networks.

4.4 Robust Schemes under Blockages

4.4.1 LoS Blockages in Integrated VLCP Systems

In practical indoor environments, the optical signals being broadcast from VLC lamps to the devices may be blocked by obstacles due to the movement of devices or human beings, as shown in Fig. 4.3 (we take Case I and Case II as examples to analyze the negative effect of blocked links on the system performance). In this case, LoS is often blocked and Non-LoS (NLoS) cannot support effective communication and positioning services, leading to the degradation of the system performance.

In Case I, for the k-th device, the optical signal from its currently associated LED lamp 3 is blocked by an obstacle, hence the received SNR value is reduced, resulting in decreasing the satisfied QoS levels and the system data rate. In this case, although the signal from LED lamp 3 is blocked, the 2D location of device k can be still successfully estimated by using the RSSI values from LED lamp 1, LED lamp 2 and LED lamp 4. However, in Case II, the optical signals being broadcast from a number of LED lamps (such as, the LED lamp 2 and LED lamp 3, even more LED lamps) to the k-th device are missing. In this case, it is hard to estimate the locations of devices with the high positioning accuracy only using less than two RSSI values. Moreover, the data rate

performance is degraded in this case, too.

According to the above analysis, how to estimate the locations of the devices with the high positioning accuracy and how guarantee the minimum data rate requirements of devices are still key challenges under blockages in dynamic integrated VLCP systems.

Hence, the following subsections introduce two proposed schemes to address the above mentioned challenges, in order to improve both the communication and positioning performance under LoS blockages.

4.4.2 Robust Communication Scheme Under Blockages

For each device, when its received optical signal from one LED lamp is blocked, the power allocated to the device at the corresponding LED lamp may be waste due to the unsuccessful communication service under the blockage. In this case, the LED lamp can allocate this part of power to other devices to enhance the system performance.

Under LoS blockages, the k-th SG signal in the frequency domain after the joint adaptive modulation, subcarrier allocation, and weighted pre-equalization can be given by

$$\mathbf{S'}_k(M_k, \boldsymbol{\rho}_k) = \sum\nolimits_{l=1}^{L} W_{k,l} \cdot \mathbf{H_k^{-1}}(\boldsymbol{\rho}_\mathbf{k}) \cdot \mathbf{S'_k}(M_\mathbf{k}, \boldsymbol{\rho}_\mathbf{k}) \tag{4.14}$$

where $W_{k,l}$ denotes the weighted pre-equalization coefficient of the l-th VLC lamp allocated on the SG of the k-th device. As mentioned before, when the optical link from one VLC lamp is blocked, the allocated electrical power to the device is set to be zero (set $W_{k,l} = 0$) and allocate this part of electrical power to other devices to enhance their QoS satisfaction levels or improve the transmission data rate. Generally, the device detects the optical link blockages from corresponding LED lamps based on the received SNR values, and then send the feedback information to the controller.

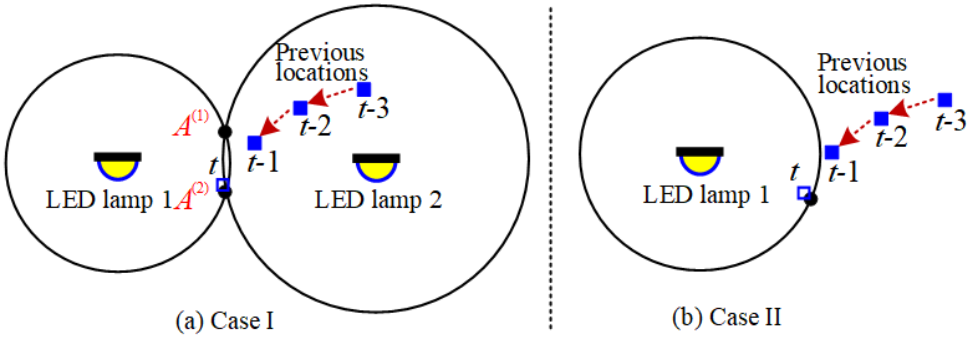

Figure 4.4: Signals transmitted from some LED lamps are blocked by obstacles.

4.4.3 Robust Positioning Scheme Under Blockages

As shown in Fig. 4.4(a), the k-th device only receives the optical signals from the LED lamp 1 and LED lamp 2 while the available signals being broadcasted from other LED lamps are blocked by the obstacles. According to the RSSI signals received from the LED lamp 1 and LED lamp 2, two circles centered at these two LED lamps are identified with black lines. The intersection of the two circles generates two possible locations (the black dots shown in Fig. 4.4(a)) of the k-th device at the time slot t, denoted by $A^{(1)}(x_{k,t}^{(1)}, y_{k,t}^{(1)})$ and $A^{(2)}(x_{k,t}^{(2)}, y_{k,t}^{(2)})$, respectively. These two possible locations $A^{(1)}$ and $A^{(2)}$ can be calculated by solving the following two equations

$$\begin{aligned} \sqrt{\left(x_1^{\text{led}} - x_{k,t}^{(1)}\right)^2 + \left(y_1^{\text{led}} - y_{k,t}^{(1)}\right)^2} &= d_{1,k,t} \\ \sqrt{\left(x_2^{\text{led}} - x_{k,t}\right)^2 + \left(y_2^{\text{led}} - y_{k,t}\right)^2} &= d_{2,k,t} \end{aligned} \tag{4.15}$$

where $d_{l,k,t}$ denotes the distance from the l-th LED lamp to device k at the time slot t which can be calculated by (4.7).

We would like to mention that the literature [75] presented a simple scheme to select the most likely current location from these two possible locations, where the scheme calculates the distances from the previous location to the two possible locations and selects the possible location as the current location with the smallest distance. However, the scheme in [75] does not consider the movement behaviors of devices, hence it still has the high positioning errors during devices' traveling under blockages.

In order to improve the positioning accuracy under blockages, we present a new robust positioning scheme by combing the PDR method [202] with the RSS-based VLP system (called PDR-assisted RSS), where PDR is the process of predicting the device' current location by using the previously locations' information.

In PDR, each device has its corresponding movement prediction model by sampling its periodical location information. When one device only receives at most two RSSI signals from the LED lamps and other optical RSSI signals are missing at one time slot, it adopts PDR to calculate its velocity components $v_{k,x}$ and $v_{k,y}$ along the X-axe and Y-axe from the previous location information $(x_{k,t-1}, y_{k,t-1})$ and $(x_{k,t-2}, y_{k,t-2})$ taken at the time slots t-1 and t-2. Here, the velocity components in the last time slot can be calculated by

$$v^x_{k,t-1} = (x_{k,t-1} - x_{k,t-2})/\tau_{t-1}; \;\; v^y_{k,t-1} = (y_{k,t-1} - y_{k,t-2})/\tau_{t-1} \tag{4.16}$$

respectively, and τ_{t-1} is the time duration at the time slot t-1.

After calculating the velocity components by (4.16) according to the two latest previous location samples, the k-th device predicts its location at the current time slot t

$$x'_{k,t} = x_{k,t-1} + v^x_{k,t-1}\tau_t; \;\; y'_{k,t} = y_{k,t-1} + v^y_{k,t-1}\tau_t \tag{4.17}$$

According to the above analysis, the k-th device predicts its current location P' (the blue hollow square in Fig. 4.4 (a)) by adopting the PDR method, and calculates the possible locations ($A^{(1)}$ and $A^{(2)}$) by using RSS positioning algorithm. In this case, the predicted location P' is close to one of the possible locations ($A^{(1)}$ and $A^{(2)}$) due to the movement behavior of devices, especially in indoor positioning environments. This allows the selection of the most likely current location of the device through comparing the distances between the predicted location and the two possible locations, i.e.,

$$d^{P' \to A^{(1)}}_{k,t} = \sqrt{(x'_{k,t} - x^{(1)}_{k,t})^2 + (y'_{k,t} - y^{(1)}_{k,t})^2} \tag{4.18}$$

$$d_{k,t}^{P' \to A^{(2)}} = \sqrt{\left(x'_{k,t} - x_{k,t}^{(2)}\right)^2 + \left(y'_{k,t} - y_{k,t}^{(2)}\right)^2} \tag{4.19}$$

The most likely current position $(x_{k,t}, y_{k,t})$ at the current time slot t is selected from the two possible locations by

$$(x_{k,t}, y_{k,t}) = \begin{cases} (x_{k,t}^{(1)}, y_{k,t}^{(1)}), \ d_{k,t}^{P' \to A^{(1)}} \leq d_{k,t}^{P' \to A^{(2)}} \\ (x_{k,t}^{(2)}, y_{k,t}^{(2)}), \ d_{k,t}^{P' \to A^{(1)}} > d_{k,t}^{P' \to A^{(2)}} \end{cases} \tag{4.20}$$

As shown in Fig. 4.4 (b), if the device only receives the RSSI signal from one LED lamp while other RSSI signals broadcast from LED lamps are missing, the device perform positioning by the following analysis. According to the RSSI signal from the LED lamp 1, one circle centered at the LED lamp 1 is identified and the possible location of the device is on the circle. By adopting the PDR method, the device predicts its current location P' (the blue hollow square in Fig. 4.4 (b)), and the most likely current position of the device (the black dot) is selected on the circle with the minimum distance from it to the predicted location P'. It is worth noticing that all RSSI signals being broadcast from all LED lamps to the device may be blocked in dynamic indoor environments, but it happens with a very small probability. In this case, the device can directly adopt the PDR positioning method to predict its current location according to the previous location samples.

4.5 Experimental Demonstration

4.5.1 Experimental Setup

As shown in Fig. 4.5, the experimental setup is provided to evaluate the system performance. We use Matlab to generated the integrated communication and positioning signal with an IFFT size of 512, then load the signal in an arbitrary waveform generator (AWG, Spectrum M4x. 6622-x4) with a sampling rate of 100 MSa/s, before adding it to the DC bias of the four LED lamps (LXK8-PW27-0016) after passing through the amplifiers and adding DC biases. After optical free-space propagation, the light

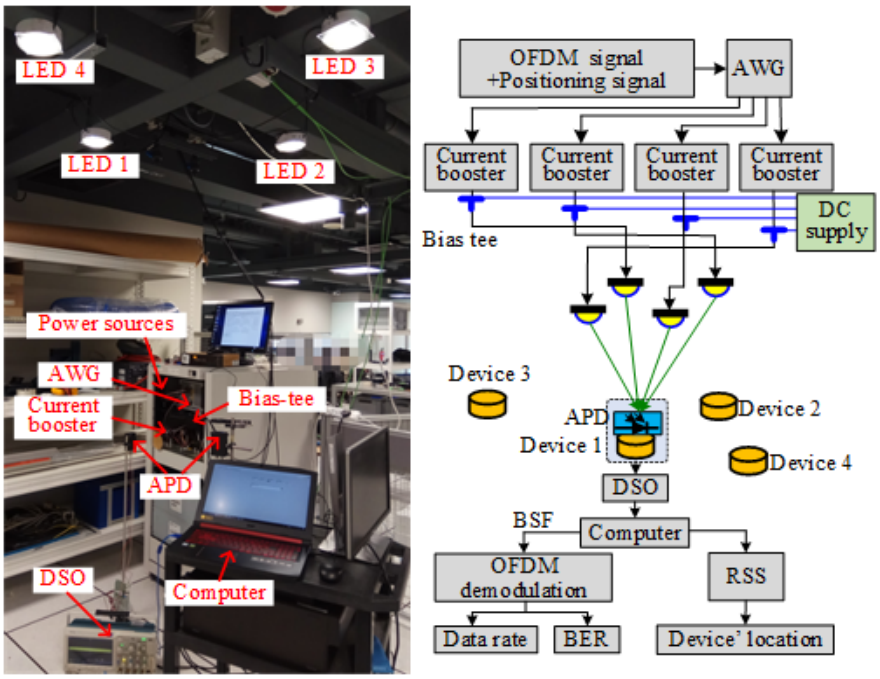

Figure 4.5: Experimental setup of the integrated VLCP system.

is detected by an avalanche PD (APD) before using a digital storage oscilloscope to record the detected signal with a sampling rate of 500 MSa/s. After that, the communication signal demodulation and the device location estimation are completed by using Matlab. The specifications of the amplifier is 811AR-16F amp (BUF634) buffer power gain 24 dB, the bias tee is made by our group with 2KHz to 500MHz, the driving current of each LED varies between 60 mA and 140 mA for different simulation settings, which is shown in Fig. 4.9. The illumination level at the receiving plane under the cell unit was 380 lux which has reached the standard of indoor illumination. The experiment is in a coverage area of 2×2×1.35 m^3. The locations of four LED lamps are (-0.4, 0.4, 1.35), (0.4, 0.4, 1.35), (-0.4, 0.4, 1.35) and (-0.4, -0.4, 1.35) with the origin (0, 0, 0) in meters. The transmission modulation bandwidth is 20 MHz and the available bandwidth is 10 MHz due to the Hermitian symmetry [184], [197]. The range of the four positioning frequencies is from 5.07 to 5.67 MHz. The modulation order $M = \{2, 4, 8, 16, 32, 64, 128, 256\}$ and $BER_{\max} = 3.8 \times 10^{-3}$. Four devices randomly

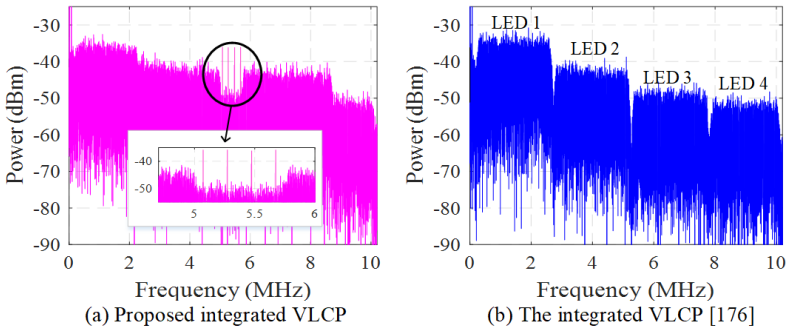

Figure 4.6: Received spectra of (a) OFDM-SCM-interleaving based integrated VLCP and (b) OFDMA based integrated VLCP [176].

locate on the receiving plane, two of them need both communication and positioning services and each requires the low data rate (1 Mbit/s), while other two devices only need communication services and each has the high data rate requirement (12.5 Mbit/s). In addition, the maximum positioning error threshold is 10 cm.

4.5.2 Performance Evaluations Under LoS Condition

Fig. 4.6 (a) and (b) indicate the received electrical spectrum of the integrated signals in the proposed OFDM-SCM-interleaving integrated VLCP system and the OFDMA based integrated VLCP system [176] when the device locates at (0m, 0m, 0m), respectively. In Fig. 4.6 (b), the power in the high-frequency subcarriers (modulated on LED 3 and LED 4) is seriously attenuated, leading to the low received SNR, which degrades the positioning accuracy in the existing design [176]. By contract, our proposed design has high SNR values for all positioning subcarriers to guarantee the positioning performance. In addition, OFDMA based VLCP in [176] has high OOBI to adjacent subbands and it needs larger GBs' spacing, while our design has negligible OOBI on the positioning frequency holes.

Fig. 4.7 shows the positioning results of the two integrated VLCP systems. We find that positioning error is low at the center areas, but is high at the edges, because of the decreased received power. The mean position errors of our proposed design and

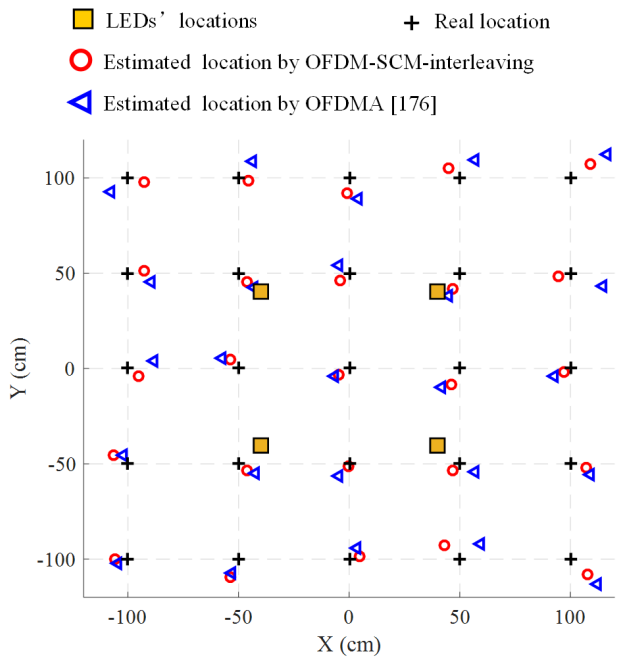

Figure 4.7: Comparisons of positioning results

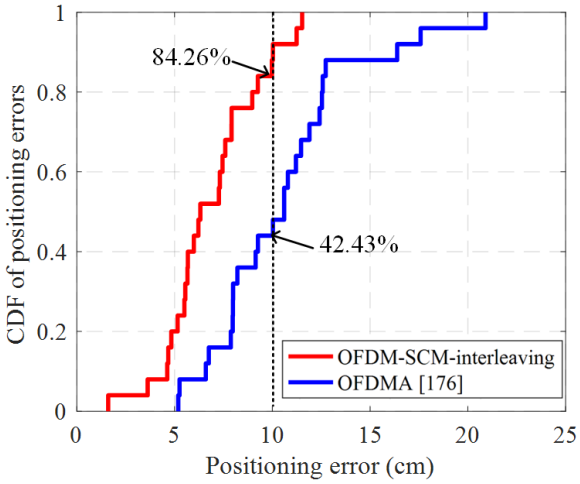

Figure 4.8: Comparisons of positioning errors' CDF.

the existing design [176] are 6.88 cm and 10.56 cm, respectively, which indicates the higher positioning accuracy achieved by our proposed design.

The CDF of the positioning errors is provided in Fig. 4.8. From Fig. 4.8, when

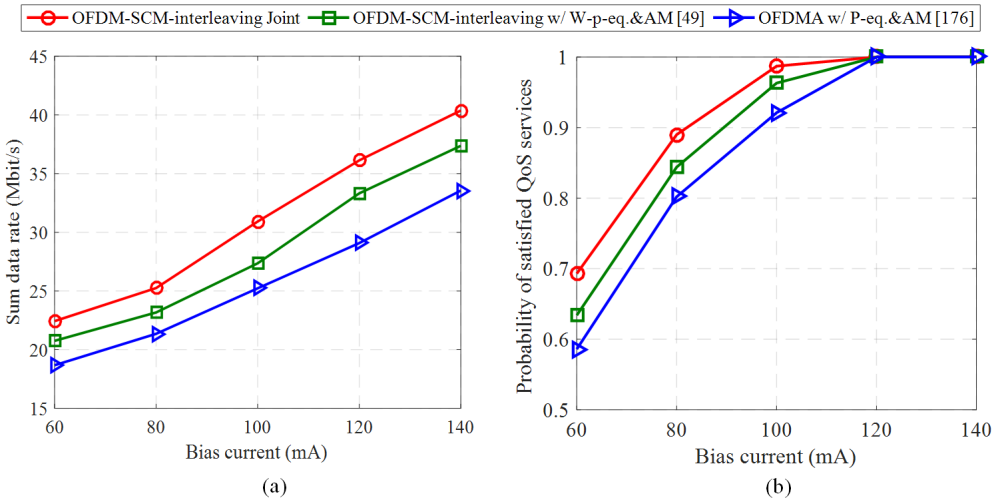

Figure 4.9: (a) Sum data rate and (b) the satisfied QoS level vs. bias current (mA).

$RSE^{max} = 10$ cm, our proposed design has the probability of 84.26 % to satisfy devices' positioning accuracy requirements, while the design in [176] only has the probability of 42.43 %.

Fig. 4.9 represents the sum data rate of devices and the satisfied QoS level versus the bias input current for the three designs (note: W-p-eq. means weighted pre-equalization and AM denotes adaptive modulation). As the increase of the input current, the performance of the sum data rate and the satisfied QoS service level increase due to the high received SNR. Our proposed design (OFDM-SCM-interleaving w/Joint) outperforms the design in [49] (OFDM-SCM-interleaving w/Wei-pre-eq.AM), because we consider subcarrier allocation in the transmission optimization design. However, the data rate performance of the design in [176] is worse, the main reasons are listed as follows: 1) it has low effective bandwidth utilization when the total bandwidth is divided into for subbands for four LED lamps as shown in Fig 4.1 (b) and the analysis shown in Section II.A; 2) four LED lamps transmit their signals independently in four subbands, which exists high OOBI at the edge of each sub-band, so it needs some number of subcarriers as GBs. Hence the low effective bandwidth utilization degrades

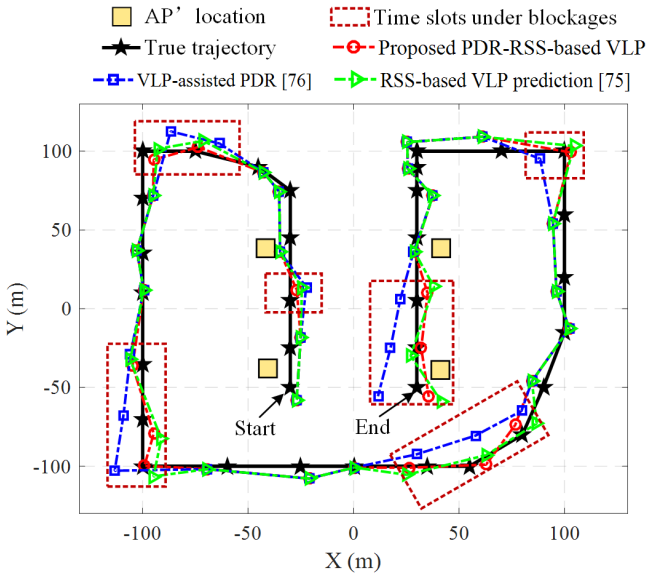

Figure 4.10: Trajectory performance comparisons of the three positioning schemes under blockages

the data rate performance in the design [176]. From Fig. 4.9(b), we can observe that our proposed design can effectively satisfy the QoS requirements.

4.5.3 Performance Evaluations Under LoS Blockages

This subsection evaluates both the communication and positioning performances of the following positioning schemes under LoS blockages: *1)* Our proposed robust positioning scheme by combining PDR the RSS-based VLP (denoted by PDR-RSS-based VLP); *2)* The VLP-assisted PDR positioning scheme, similar to [76] (denoted by VLP-assisted PDR [76]); *3)* The RSS-based VLP positioning scheme by using the previous location information to predict devices' locations under blockages [75] (denoted by RSS-based VLP prediction [75]).

The indoor tracking performances of the three positioning schemes under blockages are provided in Fig. 4.10. All the three schemes have the similar positioning accuracy performance under the LoS condition (no blockages). However, the positioning error is huge for the VLP-assisted PDR scheme [76] under blockages, and it is still increas-

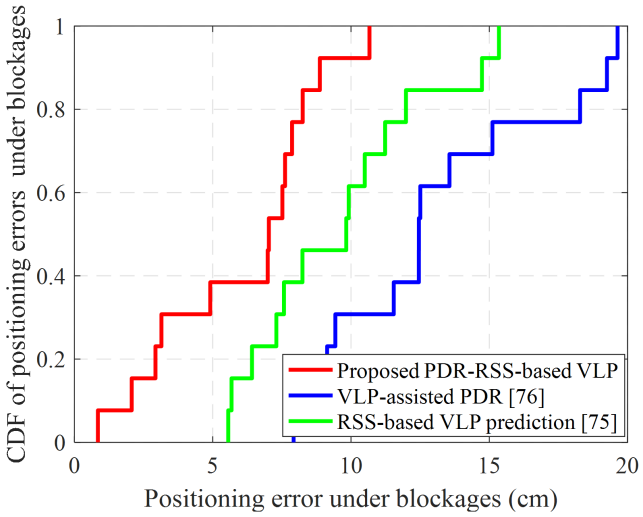

Figure 4.11: CDF of positioning errors under blockages.

ing as the increase of traveling distance in this case. Because the positioning error will gradually increase over time using the PDR method to predict devices' locations in VLP systems under blockages. By contract, the best positioning performance is achieved by using our proposed PDR-RSS-based VLP, where the information of RSS results are used to correct the positioning error under blockages, hence the trajectory is pulled back to the true path as analyzed in Section 4.4.3. In addition, the RSS-based VLP with prediction scheme [75] obtains the high positioning error under blockages, because it does not consider the movement behaviors of devices and choose the most likely predicted location based on the historical information, hence it still has the high positioning errors during devices traveling in this case.

The CDF of the positioning errors of the three schemes under blockages are shown in Fig. 4.11. The mean positioning errors of the PDR-RSS-based VLP, VLP-assisted PDR and RSS-based VLP prediction schemes under LoS blockage events are 7.08 cm, 14.72cm and 10.13 cm, respectively.

The effect of the blocking probability of LoS links on the sum data rate and the satisfied QoS level are shown in Fig. 4.12. From Fig. 4.12, the data rate and satisfied

QoS performances of all approaches are decreased upon increasing the LoS blocking probability. However, our proposed scheme with robust communication and positioning can still achieve a good performance and it outperforms other approaches with different blocking probability values. In addition, the probability of the satisfied QoS services decreases during this process, because the blockage significantly degrades the received desired power or SNR, results in failing to guarantee the different QoS requirements of devices. However, for all blocking probabilities, our proposed scheme still outperforms other schemes.

4.6 Multi-cell Integrated VLCP System Model and Problem Formulation

This section extends the system model into multi-cell integrated VLCP networks [196], where a joint AP section, bandwidth allocation and power allocation approach is proposed maximize the network data rate while guaranteeing the different QoS requirements of indoor devices.

4.6.1 System Model

We consider an indoor integrated VLCP networks, which consists of a set of L VLC APs uniformly installed on the ceiling and each VLC AP covers a confined area to generate a small optical cell, as shown in Fig. 4.13(a). In addition to offer the lighting requirements, they also set up to provide both the communication and positioning services for indoor devices. In the network, the communication and positioning signals are modulated into the APs before passing through the wireless optical channel, and each device is equipped with a PD to convert the received light into electrical signals.

In the network, a number of devices (K devices) are randomly located in the lighting coverage area, and some devices may suffer from ICI from adjacent cells when they are in the overlapped areas. There exists a central controller in the network, which connects

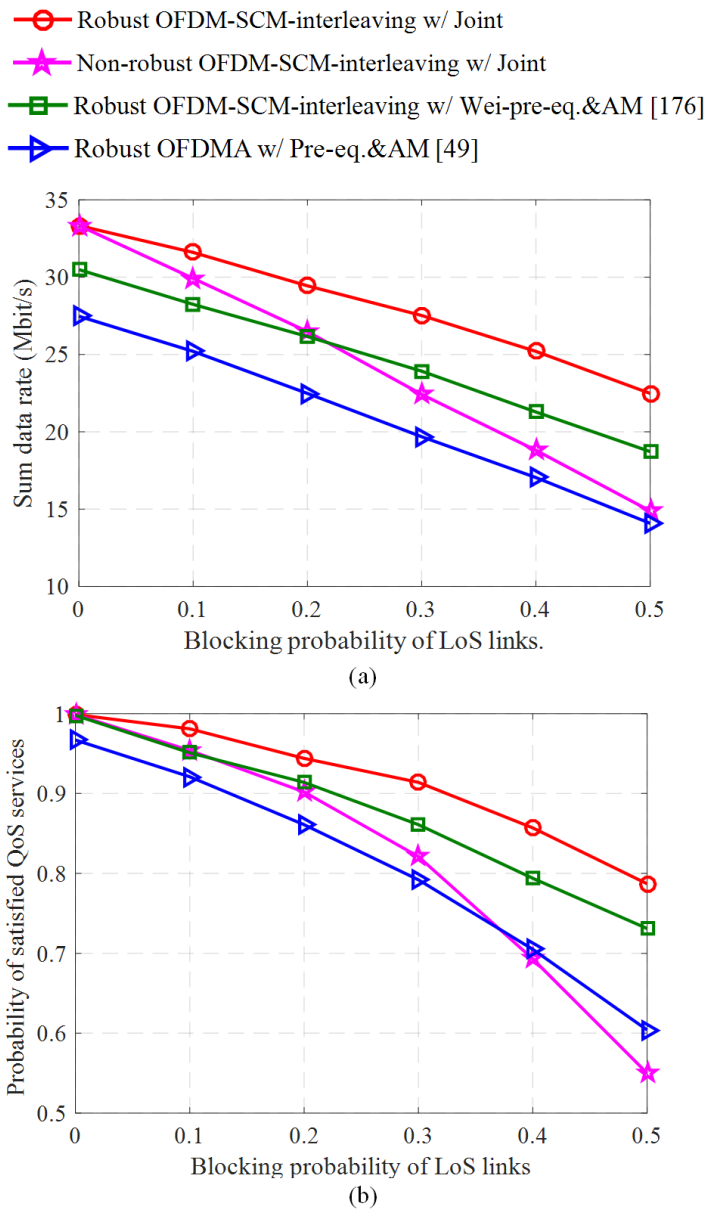

Figure 4.12: (a) Sum data rate and (b) the satisfied QoS level against the blocking probability of LoS links.

all APs to broadcast information to devices, and the uplink feedback is offered by the Wi-Fi links. After receiving the feedback information, the central controller can tackle the resource management task. The total available subcarriers is equally divided into $N+1$ SGs, where the subcarriers in the $(N+1)$-th SG are used for positioning and the remaining N SGs are served for communication. In order to improve the subcarrier utilization, the network adopts the unity frequency reuse (UFR) design in the integrated VLCP network, where the communication SGs are reused across all cells. Let $\mathcal{L}$ and $\mathcal{K}$ denote the AP set and the device set, respectively. Let $\mathcal{N}_l$ denote the SG set in the l-th cell.

At each AP, the sinusoidal signals for VLP are added with the OFDM signal after allocating the SGs to devices, where the L positioning subcarriers from f_1 to f_L are all in the $(N+1)$-th SG and the communication data for the devices are all in the N SGs. After collecting the feedback information (channel information, SINR, QoS requirements, RSSI etc.) from the devices, the communication data stream is then encoded to the OFDM signal with the adaptive QAM mapping based on the devices' different minimum data requirements and the received SINR values.

At the receiver, if the k-th device assigns the n-th SG of the l-th AP, the received SINR is given by

$$\gamma_{k,n,l}^{\mathrm{co}} = \frac{\mu^2 P_{n,l} (G_{k,n,l})^2}{\sum_{i=1, i\neq l}^{L} P_{n,i} (G_{k,n,i})^2 + \delta^2} \tag{4.21}$$

where μ is the PD's responsivity. $P_{n,l}$ is the allocated electrical power on the n-th SG at the l-th AP. $G_{k,n,l}$ represents the optical channel gain from the l-th AP to device k on the n-th SG. δ^2 is the noise power including the shot noise (denoted by δ^2_{shot}), the thermal noise (denoted by $\delta^2_{\mathrm{thermal}}$) and the inter symbol interference (ISI, denoted by δ^2_{ISI}) caused by the multipath propagation [5, 35], which can be expressed as

$$\delta^2 = \delta^2_{\mathrm{shot}} + \delta^2_{\mathrm{thermal}} + \delta^2_{\mathrm{ISI}} \tag{4.22}$$

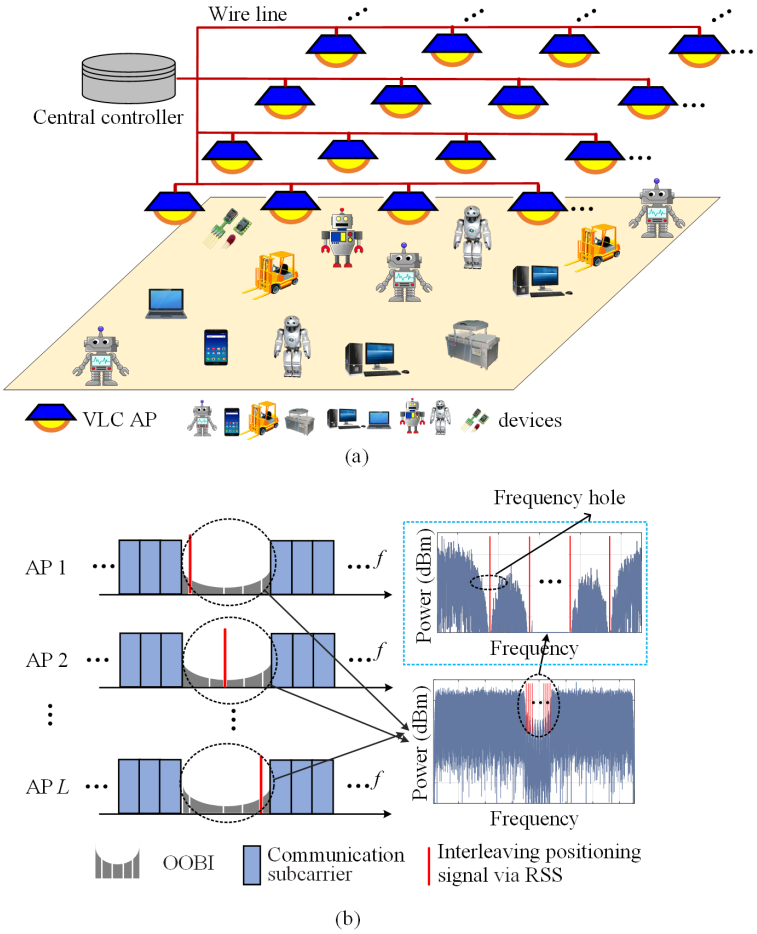

Figure 4.13: (a) The integrated VLCP network for indoor devices and (b) the spectrum structures of the integrated VLCP network.

In (4.22), the received signals at the PD through diffuse path may suffer from the multipath propagation which causes ISI in complex indoor environments. The more details about the above mentioned multipath propagation can be found in the literatures [5, 35].

Other details of the communication model and positioning model can be seen Section 4.2 in this chapter.

4.6.2 Problem Formulation

In the network, our objective is to maximize the overall network transmission data rate while guaranteeing the above mentioned QoS requirements of devices shown in Section 4.3. Here, the resource management problem (joint AP selection, SG allocation and power allocation) can be mathematically formulated as

$$\begin{aligned}
&\max_{\boldsymbol{\alpha},\boldsymbol{\rho},\boldsymbol{P}} R_{sum} = \sum_{l\in\mathcal{L}}\sum_{k\in\mathcal{K}} \alpha_{k,l} R_k \\
&s.t. \quad \text{a}: \ (4.8),\ (4.10); \\
&\text{b}: \ \alpha_{k,l},\ \rho_{k,n,l} \in \{0,1\},\ \forall k,\ \forall l, \forall n; \\
&\text{c}: \ \textstyle\sum_{l\in\mathcal{L}} \alpha_{k,l} = 1,\ \forall k; \\
&\text{d}: \ \textstyle\sum_{k\in\mathcal{K}} \sum_{n\in\mathcal{N}_l} \rho_{k,n,l} P_{n,l} \le P_{\max},\ \forall l; \\
&\text{e}: \ \textstyle\sum_{k\in\mathcal{K}} \sum_{n\in\mathcal{N}_l} \rho_{k,n,l} \le N,\ \forall l.
\end{aligned} \tag{4.23}$$

where $\boldsymbol{\alpha}$, $\boldsymbol{\rho}$ and $\boldsymbol{P}$ represent the matrix or vectors of the AP selection, SG allocation indicator, modulation order and transmit power level, respectively. In order to reduce the AP selection complexity, constraint (4.23c) is used to ensure that one device can only select a single AP to apply the communication services. Constraints (4.23d) is that the transmit power of each AP allocated to its served devices should not exceed the maximum transmit power. (4.23e) is imposed to guarantee that the sum of assembled SGs should not exceed the number of the available SGs of each AP.

4.7 Solution to the Resource Management Problem

Clearly, the optimization problem in (4.23) is a mixed-integer programming problem due to that the binary variables and the non-negative power variables are involved, as well as it is non-convex, so it cannot be solved directly. Hence, we should make the optimization problem tractable. In this section, we solve the joint optimization problem in (4.23) by decomposing it into two subproblems: 1) AP selection and SG allocation; 2) power allocation. Consequently, after solving these two subproblems alternately, we can achieve the optimized solution of the joint optimization problem in (4.23) by using an iterative algorithm.

4.7.1 AP Selection Formation

The network generally consists of multiple optical cells, hence the VLC AP selection should be considered to improve the network performance and guarantee devices' QoS requirements. The traditional max-RSSI approach [203] is widely adopted to address the AP selection problem, but it fails to enable devices to achieve the desired service qualities, because the devices may simply associate with the nearest AP with the largest RSSI value, which may result in the intense channel contention and significantly unbalanced data rate distributions. In addition, some optimal AP selection approaches [59, 66, 73, 141, 193] were presented in RF networks or VLC networks, but they have the high complexity and the perfect assumption of devices' location information.

Hence, we propose a new AP selection to find the suitable AP selection strategy among L APs composing the integrated VLCP network where devices can be associated such that: 1) VLP APs could satisfy the different QoS requirements of devices, and 2) the AP selection needs to optimize the overall network performance.

Considering the fact that different devices have different service requirements, we first divide the devices into two kinds of devices based on their different services:

Primary devices: Devices in this group have specific requirements on low service delay, high transmission reliability and service steadiness, such as instant online software installation and real-time data stream.

Secondary devices: This kind of devices are not interested in the service delay and steadiness such as short message service, web browsing, software/document downloading and email sending.

We set that primary devices have the higher priority to associate its needed AP, while second devices are with the lower priority to associate its needed AP compared with the primary devices. Let $\mathcal{K}_{\mathrm{AP},l}$ denote the set of devices currently selected by the l-th AP.

Implementation: We now carry out the VLC AP selection for devices step by step.

Step 1 (Candidate AP selection): Each device first sorts the RSSI values of all APs in the candidate-selected AP subset, and it searches the AP with the highest RSSI denoted by AP_k, which refers to the candidate-selected AP, hence we have

$$\mathrm{AP}_{(k)} = \arg \max_{l \in \mathcal{L}} (P_{k,l}^{\mathrm{rec}}) \tag{4.24}$$

If more than one devices select the same candidate AP and the corresponding AP has no device association, the AP selects the primary devices to associate its channel resource with the high priority. And other secondary devices should search their next available APs if this candidate AP has no enough channel and power resource for them, until each device searches its unique candidate AP. If more than one devices with the same priority level select the same candidate AP, the AP adopts the proportional fair (PF) priority scheduling scheme to serve the devices from the high PF-priority devices to the low PF-priority devices if the AP has enough resource [204], otherwise, the low PF-priority devices have to select their next nearby APs.

Hence, according the above analysis, each AP $l \in \mathcal{L}$ has its current candidate-served device set, which is expressed as

$$\mathcal{K}_{\mathrm{AP},l} = \{\mathrm{AP}^{*}_{(k)} : \ k \in \mathcal{K} \} \tag{4.25}$$

After the AP selection for all devices has been completed, the minimum data requirements and service quality can be effectively guaranteed. However, the network still needs to adjust the candidate AP selection strategy to address the following issues: 1) balance the data rate distributions, where some APs may be idle while other APs are busy serving devices, leading to the unbalanced resource allocation. Hence, the networks needs to adjust its AP selection strategy to optimize the overall network performance, which is shown in step 2; 2) minimize the overall ICI to improve the network performance, which is shown in step 3.

Step 2 (Resource balance based-AP selection adjustment): For the idle APs, the candidate-served device set of the l'-th idle AP is expanded first by including the nearby devices with a certain range d_0, which is written as

$$\mathcal{K}_{\mathrm{AP},l'} = (\mathcal{K}_{\mathrm{AP},l'} \cup \{k \in \mathcal{K}_{\mathrm{AP},l} : \sqrt{(x_l - x_k)^2 + (y_l - y_k)^2} \leq d_0\} \ ) \tag{4.26}$$

In (4.26), when the l'-th idle AP selects the k-th device from the l-th AP candidate-served device set: $\mathcal{K}_{\mathrm{AP},l} = \mathcal{K}_{\mathrm{AP},l} - \{k\}$, but the update subset $\mathcal{K}_{\mathrm{AP},l} \neq \emptyset$. If the k-th device was included in several idle APs, it selects the nearest idle AP.

Step 3 (ICI minimum based-AP selection adjustment): We would like to mention that the device located in the overlapping area may suffer severe ICI form adjacent cells, leading to the significant degradation of the network performance and the satisfied QoS level. However, if the device changes its decision by selecting the nearby AP with the lower ICI instead of its current associated AP , its performance and satisfied QoS level can be effectively improved. Based on this observation, the network needs to adjust the AP selection strategy to reduce the negative effect of ICI on the network performance

improvement. Here, we define the signal-to-interference ratio (SIR) as the RSSI value of the current associated AP over the sum of the RSSI values from other adjacent APs (or optical cells). When the k-th device currently associates with the l-th AP, its SIR can be written as

$$SIR_{k,l} = P_{k,l}^{\text{rec}} \Big/ \left(\sum\nolimits_{\hat{l} \in \mathcal{L},\, \hat{l} \neq l} P_{k,\hat{l}}^{\text{rec}} \right) \tag{4.27}$$

Similarly, according to the RSSI values, the device can calculate other SIR values if it selects other APs, and it compares its current $SIR_{k,l}$ with $SIR_{k,\hat{l}},\ \hat{l} \in \mathcal{L}$, finally selects the AP from the these candidate APs with the highest SIR value by

$$\text{AP}_{(k)} = \arg \max_{l \in \mathcal{L}} (SIR_{k,l}) \tag{4.28}$$

4.7.2 Suboptimal SG Allocation

We can observe that the optimization problem in (4.23) is a combinatorial problem, which has a prohibitive computational complexity if we solve it through using the exhaustive search for all the possible cases, especially when the number of devices and SGs are large in the network. Hence, we propose a low complexity scheme to achieve the suboptimal SG allocation under the constraints in (4.8).

The key principle of the proposed approach is that the primary devices first access the SGs of its selected AP, and the primary device whose rate is the farthest away from its target minimum data rate requirement has the priority to be allocated the SGs with highest channel quality to meet its minimum data rate requirement. Then, the AP allocates the SG resource to the secondary devices to meet their minimum data rate requirement. After satisfying the devices' QoS requirements, we allocate the excess SGs of each AP to the devices with high channel gains to maximize the overall network data rate.

Let Ω_k denote the SG subset allocated to the k-th device. The proposed AP selection and SG allocation approach is shown in **Algorithm 1**.

Algorithm 1 AP Selection and SG Allocation

Initialize: $\mathcal{N}_l = \{1, \ldots, N\}$, $\mathcal{K} = \{1, \ldots, K\}$, set $R_k = 0$ and $\Omega_k = \emptyset$ for $\forall k \in \mathcal{K}$.

Step 1: AP selection

1: The AP selection strategy is carried out by the candidate AP selection, resource balance and ICI minimum based-AP selection adjustment shown by Section 4.71.

Step 2: Satisfy minimum rate requirements

2: Primary devices access SGs of its selected AP with the higher priority while secondary devices are with the lower priority to access SGs. The devices with the same priority level take step 3 to step 5.

3: For any device k satisfying $R_k < R_k^{\min}$;

4: Find the device k' satisfying $R_{k,\min} - R_k \leq R_{k',\min} - R_{k'}$ for $\forall k' \in \mathcal{K}$;

5: For the device k', find SG $n' \in \mathcal{N}_l$ from its selected AP l with the highest data rate;

6: Let $\Omega_{k'} = \Omega_{k'} \cup \{n'\}$, $\mathcal{N}_l = \mathcal{N}_l - \{n'\}$, and update $R_{k'}$;

Step 3: Allocate excess SGs to maximize the sum data rate

7: If $\mathcal{N}_l \neq \emptyset$, $\forall l$, allocate the excess SGs to the devices with high channel gains to maximize the sum data rate.

The optimal AP selection and SG allocation can be achieved if we adopt the exhaustive search for all the possible SG allocation cases. In the multi-cell network with the K devices, L cells and N SGs per cell, it is prohibitive to search the optimum due to the high computational complexity, since the exhaustive search method has $O(K^{N \times L})$ possible SG allocation cases. Hence, in the system, there exists $N \times L$ communication SGs over all cells. It is obvious to see that each device needs compute the SG allocation and AP selection step which takes $N \times L$ comparison operations. For all the devices, then the total complexity of the AP selection and SG allocation is $O(K \times N \times L)$, which is greatly lower than the exhaustive search method.

4.7.3 Power Allocation

Here, given the AP selection and SG allocation strategies, we aim to obtain the optimized power allocation strategy $\boldsymbol{P}$ which includes the communication power allocation strategy $\boldsymbol{P}^{\text{co}}$ and the positioning power allocation strategy $\boldsymbol{P}^{\text{po}}$. We find that the positioning power allocation strategy $\boldsymbol{P}^{\text{po}}$ is not related to the objective function in (4.23), we use the water fulling algorithm for positioning allocation allocation to guarantee the positioning constraint (4.10) first [187, 188]. After that we achieve the optimized communication power allocation strategy $\boldsymbol{P}^{\text{co}}$ by the following analysis.

The partial Lagrange function of the problem (4.23) in term of the $\boldsymbol{P}^{\mathrm{co}}$ is expressed as

$$\begin{aligned}\Upsilon(\boldsymbol{\beta},\boldsymbol{\chi},\boldsymbol{P}^{\mathrm{co}}) = \sum_{l\in\mathcal{L}}\sum_{k\in\mathcal{K}}\alpha_{k,l}R_k + \sum_{k\in\mathcal{K}}\beta_k(R_k - R_k^{\min}) \\ + \sum_{l\in\mathcal{L}}\chi_l(P_{\max} - P_l^{\mathrm{po}} - \textstyle\sum_{k\in\mathcal{K}}\sum_{n\in\mathcal{N}_l}\rho_{k,n,l}P_{n,l})\end{aligned} \tag{4.29}$$

where $\boldsymbol{\beta} = \{\beta_k, \forall k\}$ and $\boldsymbol{\chi} = \{\chi_l, \forall l\}$ are the dual Lagrange multiplier vectors or variables for the constraints in (4.8) and (4.23d). P_l^{po} is the positioning power allocation level at the l-th VLC AP.

Then, the dual function of the Lagrange function (4.29) can be given by

$$J(\boldsymbol{\beta},\boldsymbol{\chi}) = \max_{\boldsymbol{P}^{\mathrm{co}}}\{\Upsilon(\boldsymbol{\beta},\boldsymbol{\chi},\boldsymbol{P}^{\mathrm{co}})\} \tag{4.30}$$

In (4.30), when the dual function value is optimized, we can get the optimized power allocation variables $\boldsymbol{P}^{\mathrm{co}}$. The dual problem to the original problem (4.23) can be written as

$$\begin{aligned}&\min_{\boldsymbol{\beta},\boldsymbol{\chi}}\{J(\boldsymbol{\beta},\boldsymbol{\chi})\} \\ &s.t.\ \boldsymbol{\beta}\geq\mathbf{0}, \boldsymbol{\chi}\geq\mathbf{0}.\end{aligned} \tag{4.31}$$

The value of $J(\boldsymbol{\beta},\boldsymbol{\chi})$ can be calculated by using the Lagrange dual decomposition method. Notably, $J(\boldsymbol{\beta},\boldsymbol{\chi})$ is a concave function due to the pointwise infimum of a set of affine functions of Lagrange multipliers. Hence, we can use the subgradient method to solve the optimization problem (4.23) [205].

Accordingly, we present the solution process for the AP selection, SG allocation and power allocation in integrated VLCP networks, as shown in **Algorithm 2**.

Algorithm 2 Resource Management Approach

Initialize: Set the iteration $j = 0$, set $R_{\text{sum}}(0)$, $\boldsymbol{\alpha}(0)$, $\boldsymbol{\rho}(0)$, and $\boldsymbol{P}(0)$, the maximum tolerance $\varsigma > 0$;
1: **Repeat**
2: Update the AP selection variables $\boldsymbol{\alpha}(j+1)$ and the SG allocation variables $\boldsymbol{\rho}(j+1)$ by **Algorithm 1**;
3: Update the positioning power allocation variables $\boldsymbol{P}^{\text{po}}(j+1)$ by using the water fulling method and communication power allocation variables $\boldsymbol{P}^{\text{co}}(j+1)$ by solving (4.23) using the subgradient method with the partial Lagrange function in (4.29);
4: $j \leftarrow j + 1$;
5: Update the sum data rate $R_{\text{sum}}(j)$;
6: Until $|R_{\text{sum}}(j) - R_{\text{sum}}(j-1)| \leq \varsigma$;
7: **End**
8: **Output**: $\boldsymbol{\alpha}(j)$, $\boldsymbol{\rho}(j)$ and $\boldsymbol{P}(j)$.

In this section, we solve the joint optimization problem in (4.23) by decomposing it into two subproblems: 1) AP selection and SG allocation; 2) power allocation. Consequently, after solving these two subproblems alternately, we can achieve the optimized solution of the joint optimization problem in (4.23) by using an iterative algorithm. Hence, it not an optimal solution, and it is a suboptimal solution.

By every iteration, the sum-rate is increasing. As the optimized sum-rate is bounded due to limitations in access points (APs), bandwidth and power resources, the iterative algorithm must converge to a convergence point. The optimization problem of (4.23) is composed of three AP selection, power and subchannel allocation subproblems which are solved iteratively. Consequently, the optimality criteria for the solution of optimization problem of (4.23) will be the criteria set for its constituent problems. The convergence point of the presented solution is satisfying these optimality criteria and thus provides the final solution point. Additionally, the references [72]-[74] verify the convergence property of the iterations and provide convergence conditions of the iterative algorithm.

In **Algorithm 2**, the presented resource management approach consists of SG allocation, AP selection, and power allocation. As shown in the last comment, the complexity of the AP selection and SG allocation is $O(K \times N \times L)$. For power allocation, since there exist the overall $(N + 1) \times L$ SGs of all APs (note that each AP has N

communication SGs and one positioning SG), according to [R8, Section IV-B], the power allocation step can be solved in $O((N+1)\times L)\log_2((N+1)\times L)$ operations by using the iterative algorithm over $(N+1)\times L$ SGs. As the iterative algorithm needs I iterations to coverage to the final point, hence the overall complexity of **Algorithm 2** is $O\left(I(K\times N\times L+(N+1)\times L)\log_2((N+1)\times L)\right)$.

4.7.4 Robust Handover Among APs Under Blockages

As analyzed in Section 4.4, the optical signals being broadcast from VLC APs to the devices may be blocked by obstacles due to the movement of devices or human beings. In this case, LoS is often blocked and NLoS cannot support effective communication and positioning services, leading to the degradation of the network performance.

Hence, this subsection propose a handover scheme to improve the communication performance LoS blockages in multi-cell networks. We would like to mention that the robust positioning schemes has been presented in Section 4.4.3, where the receiver will select the three highest received RSSI with the three corresponding APs to perform 2D positioning in multi-cell networks, more details can be seen in in Section 4.4.3.

The robust handover scheme for communication services can be discussed as follows.

1) Handover under blockages: Due to the mobility of devices, human beings and obstacles, for any device, its current LoS link from the associated AP may be blocked in one time slot or even a long time duration. In this case, the device's performance and satisfied QoS level are notably affected. Hence, we propose a robust handover scheme to combat the LoS link blockage in the network.

Once the device detects that its current LoS link is blocked, it reports the blockage information to the controller. The controller performs the handover mechanism for the device based on the priority level of the device.

i) Handover for primary devices: If the device's location is fixed for a long period, the controller immediately select the nearest AP to continually provide the communica-

tion services for the device. On the contrary, if the device is in the state of movement, the controller select the device's neighboring AP from the available AP subset based on the device's mobility trajectory where the device is moving toward the neighboring AP and the AP will be the nearest one for some time slots in the future. This handover mechanism aims to provide the stable and low-latency services for primary devices under blockages.

ii) Handover for secondary devices: When the device deletes the LoS blockage, the controller waits of a dwell period of τ_{wait}. When τ_{wait} expires, the controller selects one neighboring AP with the enough channel resource for the device, otherwise, the device still associates with its currently serving AP until the blocked link is recovered. This handover mechanism can effectively avoid the potential ping-pong effects by reducing the unnecessary handovers.

2) Handover under mobility: Some literatures proposed the handover mechanisms based on the location information of devices [26-[31], but they assumed that the devices' location information is perfectly known. Hence, we present a transmission handover mechanism based on the RSSI values.

Let $P_{k,l}^{\text{rec}}$ and $P_{k,\hat{l}}^{\text{rec}}$ denote RSSI values of the k-th device's currently serving AP and one candidate AP of its neighboring APs, respectively. The handover is executed when the following condition is satisfied

$$P_{k,\hat{l}}^{\text{rec}} \geq P_{k,l}^{\text{rec}} + \varepsilon, \ \ \forall \hat{l} \in \mathcal{L} \tag{4.32}$$

where ε denotes the hysteresis value of the handover margin which is also used to prevent unnecessary handovers. If the device locates in the region of the $\hat{l}$-th AP and the RSSI value satisfied (4.32) for a certain period, then the device switches the connection from its currently serving AP l to the $\hat{l}$-th AP.

4.8 Simulation Results and Discussion

In this section, simulations are conducted in Matlab 2017a to evaluate the performance of our presented integrated VLCP network, the proposed resource management approach and the robust schemes under LoS blockages.

We consider a typical indoor room with the area of 10m×10m×4m, where 4×4 VLC APs are uniformly distributed at a height of 3.75m. A number of devices are randomly distributed at two different heights (0.5m and 1m). $K/2$ devices need both communication and positioning services with the data rate requirement (1 Mbps per device) and other $K/2$ devices only require communication services with the data rate requirement (10 Mbps per device). The number of SGs in each cell is N=6. For each AP, the LED lamp semi-angle at half power and Lambertian emission order are 60^o and 1, respectively. The active area, the FOV, the concentrator refractive index and the responsivity of the PD are 1 cm^2, 110^o, 1.5 and 0.5 A/W, respectively. The gain of the optical filter is 1. The dwell period of τ_{wait} is 1 second.

The transmission modulation bandwidth is 20 MHz and the available bandwidth is 10 MHz due to the Hermitian symmetry [184, 197]. The range of the positioning frequencies is from 5.0 MHz to 6.45 MHz. In addition, the positioning error threshold is 5 cm.

4.8.1 Performance Comparisons of Integrated VLCP Networks

Fig. 4.14 and Fig. 4.15 show the positioning results and the CDF of the positioning errors over the indoor room, respectively. In Fig.4.14, the mean position error of our proposed integrated VLCP based on OFDM-SCM-interleaving and the existing integrated VLCP based on OFDMA [176] are 4.28 cm and 19.55 cm, respectively, which indicates the higher positioning accuracy achieved by our proposed integrated VLCP network. In the existing OFDMA based integrated VLCP network [176], the

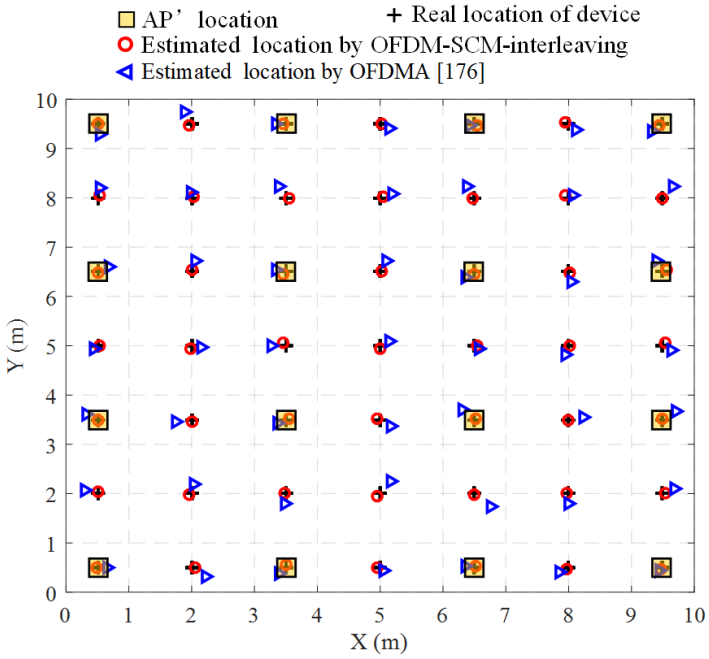

Figure 4.14: Comparisons of positioning errors' CDF.

high OOBI from OFDM signal leads to the severe interference on adjacent positioning subcarriers, which could degrade the positioning accuracy performance.

In Fig. 4.15, we can see that the positioning errors at 90% confidence for OFDM-SCM-interleaving and OFDMA are 6.82 cm and 28.17 cm, respectively, showing a significant improvement of positioning accuracy by using OFDM-SCM-interleaving in integrated VLCP networks.

4.8.2 Convergence Performance Comparisons

Fig. 4.16 illustrates the convergence of my proposed resource allocation solution in terms of the sum data rate versus the number of iterations when the total number of devices is K=100 and the transmit power per AP P_{max}= 60 mW. We can observe that from Fig. 4.16 that my proposed resource allocation solution has achieved convergence after iteration index 10, and it has the higher convergence speed than LB RM [66]. This is because that the LB RM approach [66] tries to search the optimal solution

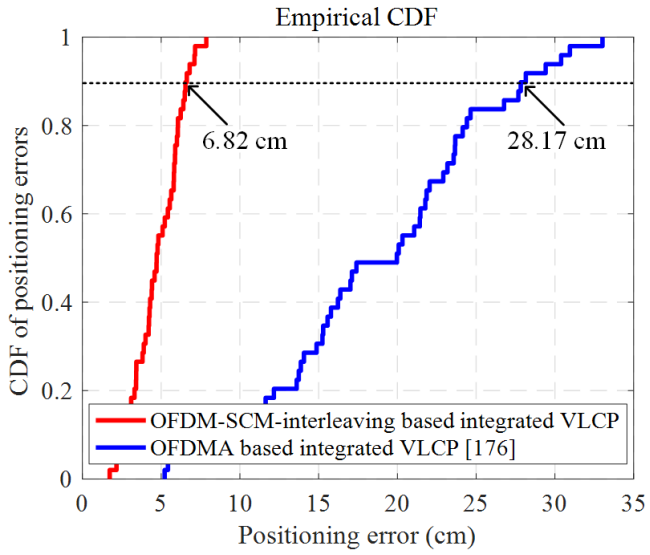

Figure 4.15: Comparisons of positioning results.

with higher computation complexity, so the convergence speed is sacrificed to achieve the improved sum data rate performance. Although LB RM outperforms my proposed QoS-driven RM in terms of the data rate, it has the higher positioning error and the lower satisfied QoS level than the proposed QoS-driven RM, which has been shown in Fig. 4.16 in my thesis. The max-RSSI RM approach requires the lower number of convergence iterations compared with other approaches (except optimal QoS-driven RM), but it achieves the worst sum data rate performance in the networks, because each device selfishly selects its own nearest AP, leading to the unbalanced resource allocation.

4.8.3 Performance Comparisons Under Different Transmit Power Levels

In this subsection, we compare the performance of different resource management approaches in our presented multi-cell integrated VLCP network, where the approaches are shown as follows: *1)* Optimal resource management approach (denoted as optimal QoS-driven RM), where the approach uses the exhaustive search method to find the

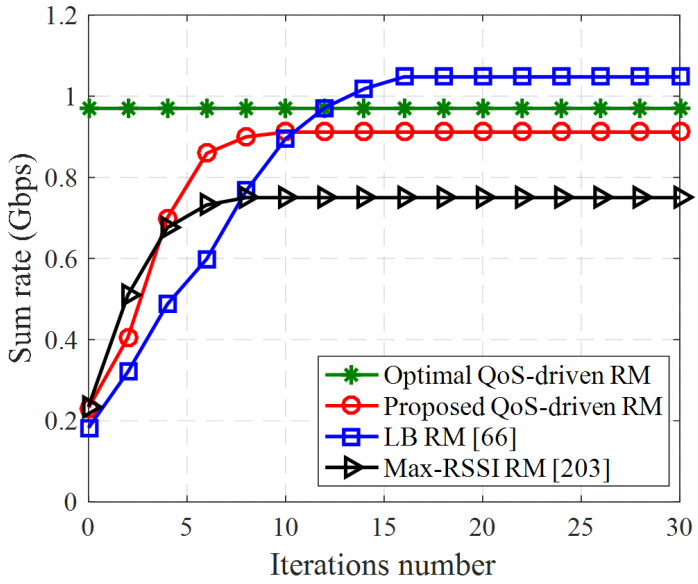

Figure 4.16: Comparisons of convergence performance.

optimal AP selection and SG allocation strategy; *2)* Our proposed suboptimal resource management approach (denoted as proposed QoS-driven RM), with the purpose of guaranteeing the QoS requirements of devices while maximizing the overall data rate; *3)* The load balancing (LB) approach without satisfying QoS requirements first [66] (denoted as LB RM [66]); *4)* The resource management approach based the maximal RSSI [203] (denoted as Max-RSSI RM [203]).

Fig. 4.16 shows the sum data rate of devices, the positioning error and the probability of satisfied QoS services versus the electronic transmit power $P_{\max}$ per AP for the four approaches, when the total number of devices is K=100 and the blocking probability of LoS link is 0.1. As the increase of $P_{\max}$, for all approaches, the sum data rate performance and the probability of satisfied QoS services increase, and the positioning error decreases. This is because that when $P_{\max}$ increases, the received SINR and received power allocated on the positioning subcarriers enhance, leading to the performance improvement.

From Fig. 4.16, although LB RM outperforms our proposed QoS-driven RM in

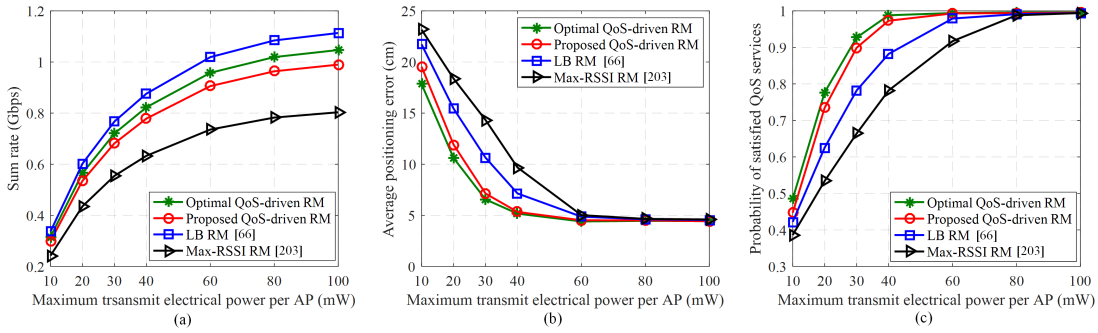

Figure 4.17: Performance evaluations and comparisons versus the maximum transmit electrical power per AP.

terms of the data rate, it has the higher positioning error and the lower satisfied QoS level than the proposed QoS-driven RM. The max-RSSI RM approach archives the worst performance in the networks, because each device selfishly selects its own nearest AP, leading to the unbalanced resource allocation.

From Fig. 4.16 (b), as the increase of $P_{\max}$, the positioning error of all approaches decreases significantly when $P_{\max} < 60$ mW, but the performance is appropriately maintained at a horizontal level when $P_{\max}$ exceeds 60 mW. Such the performance improvement results from the high received power on positioning subcarriers when $P_{\max}$ is large. Once the positioning accuracy requirements are guaranteed in the high power region, the extra power will be allocated to maximize the sum rate of devices as shown in the optimization problem (4.23), thus the positioning accuracy performance is constant when $P_{\max}$ is in the high region. In addition, in Fig. 4.16 (a), the performance improvement is not obviously when $P_{\max}$ >60 mW, because ICI is one of the key factors which limits the data rate enhancement in multi-cell networks.

4.8.4 Performance Comparisons Under Different Device Density

Fig. 4.17 shows the performance comparisons of the four approaches versus the total different numbers of device when $P_{\max} = 60$ mW and the blocking probability is 0.1.

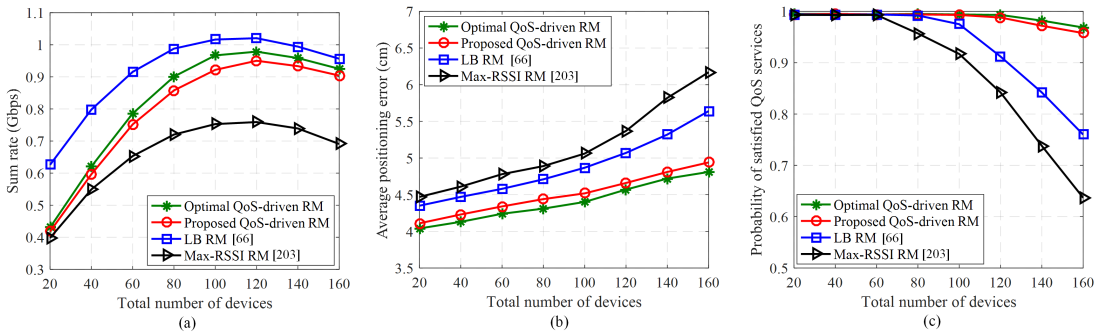

Figure 4.18: The performance evaluations and comparisons varying total number of devices.

It can be seen that the data rate is constantly increasing to a peak due to the more probability of searching devices having good channel gains to enhance the sum rate. After that, it then declines as K increases further, because the increased number of handovers limits the data rate improvement and the more resource may need to allocate to the devices with poor channel gains to support their QoS requirements. Similarly, when the number of devices is large, all devices aims to share the limited power and bandwidth resource, hence the positioning error slight increases and the satisfied QoS level reduces.

In addition, we can observe that the proposed QoS-driven RM approach has comparable data rate performances to the LB RM approach when the number of devices is large, and outperforms the max-RSSI RM approach. Moreover, the proposed QoS-driven RM approach significantly achieves the higher satisfied QoS levels and the lower positioning error than both the LB RM and max-RSSI RM approaches for the large number of devices. Because the proposed approach aims to search the QoS-driven optimized strategy to effectively meet the different QoS requirements of devices while maintaining the high data rate performance, thereby improving the device experiences in indoor networks.

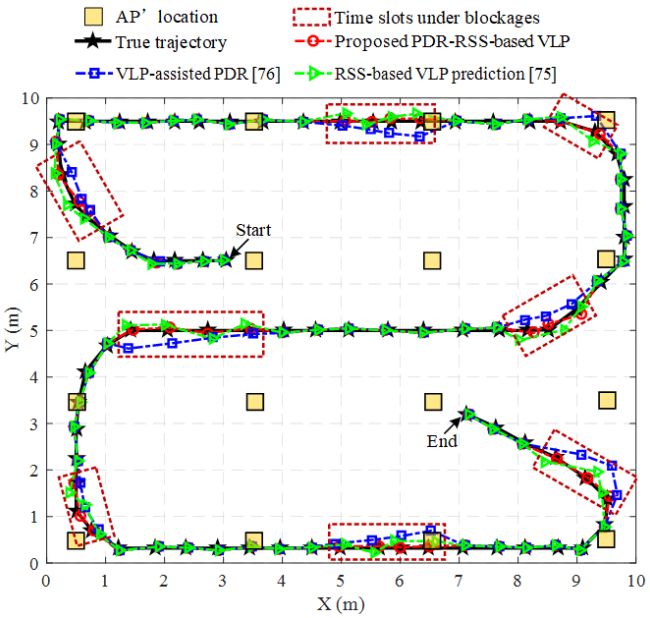

Figure 4.19: Trajectory performance comparisons of the three positioning schemes under blockages.

4.8.5 Tracking Performance Comparisons Under Blockages

This subsection compares the indoor tracking performance.

The indoor tracking performances over all the network of the three positioning schemes under blockages are provided in Fig. 4.18. All the three schemes have the similar positioning accuracy performance under the LoS condition (no blockages). However, the positioning error is huge for the VLP-assisted PDR scheme [76] under blockages, and it is still increasing as the increase of traveling distance in this case. Because the positioning error will gradually increase over time using the PDR method to predict devices' locations in VLP systems under blockages. By contract, the best positioning performance is achieved by using our proposed PDR-RSS-based VLP, where the information of RSS results are used to correct the positioning error under blockages, hence the trajectory is pulled back to the true path as analyzed in Section 4.4.3. In addition, the RSS-based VLP with prediction scheme [75] obtains the high positioning error under blockages, because it does not consider the movement behaviors of devices

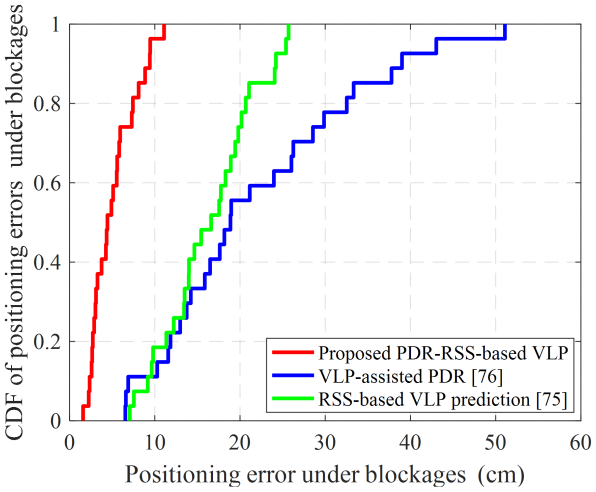

Figure 4.20: CDF of positioning errors under blockages.

and choose the most likely predicted location based on the previous information, hence it still has the high positioning errors during devices traveling in this case.

The CDF of the positioning error of the three schemes under blockages are shown in Fig. 4.19. The mean positioning errors of the PDR-RSS-based VLP, VLP-assisted PDR and RSS-based VLP prediction schemes under LoS blockage events are 5.13 cm, 21.97cm and 16.35 cm, respectively.

Fig. 4.20 shows the robustness of the three positioning schemes against the LoS blockages. When the blocking probability increases, the positioning error obviously increases for the VLP-assisted PDR and RSS-based VLP prediction schemes while it slightly increases for the PDR-RSS-based VLP scheme. Moreover, the gap of the performances between them becomes larger with the increased value of the blocking probability. The above positioning results indicate the effectiveness of the proposed robust scheme against the LoS blockages in networks.

The effect of the blocking probability of LoS links on the sum data rate and the satisfied QoS level are shown in Fig. 4.21 and Fig. 4.22, respectively. From Fig. 4.21, the data rate performances of all approaches are decreased upon increasing the LoS blocking probability. However, our proposed approach with robust handover can still

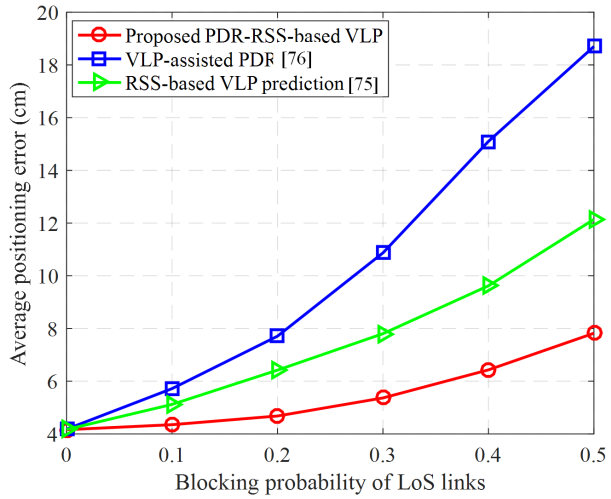

Figure 4.21: Positioning error comparisons against blockage.

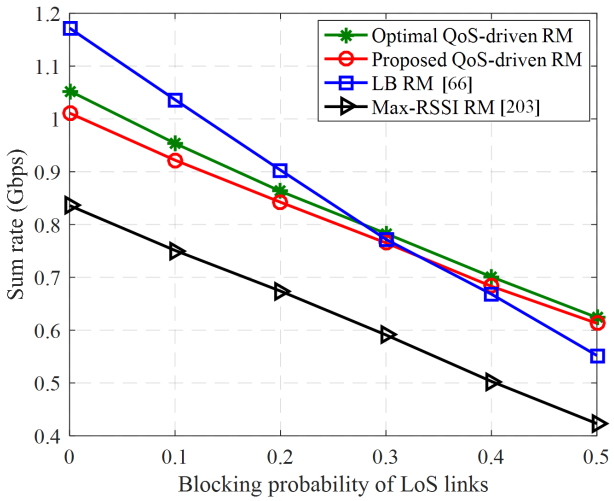

Figure 4.22: Sum data rate comparisons against blockage.

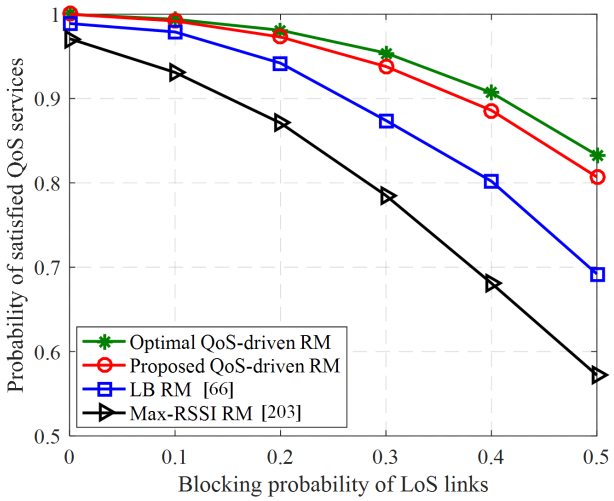

Figure 4.23: Probability of satisfied QoS services against blockage.

achieve a good performance and it outperforms the LB RM approach when the blocking probability is more than 0.3. In addition, the probability of the satisfied QoS services decreases during this process, because the blockage significantly degrades the received desired power or SINR, results in failing to guarantee the different QoS requirements of devices. However, for all blocking probabilities, our proposed approach still outperforms other approaches.

4.9 Conclusion

In this chapter, a new integrated VLCP system model has been proposed to improve both the communication and positioning performance. In order to satisfy different QoS requirements, a QoS-driven optimized joint the adaptive modulation, subcarrier allocation and adaptive weighted pre-equalization was proposed in the integrated VLCP system. The LoS blockage issue is investigated in the system, and the robust optimized schemes are presented to maintain the system performance. The experimental results verified the superiority in performance of the presented integrated VLCP system models, and also showed that the proposed design outperforms other existing adaptive

transmission designs in terms of the data rate and positioning accuracy. Moreover, this chapter also extends the system model into multi-cell integrated VLCP networks, where a joint AP selection, bandwidth allocation, adaptive modulation and power allocation approach is proposed to maximize the network data rate while guaranteeing the different QoS requirements of indoor devices. Simulation results corroborate the superiority in performance of the presented works.

Chapter 5

Interference Mitigation Design for Multi-User Multi-Cell MIMO VLC Systems

5.1 Introduction

As discussed in Section 2, general indoor environment consists of multiple optical cells and each cell may have several LED lamps. Each cell in a multi-cell VLC system is expected to simultaneously support multiple users and each user may receive signals that are broadcasted from the LED transmitters but intended for other users within the same cell. This kind of interference signal is referred to as Inter-User Interference (IUI) [46, 206], in addition to ICI, which is another critical issue that can significantly degrade the system performance in multi-user multi-cell VLC systems.

Considering that ICI greatly degrades the system capacity and reduces the satisfied QoS levels of devices in multi-cell VLC systems, various technologies have been proposed to mitigate ICI, including frequency division, precoding, using an optical differential detection as a VLC receiver (called angle diversity receiver) and resource management based on multiple access [117-146]. The overview of the main ICI mitigation techniques in multi-cell VLC systems have been provided in Section 2.3.2. (Please

see Section 2.3.2 for the more details.)

In [46, 206-207], transmitter precoding was proposed to mitigate IUI in multi-user VLC systems. In [206] and [207], transmitter precoding was achieved by solving the sum rate maximization problem subject to optical power constraints. Especially, the sum rate maximization approach in [207] did not restrict the IUI to be zero and achieved considerably high capacity. The work in [208] reported a MIMO-OFDM technique in multi-user VLC systems, and investigated the system capacity performance. In [209], an optical adaptive precoder was proposed to enhance the SINR in multi-user MIMO-VLC systems. However, the precoders in [46, 206-207] were only proposed for single-cell VLC systems where only the IUI was considered while the ICI was neglected. In practical applications, both ICI and IUI should be taken into consideration when implementing a VLC system covering a certain indoor area. To the best of our knowledge, no work has been reported on the simultaneous mitigation of ICI and IUI in indoor multi-user multi-cell MIMO-VLC systems.

In recent years, the IA technique has been proposed to efficiently separate the desired signals from the interference in wireless RF systems [210-212], which has also been applied in VLC systems. In [213, 214], IA was explored in a multi-user VLC system by assuming perfect CSI. However, the CSI is not always perfectly available at LED transmitters [46, 68], and the assumption of perfect CSI is not practical for VLC systems. Hence, a blind interference alignment scheme for achieving the multi-user MIMO VLC system capacity without CSI at the transmitter was proposed in [215]. However, the work in [216] only considered one single cell, and did not extend the framework in multi-cell VLC system where the ICI mitigation is a key challenge in practical VLC systems. For the above discussion, how to design a novel approach to mitigate both ICI and IUI based on precoding or equalizer design for indoor multi-user multi-cell MIMO-VLC systems is still a key challenge.

This chapter firstly proposes a novel joint precoder and equalizer design based on

IA to mitigate both ICI and IUI for multi-user multi-cell MIMO-VLC systems in the presence of imperfect CSI [216]. In order to achieve the optimal transmit precoding matrix and receiving equalizer matrix, we formulate the joint optimization problem through minimizing the total generated interference and mean-squared error (MSE) under optical power constraints. The proposed design aims to mitigate both IUI and ICI effectively, as well as maintain the BER at the lowest level. Furthermore, we take into account the optical channel estimation error for our formulated joint optimization problem when designing the optimal precoder and receiving equalizer in multi-user multi-cell MIMO-VLC systems. We investigate the effect of different users' locations, channel estimation error and LED/PD spacing levels on the system capacity and BER performance analytically and by simulation. Numerical results show that the proposed design achieves significant system capacity and BER improvements under imperfect CSI, compared with the MMSE and max-rate designs.

The rest of this chapter is organized as follows. In Section 5.2, we describe the model of a multi-user multi-cell MIMO-VLC system. Section 5.3 presents the joint precoder and equalizer design based on IA, and the solution to the optimization problem is given in Section 5.4. The analysis in terms of the behavior of the proposed design is presented in Section 5.5. Section 5.6 provides the simulation results and discussions. Finally, Section 5.7 concludes the chapter with the observations made in this work. The content of this chapter is related to the author's work provided in [216].

Notation: $\mathbf{I}_N$ denotes an identity matrix. $E[\cdot]$ is the expectation operator. $\mathbf{R}^{N\times M}$ denotes the set of $N \times M$ dimensional real-valued numbers, $\mathbb{R}_+^{N\times M}$ represents the set of $N \times M$ -dimensional non-negative real-valued numbers. $(\cdot)^T$, $\mathrm{Tr}\{\cdot\}$ and $(\cdot)^{-1}$ denote the transpose, the trace and the inverse of a matrix/vector, respectively. $||\cdot||_F$ denotes the Frobenius norm, $||\cdot||_l$ denotes the l-norm, vec$(\cdot)$ is the vectorization operator, and $\otimes$ denotes the Kronecker product. abs$(\cdot)$ denotes an element-wise absolute operator and 1 denotes a vector whose elements are all 1.

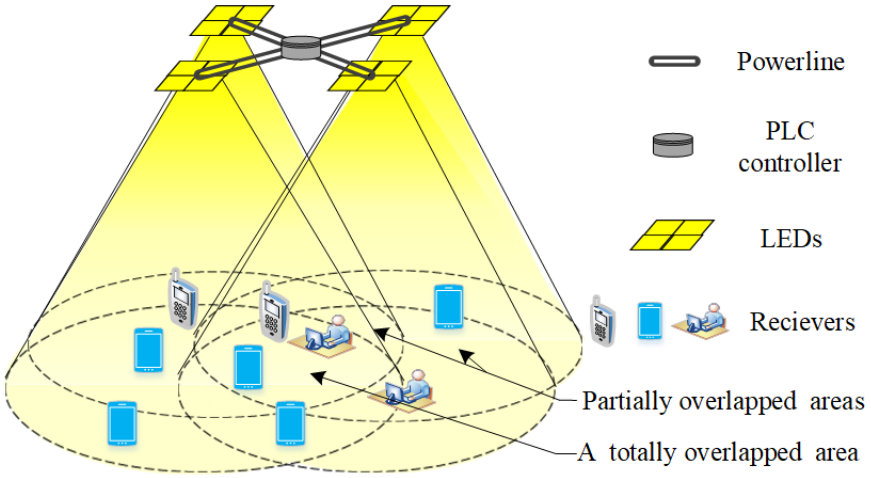

Figure 5.1: An indoor four-cell MIMO VLC system with the overlapped areas.

5.2 System Model

In practical indoor environments, multiple LED lamps are usually installed to set up a VLC system to satisfy lighting and communication requirements of users, as shown in Fig. 5.1. As in [16], we assume that these LED lamps fully cooperate with each other through a PLC backbone network to broadcast information to multiple users simultaneously, and exchange the users information (such as the channel gains) with each LED lamp through the power line communications (PLC) controller in the VLC system. There are multiple LED lamps establishing optical attocells to communicate with multiple users within its illuminated area, where each cell has multiple LED lamps and each user is equipped with multiple PDs [8-10]. Such a cellular indoor VLC system is referred to as a multi-user multi-cell MIMO VLC system in this thesis.

5.2.1 Transmitter Model

In the multi-user multi-cell MIMO-VLC system, some users suffer from ICI when they are located in the overlapped areas in addition to the IUI. Especially, the users who are located in the completely overlapped area may suffer from severe ICI, leading to

the drastic performance degradation. Assuming that the VLC system has B cells and broadcasts information to K users with each user being equipped with N_r PDs. Each cell has N_t down-facing LEDs as transmitters. The k-th user in cell b is denoted as the user (k,b). In this thesis, we consider the OOK modulation as it is typically applied in VLC systems, and $s_{k,b} \in \mathbb{R}$ is defined as the data stream transmitted to the user (k, b). $s_{k,b}$ is assumed to be a non-return-to-zero (NRZ) OOK signal which has a zero mean (i.e., $E\{s_{k,b}\} = 0$) . Since VLC systems employ the IM/DD technique, the transmitted signal should be real-valued and non-negative. This means that a DC component should be added to make sure the transmitted data is non-negative. In addition, LEDs have a limited linear drive current range where the output optical power linearly increases with the drive current [35].

With the transmitter precoding strategy and the DC component addition, the signal vector transmitted by the LED lamps in cell b can be expressed as

$$\mathbf{x}_b = \mathbf{V}_b \mathbf{s}_b + \mathbf{p}_b = \sum\nolimits_{k=1}^{K} \mathbf{v}_{k,b} s_{k,b} + \mathbf{p}_b \tag{5.1}$$

where $\mathbf{V}_b = [\mathbf{v}_{1,b}, \ldots, \mathbf{v}_{k,b}, \ldots, \mathbf{v}_{K,b}]$ is the precoding matrix in cell b and $\mathbf{v}_{k,b} \in \mathbb{R}^{N_t \times 1}$ is the precoding vector for the user (k, b); $\mathbf{s}_b = [s_{1,b}, \ldots, s_{k,b}, \ldots, s_{K,b}]^{\mathrm{T}}$ is the real-valued source symbol vector; and $\mathbf{p}_b = [p_{1,b}, \ldots, p_{N_t,b}]^{\mathrm{T}} \in \mathbb{R}_{+}^{N_t \times 1}$ denotes the DC offset optical power vector which is used to guarantee the non-negativity of the transmitted signal and adjust the illumination level in the room. The signal $x_{n,b}$ transmitted by the n-th LED lamp in cell b can be given by

$$x_{n,b} = \sum\nolimits_{k=1}^{K} v_{n,k,b} s_{k,b} + p_{n,b} \tag{5.2}$$

where $v_{n,k,b}$ is the element of $\mathbf{V}_b$ in the n-th row and k-th column. From (5.1) and (5.2), the non-negative transmitted signal in VLC systems imposes the optical constraints on the precoding matrix $\mathbf{V}_b$ in each cell. Since we choose the OOK modulation with

$s_{k,b} \in \{\pm 1\}$, the data signal before adding the DC offset at the n-th LED lamp in cell b satisfies

$$-\sum_{k=1}^{K} |v_{n,k,b}| \leq \sum_{k=1}^{K} v_{n,k,b} s_{k,b} \leq \sum_{k=1}^{K} |v_{n,k,b}| \tag{5.3}$$

In order to ensure that LED lamps can operate in the limited liner optical power range, the data signal transmitted at each LED lamp satisfies

$$-\sum_{k=1}^{K} |v_{n,k,b}| + p_{n,b} \leq x_{n,b} \leq \sum_{k=1}^{K} |v_{n,k,b}| + p_{n,b} \tag{5.4}$$

To ensure that the LED lamp drive optical power in the linear region of $[p_{\min}, p_{\max}]$, where $p_{\min}$ and $p_{\max}$ denote the minimum and maximum values of the optical power. Then, combining (5.2), (5.3) and (5.4), we have

$$\begin{cases} p_{n,b} - \sum_{k=1}^{K} |v_{n,k,b}| \geq p_{\min} \\ p_{n,b} + \sum_{k=1}^{K} |v_{n,k,b}| \leq p_{\max} \end{cases} \tag{5.5}$$

Rearranging the inequalities in (5.5), we can get the constraint of each precoding element of $\mathbf{V}_b$

$$\begin{aligned} \sum_{k=1}^{K} |v_{n,k,b}| &= \|\mathbf{v}_{n,b}\|_1 \\ &\leq \min\left\{p_{n,b} - p_{\min},\ p_{\max} - p_{n,b}\right\},\ \forall n,\ \forall b \end{aligned} \tag{5.6}$$

where $\mathbf{v}_{n,b}$ is the n-th row vector of $\mathbf{V}_b$. The constraint in (5.6) enables to select available precoding matrix $\mathbf{V}_b$ in practical indoor environments.

5.2.2 Receiver Model

At the receiver, the received signal is detected by the PDs of each user and converted back to a digital signal. Then, for the user (k, b), the received signal after the direct detection can be given by

$$\begin{aligned} \mathbf{y}_{k,b} = &\underbrace{\mathbf{H}_{k,b}^{b} \mathbf{v}_{k,b} s_{k,b}}_{\text{desiredsignal}} + \underbrace{\sum_{b' \neq b}^{B} \rho_{k,b}^{b'} \sum_{m=1}^{K} \mathbf{H}_{k,b}^{b'} \mathbf{v}_{m,b'} s_{m,b'}}_{\text{ICI}} + \\ &\underbrace{\sum_{\ell=1, \ell \neq k}^{K} \mathbf{H}_{k,b}^{b} \mathbf{v}_{\ell,b} s_{\ell,b}}_{\text{IUI}} + \underbrace{\left(\mathbf{H}_{k,b}^{b} \mathbf{p}_b + \sum_{b' \neq b}^{B} \rho_{k,b}^{b'} \mathbf{H}_{k,b}^{b'} \mathbf{p}_{b'} \right)}_{\text{DCbias}} + \mathbf{n}_{k,b} \end{aligned} \tag{5.7}$$

where $\rho_{k,b}^{b'}$ denotes a set of binary variables, i.e., $\rho_{k,b}^{b'} \in \{0,1\}$, which indicates whether the user (k,b) receives ICI from the adjacent cell b' or not. If the user (k,b) receives ICI from the cell b', then $\rho_{k,b}^{b'} = 1$; otherwise $\rho_{k,b}^{b'} = 0$. $\mathbf{H}_{k,b}^{b'} \in R_{+}^{N_r \times N_t}$ denotes the optical channel matrix from the LED lamps in cell b' to the user (k,b). In (5.7), we can see that the received signal consists of five terms. The first term is the desired signal, the second and third terms are the ICI and IUI, respectively, the fourth term is the DC offset, and the last one is the additive Gaussian noise vector with zero-mean and variance of $\delta_{k,b}^2$, which consists of the shot noise and thermal noise in VLC systems [15]. We define $h_{k,b,b'}^{j,i}$ as the optical channel gain from the j-th LED lamp in cell b' to the i-th PD of the user (k,b), and $h_{k,b,b'}^{j,i}$ is one of the elements of $\mathbf{H}_{k,b}^{b'}$. $\psi_{k,b,b'}^{j,i}$ and ψ_c denote the angle of incidence and the half-angle field-of-view (FOV) of the receiver, respectively. When $0 \leq \psi_{k,b,b'}^{j,i} \leq \psi$, $h_{k,b,b'}^{j,i}$ can be expressed as

$$h_{k,b,b'}^{j,i} = \frac{A_{k,b,b'}^{j,i}}{\left(d_{k,b,b'}^{j,i}\right)^2} R_0(\phi_{k,b,b'}^{j,i}) T_s(\psi_{k,b,b'}^{j,i}) g(\psi_{k,b,b'}^{j,i}) cos\psi_{k,b,b'}^{j,i} \tag{5.8}$$

where $A_{k,b,b'}^{j,i}$ is the active area of the PD, $\phi_{k,b,b'}^{j,i}$ is the angle of irradiance, $d_{k,b,b'}^{j,i}$ denotes the distance and $T_s(\psi_{k,b,b'}^{j,i})$ is optical filter gain. $g(\psi_{k,b,b'}^{j,i})$ is the optical concentrator gain. If $0 \leq \psi_{k,b,b'}^{j,i} \leq \psi_c$, $g(\psi_{k,b,b'}^{j,i}) = \eta/\sin^2\psi_c$; otherwise, $g(\psi_{k,b,b'}^{j,i}) = 0$, where η is the refractive index. Assuming that the LEDs radiation pattern is modelled as the Lambertian pattern, the radiant intensity $R_0(\phi_{k,b,b'}^{j,i})$ can be expressed as: $R_0(\phi_{k,b,b'}^{j,i}) = (\vartheta + 1)\cos^{\vartheta}(\phi_{k,b,b'}^{j,i})/2\pi$, where $\vartheta = \ln 2/(\ln \cos \phi_{1/2})$ denotes the order of Lambertian emission with $\phi_{1/2}$ being the LEDs semi-angle at half power.

Applying the linear equalizers at receivers, the user (k,b) achieves its own desired signal by equalizing the received signal through multiplying a receiving equalizer vector $\mathbf{u}_{k,b} \in R^{N_r \times 1}$. Then, the signal for the user (k,b) after DC removal can be expressed as

$$\tilde{\mathbf{y}}_{k,b} = \sum_{b'=1}^{B} \sum_{m=1}^{K} \rho_{k,b}^{b'} \mathbf{u}_{k,b}^{\mathrm{T}} \mathbf{H}_{k,b}^{b'} \mathbf{v}_{m,b'} s_{m,b'} + \mathbf{u}_{k,b}^{\mathrm{T}} \mathbf{n}_{k,b} \tag{5.9}$$

From (5.9), the system aims to properly mitigate the interference (IUI and ICI) and recover the desired signal for each user successfully. As multiple LED lamps are cooperating with each other based on a PLC controller, different cells can exchange information (channel state information, precoders and DC offset) to perform the proposed design based on IA, which will be discussed in the next section.

5.3 IA based Interference Mitigation Design

In this section, we propose a novel joint precoder and receiving equalizer design based on IA for multi-user multi-cell MIMO VLC systems. As each user aims to recover its own desired signal successfully, the interference (IUI and ICI) should be aligned into the subspace that is orthogonal to the receiving equalizer $\mathbf{u}_{k,b}$, and the dimension of the signal space of the desired signal needs to be equal to the number of the data streams. Therefore, the conditions for the ideal IA under perfect CSI are given as follows [210-213]

$$\mathbf{u}_{k,b}^{\mathrm{T}}\mathbf{H}_{k,b}^{b}\mathbf{v}_{\ell,b}=0, \quad \forall \ell \neq k \tag{5.10a}$$

$$\mathbf{u}_{k,b}^{\mathrm{T}}\mathbf{H}_{k,b}^{b'}\mathbf{v}_{m,b'}=0, \quad \forall b' \neq b, \forall m \tag{5.10b}$$

$$\mathrm{rank}\left\{\mathbf{u}_{k,b}^{\mathrm{T}}\mathbf{H}_{k,b}^{b}\mathbf{v}_{k,b}\right\}=d, \quad \forall k,b \tag{5.10c}$$

$$\mathbf{v}_{k,b}^{\mathrm{T}}\mathbf{v}_{k,b}{=}I_d, \quad \mathbf{u}_{k,b}^{\mathrm{T}}\mathbf{u}_{k,b}=\mathbf{I}_d \tag{5.10d}$$

where d is the number of transmitted data streams, and we set d=1 in this thesis. In addition, (5.10a) and (5.10b) imply that both IUI and ICI are perfectly mitigated, and (5.10c) satisfies the number of the transmitted data streams per user. The goal of the IA scheme in multi-user multi-cell MIMO VLC systems is to design optimal precoders and receiving equalizers as in (5.10a)-(5.10c) to align the unwanted IUI and ICI without suppressing the desired signal at each receiver. In addition, the subjection in (5.10d)

shows the precoder $\mathbf{v}_{k,b}$ and receiving equalizer $\mathbf{u}_{k,b}$ being orthogonal, which has the same goal with the conditions in (5.10a), (5.10b) and (5.10c) when we apply the IA scheme [210-213].

However, the standard IA schemes are sensitive to the channel estimation error [210-213]. Under the practical channel conditions, both IUI and ICI cannot be perfectly mitigated, resulting in the performance degradation in VLC systems. Therefore, in the following subsection, we will consider the channel estimation error in our proposed design.

5.3.1 Channel Uncertainty Model

In practical MIMO VLC systems, the CSI is not perfectly available, and hence the channel estimation error should be taken into account. We set $\mathbf{H}_{k,b}^{b'}$ and $\hat{\mathbf{H}}_{k,b}^{b}$ as the perfect CSI and estimated CSI, respectively, and $\Delta\hat{\mathbf{H}}_{k,b}^{b'}$ is the channel estimation uncertainty which is assumed as the Gaussian model with zero mean and covariance matrix $\{\Delta\hat{\mathbf{H}}_{k,b}^{b'}\Delta\hat{\mathbf{H}}_{k,b}^{b'\,\mathrm{T}}\} = \delta_e^2\mathbf{I}_d$ [46, 68]. We assume that $\Delta\hat{\mathbf{H}}_{k,b}^{b'}$ is independent of $\hat{\mathbf{H}}_{k,b}^{b'}$ [46, 68]. For simplicity, we assume all channel uncertainties $\{\Delta\hat{\mathbf{H}}_{k,b}^{b'}\}$ have an equal variance δ_e^2 .

Then, considering the estimation inaccuracy, the channel matrix $\hat{\mathbf{H}}_{k,b}^{b'}$ and the norm-bounded channel uncertainty $\Delta\hat{\mathbf{H}}_{k,b}^{b'}$ can be given by [46, 68]

$$\begin{aligned} \mathbf{H}_{k,b}^{b'} &= \hat{\mathbf{H}}_{k,b}^{b} + \Delta\hat{\mathbf{H}}_{k,b}^{b} \\ \Omega_{k,b}^{b'} &= \left\{\Delta\hat{\mathbf{H}}_{k,b}^{b'} | \mathrm{Tr}\{\Delta\hat{\mathbf{H}}_{k,b}^{b'}\Delta\hat{\mathbf{H}}_{k,b}^{b'\mathrm{T}}\} \leq \varepsilon\right\} \end{aligned} \tag{5.11}$$

where ε is the radius of the channel uncertainty region. For simplicity, we assume that the channel uncertainty regions of all channel gains are the same.

5.3.2 MMSE

In order to recover the data from the received signal, we design the optimal precoder and receiving equalizer based on the MMSE criterion, i.e., minimizing the MSE of

each user in the VLC system. Then, the MSE between the recovered data and the transmitted data of the user (k, b) can be expressed as

$$\begin{aligned}\Phi_{\mathrm{MSE},k,b} &= \left[\left\|\mathbf{u}_{k,b}^{\mathrm{T}}\mathbf{y}_{k,b} - s_{k,b}\right\|_F^2\right] \\ &= \left[\mathrm{Tr}\left\{\left(\mathbf{u}_{k,b}^{\mathrm{T}}\mathbf{y}_{k,b} - s_{k,b}\right)\left(\mathbf{u}_{k,b}^{\mathrm{T}}\mathbf{y}_{k,b} - s_{k,b}\right)^{\mathrm{T}}\right\}\right] \\ &= \left[\mu^2\mathrm{Tr}\left\{\sum_{b'=1}^{B}\sum_{m=1}^{K}\mathbf{u}_{k,b}^{\mathrm{T}}\mathbf{H}_{k,b}^{b'}\mathbf{v}_{m,b'}\mathbf{v}_{m,b'}^{\mathrm{T}}\mathbf{H}_{k,b}^{b'\mathrm{T}}\mathbf{u}_{k,b}\right.\right. \\ &\quad \left.\left.-\mathbf{v}_{k,b}^{\mathrm{T}}\mathbf{H}_{k,b}^{b'\mathrm{T}}\mathbf{u}_{k,b} - \mathbf{u}_{k,b}^{\mathrm{T}}\mathbf{H}_{k,b}^{b'}\mathbf{v}_{k,b}\right]\right\} + \mu^2\end{aligned} \tag{5.12}$$

In (5.12), we assume the transmitted data $\{s_{k,b}s_{m,b'}\} = 0$, $k \neq \ell$ and $b' \neq b$, and the noise vector $\mathbf{n}_{k,b}$ are independent of $s_{k,b}$ and $\mathbf{H}_{k,b}^{b}$ [46, 68]. denotes the covariance of μ^2.

The objective function $\Phi_{\mathrm{MSE},k,b}$ in (5.12) doesnt consider the channel estimation error. Taking the channel uncertainty (5.11) into account, the function in (5.12) can be modified as

$$\begin{aligned}\widehat{\Phi}_{\mathrm{MSE},k,b} \leq \mu^2\mathrm{Tr}\Bigg(&\mathbf{u}_{k,b}^{\mathrm{T}}\left[\sum_{b'=1}^{B}\sum_{m=1}^{K}\hat{\mathbf{H}}_{k,b}^{b'}\mathbf{v}_{m,b'}\mathbf{v}_{m,b'}^{\mathrm{T}}\hat{\mathbf{H}}_{k,b}^{b'\mathrm{T}}\right. \\ &\left.+\sum_{b'=1}^{B}\sum_{m=1}^{K}\varepsilon\mathrm{Tr}\left\{\mathbf{v}_{m,b'}\mathbf{v}_{m,b'}^{\mathrm{T}}\right\}\mathbf{I}_{N_r}\right]\mathbf{u}_{k,b} - \mathbf{v}_{k,b}^{T}\hat{\mathbf{H}}_{k,b}^{b'\mathrm{T}}\mathbf{u}_{k,b} \\ &-\mathbf{u}_{k,b}^{\mathrm{T}}\hat{\mathbf{H}}_{k,b}^{b'\mathrm{T}}\mathbf{v}_{k,b}\Bigg) + \mu^2\end{aligned} \tag{5.13}$$

From (5.12) and (5.13), our goal is to design the optimal transmit precoder $\mathbf{v}_{k,b}$ and receiving equalizer $\mathbf{u}_{k,b}$ based on IA to minimize the MSE for the multi-user multi-cell VLC system while satisfying the optical power constraints (5.6). Then, the optimization problem can be formulated as

$$\min_{\mathbf{v}_{k,b},\mathbf{u}_{k,b},\forall k,\forall b}\sum_{b=1}^{B}\sum_{k=1}^{K}\widehat{\Phi}_{\mathrm{MSE},k,b} \tag{5.14a}$$

$$s.t.\mathbf{v}_{k,b}^{\mathrm{T}}\mathbf{v}_{k,b} = I_d,\forall k,\forall b \tag{5.14b}$$

$$\mathbf{u}_{k,b}^{\mathrm{T}}\mathbf{u}_{k,b} = \mathbf{I}_d,\forall k,\forall b \tag{5.14c}$$

$$\|\mathbf{v}_{n,b}\|_1 \leq \min\left\{p_{n,b} - p_{\min},\ p_{\max} - p_{n,b}\right\},\forall n,\forall b \tag{5.14d}$$

5.3.3 Solution for Interference Mitigation Design

As we can see, the problem in (5.14) is a joint optimization problem since the transmit precoders and receiving equalizers are involved and the optimization problem in (5.14) is not convex with these variables, which is hard to solve in general. Here, we divide it into two subproblems and solve them individually, and then optimize the precoder and equalizer iteratively by applying an iteration scheme.

5.3.3.1 Transmit Precoder Selection

Without loss of generality, we aim to achieve the optimal precoder of each cell by solving the problem in (5.14) when the receiving equalizer set $\{\mathbf{u}_{k,b}\}$ of all users in all cells are given. However, it is hard to implement the traditional optimization algorithms with the relaxations due to the element-wise absolute operator in the constraint (5.14d). Hence, we apply a matrix analysis to transform the optimization problem into a convex linearly constrained quadratic program (LCQP) [217]. According to the matrix analysis [217], we have the properties that $\mathrm{Tr}\{\mathbf{ABA}^{\mathrm{T}}\} = vec(\mathbf{A})(\mathbf{B}\otimes\mathbf{I})vec(\mathbf{A})^{\mathrm{T}}$ and $\mathrm{Tr}\{\mathbf{AB}\} = \mathrm{Tr}\{\mathbf{BA}\}$. In the VLC system, the matrixes and vectors are all real values, hence the first part of the objective function in (5.13) is rewritten as

$$\begin{aligned}&\mathrm{Tr}\left\{\mathbf{u}_{k,b}^{\mathrm{T}}\hat{\mathbf{H}}_{k,b}^{b'}\mathbf{v}_{m,b'}\mathbf{v}_{m,b'}^{\mathrm{T}}\hat{\mathbf{H}}_{k,b}^{b'\mathrm{T}}\mathbf{u}_{k,b}\right\}\\&= vec\Big(\mathbf{v}_{m,b'}^{\mathrm{T}}\Big)^{\mathrm{T}}\left(\hat{\mathbf{H}}_{k,b}^{b'\mathrm{T}}\mathbf{u}_{k,b}\mathbf{u}_{k,b}^{\mathrm{T}}\hat{\mathbf{H}}_{k,b}^{b'}\otimes\mathbf{I}_{N_r}\right)vec\left(\mathbf{v}_{m,b'}^{\mathrm{T}}\right)\end{aligned} \tag{5.15}$$

The above term is quadratic and hence other parts in (5.13) are linear or constant. For the above analysis, we can transform the optimization problem in (5.14) into a convex LCQP problem. And a Matlab software package is used to solve convex LCQP problems based on the semi-definite programming (SDP) (called CVX [218]), which can effectively achieve the optimal precoder $\mathbf{V}_b$ of each cell by solving the transformed problem when the receiving equalizer set $\{\mathbf{u}_{k,b}\}$ of all users in all cells are given.

5.3.3.2 Receiving Equalizer Selection

Since the constraint (5.14d) has nothing to do with the equalizer at each receiver, when the precoder $\mathbf{V}_b$ of each cell is given, the corresponding optimization problem under the channel estimation error can be expressed as

$$\min_{\mathbf{u}_{k,b},\forall k,\forall b} \sum_{b=1}^{B}\sum_{k=1}^{K} \widehat{\Phi}_{\mathrm{MSE},k,b} \tag{5.16a}$$

$$s.t. \mathbf{u}_{k,b}^{\mathrm{T}}\mathbf{u}_{k,b} = \mathbf{I}_d, \forall k, \forall b \tag{5.16b}$$

In order to achieve the receiving equalizer $\mathbf{u}_{k,b}$, we differentiate $\widehat{\Phi}_{\mathrm{MSE},k,b}$ with respect to $\mathbf{u}_{k,b}$, and get the following equation

$$\begin{aligned}\frac{\partial\widehat{\Phi}_{\mathrm{MSE},k,b}}{\partial\mathbf{u}_{k,b}} = \mathbf{u}_{k,b}^{\mathrm{T}}\Bigg(&\sum_{b'=1}^{B}\sum_{m=1}^{K}\hat{\mathbf{H}}_{k,b}^{b'}\mathbf{v}_{m,b'}\mathbf{v}_{m,b'}^{\mathrm{T}}\hat{\mathbf{H}}_{k,b}^{b'\mathrm{T}} \\ &+\sum_{b'=1}^{B}\sum_{m=1}^{K}\varepsilon\mathrm{Tr}\left\{\mathbf{V}_{m,b'}\mathbf{V}_{m,b'}^{\mathrm{T}}\right\}\mathbf{I}_{N_r}\Bigg) - \mathbf{V}_{k,b}^{T}\hat{\mathbf{H}}_{k,b}^{b'\mathrm{T}}\end{aligned} \tag{5.17}$$

Then, we set $\partial\widehat{\Phi}_{\mathrm{MSE},k,b}/\partial\mathbf{u}_{k,b}$ equal to zero, the optimal receiving equalizer for the user (k,b) can be obtained by

$$\begin{aligned}\mathbf{u}_{k,b}^{*} = \Bigg(&\sum_{b'=1}^{B}\sum_{m=1}^{K}\hat{\mathbf{H}}_{k,b}^{b'}\mathbf{v}_{m,b'}\mathbf{v}_{m,b'}^{\mathrm{T}}\hat{\mathbf{H}}_{k,b}^{b'\mathrm{T}} \\ &+\sum_{b'=1}^{B}\sum_{m=1}^{K}\varepsilon\mathrm{Tr}\left\{\mathbf{v}_{m,b'}\mathbf{v}_{m,b'}^{\mathrm{T}}\right\}\mathbf{I}_{N_r}\Bigg)^{-1}\end{aligned} \tag{5.18}$$

5.3.3.3 Iterative Algorithm

We apply an iterative method to update the precoder $\mathbf{v}_{k,b}$ and receiving equalizer $\mathbf{u}_{k,b}$ for all users in all cells iteratively, which is concisely presented in **Algorithm 1**. The objective function in (5.14a) are reduced iteratively through adjusting and updating $\mathbf{v}_{k,b}$ and $\mathbf{u}_{k,b}$ at each iteration. Hence, we can achieve the optimal precoder and receiving equalizer iteratively, and terminates when it converges. After solving the optimization of the transmit precoder and receiving equalizer in the PLC controller, the LED transmitters will send the information of the equalizer to each user. In addition, we will give the convergence analysis in the next section.

Algorithm 1 Iterative scheme for the joint design of $\mathbf{v}_{k,b}$ and $\mathbf{u}_{k,b}$

Initialization:

1: Set the optical power level $\mathbf{p}_b$ for each cell;

2: Initialize the unitary precoder matrix $\mathbf{v}_{k,b}$, $\forall k$,$\forall b$ and satisfy the constraint (5.14d);

3: Set the desired accuracy ζ and the maximum number of iterations $N^{\max}$, let $n = 1$;

Repeat:

4: Given the precoder set $\{\mathbf{V}_b\}_{b=1}^{B}$, compute $\mathbf{u}_{k,b}$ based on (5.18);

5: With all the receiving equalizer $\mathbf{u}_{k,b}$, $\forall k$, $\forall b$, update $\mathbf{v}_{k,b}$ by using the CVX software;

6: $n := n + 1$;

7: **Until:** $\frac{1}{B}\sum_{b=1}^{B} ||\mathbf{V}_b(n) - \mathbf{V}_b(n)||^2 \leq \zeta$ or $n \geq N^{\max}$, go to the next step;

Output: $\mathbf{v}_{k,b}$ and $\mathbf{u}_{k,b}$, $\forall k$, $\forall b$.

5.4 Performance Analysis

5.4.1 Data Rate Loss

In this subsection, we analyze the data rate loss performance of the proposed design. The data rate of the user (k, b) under the channel estimation error is given by $R_{k,b} = \log_2(1 + \gamma_{k,b})$, and $\gamma_{k,b}$ is the received SINR, which can be given by

$$\gamma_{k,b} = \frac{\left\| \mathbf{u}_{k,b}^{\mathrm{T}} (\hat{\mathbf{H}}_{k,b}^{b} + \Delta\hat{\mathbf{H}}_{k,b}^{b}) \mathbf{v}_{k,b} \right\|^2}{I_{k,b} + \delta_{k,b}^2} \tag{5.19}$$

where $I_{k,b}$ is the total interference of IUI and ICI to the user, which can be expressed as

$I_{k,b} = \sum_{\ell \neq k}^{K} ||\mathbf{u}_{k,b}^{\mathrm{T}} (\hat{\mathbf{H}}_{k,b}^{b} + \Delta\hat{\mathbf{H}}_{k,b}^{b}) \mathbf{v}_{\ell,b}||^2 + \sum_{b' \neq b}^{B} \rho_{k,b}^{b'} \sum_{m=1}^{K} ||\mathbf{u}_{k,b}^{\mathrm{T}} (\hat{\mathbf{H}}_{k,b}^{b'} + \Delta\hat{\mathbf{H}}_{k,b}^{b'}) \mathbf{v}_{m,b'}||^2$.

Firstly, we define the rate loss of the user as (k, b) as $\Delta R_{k,b}$, which is the difference between the ideal data rate $\tilde{R}_{k,b}$ of the user (k, b) with the ideal joint precoder and equalizer design (where full CSI is known in advance) and the data rate $R_{k,b}$ with our

proposed design. Then, the rate loss of the user (k, b) is expressed as

$$\begin{aligned}\Delta R_{k,b} &= \tilde{R}_{k,b} - R_{k,b} \\ &= E\left[\log_2\left(\delta_{k,b}^2 + \left\|\tilde{\mathbf{u}}_{k,b}^{\mathrm{T}}\mathbf{H}_{k,b}^b\tilde{\mathbf{v}}_{k,b}\right\|^2\right)\right] - E\left[\log_2\left(\delta_{k,b}^2 + I_{k,b}\right.\right. \\ &\quad \left.\left.+\left\|\mathbf{u}_{k,b}^{\mathrm{T}}\mathbf{H}_{k,b}^b\mathbf{v}_{k,b}\right\|^2\right)\right] \quad - E_{\boldsymbol{\Delta}}\left[\log_2\left(\delta_{k,b}^2\right)\right] \\ &\quad + E\left[\log_2\left(I_{k,b} + \delta_{k,b}^2\right)\right]\end{aligned} \tag{5.20}$$

where $\tilde{\mathbf{v}}_{k,b}$ and $\tilde{\mathbf{u}}_{k,b}$ denote the ideal precoder and receiving equalizer for the user (k, b). Since $I_{k,b} \geq 0$, and $\log(\cdot)$ is a strictly monotonically increasing function, we can obtain

$$\begin{aligned}&\Delta R_{k,b} \leq E\left[\log_2\left(\delta_{k,b}^2 + \left\|\tilde{\mathbf{u}}_{k,b}^{\mathrm{T}}\mathbf{H}_{k,b}^b\tilde{\mathbf{v}}_{k,b}\right\|^2\right)\right] \\ &-E\left[\log_2\left(\delta_{k,b}^2 + \left\|\mathbf{u}_{k,b}^{\mathrm{T}}\mathbf{H}_{k,b}^b\mathbf{v}_{k,b}\right\|^2\right)\right] + E\left[\log_2\left(1 + \tfrac{I_{k,b}}{\delta_{k,b}^2}\right)\right]\end{aligned} \tag{5.21}$$

Note $E[\log_2(1 + ||\tilde{\mathbf{u}}_{k,b}^{\mathrm{T}}\mathbf{H}_{k,b}^b\tilde{\mathbf{v}}_{k,b}||^2)] = E[\log_2(1 + ||\mathbf{u}_{k,b}^{\mathrm{T}}\mathbf{H}_{k,b}^b\mathbf{v}_{k,b}||^2)]$, based on the Theorem 1 in [219]. Using the Jensens inequality, the upper bound of the data rate loss of the user is

$$\Delta R_{k,b} \leq E\left[\log_2\left(1 + I_{k,b}/\delta^2\right)\right] \leq \log_2\left(1 + E\left[I_{k,b}\right]/\delta_{k,b}^2\right) \tag{5.22}$$

From (5.20)-(5.22), we can comprehend that one of the key effects on the data rate loss is determined by the power of the interference leakage, such as IUI and ICI. Therefore, the design of the precoder $\mathbf{v}_{k,b}$ and receiving equalizer $\mathbf{u}_{k,b}$ is important in the multi-user multi-cell MIMO VLC systems. Hence, this thesis proposes the joint precoder and equalizer design based on IA for ICI and IUI mitigation in multi-user multi-cell MIMO VLC systems.

5.4.2 Convergence of the Proposed Design

For the optimization problem in (5.14), we can observe that the proposed design based on IA aims to minimize the objective function in (5.14a) by using the iterative method to update the precoder $\mathbf{v}_{k,b}$ and receiving equalizer $\mathbf{u}_{k,b}$, k=1,$\cdots$,K, b=1,$\cdots$,B. Firstly, we

minimize the objective function (5.14a) by fixing the set of the variables $\mathbf{u}_{k,b}$, k=1,$\cdots$,K, b=1,$\cdots$,B, so that the optimization problem in (5.14) reduces to a convex function of the variables $\mathbf{v}_{k,b}$, k=1,$\cdots$,K, b=1,$\cdots$,B, which can be solved by using the CVX tool. Then, by giving a set of the precoder variables $\mathbf{v}_{k,b}$, k=1,$\cdots$,K, b=1,$\cdots$,B, we obtain the receiving equalizer variables $\mathbf{u}_{k,b}$,k=1,$\cdots$,K, b=1,$\cdots$,B by minimizing the objective function (5.14a). The objective function is nonnegative, and it is reduced by adjusting the set of precoder and receiving equalizer variables at each iteration. As a result, the convergence of the proposed design can be achieved [210-212].

5.4.3 Comparison with Existing Popular Designs

Generally, the MMSE design [46, 68] and the sum-rate maximization design [207] are the two existing popular designs applied to improve the system performance in VLC systems. However, the works in [46, 68] only investigated the system performance in single-cell VLC systems without considering ICI mitigation or in multi-cell VLC systems without considering IUI mitigation. Hence, when applying these two designs in multi-user multi-cell MIMO VLC system, the optimization problems can be expressed as follows:

(i) The joint precoder and receiving equalizer design based on MMSE [46, 68] (denoted as the MMSE design):

$$\begin{aligned} &\min_{\mathbf{V}_{k,b},\mathbf{U}_{k,b},\forall k,\forall b} \left[||\mathbf{u}_{k,b}^{\mathrm{T}}\mathbf{y}_{k,b} - s_{k,b}||_F^2 \right] \\ &s.t.\ \ \|\mathbf{v}_{n,b}\|_1 \leq \min\left\{p_{n,b} - p_{\min},\ p_{\max} - p_{n,b}\right\},\ \ \forall n,\ \ \forall b \end{aligned} \tag{5.23}$$

As the solution of the optimization problem in (5.23) is similar to that in [46, 68], we do not give the details of the solution process.

(ii) The joint precoder and receiving equalizer design based on the sum-rate maxi-

mization design [207] (denoted as the max-rate design):

$$\begin{aligned} &\max_{\mathbf{V}_{k,b},\mathbf{U}_{k,b,\forall k,\forall b}} \quad \sum_{k=1}^{K} \log\left(1+\gamma_{k,b}\right) \\ &s.t. \quad \gamma_{k,b} \geq \bar{\gamma}_{k,b}, \forall k \\ &\left\|\mathbf{v}_{n,b}\right\|_1 \leq \min\left\{p_{n,b}-p_{\min},\ p_{\max}-p_{n,b}\right\},\ \forall n,\ \forall b \end{aligned} \tag{5.24}$$

Since the solution of the optimization problem in (5.24) is similar to that in [207], we do not give the details of the solution process.

From the above two optimization problem formulations of the MMSE and max-rate designs, we can observe that these two designs still fail to consider both ICI and IUI mitigations simultaneously in multi-user multi-cell VLC systems, resulting in the transmission rate loss according to the rate loss analysis in Section IV.A. Hence, this motivates us to propose the joint precoder and equalizer design based on IA in multi-user multi-cell MIMO VLC systems.

5.4.4 Computational Complexity Analysis

Here, we analyze the computational complexity of the proposed design and compare it with the MMSE and max-rate designs. For our proposed design, in order to update the receiving equalizer $\mathbf{u}_{k,b}$ for the user (k,b), it requires the following computational operations: (i) computing $\sum_{b'=1}^{B}\sum_{m=1}^{K}\mathbf{H}_{k,b}^{b'}\mathbf{v}_{m,b'}\mathbf{v}_{m,b'}^{\mathrm{T}}\mathbf{H}_{k,b}^{b'\mathrm{T}}$ in $O(2BKN_tN_r+BKN_t^2)$, (ii) computing the inversion in $O(N_r^3)$, and (iii) the matrix multiplications of commuting $\mathbf{H}_{k,b}^{b'}\mathbf{v}_{m,b'}$ in $O(N_tN_r)$. Then, the total computational complexity of updating the receiving equalizers $\mathbf{u}_{k,b}$, k=1,$\cdots$,K, b=1,$\cdots$,B for all users in all cells is $O(BK(2BKN_tN_r+BKN_t^2+N_tN_r+N_r^3))$. In order to get the precoder $\mathbf{v}_{k,b}$, we directly solve the transformed optimization problem (5.14) using the CVX software package, and the complexity for the precoder calculation in the problem (5.14) is $O(B(N_t+N_rK)^{9/2}\log(1/\zeta))$ [220], where ζ is the accuracy target. Then, the overall complexity of the proposed design is $O(L(BK(BKN_tN_r+BKN_t^2+N_tN_r+N_r^3+$

Table 5.1: Simulation Parameters

Parameters	Values		Parameters	Values
Room size (length × width × height)	8 m × 8 m × 3 m		PD concentrator refractive index	1.5
Number of cells	4		PD area	0.5 cm^2
Number of LED lamps per cell	2		Gain of optical filter	1.0
Number of users per cell	2		PD responsivity	0.5 A/W
Number of PDs per user	2		PD full-angle FOV	120°
LED half-angle FOV	60°		System bandwidth	20 MHz
LED Lambertian emission order	1			

$B(N_t + N_rK)^{9/2}\cdot\log(1/\zeta)))$, where L denotes the number of the iterations until the convergence of the proposed design. When applying the MMSE design, the total complexity of this design is $O(L(BK(BKN_tN_r+BKN_t^2+N_tN_r+N_r^3+B(N_t + N_rK)^{9/2}\log(1/\zeta)))$. Through the above complexity analysis of the two existing designs, our proposed design has the similar complexity as the MMSE design. It is necessary to note that the proposed design and the MMSE design have a higher computational complexity than that of the max-rate design in multi-user multi-cell MIMO VLC systems, but they can provide a better performance than the max-rate design, and we will give the performance analysis in the next section.

5.5 Numerical Results and Discussions

In this section, we evaluate the performance of our proposed joint precoder and equalizer design and compare it with the MMSE design and the max-rate design. In order to make the fair performance comparison, the channel estimation error is considered in both the MMSE and max-rate designs.

The system parameters used in this thesis are listed in Table 5.1. The receiving plane is 2.15 m below the room ceiling. For the channel estimation error, we use

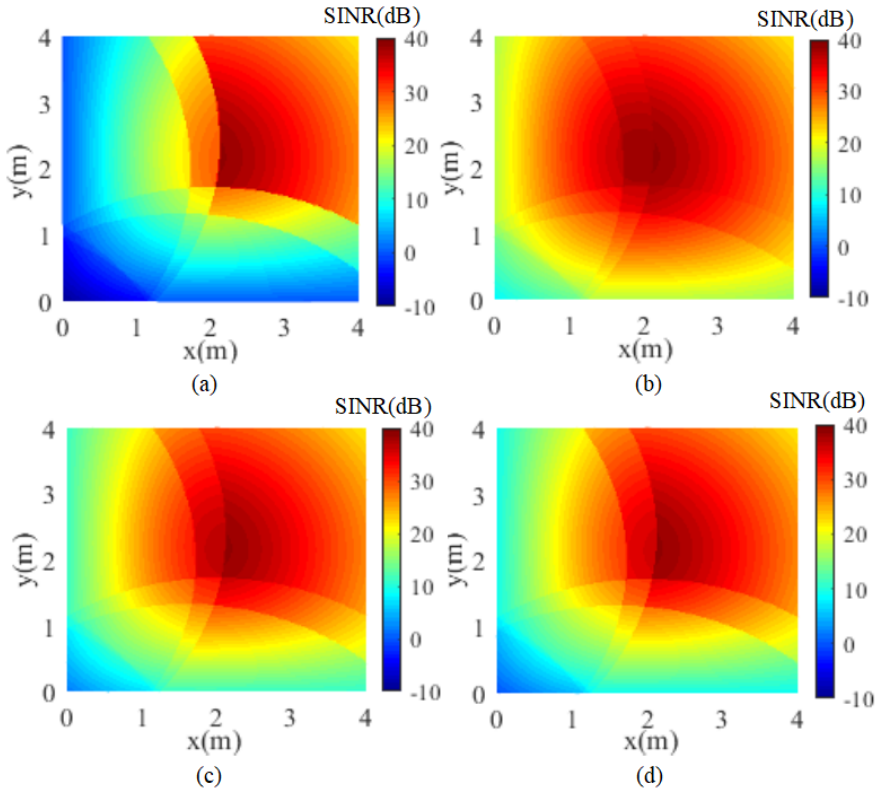

Figure 5.2: The SINR distribution (a) without any design, (b) with our proposed design, (c) with the MMSE design and (d) with the max-rate design.

the normalized error standard deviation: $\sigma = \delta_e/(||vec(\tilde{\mathbf{H}}_{k,b}^{b'})||_1/N_tN_r)$ [46, 68]. The spacing between two adjacent LED lamps in the same cell and the spacing between two PDs of each user are denoted by L_t and L_r, respectively. The four LED lamps in each cell are installed at the center of ceiling. Without loss of generality, the optical power $p_{n,b}$ of each LED lamp is set to be identical as $p_{n,b} = p$, $\forall n$, $\forall b$, and the limited dynamic range of the optical power p per LED lamp can be varied from 4 to 22 W (note: $p_{\min}$=4 W, $p_{\max}$=22 W) [221].

Fig. 5.2 shows the SINR distributions of one cell (i.e. a quarter of the room) for different designs, where the spacing of LED lamps is L_t=0.7 m and the optical power per LED lamp is 12 W. From Fig. 5.2, we can observe that the SINR values on

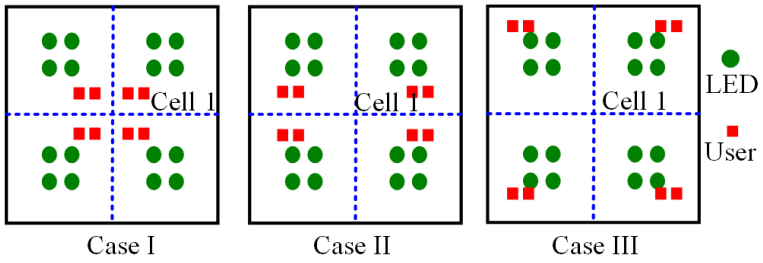

Figure 5.3: Three cases of users' locations for the four-cell VLC system.

the boundaries of adjacent cells are low, especially for the original SINR distribution without any design in Fig. 5.2 (a). However, our proposed joint precoder and equalizer design based on IA significantly outperforms other designs in terms of the average SINR performance on the boundaries of adjacent cells, because our proposed design aims to choose optimal precoders and receiving equalizers based on the IA technique, which can effectively minimize the ICI. Therefore, our proposed design based on IA has the advantage of the ICI suppression in multi-cell VLC systems.

In this subsection, we evaluate the performance with the three cases of the users locations. Firstly, we give the following three cases of users' locations when the spacing of LED lamps and PDs are L_t=0.7 m and L_r=0.07 m, receptively. The three cases of users locations are shown in Fig. 5.3. Here, we only give parameters with one quadrant (i.e. Cell 1) of the indoor room in Table 5.2, due to the geometric symmetry of the locations of four cells in the room. Case I: users locate in the totally overlapped area, where they suffer ICI from other three adjacent cells. Case II: users locate in the partially overlapped area, where they suffer ICI only from one adjacent cell. Case III: users locate in the non-overlapped area, where they do not suffer ICI from adjacent cells. All users in the above three cases receive IUI in its own cell.

Fig. 5.4 and Fig. 5.5 show the throughput and BER performance of the three designs with the different optical power levels and three cases of users locations, when the channel estimation error is $\sigma = 0.025$. We can see that all the three designs

Table 5.2: Locations of the in the Cell 1 (Unit: m)

	PDs of User 1	PDs of User 2
Case I	[0.6, 1.0, 0.85] [0.7, 1.0, 0.85]	[1.0, 1.0, 0.85] [1.1, 1.0, 0.85]
Case II	[2.8, 1.0, 0.85] [2.9, 1.0, 0.85]	[3.2, 1.0, 0.85] [3.3, 1.0, 0.85]
Case III	[2.8, 3.0, 0.85] [2.9, 3.0, 0.85]	[3.2, 3.0, 0.85] [3.3, 3.0, 0.85]

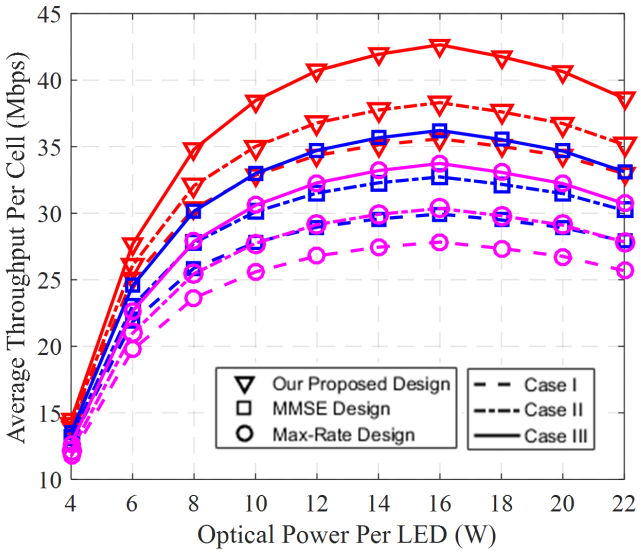

Figure 5.4: Average throughput per cell vs. optical power per LED lamp.

enhance the system performance as the optical power increases when p is less than p_{ave}=($p_{\min}$+$p_{\max}$)/2=16 W, but the performance degrades when p exceeds p_{ave}. This is because the constraint in (5.14d) determines the available set of precoding matrix. The feasible range of precoding matrix becomes large as p increases when $p \leq p_{\text{ave}}$, hence a better solution can be obtained in the system with this broader range of precoding matrix. In contrast, the feasible range of the precoding matrix becomes limited with the increase of p when $p \geq p_{\text{ave}}$, which degrades the system performance under this situation.

From Fig. 5.4 and Fig. 5.5, we can observe that the performance of the Case III is

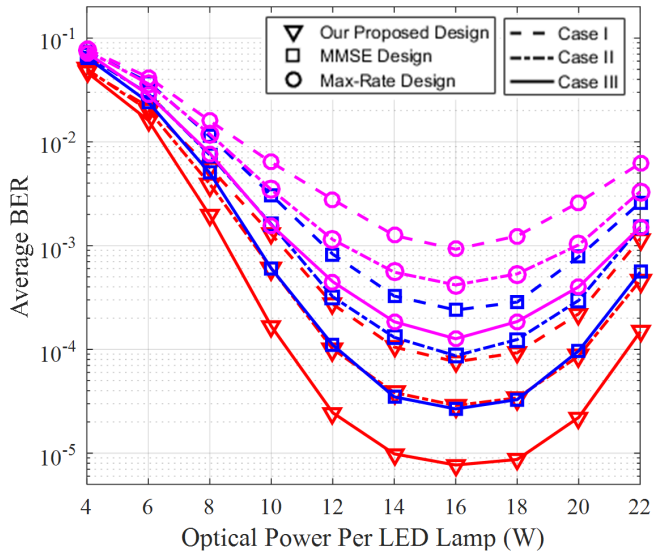

Figure 5.5: Average BER performance vs. optical power per LED lamp.

better than that of the Cases I and II. This is because that the users in last two cases suffer ICI from adjacent cells, which degrades the system performance, especially the users in Case I suffer serious ICI due to their locations in the totally overlapped area.

From Fig. 5.4 and Fig. 5.5, our proposed design achieves much higher throughput and better BER performance than other two designs. Especially, the advantage becomes more significant in the high optical power region (from 8 to 22 W). This is because the interference is one of the key factors on the data rate loss as the background noise is no longer dominant. Our proposed joint precoder and equalizer design based on IA mitigates both IUI and ICI effectively, and hence the performance is improved compared with other two designs. As shown in Fig. 5.4, when the optical power is 12 W per LED lamp, our proposed design achieves a throughput improvement of up to 18.2% and 28.7% compared with the MMSE design and the max-rate design under Case I, respectively. As shown in Fig. 5.5, our proposed design can save about 1.4 and 4.3 W transmit optical power per LED lamp as compared with the MMSE design and the max-rate design at a target BER of 10^{-3} under Case I, respectively.

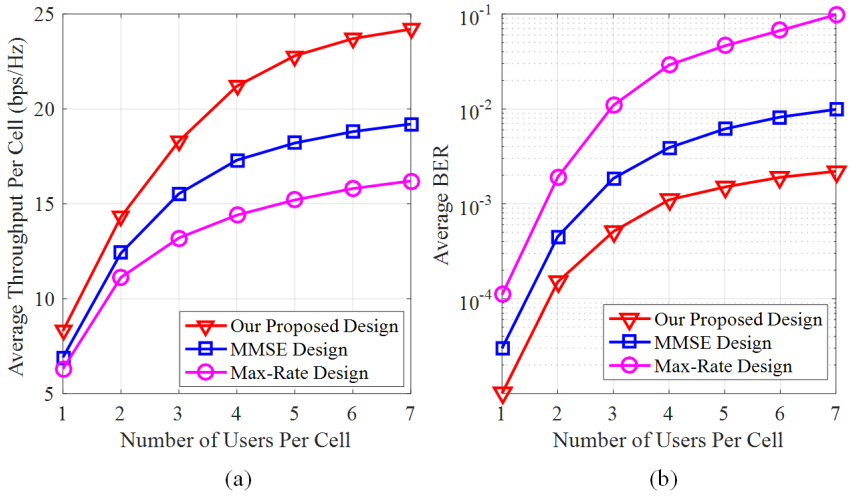

Figure 5.6: Performance comparisons vs. the different numbers of users per cell.

Figs. 5.6 (a) and (b) show the average throughput per cell and average BER performance under different numbers of users per cell when the optical power per LED is p= 12W and the channel estimation error is $\sigma = 0.025$. (Note: We run the simulation 500 times with random user locations and obtain the average statistics). We can observe that both the average throughput per cell and the average BER increase with the increased number of users per cell. When there are more users within a cell, the inter-user interference becomes higher, which has a negative effect on the throughput improvement and the BER performance. That is why the throughput improvement is not obviously when the number of users is large in VLC systems. However, compared with the other designs, the proposed design based on IA has the better performance by effectively suppressing both the IUI and ICI. Moreover, the gap of the performances obtained by the proposed design and the other two designs becomes larger with the increased number of users, which indicates that the proposed design is more suitable for VLC systems with a large number of users.

In Figs. 5.7 (a) and (b), we show the throughput and BER performance for all the three designs under different levels of channel estimation error (we take the Case I as an

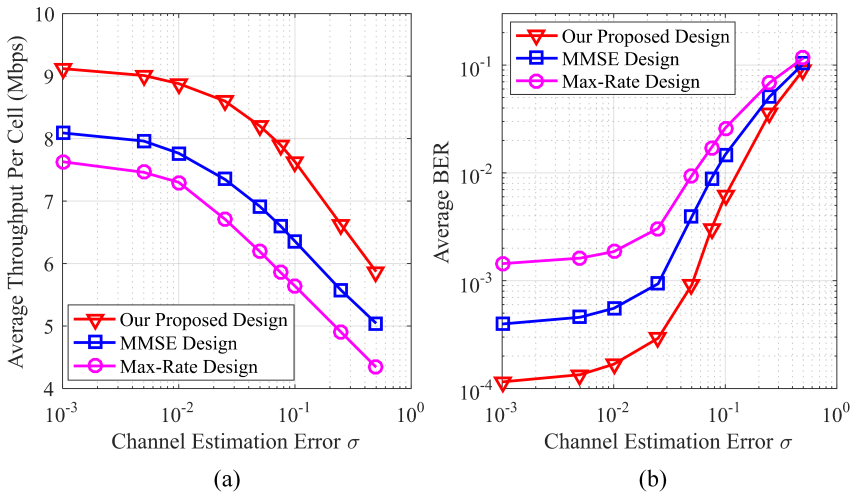

Figure 5.7: Performance comparisons against the channel estimation error.

example), when the optical power per LED is p= 12 W, and the spacing of LED lamps and spacing of PDs are L_t=0.7 m and L_r=0.07 m, respectively. It can be observed that the performance of all three approaches degrades as the increase of channel estimation error value. This is because under a relatively high channel estimation error value, the optimal design of precoders and receiving equalizers is unable to cancel IUI and ICI perfectly, and hence the degradation of the system performance at the high channel estimation error value becomes obviously. However, among the three designs, the max-rate design is most sensitive to the channel estimation error, while our proposed design based on IA achieves the better performance than other two designs over all the channel estimation error values.

Figs. 5.8 (a) and (b) depict the throughput and BER performance for all the three designs with different LED/PD spacing (L_t, L_r) in cm (we take the Case I as an example), when the optical power per LED lamp is p= 12W and the channel estimation error is $\sigma = 0.025$. We can see that a smaller LED/PD spacing results in a considerable throughput reduction. This is because the smaller LED/PD spacing leads to a higher channel correlation in the MIMO VLC system, resulting in the noise enhancement at

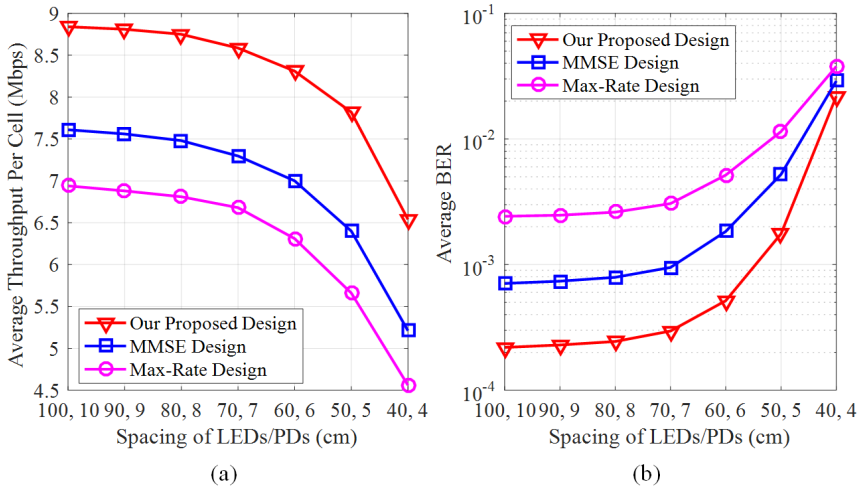

Figure 5.8: Performance comparisons vs. the spacing of LEDs/PDs.

the receivers. However, our proposed design still achieves the best throughput and BER performance among the three designs.

In short, our proposed design achieves the better throughput and BER performance than the other two designs under the different channel estimation error and small LED/PD spacing in multi-user multi-cell MIMO VLC systems.

Fig. 5.9 presents the performance convergence of the achievable throughput per cell for the three designs when the transmit optical power is 12 W per LED lamp, the channel estimation error is $\sigma = 0.025$ as well as the spacing of LEDs/PDs are L_t=0.7 m and L_r=0.07 m. We can see that the proposed design has almost the same convergence rate as the other two designs, and the throughput converges after about 22 iterations. Moreover, the proposed design achieves the higher throughput than other two designs. In addition, for the real length of the execution for the proposed solution to obtain a final result, the three solutions need about 0.63 second to achieve the convergence point conducted in the Matlab 2016a environment on a PC with Intel(R) Core (TM) i7-6700 CPU @ 3.40 GHz, 16 RAM, and the operating system is Windows 10 Ultimate 64 bits.

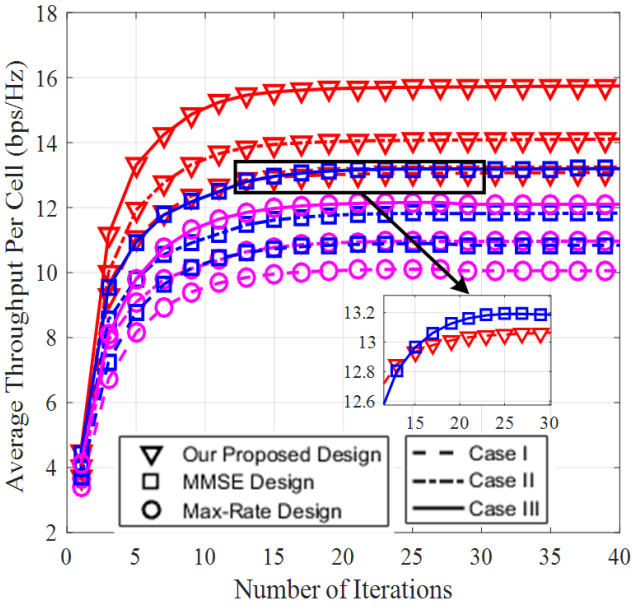

Figure 5.9: Convergence for the three designs.

5.6 Conclusion

In this chapter, I propose a novel joint precoder and receiving equalizer design based on IA for multi-user multi-cell MIMO VLC systems under imperfect CSI, in order to effectively mitigate both IUI and ICI. Specifically, we formulate the joint optimization problem by minimizing the system MSE under the unique optical power constraints in VLC. Furthermore, we take into account the channel estimation error in our formulated optimization problem when designing the optimal precoders and receiving equalizers in multi-user multi-cell MIMO VLC systems. Numerical results show that the proposed design achieves a better system capacity and BER performance as compared with the MMSE and max-rate designs. When the optical power is 12 W per LED lamp, our proposed scheme achieves a throughput improvement of up to 18.2% and 28.7% as compared with the MMSE and max-rate designs, respectively. In addition, the proposed design saves about 1.4 and 4.3 W optical power per LED lamp as compared

with the MMSE and max-rate designs, respectively, at a targeted BER of 10^{-3}.

Chapter 6

Energy-Efficient Resource Management by Heterogeneous RF/VLC for IoT Networks

6.1 Introduction

With the various application services of devices (e.g. mobile phones, monitors, and sensors) in wireless networks, Internet of Things (IoT) has been emerging as a promising vision for the next generation networks through realizing the smart manufacturing, smart grid, and smart city [222, 223]. In order to overcome the shortcoming of the limited bandwidths in RF band and provide high-speed transmission rate for indoor devices, many studies [224, 225] have reported VLC for indoor IoT networks to offer the high data transmission rates and guarantee different QoS requirements of IoT devices. In [224], a VLC-based IoT architecture was presented for indoor and outdoor deployments of VLC systems. Considering that there exist energy-constrained IoT devices, the literatures [225] and [226] proposed the light energy harvesting models to support both the communication services and energy harvesting purposes.

However, VLC still remains some key challenges, e.g., strong dependence on LoS links and small coverage [7, 21]. To overcome the limitations, researchers presented

hybrid or heterogeneous RF/VLC networks with high reliable properties [70, 152, 227-223], where RF is capable of offering reliable connectivity with the wide-area coverage and VLC can provide the high transmission data rate. In hybrid RF and VLC networks, load balancing technology has been proposed to optimize the network association with considering devices' QoS requirements, where the literatures [70, 152, 227, 228] studied the vertical handover between VLC and RF communications, while Li *et al.* [229] investigated several cooperative formations of VLC cells to improve the network throughput. In such a network, due to the specific statistical delay constraints of devices, the resource allocation under delay-guarantee constraints was considered into the optimization problem [230, 231]. In addition, the authors in [73, 232, 233] proposed RF/VLC access point selection approaches to ensure users' QoS requirements in heterogeneous networks, especially, the reinforcement learning (RL) tool is applied to solve the decision making problem in heterogeneous RF/VLC networks [232, 233].

Besides the sum data rate improvement and the network latency decrease, the EE maximization in heterogeneous RF/VLC networks have been investigated recently [72, 74, 158, 234], which is an important performance metric in wireless communications. The authors in [72] and [74] proposed energy-efficient subchannel and power allocation approaches to maximize EE under the minimum data rate requirements of users in hybrid or heterogeneous RF/VLC networks, while Khreishah *et al.* [158] focused on the power consumption minimization and the acceptable illumination level maintenance. In addition, a coordinated beamforming approach was proposed to maximize the network EE with considering QoS constraints in downlink heterogeneous RF/VLC networks [234]. The above reported works have the ability to improve the communication performance, but the practical indoor environments may have different QoS requirements, such as IoT devices may need high transmission data rates while industrial IoT devices (industrial purpose, sensors, machines, robots etc.) generally have strict latency and reliability requirements [235]. For instance, industrial automation may require

end-to-end latencies in the range of 1-5 ms with the transmission reliability of 99.999 % or higher [235, 236].These networks will be highly complex and heterogeneous under different QoS requirements. In addition, the joint uplink and downlink resource management has not been investigated before in heterogeneous RF/VLC networks.

Motivated by the above observations, this chapter presents an energy-efficient resource management based on the heterogeneous RF/VLC architecture for industrial networks to guarantee the diverse requirements (high reliability, low latency and high data rate) of IIoT and IoT devices [237, 238]. In the network, RF is capable of offering the reliable connectivity and VLC has the ability to provide high transmission data rate. A joint uplink and downlink resource management (network selection, subchannel assignment and power management) approach is proposed to satisfy different QoS requirements, and the energy-efficient resource management problem is modelled as a RL framework, thus the network is capable of intelligently making decisions based on the instantaneous observations. In order to enable the IoT network with high intelligence, a new deep post-decision state (PDS) based experience replay and transfer (PDS-ERT) RL algorithm is proposed to realize intelligent resource management, with the purpose of maximizing the network EE while ensuring the minimum data rate constraints and the strict URLLC requirements. Simulation results corroborate the superiority in performance of the presented heterogeneous network, and verify that the proposed PDS-ERT learning algorithm outperforms other existing algorithms in terms of meeting the EE and the QoS requirements.

The rest of this chapter is organized as follows. The heterogeneous RF/VLC network architecture is presented in Section 6.2. Section 6.3 formulates the energy-efficient resource management problem. The proposed deep PDS-ERT learning algorithm is provided in Section 6.4. Simulation results are presented in Section 6.5 and Section 6.6 concludes the chapter. The content of this chapter is related to the author's work provided in [237, 238].

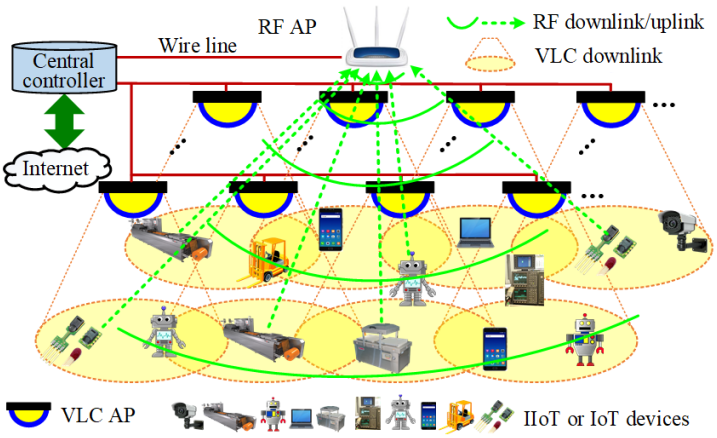

Figure 6.1: The indoor heterogeneous RF/VLC IoT network.

6.2 System Model

6.2.1 Heterogeneous RF/VLC IoT Network Architecture

The IoT network may consist of a large number IoT devices (computers, smartphones, tablets etc.) and IIoT devices (sensors, machines, actuators, robots etc.), as shown in Fig. 6.1, resulting in different QoS requirements of communication services, such as ranging from high reliability and low latency to high data rates. Conventional RF networks may fail to support the large number of devices with different QoS requirements due to the limited RF spectrum and energy resources. To address these issues, we present a new heterogeneous RF/VLC network structure to support different QoS requirements in IoT networks.

First of all, we divide the IIoT and IoT devices into two groups based on their different QoS requirements:

Group 1: the URLLC services of the devices (generally are IIoT devices) have specific requirements on low latency and high reliability but have much looser constraints on the high date rate. For example, each sensor reports a small amount of collected data to the central controller (uplink) or the central controller sends the low bit rate information to each actuator(downlink) within the strict latency requirements.

Group 2: the normal services of the devices (commonly are IoT devices) have the high data rate requirements but are less interested in the latency and reliability requirements, such as the high quality image, video and webpage.

We set that the devices in the **group 1** are with the higher priority to access the channel resource to guarantee the high reliability and low latency requirements, while the devices in the **group 2** are with the lower priority to access channel resource.

A heterogeneous RF/VLC IoT network architecture is presented to support the above mentioned different services, as shown in Fig. 6.1, where a number of VLC APs (refer to femtocells) are uniformly attached on the room ceiling and one RF AP (refers to microcell) is placed in the center. Each VLC AP contains one LED lamp based luminaries devices offering both lighting requirements and communications services, and every VLC AP covers a confined area to generate a small optical cell. By contrast, the RF AP provides the coverage for the entire room. Both the VLC and RF APs connect the Internet to perform the communication services, where VLC APs broadcast information to devices through visible light signals and the RF AP provides communication services by the RF signals. Considering the unpractical components and challenges of the wireless VLC uplink [147, 149. 239], VLC only offers the downlink data streams while RF provides both the uplink and downlink data streams. We would like to mentioned that due to human activities and device mobility, the VLC LoS communication link may be intermittently interrupted or blocked of a number for time slots, called blocked LoS VLC links, and the blocked VLC links may not support general communication services [147, 149]. Under this heterogeneous network, RF is capable of offering wide-area coverage and VLC has the ability to provide high transmission data rate due to the abundant bandwidth resources across multiple optimal cells. Motivated by the above analysis, the RF AP mainly provides the URLLC services of the devices in **group 1** due to its wide-area coverage, while VLC APs mainly support the normal services of the devices in **group 2** due to its offering high transmission data rate.

In addition, the IoT device's priority depends on its QoS requirements or application services, when the IoT device changes its application services, it will report this information to the central controller in the IoT network by the RF uplink, and hence the IoT device will be assigned to the channel resource based on its current priority. For example, one device in **group 2** with the normal service currently applies the URLLC services with the low latency and high reliability, it will report this information to the central controller and then it will be classified into **group 1** with the higher priority to access the channel resource to guarantee the high reliability and low latency requirements.

In the IoT network, a number of IIoT and IoT devices are randomly distributed on the floor, where the device (mainly IIoT device) requiring the URLLC service is equipped one RF enabled transceiver, and the device (mainly IoT device) needing the uplink/downlink data rate is equipped with one VLC receiver (called PD) and one RF enabled transceiver. The network selection (RF or VLC) decision-making problem can be formulated as a MDP with the goal of maximizing the reward function, and solved with the proposed RL algorithm, which will be provided in Section 5.3 and Section 5.4.

The number of VLC APs, devices, subchannels per VLC AP and subchannels per RF AP are denoted by C, K, N^{VLC} and N^{RF}, respectively. The set of VLC APs and devices are denoted as $\mathcal{C} = \{1, \ldots, C\}$ and $\mathcal{K} = \{1, \ldots, K\}$, respectively. Let $\mathcal{N}^{\mathrm{VLC}} = \{1, \ldots, N^{\mathrm{VLC}}\}$ and $\mathcal{N}^{\mathrm{RF}} = \{1, \ldots, N^{\mathrm{RF}}\}$ represent the subchannel sets of per VLC AP and RF AP, respectively, where the subchannels for VLC are reused across all optical cells. The network employs OFDMA to serve devices.

6.2.2 VLC Channel Model

In VLC networks, the VLC LoS links can support the successful communication services while the blocked LoS VLC links cannot provide the high transmission data rate services [147, 149]. For the VLC link, the LOS channel gain from one AP to one device is

expressed as

$$h^{\mathrm{VLC}} = \frac{(\vartheta+1)A_r}{2\pi(d^{\mathrm{VLC}})^2}\cos^{\vartheta}(\phi)T_s(\psi)g(\psi)cos\psi \tag{6.1}$$

where A_r is the active area of the PD. d^{VLC} and ψ denote the distance and the angle of incidence between the LED and the device, respectively. ϕ is the angle of irradiance from the LED to the device. ϑ is the order of Lambertian emission with $\vartheta = -\ln 2/(\ln\cos\phi_{1/2})$ with $\phi_{1/2}$ being the LED's semi-angle at half power. $T_s(\psi)$ and $g(\psi)$ are the gain of the optical filter and the optical concentrator gain at the PD, respectively. $g(\psi)$ can be expressed as: $g(\psi) = \eta/\sin^2\psi_c$ when $0 \le \psi \le \psi_c$, and $g(\psi) = 0$ if $\psi_c < \psi$, where ψ_c and η are the semi-angle FOV of the PD and the refractive index, respectively.

As shown in Fig. 6.1, due to the multiple VLC APs deployment, the devices locate in the overlapped areas may suffer ICI from adjacent cells. If the k-th device ($k \in \mathcal{K}$) is assigned to VLC AP $c \in \mathcal{C}$ on the n-th subchannel ($n \in \mathcal{N}^{\mathrm{VLC}}$), the received SINR of the device is expressed as [72, 232, 233]

$$\gamma_{k,n}^{\mathrm{VLC}} = \frac{\mu^2 P_{n,c}^{\mathrm{VLC}}(h_{k,n,c}^{\mathrm{VLC}})^2}{\mu^2\sum_{c'\in\mathcal{C}} P_{n,c'}^{\mathrm{VLC}}(h_{k,n,c'}^{\mathrm{VLC}})^2 + N_0^{\mathrm{VLC}}B_{sub}^{\mathrm{VLC}}} \tag{6.2}$$

where μ is the PD's responsivity, $P_{n,c}^{\mathrm{VLC}}$ indicates the allocated transmit electrical power on the n-th subchannel of the c-th VLC AP, $h_{k,n,c}^{\mathrm{VLC}}$ is the VLC channel gain from the c-th VLC AP to device k on the n-th subchannel, N_0^{VLC} represents the power spectral density (PSD) of noise at the PD, B_{sub}^{VLC} is the subchannel bandwidth $B_{sub}^{\mathrm{VLC}} = B^{\mathrm{VLC}}/N^{\mathrm{VLC}}$ with B^{VLC} being the VLC transmission bandwidth.

Hence, the data rate of k-th device associated by VLC AP c can be expressed as

$$R_k^{\mathrm{VLC}} = \sum_{n\in\mathcal{N}^{\mathrm{VLC}}} \rho_{k,n,c}^{\mathrm{VLC}}\frac{B_{sub}^{\mathrm{VLC}}}{2}\log_2(1+\gamma_{k,n,c}^{\mathrm{VLC}}) \tag{6.3}$$

where $\rho_{k,n,c}^{\mathrm{VLC}}$ is a binary variable, $\rho_{k,n,c}^{\mathrm{VLC}} \in \{0,1\}$, $\rho_{k,n,c}^{\mathrm{VLC}}$ =1 represents that the k-th device assigns the n-th subchannel of VLC AP c ; otherwise, $\rho_{k,n,c}^{\mathrm{VLC}}$ =0. The scaling factor 1/2 is due to the Hermitian symmetry [184, 197].

6.2.3 RF Channel Model

Each indoor room deploys one RF AP to be acted as one cell. The device may receive the ICI from adjacent rooms, when the device locates in the overlapped areas. In the RF network, the channel gain captures both the path loss and the channel fading, which is typically given by [240]

$$g_{k,n}^{\mathrm{RF}} = 10^{-PL_k[dB]/10} \tag{6.4}$$

where $PL_k[dB]$ is the RF path loss of the k-th device in dB, which is expressed as [240]

$$PL_k[dB] = A\log_{10}(d_k^{\mathrm{RF}}) + B + E\log_{10}(f_c/5) + X \tag{6.5}$$

where d_k^{RF} is the distance from the RF AP to the k-th device and f_c denotes the carrier frequency in GHz. A, B and E are constants depending on the propagation model. For the LOS propagation, A=18.7, B= 46.8 and E = 20. For NLOS scenario, we have A= 36.8, B= 43.8 and E= 20. X indicates the wall penetration loss in the NLOS scenario, we set $X = 5(N_{\mathrm{wall}} - 1)$ for thin walls or obstacles, where N_{wall} is the number of obstacles between the RF AP and the device.

Let M denote the number of the adjacent indoor rooms (or adjacent cells) and let m denote the m-th adjacent indoor room. For downlink, if the k-th device is assigned to the RF AP on the n-th subchannel ($n \in \mathcal{N}^{\mathrm{RF}}$), the received SINR of the device is given by

$$\gamma_{k,n}^{\mathrm{RF,D}} = \frac{P_n^{\mathrm{RF,D}} g_{k,n}^{\mathrm{RF}}}{\sum_{m=1}^{M} P_{n,m}^{\mathrm{RF,D}} g_{k,n,m}^{\mathrm{RF}} + N_0^{\mathrm{RF}} B_{sub}^{\mathrm{RF}}} \tag{6.6}$$

where $P_n^{\mathrm{RF,D}}$ and $P_{n,m}^{\mathrm{RF,D}}$ are the allocated transmit power on the n-th subchannel of the corresponding RF AP and the m-th adjacent RF AP, respectively. $g_{k,n,m}^{\mathrm{RF}}$ is the RF interference channel gain from the RF AP in the m-th adjacent RF cell to the

k-th device. N_0^{RF} represents the PSD of noise at the receiver, B_{sub}^{RF} is the subchannel bandwidth $B_{sub}^{\mathrm{RF}} = B^{\mathrm{RF}}/N^{\mathrm{RF}}$ with B^{RF} being the RF AP bandwidth.

For uplink, the received SINR at the RF AP from the k-th device on the n-th subchannel is

$$\gamma_{k,n}^{\mathrm{RF,U}} = \frac{P_{k,n}^{\mathrm{RF,U}} g_{k,n}^{\mathrm{RF}}}{\sum_{m=1}^{M} P_{k',n,m}^{\mathrm{RF,U}} g_{k',n,m}^{\mathrm{RF}} + N_0^{\mathrm{RF}} B_{sub}^{\mathrm{RF}}} \tag{6.7}$$

where $P_{k,n}^{\mathrm{RF,U}}$ and $P_{k',n,m}^{\mathrm{RF,U}}$ are the transmit power of the k-th device on subchannel n in its associated cell and the the k'-th device on subchannel n in the m-th adjacent RF cell, respectively. $g_{k',n,m}^{\mathrm{RF}}$ is the RF interference channel gain from the k'-th device in the m-th adjacent RF cell to the current RF AP.

Hence, the achievable data rates of downlink and uplink are defined as

$$R_k^{\mathrm{RF,D}} = \sum_{n \in \mathcal{N}^{\mathrm{RF}}} \rho_{k,n}^{\mathrm{RF,D}} B_{sub}^{\mathrm{RF}} \log_2(1 + \gamma_{k,n}^{\mathrm{RF,D}}) \tag{6.8}$$

$$R_k^{\mathrm{RF,U}} = \sum_{n \in \mathcal{N}^{\mathrm{RF}}} \rho_{k,n}^{\mathrm{RF,U}} B_{sub}^{\mathrm{RF}} \log_2(1 + \gamma_{k,n}^{\mathrm{RF,U}}) \tag{6.9}$$

respectively, where $\rho_{k,n}^{\mathrm{RF,D}}$ and $\rho_{k,n}^{\mathrm{RF,U}}$ are the channel assignment indicators, and they are binary values of "1" or "0".

6.3 Network Requirements and Problem Formulation

In this section, we formulate the energy-efficient resource management problem (joint network selection, subchannel assignment and power management) in the heterogeneous RF/VLC IoT network with the objective of maximizing the network EE while guaranteeing the QoS requirements of IIoT or IoT devices. We take these practical requirements into account as constraints in the mathematical way, and the decision making problem is modelled as a MDP [232, 233, 241].

6.3.1 Requirements of IIoT and IoT Devices

1) URLLC requirements: The real-time industrial control applications (URLLC services) have strict latency and transmission reliability requirements, but they are not interested in the high data rate. This subsection investigates how to model the URLLC requirements in a mathematical way.

For URLLC services, we assume that the k-th IIoT device or transmitter follows the independent and identically distributed Poisson distribution with the packet arrival rate λ and the data packet size L^{packet} in bytes [242]. Generally, the total latency (T_{l}) of one packet consists of the waiting time of the packet to be served in the queue (T_{w}), the transmission time (T_{t}), the channel access delay (T_{a}), the backhaul delay (T_{b}), the packet reception delay (T_{r}) and the processing delay (T_{p}), which can be expressed as [243]

$$T_{\text{l}} = T_{\text{w}} + T_{\text{t}} + T_{\text{a}} + T_{\text{b}} + T_{\text{r}} + T_{\text{p}} \tag{6.10}$$

In (6.10), the transmission time of one packet is calculated by $T_{\text{t}} = L^{\text{packet}}/R^{\text{d}}$, where R^{d} is the achievable link data rate.

Due to the latency requirement, each packet in URLLC should be successfully transmitted in a limited time duration. Let $T_{\max}$ denote the maximum tolerable latency threshold of each transmission packet, the latency constraint can be guaranteed by controlling the probability of T_{l} exceeding the threshold value $T_{\max}$, which can be expressed as

$$p^{\text{Lat}} = \Pr\left\{T_{\text{l}} \geq T_{\max}\right\} \leq p^{\text{Lat}}_{\max} \tag{6.11}$$

where $p^{\text{Lat}}_{\max}$ denotes the maximum violation probability.

In this thesis, the outage probability is used to characterize the reliability requirement and it can be defined as the probability that the received SINR ($\gamma_{k,n}$) at the

receiver is lower than the target threshold $\gamma_{k,n}^{\text{tar}}$. Then, the requirement on the reliability is satisfied by controlling the outage probability, $\Pr\{\gamma_{k,n} < \gamma_{k,n}^{\text{tar}}\}$. And the outage probability cannot beyond the violation probability $p_{\max}^{\text{Rel}}$, which can be given by

$$p_m^{\text{Rel}} = \Pr\left\{\gamma_{k,n} < \gamma_{k,n}^{\text{tar}}\right\} \leq p_{\max}^{\text{Rel}} \tag{6.12}$$

2) Minimum data rate requirements: As illustrated above, for the normal services, some IIoT devices and IoT devices may require the high data rates, though the latency is of less significance. Hence, the minimum data rate requirements of these devices should be considered in resource management. Let R_k denote the k-th device' current data rate, the minimum data rate requirement can be satisfied by controlling the probability of the unsatisfied normal service (p_k^{Nor}), where R_k fails to achieve its minimum data rate threshold $R_k^{\min}$, which can be given by

$$p_k^{\text{Nor}} = \Pr\{R_k < R_k^{\min}\} \leq p_{\max}^{\text{Nor}} \tag{6.13}$$

where $p_{\max}^{\text{Nor}}$ denotes the maximum violation probability.

6.3.2 Problem Formulation

The total achievable data rate and the total power consumption can be calculated as

$$R = \sum_{k\in\mathcal{K}}\sum_{c\in\mathcal{C}} \alpha_{k,c} R_{k,c}^{\text{VLC}} + \sum_{k\in\mathcal{K}} \beta_k R_k^{\text{RF,D}} + \sum_{k\in\mathcal{K}} \beta_k R_k^{\text{RF,U}} \tag{6.14}$$

$$\begin{aligned} P = {} & C P_{\text{fix}}^{\text{VLC}} + P_{\text{fix}}^{\text{RF}} + \sum_{k\in\mathcal{K}}\sum_{c\in\mathcal{C}} \sum_{n\in\mathcal{N}^{\text{VLC}}} \alpha_{k,c}\rho_{k,n,c}^{\text{VLC}} P_{n,c}^{\text{VLC}} \\ & \sum_{k\in\mathcal{K}} \Big(\sum_{n\in\mathcal{N}^{\text{RF}}} (\rho_{k,n}^{\text{RF,D}} P_n^{\text{RF,D}} + \rho_{k,n}^{\text{RF,U}} P_{k,n}^{\text{RF,U}}) + P_{\text{cir}} \Big) \end{aligned} \tag{6.15}$$

respectively, where $\alpha_{k,l}$ and β_k denote the association between a device and a VLC AP or a RF AP, respectively, both having binary values of "1" or "0" to indicate that there exists a selection or no selection exists. In addition, $P_{\text{fix}}^{\text{RF}}$ and $P_{\text{fix}}^{\text{VLC}}$ denote the fixed power consumption of the RF AP and each VLC AP, respectively, resulting from the AP

hardware power consumption (circuit operation, data processing, backhaul connection, etc.). Note that $P_{\text{fix}}^{\text{VLC}}$ also includes the optical power using for illumination. P_{cir} is the circuit power consumption of one device.

Our goal is to maximize the network EE (EE is defined as the radio of the overall data rate and the total power consumption: $\eta_{EE} = R/P$) while guaranteeing the mentioned QoS requirements of devices in Section 6.3.1. This chapter presents a utility function (also called reward function) in the heterogeneous integrate RF/VLC IoT network, which can be expressed as

$$r = \eta_{EE} - \omega_1 \sum_{k \in \mathcal{K}} p_k^{\text{Lat}} - \omega_2 \sum_{k \in \mathcal{K}} p_k^{\text{Rel}} - \omega_3 (\sum_{k \in \mathcal{K}} p_k^{\text{Nor}}) \tag{6.16}$$

where the part 1 is the network benefit (the overall EE in Kbit/J), the part 2, part 3 and part 4 are the cost functions in terms of the unsatisfied latency, unsatisfied reliability and unsatisfied minimum data rate requirements, respectively. The coefficient ω_i, $i \in \{1, 2, 3\}$ are the weights of the last three parts, which are used to balance the benefit and the cost.

Similar to the works [232, 233, 241], this work adopts MDP to model the intelligent resource management decision making in indoor IoT neworks. Generally, MDP can be defined as a tuple $(\mathcal{S}, \mathcal{A}, \mathbb{P}, r, \xi)$, where the main elements of the MDP can be defined as:

Agents: The RF AP, VLC APs and active devices.

State space $\mathcal{S}$: In the heterogeneous IoT network, the network state can be defined as the subchannel occupy status (idle or busy), the channel quality (SINR value), the service application types (normal services (low priority) and URLLC services (high priority)), service satisfaction (reliability, latency and minimum data rate).

Action space $\mathcal{A}$: In each time slot, the agent will take the action $a \in \mathcal{A}$ according to the current state s, where the action includes the VLC or RF AP selection, the subchannel assignment and the transmit power management.

Transition probability $\mathbb{P}$: The transition probability $\mathbb{P}(s'|s,a)$ captures the probability that the agent takes the action $a \in \mathcal{A}$ from the state $s \in \mathcal{S}$ to a new state $s' \in \mathcal{S}$.

Reward r: After taking one action, the agent will obtain an immediate reward r from the environment where the learning process is driven by the reward. We have built the reward function shown in (6.16), which decides that the policy that the agent finds. $\xi \in [0,1)$ is a discount factor.

Policy: The policy is a function that can be deterministic or stochastic, which decides the the action selection with the given state. Let $\pi(s)$ denotes a policy: $\pi(s) : \mathcal{S} \rightarrow \mathcal{A}$, which is a mapping from the state space $\mathcal{S}$ to the action space $\mathcal{A}$.

In heterogeneous IoT network, each agent tries to search the policy $\pi(s)$ to improve its immediate reward r. Let $V^{\pi}(s)$ denotes the value function, which is also a cumulative discounted reward, and it can be calculated by

$$\begin{aligned} V(s) &= E_{\pi}\left\{\sum_{t=1}^{\infty}\gamma^{t} r(s_t,a_t)|s_0 = s\right\} \\ &= E_{\pi}\left\{r(s,a_t) + \xi \int_{s'\in S}(s'|s,a)V(s')ds'\right\} \end{aligned} \tag{6.17}$$

The optimal strategy $\pi^{*}(s)$ can be achieved by satisfying the Bellman equation: $V^{*}(s) = \max_{a\in A} V(s)$ [241]. Once the optimal strategy $\pi^{*}(s)$ is achieved by maximizing the cumulative reward from the beginning, it implements the intelligent resource management in heterogeneous IoT networks.

Q-learning is a well-known RL algorithm for policy learning in wireless networks. Let $Q(s,a)$ denote the Q-function of the state-action pair (s, a), which is also the expected utility. The value function $V(s)$ is the maximum Q-function over the feasible actions at the sate s. The Q-function can be updated at the end of each time stage, which is

$$Q_{t+1}(s_t,a_t) = (1-\alpha_t)Q_t(s_t,a_t) + \alpha_t\left[r(s_t,a_t) + \xi V_t(s_{t+1})\right] \tag{6.18}$$

where $\alpha_t \in (0,1]$ is a time-varying learning rate. When the learning rate α_t admits $\sum_{t=1}^{\infty}\alpha_t = \infty$ and $\sum_{t=1}^{\infty}\alpha_t^2 < \infty$, then the Q-function $Q_t(s,a)$ will converge to the

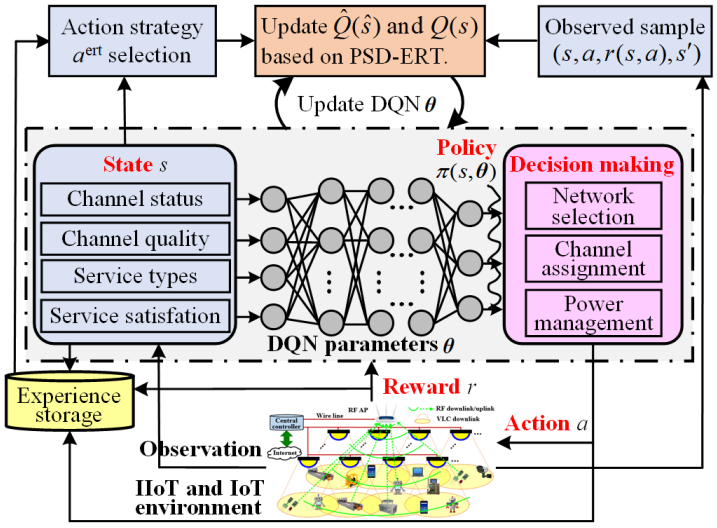

Figure 6.2: Deep PDS-ERT learning based intelligent resource management.

optimal value $Q^*(s,a)$ by $V_t(s_t) = \max_{a \in A} Q_t(s_t, a_t)$ [241].

6.4 Proposed Deep PDS-ERT-based Intelligent Resource Management

As illustrated in the above section, the policy can be numerically learned by adopting the Q-learning, policy gradient schemes and DQN algorithms [241]. However, Q-learning cannot deal with continuous state-action spaces and the policy gradient may converge to the local optimal position. Although DQN has the ability to handle the continuous control problem under high-dimensional sensory inputs, its nonlinear function approximator is known to be unstable or even to diverge. Moreover, it also needs a large number training samples to guarantee the training efficiency, all the above mentioned factors may limit the application in URLLC IoT IoT networks.

To overcome the above problems, we propose a deep PDS-ERT learning algorithm, as shown in Fig. 6.2, to accelerate the learning rate, enhance the learning efficiency and ensure the learning stability towards the optimal policy for the resource management in the heterogeneous IoT network. In details, the agent can utilize the learned strategies

from the historical experience and the other agents, and integrate the PDS-learning principle into the conventional DRL to learn the unknown dynamics. The main procedures of the proposed PDS-ERT learning based intelligent resource management are presented in the following subsections.

6.4.1 Experience Replay and Transfer

In RL, the policy strategy $\pi(s, a)$ determines the resource management strategy in heterogeneous IoT networks. In order to improve the learning efficiency, a modified experience replay and transfer mechanism is presented for policy learning by utilizing the historical knowledge or using the learned knowledge from other agents.

1) Policy strategy selection: One of the important processes of the experience replay and transfer mechanism is that how to find the most useful learned policy strategy (e.g., network selection, subchannel assignment and power management) from the historical knowledge, or search one agent as the expert agent to utilize the learned policy strategy from the expert. Instead of blindly searching the expert agent or the historical experience [233], the agent calculates the similarity level between the current agent and other active agents (or the historical knowledge) by evaluating the following three metrics: (1) service information, which refers to URLLC services and the normal services; (2) the device information, which includes the device position and mobility behavior; (3) the channel information, which contains the channel SINR values and assignment indicators, etc.

The mentioned similarity can be calculated by applying the Bregman Ball method [241], where Bregman Ball is acted as the minimum manifold with a central Z_{cen}, and a radius R_{rad}. Any information point Z_{poi} is inside this ball, and the agent searches the information point which has the most strong similarity with Z_{cen}. The distance between any information point and the central Z_{cen} is expressed as [244]

$$B(Z_{\text{cen}}, R_{\text{rad}}) = \{Z_{\text{poi}} \in Z : D(Z_{\text{poi}}, Z_{\text{cen}}) \leq R_{\text{rad}}\} \tag{6.19}$$

where $D(a, b)$ is the Bregman divergence [244], which is also the manifold distance between two data points. Once the highest similarity value between the learning agent and the expert agent or historical information is achieved, the learning agent can utilize the policy strategy.

2) Overall action strategy: As analyzed above, after finding the most suitable historical policy or transferred policy strategy by adopting the experience replay and transfer mechanism [40], the agent utilizes the learned action strategy a^{ert} and its current native action a^{na} to generate an overall action. Accordingly, at the state s, the overall action can be selected by

$$a^{\text{ov}} = \varsigma a^{\text{ert}} + (1 - \varsigma) a^{\text{na}} \tag{6.20}$$

where $\varsigma \in [0, 1]$ denotes the transfer rate, which will be reduced after every learning step to gradually remove the effect of the historical or transferred policy information on the new policy.

3) Experience collection: In order to avoid storing the unreliable experience, after interacting with the environment, the learned experience $e_t = (s_t, a_t, r_t, s_{t+1})$ with the best reward is recorded in the relay memory. If the capacity of the relay is full, the relay memory will make room for the new collected experience by the following two steps.

i) Experience combination: We combine some historical experience data into one data point if they have similar functions by using the the Bregman Ball concept [39].

ii) Experience deletion: If the capacity of the memory is full and the new collected experience needs to be stored in the memory, the least used historical experience is deleted from the memory. Because the least used experience have tiny contribution to the learning process.

6.4.2 Deep PDS-ERT Learning based Resource Management

In this subsection, deep PDS-ERT is developed by incorporating the experience replay and transfer mechanism into the deep PDS-learning algorithm. In particular, instead of directly using the selected native action strategy a_t^{na} to update the Q-function $Q(s_t)$, the historical or transferred action strategy a_t^{ert} can be utilized to exploit the extra information to improve learning speed and efficiency. Similar to the classical PDS [242], PDS-ERT can be described as the immediate network state that is achieved after the known information occurs, but before the unknown information takes place.

After achieving the corresponding overall action a_t^{ov} by (6.20), each deep PDS-ERT learning agent obtains an immediate known reward $r_{\mathrm{k}}(s_t, a_t^{\mathrm{ov}})$ and then the state s_t transits to the post-decision sate $\hat{s}_t$ ($\hat{s}_t \in \hat{S}$ with $\hat{S}$ being the set of PDS-ERT) with a known transition probability $\mathbb{P}_{\mathrm{k}}(\hat{s}_t|s_t, a_t^{\mathrm{ov}})$. Afterward, PDS-ERT transits the current state $\hat{s}_t$ to the next state s_{t+1} with an unknown transition probability $\mathbb{P}_{\mathrm{u}}(s_{t+1}|\hat{s}_t, a_t^{\mathrm{ov}})$ and an unknown reward $r_{\mathrm{u}}(\hat{s}_t, a_t^{\mathrm{ov}})$ is feedback to the agent. Mathematically, the transition probability from the current state s_t to the next state s_{t+1} with PDS-ERT admits

$$\mathbb{P}(s_{t+1}|s_t, a_t^{\mathrm{ov}}) = \int_{\hat{s}\in\hat{\mathbb{S}}} \mathbb{P}_{\mathrm{u}}(s_{t+1}|\hat{s}_t, a_t^{\mathrm{ov}})\mathbb{P}_{\mathrm{k}}(\hat{s}_t|s_t, a_t^{\mathrm{ov}})d\hat{s} \tag{6.21}$$

The reward consists of the known and unknown rewards at $\hat{s}_t$ and s_{t+1},

$$r(s_t, a_t^{\mathrm{ov}}) = r_{\mathrm{k}}(s_t, a_t^{\mathrm{ov}}) + \int_{\hat{s}\in\hat{\mathbb{S}}} \mathbb{P}_{\mathrm{k}}(\hat{s}_t|s_t, a_t^{\mathrm{ov}})r_{\mathrm{u}}(\hat{s}_t, a_t^{\mathrm{ov}})d\hat{s} \tag{6.22}$$

Then, the PDS-ERT quality Q-function with the PDS-ERT state-action pair $(\hat{s}_t, a_t^{\mathrm{ov}})$ and the general Q-function can be expressed as, respectively

$$\hat{Q}_t(\hat{s}_t, a_t^{\mathrm{ov}}) = r_{\mathrm{u}}(\hat{s}_t, a_t^{\mathrm{ov}}) + \int_{s_{t+1}\in\mathbb{S}} \mathbb{P}_{\mathrm{u}}(s_{t+1}|\hat{s}_t, a_t^{\mathrm{ov}})V_t(s_{t+1})ds \tag{6.23}$$

$$Q_t(s_t, a_t^{\mathrm{ov}}) = r_{\mathrm{k}}(\hat{s}_t, a_t^{\mathrm{ov}}) + \int_{\hat{s}\in\hat{\mathbb{S}}} \mathbb{P}_{\mathrm{k}}(\hat{s}_t|s_t, a_t^{\mathrm{ov}})\hat{Q}_t(\hat{s}_t, a_t^{\mathrm{ov}})d\hat{s} \tag{6.24}$$

After obtaining the sample $(s_t, a_t, r_{\mathrm{k}}(\hat{s}_t, a_t^{\mathrm{ov}}), \hat{s}_t, r_{\mathrm{u}}(\hat{s}_t,\ a_t^{\mathrm{ov}}), s_{t+1})$, the PDS-ERT quality value function is updated

$$\hat{Q}_{t+1}(\hat{s}_t, a_t^{\mathrm{ov}}) = (1-\alpha_t)\hat{Q}_t(\hat{s}_t, a_t^{\mathrm{ov}}) + \alpha_t[r_{\mathrm{u}}(\hat{s}_t, a_t^{\mathrm{ov}}) + \xi V_t(s_{t+1})] \tag{6.25}$$

After obtaining $\hat{Q}_{t+1}$ in (6.25), Q_{t+1} can be updated in (6.24) by replacing $\hat{Q}_t$ by $\hat{Q}_{t+1}$.

According to the above presented PDS-ERT, the deep PDS-ERT learning algorithm is presented to solve the intelligent resource management problem. As shown in Fig. 6.2, in the proposed deep PDS-ERT learning algorithm, at each time stage, after updating Eq. (6.23) and (6.24) on the overall action a_t^{ov} and the observed sample $(s_t, a_t, r(s_t, a_t), s_{t+1})$ by PDS-ERT, the classical DQN is applied to approximate the Q-function $Q(s_t, a_t^{\mathrm{ov}}, \boldsymbol{\theta}_t)$ of $Q(s_t, a_t^{\mathrm{ov}})$ through minimizing the following loss function at each time stage

$$L_t(\boldsymbol{\theta}_t) = \{r(s_t, a_t^{\mathrm{ov}}) + \xi \max_{a \in \mathcal{A}} Q_t(s_{t+1}, a_{t+1}^{\mathrm{ov}}, \boldsymbol{\theta}_t) - Q_t(s_t, a_t^{\mathrm{ov}}, \boldsymbol{\theta}_t)\}^2 \tag{6.26}$$

One key feature of using DQN is to sample the loss functions in (6.26) at each iteration to reduce the computational cost for the large-scale-state learning problems [241, 244]. The procedures to implement DQN can be found in [241, 244].

The DQN parameters $\boldsymbol{\theta}$ can be achieved by applying the gradient descent method, which is given by

$$\boldsymbol{\theta}_{t+1} = \boldsymbol{\theta}_t + \beta_{\boldsymbol{\theta}_t} \nabla Loss_t(\boldsymbol{\theta}_t) \tag{6.27}$$

where $\beta_{\boldsymbol{\theta}_t}$ is the learning rate of the DQN parameters $\boldsymbol{\theta}_t$.

After that, each agent (RF AP, VLC AP and device) will take the action based on the selected policy strategy $\pi(s_t, \boldsymbol{\theta_t})$, which can be achieved by

$$\pi(s_t, \boldsymbol{\theta}_t) = \arg\max_{a \in \mathcal{A}} \{Q_t(s_t, a_t^{\mathrm{ov}}, \boldsymbol{\theta}_t)\} \tag{6.28}$$

Theorem 1: The proposed PDS-ERT learning converges to the optimal point of the MDP when the learning rate α_t admits $\sum_{t=1}^{\infty} \alpha_t = \infty$ and $\sum_{t=1}^{\infty} \alpha_t^2 < \infty$.

Proof: If each action is executed under an infinite number of iterations, in other words, the learning policy is greedy with the infinite explorations, the function $Q(s, a)$ and the policy strategy $\pi(s, a)$ will gradually converge to the final points, respectively, with a probability of 1 [241, 242]. Due to space limitations, please see [232, 245] for the full proof.

As most DRL algorithms, my proposed deep PDS-ERT learning based resource management consists of two stages, the training stage and implement stage [241], [244] and [245]. The training process of the proposed allocation is shown in **Algorithm 1**. We denote the sets of the historical state space and action space in the memory as $\mathcal{S}'$ and $\mathcal{A}'$, respectively, and denote the current state space and action space as $\mathcal{S}$ and $\mathcal{A}$, respectively.

For the training stage, it needs a large number of the collected data to train the learning model. In DNN, let L, Z_0 and Z_l denote the training layers, the size of the input layer (which is proportional to the number of states) and the number of neurons in the l-th layer. The computational complexity in each time step for the agent is $O(Z_0 Z_l + \sum_{l=1}^{L-1} Z_l Z_{l+1})$. In the training phase, each mini-batch has Z^{epi} episodes with each episode being T time steps, each trained model is completed over I iterations until convergence. Hence, the total computational complexity in DNN is $O\left(IZ^{\text{epi}}T(Z_0 Z_l + \sum_{l=1}^{L-1} Z_l Z_{l+1})\right)$. The high computational complexity of the DNN training phase can be performed offline for a finite number of episodes at a centralized powerful unit (such as the central controller) [241], [245].

In ERT, since the relay buffer size is D, the system requires to make both updating and sampling $O\left(\log_2(D)\right)$ operations, so the computation complexity of the ERT scheme is $O\left(\log_2(D)\right)$.

According the above analysis, the complexity of the DQN algorithm and the deep PDS-ERT learning algorithm are $O\left(IZ^{\text{epi}}T(Z_0Z_l+\sum_{l=1}^{L-1}Z_lZ_{l+1})+|\mathcal{S}|^2\times|\mathcal{A}|)\right)$ and $O\left(IZ^{\text{epi}}T(Z_0Z_l+\sum_{l=1}^{L-1}Z_lZ_{l+1})+|\mathcal{S}|^2\times|\mathcal{A}|+|\mathcal{S}'|^2\times|\mathcal{A}'|)+\log_2(D)\right)$, indicating that the complexity of the proposed algorithm is slightly higher than the classical DQN learning algorithm. However, our proposed algorithm achieves the better performance than the classical DQN algorithm, which have been shown in the Section 6.5.

It worth noting that the trained DQN models for agents rarely need to be updated; updates happen when the environment have been greatly changed, possibly once a week or even a month, mainly depending on the environment dynamics and service requirements [241, 242, 245]. .

At one decision stage (implement state), the sample complexity of the action selection and learning update of the classical Q-learning algorithm and DQN are $O(|\mathcal{S}|\times|\mathcal{A}|)$ and $O(|\mathcal{S}|^2\times|\mathcal{A}|)$ [241, 242, 245], respectively. As expected, the proposed deep PDS-ERT learning algorithm by utilizing the historical learning ecperience. Here, the sample complexity of the action selection and learning update of the proposed deep PDS-ERT learning algorithm is $O(|\mathcal{S}'|^2\times|\mathcal{A}'|+|\mathcal{S}|^2\times|\mathcal{A}|)$ [241, 242, 245], which is relatively higher than that of the classical Q-learning algorithm and the DQN learning algorithm.

In addition to the above mentioned extra computational complexity, our proposed deep PDS-ERT learning algorithm needs a memory of $|\mathcal{S}'|\times|\mathcal{A}'|$ to store the historical learning knowledge, compared with the classical Q-learning algorithm and the DQN learning algorithm [241, 242, 245].

We would like to mention that the training time is quite long in my python platform, but the training time is not included into the time of the decision making time. After training the learning model (which can be assume the learning model has already existed), so the network only directly load the learning model to make decision in the implement stage, where the response time of the decision making in my python simulation platform is about 1.87 ms per epoch in a PC with Intel(R) Core (TM) i7-

6700 CPU @ 3.40 GHz, 16 RAM, and the operating system is Windows 10 Ultimate 64 bits, which is available in the real-time communication networks. As suggested, I have added the above discussion in Section 6.4.2 in the revised thesis.

The proposed deep PDS-ERT learning algorithm based intelligent resource management in heterogeneous RF/VLC IoT networks is shown in **Algorithm 1**.

Algorithm 1 Deep PDS-ERT Learning based Intelligent Resource Management

Input: the discount factor ξ, IIoT and IoT environment simulators and the samples of historical knowledge.

Initialize: the network state s_0, value function $V(s_0)$, policy strategy $\pi(s_0)$, and the DQN with parameters $\boldsymbol{\theta}_0$;
for each time step t=0, 1, 2, ... **do**
  The agent observes the state s_t;
  if the agent applies new services or has poor performance **then**
    Search the expert agent with the highest similarity;
    Obtain the transferred action strategy a_t^{ert} from the expert;
    Select the overall action by (6.20) and update the transfer rate ς;
    Perform deep PDS-ER from step 10 to step 17;
  else
  The agent selects the action a_t^{na} with a probability ε or choose a_t^{na} by satisfying $a_t^{\text{na}} = \arg\max_{a\in\mathcal{A}} Q_t(s_t, a, \boldsymbol{\theta})$;
  Search the historical action a_t^{ert} with the highest similarity from the experience replay memory;
  With a_t^{na} and a_t^{ert}, calculate the overall action a_t^{ov} by (6.20);
  After executing action a_t^{ov}, the agent gets the reward $r(s_t, a_t^{\text{ov}})$ and observes a new state s_{t+1} from the environment;
  The agent stores the experience $e_t = (s_t, a_t^{\text{ov}}, r(s_t, a_t^{\text{ov}}), s_{t+1})$ into its replay memory. If the capacity of the relay memory is full, the least used historical experience is dropped;
  Observe PDS tuple $(s_t, a_t^{\text{ov}}, \hat{s}_t, r(s_t, a_t^{\text{ov}}), s_{t+1})$, the agent updates the Q-function $\hat{Q}_t(\hat{s}_t, a_t^{\text{ov}})$ and $Q_t(s_t, a_t^{\text{ov}})$ by (6.23) and (6.24), respectively;
  Update the DQN parameters $\boldsymbol{\theta}_t$ by (6.27);
  Reset the DQN evaluation network by $\boldsymbol{\theta}_{t+1}$=$\boldsymbol{\theta}_t$;
  end if
end for
Output: RF/VLC network selection, subchannel assignment and power management.

6.5 Numerical Results and Analysis

In this section, simulation results are conducted in Python to evaluate the performance of our presented heterogeneous RF/VLC IoT network and the proposed deep PDS-ERT

learning based intelligent resource management.

We consider an indoor IoT room with the area of 24m×24m×6m, where 6×6 VLC APs (uniform distribution) and a RF AP (locate in the center) are distributed at a height of 5 m. Additionally, the room is entirely covered by the RF AP. A number of devices ($K/2$ IIoT devices and $K/2$ IoT devices) are randomly distributed at four different heights (0.5m, 1m, 1.5m and 2m). The RF AP has the carrier frequency of 2.4 GHz, the bandwidth of B^{RF}=10 MHz, the number subchannels of N^{RF}=32, the maximum transmit power of 250 mW, the fixed power consumption of $P_{\mathrm{fix}}^{\mathrm{RF}}$=6.7 W, and the PSD noise of N_0^{RF}=-173 dBm/Hz [184, 197]. Each VLC AP has the transmission bandwidth of B^{VLC}=20 MHz (the available bandwidth is 10 MHz due to the Hermitian symmetry [184, 197]), the number of subchannels N^{VLC}=16, the maximum transmit electronic power of 250W, the fixed power consumption of $P_{\mathrm{fix}}^{\mathrm{VLC}}$=4W and the PSD noise of $N_0^{\mathrm{VLC}} = 10^{-21}\mathrm{A}^2/\mathrm{Hz}$. Each device has the circuit power consumption of P_{cir}=5mW and the maximum transmit power of $P_{k,\max}^{\mathrm{RF}}$=30mW. The LED lamp semi-angle at half power and Lambertian emission order are 60^o and 1, respectively. The active area, the FOV, the concentrator refractive index and the responsivity of the PD are 1 cm^2, 90^o, 1.5 and 0.5 A/W, respectively. The gain of the optical filter is 1.

For the URLLC services, we set the maximum latency threshold T_{max}=1ms with $T_{\mathrm{a}} + T_{\mathrm{b}}$=0.1ms and $T_{\mathrm{r}} + T_{\mathrm{p}}$=0.3ms [243], the transmission reliability is 0.999 with each message size being 250 bytes and the SINR threshold is 5dB. For the normal services, the minimum data rate is set as 3 Mbps in downlink and 0.5 Mbps in uplink. Each time slot is 1ms. LOS blocking probability for both VLC and RF links is 0.05. We set ω_1=ω_2=10^5 and ω_3=2×10^4 to balance the benefit and the costs in (6.16) [232, 233]. In RL, the discount parameter ξ=0.98 and the learning rate a_t=0.02. The DNN has three hidden layers with each hidden layer being with 50 neurons.

In this section, we present the performance comparisons of the following IoT networks: 1. our presented heterogeneous RF/VLC IoT network (denoted by RF/VLC);

2. the network service is performed using two RF APs (denoted by RF/RF) and the two carrier frequencies are 2.4 GHz and 5 GHz, where the network total bandwidth is 20 MHz to ensure a fair comparison with the RF/VLC network. Moreover, we also compare the performance of our proposed deep PDS-ERT learning algorithm based intelligent resource management with the following existing algorithms: 1. Deep PDS learning [245] (denoted by Deep PDS [245]); 2. Q-learning algorithm with knowledge transfer [233] (denoted by QKT-learning [233]); 3. decomposing the optimization problem into two subproblems: i). network selection and subchannel assignment, ii). transmit power management, and solve it iteratively in a centralized way, similar to [72] (denoted as Baseline 1).

Fig. 6.3 shows the EE per device, the probability of satisfied normal services, the average URLLC latency per packet and the reliability of URLLC services against the device density when the packet arrival rate is λ=0.12 packets/slot/per IIoT source. As seen in Fig. 6.3 (a), the higher the number of devices, the lower EE per device achieves, since the ICI becomes more pervasive in the VLC RF networks which limits the data rate improvement, and the power consumption as well as the subchannel assignment increase in the VLC RF networks under the high-density scenario of devices, leading to the EE degradation. From Fig. 6.3 (b) to Fig. 6.3 (d), the probability of the satisfied normal services and URLLC reliability decrease and the URLLC latency increases as the increase number of devices. This is because that under the fixed power and bandwidth resource, the large number of services need to be completed and different QoS requirements should to be guaranteed, the network may fail to support all the services' requirements, leading to bring down the performance in the high-density scenario. However, the presented heterogeneous RF/VLC network still outperforms the RF/RF network, and the proposed deep PDS-RET learning algorithm achieves the best performance among the existing algorithms.

We study in Fig. 6.4 how the performances vary with the packet arrival rate (λ)

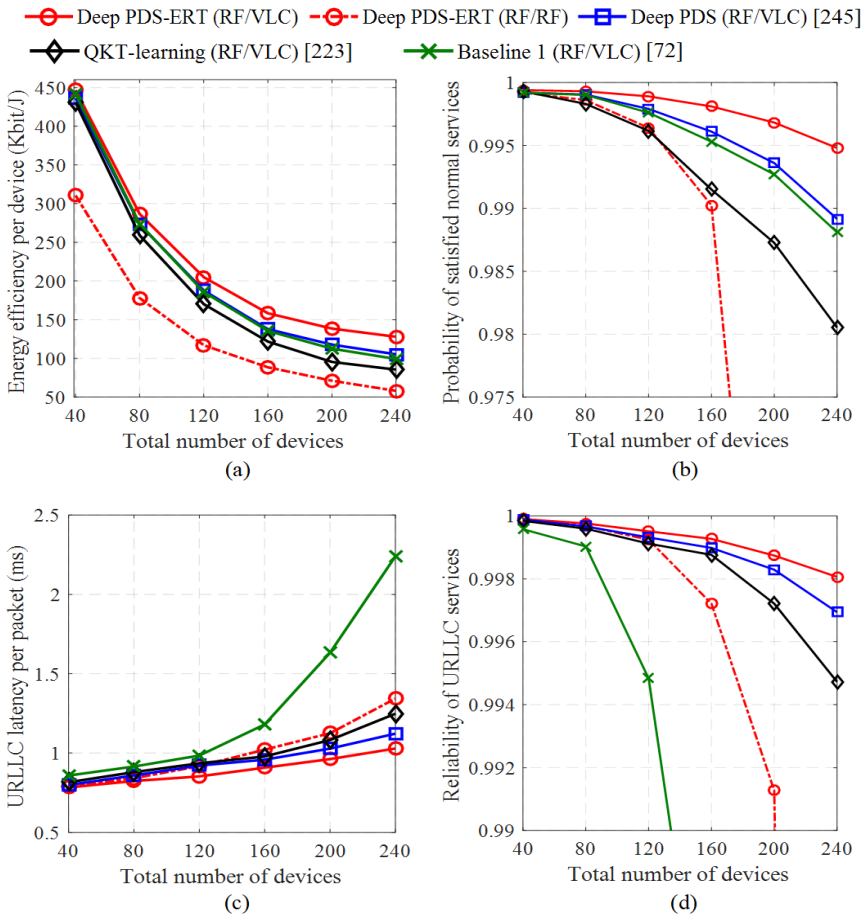

Figure 6.3: Performance comparisons with varying total numbers of devices.

when K=160. We can observe that the EE value increases with λ to a peak due to the increased network throughput when more packets transmit in the network. The power consumption also increases during this process, but the improvement rate of the network throughput is quite bigger than that of the power consumption, leading to EE enhancement. After that, it then slightly declines because of continuing to increase λ will increase frequent connections and waiting time in the queue, leading to more power consumption. In this case, the throughput enhancement fails to compensate the cost of

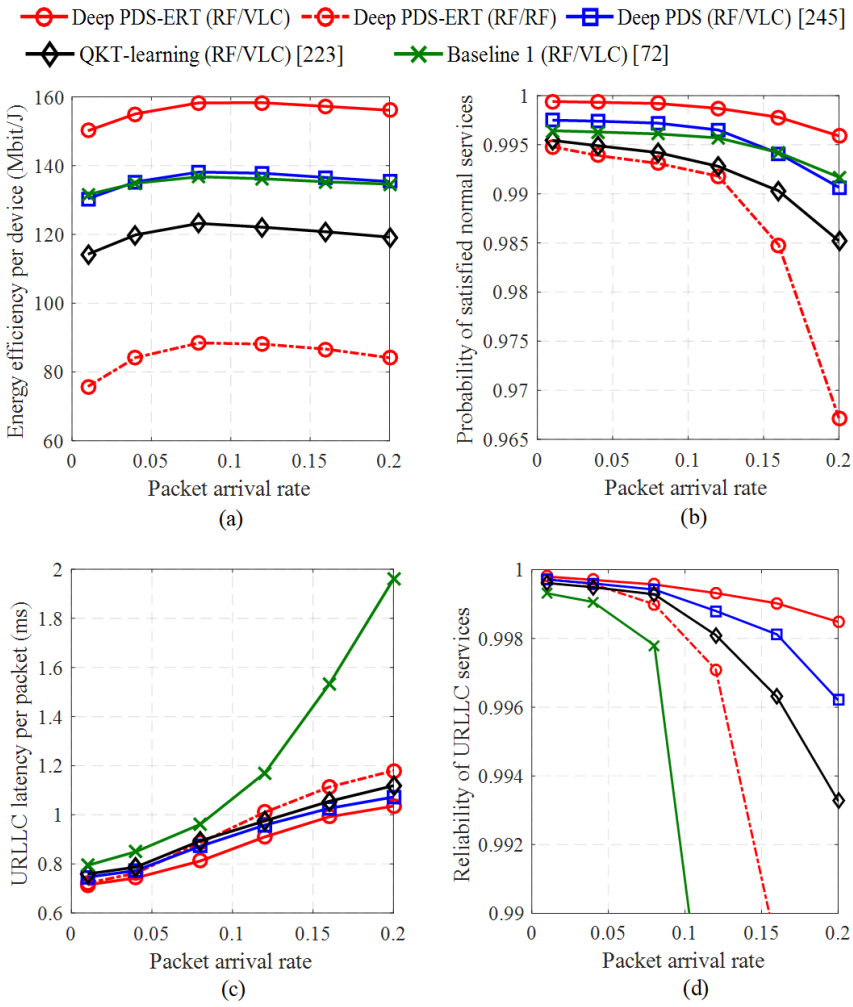

Figure 6.4: Performance comparisons vs. packet arrival rate of URLLC services.

consuming more total power, which slightly decreases the EE performance. It is worth noting that compared with RF/VLC, the performance of RF/RF is much sensitive to λ due to the limited bandwidth. Even the decreased performances happen with the increase of λ, our proposed deep PDS-RET learning algorithm still achieves the best performance.

Let us now quantify the effect of the blocking probability of RF&VLC links on the network performance, when K= 160 and λ =0.12 packets/slot/per IIoT source, as shown in Fig. 6.5. As seen in Fig. 6.5 (a), when the blocking probability is

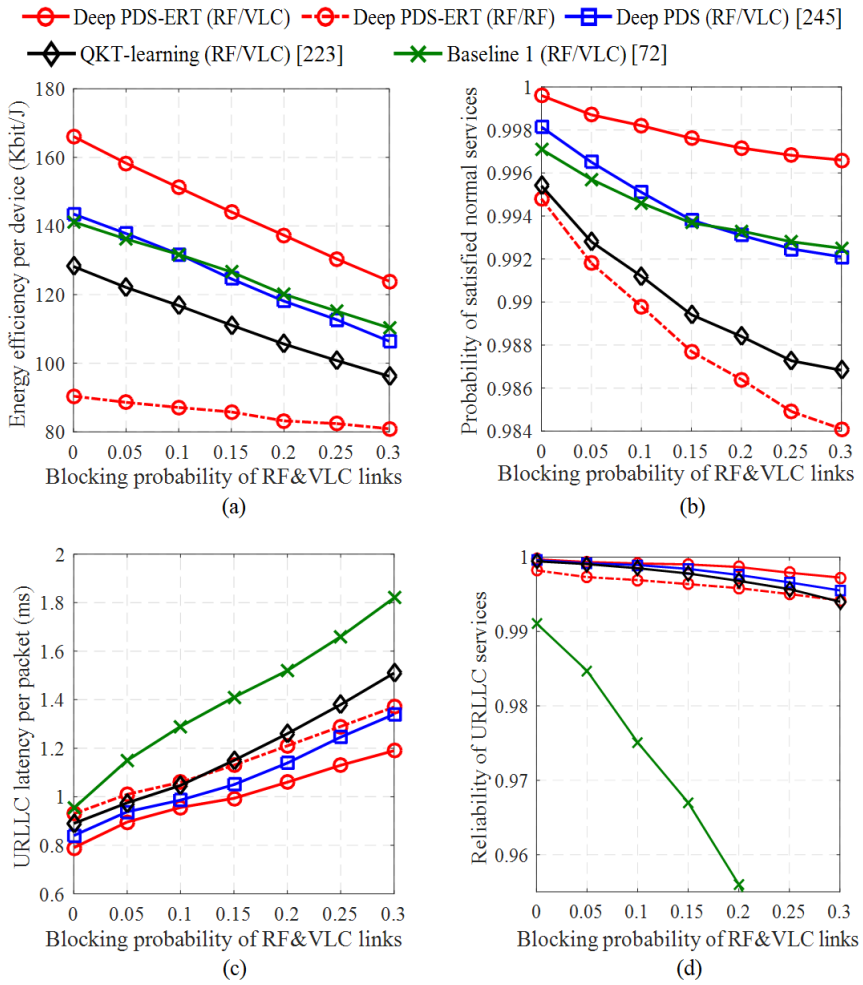

Figure 6.5: The performance evaluations and The performance evaluations and comparisons vs. blocking probability of RF&VLC links.

increased, the EE performance obviously declines in RF&VLC networks while it is slightly reduced for RF/RF networks. This is because the blocked links in the VLC network unsuccessfully provides the high transmission data rate, while the effect of blocked links can be negligible in the RF network. From Fig. 6.5 (b) to Fig. 6.5 (d), the probability of the satisfied normal services and URLLC reliability decrease, and the URLLC latency increases during this process, because the blockage degrades the received SINR value, results in failing to guarantee the different QoS requirements of

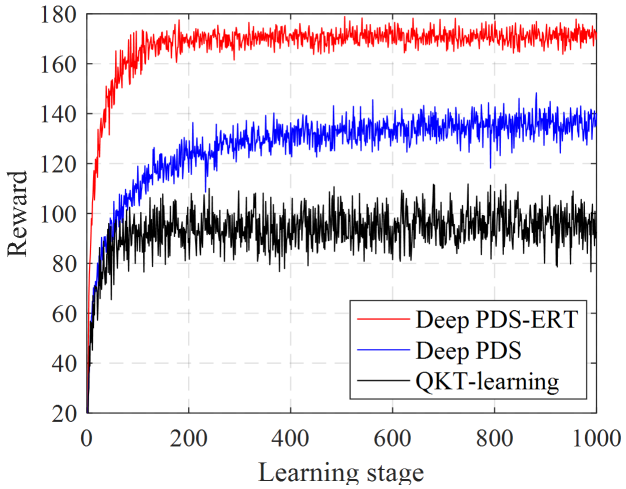

Figure 6.6: Learning process comparisons of RL algorithms.

devices. However, for all blocking probabilities, our proposed solution still outperforms other solutions (network architecture and algorithms).

In Fig. 6.6, we show the learning process of the RL algorithms in terms of the reward when $K=$ 120 and λ =0.12 packets/slot/per IIoT source. Clearly, the deep PDS-RET and QKT-learning algorithms achieve the faster convergence than that of the deep PDS learning algorithm, but QKT-learning has the lowest performance in large-scale networks. The deep PDS-ERT learning algorithm achieves the best reward value, the fastest convergence and the most stability (less fluctuations) by utilizing the historical experience strategy to improve the learning efficiency and convergence speed, compared with other RL algorithms.

From Fig. 6.3 to Fig. 6.6, the proposed deep PDS-RET learning algorithm based heterogeneous RF/VLC can effectively meet the energy-efficient communications, guarantee the strict URLLC requirements and ensure the high data rate demands at different scenarios in IoT networks.

Here, the entire execution delay of the proposed algorithm consists of the learning delay and the packet successful transmission completion delay [233], [241]. Fig. 6.7

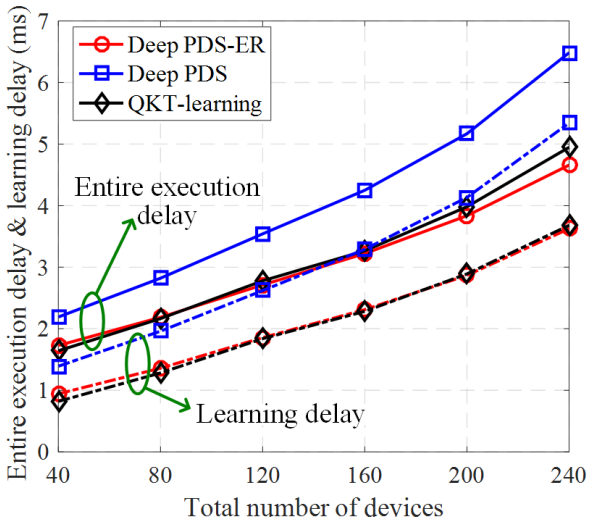

Figure 6.7: The entire execution delay and learning delay per epoch.

shows the entire execution delay and learning delay per epoch of the proposed algorithms and compared algorithms. From Fig. 6.7, we can find that as the number of total devices increases, both the entire execution delay and learning delay of all the reinforcement learning algorithms increases. This is because that the network states increase during this process, so the network environment becomes more complex, finally all reinforcement learning algorithms need more processing time to iteratively search the final policy. In addition, my proposed deep PDS-ERT learning algorithm has lower entire execution delay and the learning delay than other algorithms, because PDS and ERT mechanisms are adopted to improve the learning convergence speed.

6.6 Conclusion

This chapter presented a heterogeneous RF/VLC network architecture for wireless IoT networks to support different QoS requirements (ranging from high reliability and low latency to high data rates) of IIoT and IoT devices. Based on the heterogeneous IoT network, this chapter formulated an energy-efficient resource management decision-

making problem (joint network selection, subchannel assignment and power management) as a MDP, and a new deep PDS-ERT learning algorithm is proposed to learn the optimal policy for the intelligent resource management in heterogeneous IoT networks, which accelerates the learning rate and improves the learning efficiency. Simulation results verified the effectiveness of the presented heterogeneous RF/VLC IoT network and also showed that the proposed deep PDS-ERT learning algorithm outperforms other existing algorithms.

Chapter 7

Conclusions and Future Works

7.1 Conclusions

VLC and VLP based on white LEDs have been emerging as two promising candidates for indoor wireless communication and positioning. In this thesis, the investigations of newly proposed integrated VLCP system models, interference mitigation schemes for multi-cell VLC systems, robust designs under LoS blockages and resource management approach for hybrid RF/VLC networks have been explored and presented to improve the system performance and guarantee indoor derives' different QoS requirements.

In Chapter 3, an integrated VLCP system using FBMC-SCM and PDOA was presented to achieve both the communication and positioning services, where the presented integrated VLCP system is capable of suppressing the OOBI and hence improve the performance of positioning accuracy compared with OFDM-SCM based VLCP systems. Simulation results versify that the VLCP system using FBMC-SCM requires much reduced GBs in comparison to that using OFDM-SCM, and therefore achieves a higher spectral efficiency and improved positioning accuracy. In addition, the experimental results showed that, in a coverage area of 1.2×1.2 m^2 with a height of 2.1 m, the mean position errors using OFDM-SCM and FBMC-SCM for a GB of 0.7 MHz are 10.91 and 6.08 cm, respectively. Moreover, a comparable BER performance can

be achieved for both OFDM-SCM and FBMC-SCM. Due to the negligible GBs when using FBMC-SCM, the effective bandwidth utilization ratio of the integrated VLCP system is improved from 72% to 98% when OFDM-SCM is replaced by FBMC-SCM.

Chapter 4 presented a new integrated VLCP system model based on OFDM-SCM-interleaving to improve both the communication and positioning performance with the low signal processing complexity compared with FBMC-SCM based integrated VLCP system. In order to guarantee the minimum data rate and positioning accuracy requirements, a QoS-driven optimized design with joint adaptive modulation, subcarrier allocation and adaptive weighted pre-equalization was proposed to maximize the system transmission data rate while guaranteeing different QoS requirements. The LoS blockage issue was investigated in the system, and the robust optimized schemes were presented to maintain the system performance. The experimental results corroborated the superiority in performance of the presented integrated VLCP system model, and verified that the proposed design outperforms other existing adaptive transmission designs in terms of effectively enhancing the data rate, improving the positioning accuracy and guaranteeing devices QoS requirements.

In chapter 4, the integrated VLCP system model was also extended into multi-cell integrated VLCP networks. A joint AP selection, bandwidth allocation, adaptive modulation and power allocation approach was proposed maximize the network data rate while guaranteeing the different QoS requirements of indoor devices. A low-complexity solution was presented to solve the optimization problem. Moreover, the LoS blockage issue was investigated in networks, and the robust optimized schemes were presented to maintain the network performance. The simulation results corroborated the superiority in performance of the presented integrated VLCP network and the proposed resource management approach.

In Chapter 5, a novel joint precoder and equalizer design based on IA was proposed to mitigate both ICI and IUI for multi-user multi-cell MIMO-VLC systems in

the presence of both perfect and imperfect CSI. In order to achieve the optimal transmit precoding matrix and receiving equalizer matrix, the thesis formulated the joint optimization problem through minimizing the total generated interference and MSE under optical power constraints. The proposed design aims to mitigate both IUI and ICI effectively, as well as maintain the BER at the lowest level. Furthermore, the thesis took into account the optical channel estimation error for our formulated joint optimization problem when designing the optimal precoder and receiving equalizer in multi-user multi-cell MIMO-VLC systems. The thesis investigated the effect of different users' locations, channel estimation error and LED/PD spacing levels on the system capacity and BER performance analytically and by simulation. Numerical results showed that the proposed design achieves significant system capacity and BER improvements under imperfect CSI, compared with the MMSE and max-rate designs.

In Chapter 6, considering the fact that there exists a large number of devices in indoor IoT networks, and different devices have different QoS requirements, ranging from ultra-reliable and low-latency communications to high transmission data rates. These indoor networks will be highly complex and heterogeneous, as well as the spectrum and energy resources are severely limited. Hence, this thesis presented a heterogeneous RF/VLC IoT network architecture to guarantee different QoS requirements, where RF is capable of offering wide-area coverage and VLC has the ability to provide high transmission data rate. A joint uplink and downlink energy-efficient resource management decision-making problem (network selection, subchannel assignment and power management) was formulated as a Markov decision process. In addition, a new deep PDS based experience replay and transfer (PDS-ERT) RL algorithm was proposed to learn the optimal policy. Simulation results corroborated the superiority in performance of the presented heterogeneous network, and verified that the proposed PDS-ERT learning algorithm outperforms other existing algorithms in terms of meeting the energy efficiency and the QoS requirements.

7.2 Future Works

In this thesis, integrated VLCP systems models, ICI mitigation approach, resource management strategy and robust optimized schemes were presented to improve both the communication and positioning performance while guaranteeing devices' different QoS requirements. In addition to the above mentioned works, the following works are worth to be investigated in the future.

Chapter 3 presented the FBMC-SCM based integrated VLCP system via PDOA positioning algorithm and Chapter 4 proposed a new integrated VLCP system model based on OFDM-SCM-interleaving via RSS positioning algorithm. However, it has been shown in [39, 116] that there exists the position shifting effect in practical PDOA-based VLP systems caused by the nonuniform initial time delay pattern of the commercial off-the-shelf LEDs, which directly degrades the positioning accuracy. In addition, most studies have reported that RSS has low positioning accuracy when the device locates at the edges, or corners of the experimental and simulative environments. So far, the solutions to these two problems have not yet been well explored in indoor positioning. Hence, it is of great importance to develop an improved positioning scheme to overcome the above mentioned problems.

In indoor environments, there exist some energy-constrained devices, e.g., sensors for monitoring, humidity and indoor air quality, etc. Hence, it is important to extend the lifetime of the devices due to their limited energy budget. In our presented heterogeneous RF/VLC IoT network analyzed in Chapter 6, at each IoT or IIoT device, light energy harvesting is achieved by using PD and the harvested energy is used for collected data reporting through the RF uplink. However, achieving both the energy harvesting in VLC systems might violate the illumination requirements, because VLC systems need to provide energy and information to indoor devices. As a result, the investigation of the above mentioned functions in heterogeneous RF/VLC networks

by formulating optimization problems that allocate DC bias, transferred energy, and available resources is needed.

This thesis pays attention to the investigations of the indoor VLC and VLP systems, but these techniques can not be directly applied in outdoor VLC or VLP systems. Before extending the techniques in outdoor VLC networks, the following issues should be considered: 1) the negative effect of the sum light on the optical signal detection at the receiver side; 2) the outdoor VLC channel links are not stable and static due to the atmosphere pressure as well as the inhomogeneities in the temperature; 3) the poor channel quality due to the long transmission distance. Therefore, it is necessary to develop efficient techniques to overcome the above mentioned issues before applying the indoor VLC technologies into outside VLC networks.

The heterogeneous RF/VLC IoT network is generally complex under the different QoS requirements of devices, the presented heterogeneous network architecture and the proposed deep reinforcement leaning algorithm presented in Chapter 6 mainly focused on the vertical transmission mode selection. However, the practical indoor environment needs both the vertical and horizontal handover processes to guarantee both the connectivity and QoS requirements of mobile IoT devices. For the vertical handover mechanism, the mobile device can connect the RF links when the VLC LoS link is blocked or it may connect the VLC links if it needs the high data rate transmission. For the horizontal handover, the handover is mainly deployed in VLC networks to avoid the effect of ICI and maintain the communication connectivity of mobile devices. Therefore, how to effectively implement both the vertical and horizontal handover mechanisms need to be considered in the future works.

Publication list

Journal

[1] **H. L. Yang**, C. Chen, W. D Zhong, A. Alphones, S. Zhang and P. F. Du, "Demonstration of a quasi-gapless integrated visible light communication and positioning system," *IEEE Photon. Technol. Lett.*, vol. 30, no. 23, pp. 2001-2004, Dec. 2018. (related to Chapter 3)

[2] **H. L. Yang**, W. D. Zhong, A. Alphones, C. Chen, S. Zhang and P. F. Du, "Coordinated resource allocation-based integrated visible light communication and positioning systems for indoor IoT," Revision was submitted to *IEEE Trans. Wireless Commun.* (related to Chapter 3)

[3] **H. L. Yang**, P. F. Du, W. D. Zhong, C. Chen, A. Alphones and S. Zhang, "Reinforcement learning based intelligent resource allocation for integrated VLCP systems," *IEEE Wireless Commun. Lett.*, vol. 8, no. 4, pp. 1204-1207, Aug. 2019. (related to Chapter 4)

[4] **H. L. Yang**, W. D. Zhong, C. Chen, A. Alphones, and P. Du, "QoS-driven optimized design-based integrated visible light communication and positioning for indoor IoT networks," *IEEE Internet of Things J.*, vol. 7, no. 1, pp. 269-283, Jan. 2020. (related to Chapter 4)

[5] **H. L. Yang**, C. Chen, W. D. Zhong and A. Alphones, "Joint precoder and equalizer design for multi-user multi-cell MIMO VLC systems," *IEEE Trans. Veh. Technol.*, vol. 67, no. 12, pp. 11354-11364, Dec. 2018. (related to Chapter 5)

[6] **H. L. Yang**, C. Chen and W. D. Zhong, "Cognitive multi-cell visible light communication with hybrid underlay/overlay resource allocation," *IEEE Photon. Technol. Lett.*, vol. 30, no. 12, pp. 1135-1138, Jun. 2018. (related to Chapter 6)

[7] **H. L. Yang**, C. Chen, W. D. Zhong and A. Alphones, "Learning-based energy-efficient resource management by heterogeneous RF/VLC for ultra-reliable low-latency industrial IoT networks," Accepted for publication in *IEEE Trans. Ind. Informat.* (related to Chapter 6)

[8] **H. L. Yang**, W. D. Zhong, C. Chen and A. Alphones, "Integration of visible light communication and positioning within 5G networks for Internet of Things," Revision was submitted to *IEEE Network*.

[9] C. Chen, W. D. Zhong, **H. L. Yang**, S. Zhang and P. F. Du, "Reduction of SINR fluctuation in indoor multi-cell VLC systems using optimized angle diversity receiver," *J. Lightw. Technol.*, vol. 36, no. 17, pp. 3603-3610, Sept. 2018.

Conference

[10] **H. L. Yang**, C. Chen, W. D. Zhong, "An integrated indoor visible light communication and positioning system based on FBMC-SCM," *IEEE Photon. Conf.*, pp. 129-130, 2017. (related to Chapter 3)

[11] **H. L. Yang**, C. Chen, W. D. Zhong and A. Alphones, "Resource allocation for multi-user integrated visible light communication and positioning systems," in *Proc. IEEE Int. Conf. Commun. (ICC)*, pp. 1-6, Shanghai, China, May 2019. (related to Chapter 4)

[12] C. Chen, Y. Yang, X. Deng, P. F. Du, **H. L. Yang**, Z. Chen, and W.-D. Zhong, "NOMA for MIMO visible light communications: a spatial domain perspective," Accepted for presentation in *IEEE Global Communication Conf. (GLOBECOM)*, 2019.

[13] **H. L. Yang**, A. Alphones, W. D. Zhong, C. Chen, P. F. Du, and S. Zhang, "QoS-driven optimized design in a new integrated visible light communication and positioning system," Accepted by *Proc. IEEE Int. Conf. Commun. (ICC)*, Jun., Dublin, Ireland, 2020. (related to Chapter 4)

Bibliography

[1] L. Hanzo, H. Haas, S. Imre, D. OBrien, M. Rupp, and L. Gyongyosi, "Wireless myths, realities, futures: From 3G/4G to optical and quantum wireless," *Proc. IEEE*, vol. 100, pp. 1853-1888, 2012.

[2] J. An, K. Yang, J. Wu, N. Ye, S. Guo and Z. Liao, "Achieving sustainable ultra-dense heterogeneous networks for 5G," *IEEE Commun. Mag.*, vol. 55, no. 12, pp. 84-90, Dec. 2017.

[3] Y. Li, Y. Zhang, K. Luo, T. Jiang, Z. Li and W. Peng, "Ultra-dense hetNets meet big data: green frameworks, techniques, and approaches," *IEEE Commun. Mag.*, vol. 56, no. 6, pp. 56-63, Jun. 2018.

[4] S. Wu, H. Wang and C. Youn, "Visible light communications for 5G wireless networking systems: from fixed to mobile communications," *IEEE Network*, vol. 28, no. 6, pp. 41-45, Nov.-Dec. 2014.

[5] P. Pathak, X. Feng, P. Hu, and P. Mohapatra, "Visible light communication, networking, and sensing: a survey, potential and challenges," *IEEE Commun. Surveys Tuts.*, vol. 17, no. 4, pp. 2047-2077, 2015.

[6] M. B. Rahaim and T. D. C. Little, "Toward practical integration of dual-use VLC within 5G networks," *IEEE Wireless Commun.*, vol. 22, no. 4, pp. 97-103, Aug. 2015.

[7] D. Karunatilaka, F. Zafar, V. Kalavally, and R. Parthiban, "LED based indoor visible light communications: State of the art," *IEEE Commun. Surveys Tuts.*, vol. 17, no. 3, pp. 1649-1678, 3rd Quart. 2015.

[8] United States Department of Energy. Energy Savings Forecast of Solid-State Lighting in General Illumination Applications. [Online]. Available: http://apps1.eere.energy.gov/ buildings/publications/pdfs/ssl/energysavingsforecast14.pdf.

[9] Y. Tanaka, S. Haruyama, and M. Nakagawa, "Wireless optical transmissions with white colored LED for wireless home links," in *Proc. IEEE Int. Symp. PIMRC*, vol. 2, pp. 1325- 1329, 2000.

[10] T. Komine and M. Nakagawa, "Fundamental analysis for visible-light communication system using LED lights," *IEEE Trans. Consum. Electron.*, vol. 50, no. 1, pp. 100-107, 2004.

[11] Visible Light Communications Consortium (VLCC). [Online]. Available: http://www. vlcc. net/.

[12] IEEE Standard for Local and Metropolitan Area Networks-Part 15.7: Short-Range Wireless Optical Communication Using Visible Light, IEEE Std. 802.15.7, 2011.

[13] F. Che, L. Wu, B. Hussain, X. Li and C. P. Yue, "A fully integrated IEEE 802.15.7 visible light communication transmitter with on-chip 8-W 85% efficiency boost LED driver," *J. Lightw. Technol.*, vol. 34, no. 10, pp. 2419-2430, May, 2016.

[14] C. Yang, Y. Wang, Y. Wang, X. Huang, and N. Chi, "Demonstration of high speed multi-user multi-carrier CDMA visiblelight communication," *Opt. Commun.*, vol. 336, pp. 269-272,2015.

[15] X. Liu, et al., "Gbps Long-Distance real-time visible light communications using a high-bandwidthGaN-based micro-LED," *IEEE Photon. J.*, vol. 9, no. 6, pp.1-9, Dec. 2017.

[16] D. Tsonev, et al.,"A 3-Gb/s single-LED OFDM-based wireless VLC link using a gallium nitride μLED," *IEEE Photon. Technol. Lett.*, vol. 26, no.7, pp. 637-640, Apr. 2014.

[17] "Standards News" *IEEE Commun. Standards Mag.*, vol. 2, no. 4, pp. 12-17, Dec.2018.

[18] Z. Ghassemlooy, W. Popoola, and S. Rajbhandari, Optical Wireless Communications, System and Channel Modelling With Matlab. London, U.K.: CRC Press, 2012.

[19] S. Arnon, J. R. Barry, G. K. Karagiannidis, R. Schober, and M. Uysal, Eds., Advanced Optical Wireless Communication. Cambridge University Press, 2012.

[20] A. Sevincer, A.Bhattarai, M. Bilgi, M. Yuksel, and N. Pala, "LIGHTNETs: Smart LIGHTing and mobile optical wireless NETworks - A survey," *IEEE Commun. Surveys Tuts.*, vol. 15, no. 4, pp. 1620-1641, 4th quarter 2013.

[21] H. Haas, L. Yin, Y. Wang, and C. Chen, "What is LiFi?" *J. Lightw. Technol.*, vol. 34, no. 6, pp. 1533-1544, Mar. 2016.

[22] S. Y. Jung, andS. Hann, "TDOA-based optical wireless indoor localization usingLED ceiling lamps," *IEEE Trans. Consum. Electron.*, vol. 57,no. 4, pp. 1592-1597, Nov. 2011.

[23] J. Armstrong, Y. Sekercioglu, and A. Neild, "Visible light positioning: A roadmap for international standardization," *IEEE Commun.Mag.*, vol. 51, pp. 68-73, Dec. 2013

[24] H.-S. Kim, D.-R. Kim, S.-H.Yang, Y.-H. Son, and S.-K. Han, "An indoor visible light communication positioning system using a RF carrier allocation technique," *J. Lightw. Technol.*, vol. 31, pp. 134-144, Jan.2013.

[25] M. F. Keskin, A. D. Sezer, and S. Gezici, "Localization via visible light systems," *Proc. IEEE*, vol. 106, pp. 1063-1088, Jun. 2018.

[26] Peter H. Dana. Global Positioning System Overview. http://www.colorado.edu/ geography/gcraft/notes/gps/gpsf.html, 1994. [Online; accessed 19-November-2016].

[27] Hui Liu, Houshang Darabi, PatBanerjee, and Jing Liu, "Survey of wireless indoor positioning techniques and systems," *IEEE Trans. Sys., Man, and Cybernetics*, Part C, vol. 37, no. 6, pp.1067-1080, May 2007.

[28] Paul A Zandbergen, “Accuracy of iphone locations: Comparison of assisted gps, wifi and cellular positioning,” *Trans. in GIS*, vol. 13, pp. 5-25, 2009.

[29] S. Zhou and J. K. Pollard, “Position measurement using bluetooth,” *IEEE Trans. Consumer Electron.*, vol. 52, no. 2, pp.555-558, Mar. 2006.

[30] Y. Wang, X. Yang, Y. Zhao, Y. Liu, and L. Cuthbert, “Bluetooth positioning using rssi and triangulation methods,” In *Proc. IEEE 10th Consumer Commun. and Net. Conf. (CCNC)*, pp. 837-842, 2013.

[31] L. M. Ni, Y. Liu, Y. C. Lau, and A P. Landmarc, “indoor location sensing using active fid,” *Wireless netw.*, vol. 10, no. 6, pp. 701-710,2004.

[32] P. K. Yoon, S. Zihajehzadeh, B. S. Kang, and E. J. Park, “Robust biomechanical model-based 3-D indoor localization and tracking method using UWB and IMU,” *IEEE Sens. J.*, vol. 17,no. 4, pp. 1084-1096, Feb. 2017.

[33] Y. Xu, Z. Wang, P. Liu,J. Chen, S. Han, C. Yu, and J. Yu, “Accuracy analysis and improvement of visible light positioning based on VLC system using orthogonal frequency division multiple access,” *Opt. Express*, vol. 26, no. 7, pp. 9230-9242, Apr. 2018.

[34] X. Zhang, J. Duan, Y. Fu, and A. Shi, “Theoretical accuracy analysis of indoor visible light communication positioning system based on received signal strength indicator,” *J. Lightw. Technol.*, vol. 32, no. 21, pp. 4180- 4186, 1 Nov., 2014.

[35] W. Gu, M. Aminikashani, P. Deng, and M. Kavehrad, “Impact of multipath reflections on the performance of indoor visible light positioning systems,” *J. Lightw. Technol.*, vol. 34, no. 10, pp.2578-2587, May 2016.

[36] S. H. Yang, H. S. Kim, Y. H. Son, and S.K. Han, “Three-dimensional visible light indoor localization using AOA and RSS with multiple optical receivers,” *J. Lightw. Technol.*, vol. 32, no. 14, pp.2480-2485, Jul. 2014.

[37] R. Zhang, W. Zhong, K. Qian, and D. Wu, “Image sensor based visible light positioning system with improved positioning algorithm,” *IEEE Access*, vol. 5, pp. 6087-6094, Feb. 2017.

[38] P. Du, S. Zhang, C. Chen, A. Alphones, and W. Zhong, “Demonstration of a low-complexity indoor visible light positioning system using an enhanced TDOA scheme,” *IEEE Photon. J.*, vol. 10, no. 4, pp. 1-10, Aug. 2018.

[39] S. Zhang, W.-D. Zhong, P. F. Du, and C. Chen, “Experimental demonstration of indoor sub-decimeter accuracy VLP system using differential PDOA,” *IEEE Photon. Technol. Lett.*, vol. 30, no. 19, pp. 1703-1706, Oct. 2018.

[40] M. F. Keskin, A. D.Sezer, and S. Gezici, “Optimal and robust power allocation for visible light positioning systems under illumination constraints,” *IEEE Trans. Commun.*, vol. 67, no. 1, pp. 527-542, Jan.2019.

[41] S. Yang, E. Jung and S. Han, “Indoor location estimation based on LED visible light communication using multiple optical receivers,” *IEEE Commun. Lett.*, vol. 17, no. 9, pp.1834-1837, Sep. 2013.

[42] A. Naz, H. M. Asif, T. Umer and B. S. Kim, “PDOA based indoor positioning using visible light communication,” *IEEE Access*, vol. 6, pp. 7557-7564,Sep. 2018.

[43] W. Sakpere, M. Adeyeye-Oshin, and N.B.W. Mlitwa,"A state-of-the-art survey of indoor positioning and navigation systems and technologies," *South African Comp. Journal*, vol. 29, no. 3, pp. 145-197, Dec. 2017.

[44] X. Li, B. Hussain, J. Kang,H. S. Kwok and C. P. Yue, "Smart μLED Display-VLC System With a PD-Based/Camera-Based Receiver for NFC Applications," *IEEE Photon. J.*, vol. 11, no. 1, pp. 1-8, Feb. 2019.

[45] S. Cincotta, C. He, A. Neild and J. Armstrong, "QADA-PLUS: a novel two-stage receiver for visible light positioning," in *Pro. IEEE 2018 IPIN*, Nantes, 2018, pp.1-5.

[46] K. Ying, H. Qian, R. J. Baxley and S. Yao, "Joint optimization precoder and equalizer in MIMO VLC systems," *IEEE J. Sel. Areas Commun.*, vol. 33, no. 9, pp. 1949-1958, Sep. 2015.

[47] Y. Hong, T. Wu and L. Chen, "On the performance of adaptive MIMO-OFDM indoor visible light communications," *IEEE Photon. Technol. Lett.*, vol. 28, no.8, pp. 907-910, Apr. 2016.

[48] L. M. Hao, D. O'Brien, G. Faulkner, *et al.*, "High-speed visible light communications using multiple-resonant equalization," *IEEE Photon. Technol. Lett.*, vol. 20, no. 14, pp. 1243-1245, Agu.2008.

[49] Y. Wang, L. Tao, Y. Wang and N. Chi, "High speed WDM VLC system based on multi-band CAP64 with weightedpre-equalization and modified CMMA based post-equalization," *IEEE Commun. Lett.*, vol. 18, no. 10, pp. 1719-1722, Oct.2014.

[50] D. Tsonev et al., "A 3-Gb/s single-LED OFDM-based wireless VLC link using a gallium nitride LED," *IEEE Photon. Technol. Lett.*, vol. 26, no. 7, pp. 637-640, Apr. 2014.

[51] H. Elgala, R. Mesleh and H. Haas, "Indoor broadcasting via white LEDs and OFDM," *IEEE Trans. Consumer Electro.*, vol. 55, no. 3, pp. 1127-1134, Aug. 2009.

[52] C. Chen, W.-D. Zhong, H. L. Yang, and P. F. Du, "On the performance of MIMO-NOMA-based visible light communication systems," IEEE Photon. Technol. Lett., vol. 30, no. 4, pp.307-310, Feb. 2018.

[53] S. Feng, R. Zhang, W. Xu and L. Hanzo, "Multiple access design for ultra-dense VLC networks: orthogonal vs non-orthogonal," *IEEE Trans. Commun.*, vol.67, no. 3, pp. 2218-2232, Mar. 2019.

[54] B. Lin et al., "Experimental demonstration of OFDM/OQAM transmission for visible light communications," *IEEE Photonics J.*, vol. 8, no. 5, pp. 1-10, Oct. 2016.

[55] T. Yuan, Y. Xu, Y. Wang, P. Han and J. Chen, "A tilt receiver correction method for visible light positioning using machine learning method," *IEEE Photo. J.*, vol. 10, no. 6, pp. 1-12, Dec. 2018.

[56] S. Büyükeorak and G.Karabulut Kurt, "A bayesian perspective on RSS based localization for visible light communication with heterogeneous networks extension," *IEEE Access*, vol. 5, pp. 17487-17500, May 2017.

[57] W. Guan, X. Chen, M. Huang, Z. Liu, Y. Wu and Y. Chen, "High-speed robust dynamic positioning and tracking method based on visual visible light communication

Using optical flow detection and Bayesian Forecast," *IEEE Photo. J.*, vol. 10, no. 3, pp.1-22, Jun. 2018.

[58] C. Chen, S. Videv, D. Tsonev, and H. Haas, "Fractional frequency reuse in DCO-OFDM-based optical attocell networks," *J. Lightw. Technol.*, vol. 33, no. 19, pp. 3986-4000, Oct. 2015.

[59] C. Chen, W.-D. Zhong, H. L. Yang, S. Zhang, and P. F. Du, "Reduction of SINR fluctuation in indoor multi-cell VLC systems using optimized angle diversity receiver," *J. Lightw. Technol.*, vol. 36, no. 17, pp. 3603-3610, Sept. 2018.

[60] H. Kazemi, M. Safari and H. Haas, "A wireless optical backhaul solution for optical attocell networks," *IEEE Trans. Wireless Commun.*, vol. 18, no. 2, pp. 807-823, Feb. 2019.

[61] Y.Xu, Z. Wang, P. Liu, J. Chen, S. Han, C. Yu, and J. Yu, "Accuracyanalysis and improvement of visible light positioning based on VLCsystem using orthogonal frequency division multiple access,"Opt. Express, vol. 26, no. 7, pp. 9230-9242, Apr. 2018.

[62] M. Aminikashani, W. Gu, and M. Kavehrad, "Indoor positioning with OFDM visible light communications," in IEEE Consum.Commun. Netw. Conf., Las Vegas, NV, USA, 2016, pp.505-510.

[63] B. Lin, X. Tang, Z. Ghassemlooy, C. Lin, and Y. Li, "Experimental demonstration of an indoor VLC positioning system based on OFDMA," *IEEE Photon. J.*, vol. 9, no. 2, pp.1-9, Apr. 2017.

[64] H. Kazemi and H. Haas, "Downlink cooperation with fractional frequency reuse in DCO-OFDMA optical attocell networks," *IEEE Int. Conf. Commun. (ICC)*, Kuala Lumpur, 2016, pp. 1-6.

[65] H. Kim, D. Kim, S. Yang, Y. Son, and S.-K. Han, "Mitigation of inter-cell interference utilizing carrier allocation in visible light communication system," *IEEE Commun. Lett.*, vol. 16, no. 4, pp. 526-529, Jan. 2012.

[66] X. Li, F. Jin, R. Zhang, J. Wang, Z. Xu and L. Hanzo, "Users first: User-centric Cluster formation for interference-mitigation in visible-light networks," *IEEE Trans. Wireless Commun.*, vol. 15, no. 1, pp. 39-53, Jan. 2016.

[67] T. V. Pham and A. T. Pham, "Coordination/cooperation strategies and optimal zero-forcing precoding design for multi-user multi-cell VLC networks," *IEEE Trans. Wireless Commun.*, vol. 67, no.6, pp. 4240-4251, Jun. 2019.

[68] H. Ma, L. Lampe, and S. Hranilovic, "Coordinated broadcasting for multiuser indoor visible light communication systems," *IEEE Trans. Commun.*, vol. 63, no. 9, pp. 3313-3324, Sep. 2015.

[69] J. Lian, and M. Brandt-Pearce, "Multiuser MIMO indoor visible light communication system using spatial multiplexing," *J. Lightw. Technol.*, vol. 35, no. 23, pp. 5024-5033, Dec. 2017.

[70] F. Wang, Z.Wang, C. Qian, L. Dai and Z. Yang, "Efficient vertical handover scheme for heterogeneous VLC-RF systems," *IEEE/OSA J. Opt. Commun. Netw.*, vol. 7, no. 12, pp. 1172-1180, Dec. 2015.

[71] M. Hammouda, S. Ak?n, A. M. Vegni, H. Haas and J. Peissig, “Link selection in hybrid RF/VLC systems under statistical queueing constraints,” *IEEE Trans. Wireless Commun.*, vol. 17, no. 4, pp. 2738-2754, Apr. 2018.

[72] H. Zhang, N. Liu, K. Long, J. Cheng, V. C. M. Leung, and L. Hanzo, “Energy efficient subchannel and power allocation for software-defined heterogeneous VLC and RF networks,” *IEEE J. Sel. Areas Commun.*, vol. 36, no. 3, pp. 658-670,Mar. 2018.

[73] W. Ma and L. Zhang, “QoE-driven optimized load balancing design for hybrid LiFi and WiFi networks,” *IEEE Commun. Lett.*, vol. 22, no. 11, pp. 2354-2357, Nov. 2018.

[74] M. Kashef, M. Ismail, M. Abdallah, K. A. Qaraqe and E. Serpedin, “Energy efficient resource allocation for mixed RF/VLC heterogeneous wireless networks,” *IEEE J. Sel. Areas Commun.*, vol. 34, no. 4, pp. 883-893, Apr. 2016.

[75] A. R. Jimenez, F. Seco, C. Prieto, and J. Guevara, “A comparison of pedestrian dead-reckoning algorithms using a low-cost MEMS IMU,” in *Proc. IEEE WISP*, Budapest,2009, pp. 37-42.

[76] Y. Wang and H. Zhao, “Improved smartphone-based indoor pedestrian dead reckoning assisted by visible light positioning,” *IEEE Sensors J.*, vol. 19, no.8, pp. 2902-2908, Apr. 2019.

[77] F. R. Gfeller and U. Bapst, “Wireless in-house data communication via diffuse infrared radiation,” *Proc. IEEE*, vol. 67, no. 11, pp. 1474-1486, 1979.

[78] L. Zeng, D. O’Brien, H. L. Minh, G. E. Faulkner, K.Lee, D. Jung, Y. Oh, and E. Won, “High data rate multiple input multiple output (MIMO) optical wireless communications using whiteLED lighting,” *IEEE J. Sel. Areas Commun.*, vol. 27, no. 9,pp. 1654-1662, Apr. 2009.

[79] J. McKendry, R. Green, A. Kelly, Z. Gong, B. Guilhabert, D. Massoubre, E. Gu, and M. Dawson, “High-speed visible light communications using individual pixels in a micro light-emitting diode array,” *IEEE Photon. Technol. Lett.*, vol. 22, no. 18, pp. 1346-1348, Jul. 2010.

[80] C.Tsai and Z.-Fan Xu, “Line-of-sight visible light communications with InGaN-based resonant cavity LEDs,” *IEEE Photon. Technol. Lett.*, vol. 25, no. 18, pp. 1793-1796, Dec. 2013.

[81] H. Minh, D. O’Brien, G. Faulkner, L. Zeng, K. Lee, D. Jung, Y. Oh,and E. Won, “100-Mbit/s NRZ visible light communications using a post-equalized white LED,” IEEE Photon. Technol. Lett., vol.21, no. 15, pp. 1063-1065, Aug. 2009.

[82] Z. Li and C. Zhang, “Animproved FD-DFE structure for downlink VLC systems based on SC-FDMA,” *IEEE Commun. Lett.*, vol. 22, no. 4, pp. 736-739,Apr. 2018.

[83] J. Sung, C. Yeh, C. Chow, W. Lin, and Y. Liu, “Orthogonal frequency-division multiplexing access (OFDMA) based wireless visible light communication (VLC) system,” *Opt. Commun.*, vol. 355, pp. 261-268, May 2015.

[84] H. Burchardt, N. Serafimovski, D. Tsonev, S. Videv, and H. Haas, “VLC: Beyond point-to-point communication,” *IEEE Commun. Mag.*, vol. 52, no. 7, pp. 98-105, 2014.

[85] L. Zeng, D. O’Brien, H. L. Minh,G. E. Faulkner, K. Lee, D. Jung, Y. Oh, and E. Won, “High data rate multiple input multiple output (MIMO) optical wireless

communications using white LED lighting," *IEEE J. Sel. Areas Commun.*, vol. 27, no. 9, pp. 1654-1662, Oct. 2009.

[86] H. Yang, and L. Chen, "On the performance of adaptive MIMO-OFDM indoor visible light communications," *IEEE Photon. Technol. Lett.*, vol. 28, no. 8, pp. 907-910, 2015.

[87] T. Fath and H. Haas, "Performance comparison of MIMO techniques for optical wireless communication in indoor environments," *IEEE Trans. Commun.*, vol. 61, no. 2, pp. 733- 742, Feb. 2013.

[88] L. Wei, H. Zhang, and J. Song, "Experimental demonstration of a cubic receiver based MIMO visible light communication system," *IEEE Photon. J.*, vol. 9, no. 1, Mar. 2017.

[89] R. Mesleh, H. Haas, S. Sinanovic, C. Ahn, and S. Yun, "Spatial modulation," *IEEE Trans. Veh. Technol.*, vol. 57, no. 4, pp. 2228-2241, 2008.

[90] K. Xu, H. Yu and Y. Zhu, "Channel-adapted spatial modulation for massive MIMO visible light communications," *IEEE Photon. Technol. Lett.*, vol. 28, no. 23, pp.2693-2696, 1 Dec. 2016.

[91] B. Anitha Vijayalakshmi, And M. Nesa Sudha, "A novel approach to using energy-efficient LED-based visible light communication in hospitals," *Intelligent and Efficient Electr. Sys.*, volume 446, pp 197-204, Jan. 2018.

[92] https://visiblelightcomm.com/top-10-visible-light-communications-applications/.

[93] T. Yamazato, et al., "Image-sensor-based visible light communication for automotive applications," *IEEE Commun. Mag.*, vol. 52, no. 7, pp. 88-97, Jul. 2014.

[94] R. Corsini, *et al.*, "Free space optical communication in the visible bandwidth for V2V safety critical protocols," *IEEE IWCMC*, Limassol, 2012, pp. 1097-1102.

[95] H. Uema, T. Matsumura, S. Saito, and Y. Murata, "Research and development on underwater visible light communication systems," *Electron. Commun. Japan*, vol. 98, no. 3, pp. 9-13, May 2015.

[96] N. Anous, M.Abdallah, M. Uysal and K. Qaraqe, "Performance evaluation of LOS and NLOS vertical inhomogeneous links in underwater visible light communications," *IEEE Access*, vol. 6, pp. 22408-22420, Jan.2018.

[97] http://www.personal.psu.edu/gvw5074/opticalcomm.html.

[98] J.Armstrong, Y. A. Sekercioglu and A. Neild, "Visible light positioning: a roadmap for international standardization," *IEEE Commun. Mag.*, vol. 51, no. 12, pp. 68-73, Dec. 2013.

[99] L. Li, P. Hu, C. Peng, G. Shen, and F. Zhao, "Epsilon: A visible light based positioning system," in *IEEE 11th USENIX NSDI*, Seattle, WA, pp. 331-343, 2014.

[100] X. Guo, F.Hu, N. R. Elikplim and L. Li, "Indoor localization using visible light via two-layer fusion network," *IEEE Access*, vol. 7, pp. 16421-16430, Apr. 2019.

[101] Y. Zhuang et al., "A survey of positioning systems using visible LED lights," *IEEE Commun. Surveys Tuts.*, vol. 20, no. 3, pp. 1963-1988, 3Qt 2018.

[102] Y. Hou, S. Xiao, M. Bi, Y. Xue, W. Pan and W. Hu, "Single LED beacon-based 3-D indoor positioning using off-the-shelf devices," *IEEE Photon. J.*, vol. 8, no. 6, pp. 1-11, Dec. 2016.

[103] M. Yasir, S.-W. Ho, and B. N. Vellambi, "Indoor positioning system using visible light and accelerometer," *J. Lightw. Technol.*, vol. 32, no. 19, pp. 3306-3316, Oct.1, 2014.

[104] G. B. Prince and T. D. C. Little, "A two phase hybrid RSS/AoA algorithm for indoor device localization using visible light," *in Proc. IEEE Glob. Commun. Conf. (GLOBECOM)*, Anaheim, CA, USA, 2012, pp. 3347-3352.

[105] H. Steendam, T. Q. Wang, and J. Armstrong, "Cramer-Rao bound for AOA-based VLP with an aperture-based receiver," in *Proc. IEEE Int. Conf. Commun. (ICC)*, May 2017, pp. 1-6.

[106] H. Steendam, "A 3-D positioning algorithm for AOA-based VLP with an aperture-based receiver," *IEEE J. Sel. Areas Commun.*, vol.36, no. 1, pp. 23-33, Jan. 2018.

[107] T.Q. Wang, Y. A. Sekercioglu, A. Neild, and J. Armstrong, "Position accuracy of time-of arrival based ranging using visible light with application in indoor localization systems," *J. Lightw. Technol.*, vol. 31, no. 20, pp. 3302-3308, Oct. 15, 2013.

[108] T. Akiyama, M. Sugimoto and H. Hashizume, "Time-of-arrival-based smartphone localization using visible light communication," in *IEEE IPIN*, Sapporo, 2017, pp. 1-7.

[109] M. F. Keskin, S. Gezici, and O. Arikan, "Direct and two-step positioning invisible light systems," *IEEE Trans. Commun.*, vol. 66, no.1, pp. 239-254, Jan. 2018.

[110] T.-H. Do and M. Yoo, "TDOA-based indoor positioning using visible light," *Photon. Netw. Commun.*, vol. 27, no. 2, pp. 80-88, Jan.2014.

[111] K. Panta and J. Armstrong, "Indoor localization using white LEDs," *Electron. Lett.*, vol. 48, no. 4, pp. 228-230, Nov.2012.

[112] A. Taparugssanagorn, S. Siwamogsatham, and C. Pomalaza-Raez,"A hexagonal coverage LED-ID indoor positioning based on TDOA with extended Kalman filter," in *Proc. IEEE 37th Annu. Comput. Softw. Appl. Conf. (COMPSAC)*, Kyoto, Japan, 2013, pp.742-747.

[113] T.-H. Do, J. Hwang, and M. Yoo, "TDoA based indoor visible light positioning systems," in *Proc. Int. Conf. Ubiquitous Future Netw. (ICUFN)*, Da Nang, Vietnam, 2013, pp. 456-458.

[114] R. Roberts, P. Gopalakrishnan, and S. Rathi, "Visible light positioning: Automotive use case," in *Proc. IEEE Veh. Netw. Conf. (VNC)*, Dec. 2010, pp. 309-314.

[115] J. H.Y. Nah, R. Parthiban, and M. H. Jaward, "Visible light communications localization using TDOA based coherent heterodyne detection," in *Proc. IEEE Int. Conf. Photon. (ICP)*, Oct. 2013, pp. 247-249.

[116] S. Zhang, P. Du, C. Chen, W. Zhong and A. Alphones, "Robust 3D indoor VLP system based on ANN using hybrid RSS/PDOA," *IEEE Access*, vol. 7, pp. 47769-47780, Mar. 2019.

[117] C. Chen, S. Videv, D. Tsonev, and H. Haas, "Fractional frequency reuse in DCO-OFDM-based optical attocell networks," *J. Lightw. Technol.*, vol. 33, no. 19, pp.3986-4000, Oct. 2015.

[118] H.-S. Kim, D.-R. Kim, S.-H. Yang, Y.-H. Son, and S.-K. Han, "Mitigation of inter-cell interference utilizing carrier allocation in visible light communication system," *IEEE Commun. Lett.*, vol. 16, no. 4, pp. 526-529, Apr. 2012.

[119] Y. Chen, S. Li and H. Liu, "Dynamic frequency reuse based on improved tabu search in multi-user visible light communication networks," *IEEE Access*, vol. 7, pp.35173-35183, Jun. 2019.

[120] S. Jung, D. Kwon, S. Yang, and S.-K. Han, "Inter-cell interference mitigation in multicellular visible light communications," *Opt. Exp.*, vol. 24, no. 8, pp. 8512-8526, Apr. 2016.

[121] X. Li, F. Jin, R. Zhang, J. Wang, Z. Xu, and L. Hanzo, "Users first: user-centric cluster formation for interference-mitigation in visible-light networks," *IEEE Trans. Wireless Commun.*, vol. 15, no. 1, pp. 39-53, Jan. 2016.

[122] D. Bykhovsky and S. Arnon, "Multiple access resource allocation invisible light communication systems," *J. Lightw. Technol.*, vol. 32, no. 8, pp. 1594-1600, Apr. 2014.

[123] K. Zhou, C. Gong and Z. Xu, "Color planning and inter-cell interference coordination for multicolor visible light communication networks" *J. Lightw. Technol.*, vol.35, no. 22, pp. 4980-4993, Nov. 2017.

[124] S. Jung, D. Kwon, S. Yang and S. Han, "Reduction of inter-cell interference in asynchronous multi-cellular VLC by using OFDMA-based cell partitioning" in *IEEE ICTON*, Trento, 2016, pp. 1-4.

[125] H. Ma, L.Lampe and S. Hranilovic, "Coordinated broadcasting for multiuser indoor visible light communication systems," *IEEE Trans. Commun.*, vol. 63, no. 9, pp. 3313-3324, Sep. 2015.

[126] T. V. Pham, H. Le-Minh, and A. T. Pham, "Multi-cell VLC: Multi-user downlink capacity with coordinated precoding," in *Proc. IEEE Int. Conf. Commun. (ICC)*, May 2017, pp. 469-474.

[127] T. V. Pham and T. A.Pham, "Cooperation strategies and optimal precoding design formulti-user multi-cell VLC networks," in *Proc. IEEE Global Commun. Conf. (GLOBECOM)*, Dec. 2017, pp. 1-6.

[128] T. V. Phamand A. T. Pham, "Coordination/cooperation strategies and optimal zero-forcing precoding design for multi-user multi-cell VLCnetworks," *IEEE Trans. Commun.*, vol. 67, no. 6, pp.4240-4251, Jun. 2019.

[129] A. Adnan-Quidan, M. Morales-Cespedes and A. Garcia-Armada, "Aligning the light based on the network topology for visible light communications," in *Proc. IEEE Int. Conf. Commun. (ICC)*, Kansas City, MO, 2018,pp. 1-6.

[130] M. Obeed, H. Dahrouj, A. M. Salhab, S. A. Zummo and M. Alouini, "DC-Bias allocation in cooperative VLC networks via joint information and energy transfer," in *Proc. IEEE Global Commun. Conf. (GLOBECOM)*, Abu Dhabi, United Arab Emirates, 2018, pp. 1-6.

[131] H. Le Minh, *et al.*, "A 1.25-Gb/s Indoor cellular optical wireless communications demonstrator," *IEEE Photon. Technol. Lett.*, vol. 22, no. 21, pp. 1598-1600, Nov. 2010.

[132] Z. Cheng, N. Serafimovski, and H. Haas, "Angle diversity for an indoor cellular visible light communication system," in *Proc. Veh. Technol. Conf. (TVC) Spring*, 2014, pp. 1-5.

[133] Z.Chen, D. Tsonev, and H. Haas, "Improving SINR in indoor cellular visible light communication networks," in *Proc. IEEE Int. Conf. Commun. (ICC)*, Jun. 2014, pp. 3383-3388.

[134] Z. Chen, D. A. Basnayaka, X. Wu and H. Haas, "Interference mitigation for indoor optical attocell networks using an angle diversity receiver," *J. Lightw. Technol.*, vol. 36, no. 18, pp.3866-3881, Sept. 2018.

[135] C. Chen, W. Zhong, H. Yang, S. Zhang and P. Du, "Reduction of SINR fluctuation in indoor multi-cell VLC systems using optimized angle diversity receiver," *J. Lightw. Technol.*, vol. 36, no. 17, pp. 3603-3610, Sept. 2018.

[136] Z. Chen, D. A. Basnayaka, and H. Haas, "Space division multiple access for optical attocell network using angle diversity transmitters," *J. Lightw. Technol.*, vol. 35, no.11, pp. 2118-2131, 1 Jun. 2017.

[137] H. Tran, G. Kaddoum, P. D. Diamantoulakis, C. Abou-Rjeily, and G. K. Karagiannidis,"Ultra-small cell networks with collaborative RF and lightwave power transfer," to appear in *IEEE Trans. Commun.*.

[138] S. Feng, R. Zhang, X. Li, Q. Wang, and L. Hanzo, "Dynamic throughput maximization for the user-centric visible light downlink in the face of practical considerations," *IEEE Trans. Wireless Commun.*, vol. 17, no. 8, pp. 5001-5015, Aug. 2018.

[139] M. Obeed, A. M. Salhab, S. A. Zummo, and M. Alouini, "New algorithms for energy-efficient VLC networks withuser-centric cell formation," *IEEE Trans. Green Commun. Netw.*, vol. 3, no. 1, pp. 108-121, Mar. 2019.

[140] X. Li, R. Zhang and L. Hanzo, "Optimization of visible-light optical wireless Systems: network-centric versususer-centric designs," *IEEE Commun. Surveys Tuts.*, vol. 20,no. 3, pp. 1878-1904, 3rd Quart., 2018.

[141] R. Jiang, Q. Wang, H. Haas and Z. Wang, "Joint user association and power allocation for cell-free visible light communication networks," *IEEE J. Sel. Areas Commun.*, vol. 36, no. 1, pp.136-148, Jan. 2018.

[142] A. Ibrahim, T.Ismail and K. Elsayed, "Optimized radio resource allocation scheme for indoor optical wireless communication," in *Proc. IEEE ICTON*, Girona, 2017, pp. 1-4.

[143] Y. Fu, Y. Hong, L. Chen and C. W. Sung, "Enhanced power allocation for sum rate maximization in OFDM-NOMA VLC systems," *IEEE Photon. Technol. Lett.*, vol.30, no. 13, pp. 1218-1221, Jul. 2018.

[144] S. Feng, R. Zhang, W. Xu and L. Hanzo, "Multiple access design for ultra-dense VLC networks: orthogonal vs non-orthogonal," *IEEE Trans. Commun.*, vol. 67, no. 3, pp. 2218-2232, Mar. 2019.

[145] X. Zhang, Q. Gao, C. Gong and Z. Xu, “User grouping and power allocation for NOMA visible light communication multi-cell networks,” *IEEE Commun. Lett.*, vol. 21, no. 4, pp. 777-780,Apr. 2017.

[146] Q. Li, T. Shang, T. Tang and Z. Dong, “Optimal power allocation scheme Based on multi-factor control inindoor NOMA-VLC systems,” to appear to *IEEE Access*.

[147] S. Shao *et al.*, “Design and analysis of a visible-light-communication enhancedWiFi system,” *IEEE/OSA J. Opt. Commun. Netw.*, vol. 7, no.10, pp. 960-973, Oct. 2015.

[148] F. Wang, Z. Wang, C. Qian, L. Dai and Z. Yang, “Efficient verticalhandover scheme for heterogeneous VLC-RF systems,” *IEEE/OSAJ. Opt. Commun. Netw.*, vol. 7, no. 12, pp. 1172-1180, Dec. 2015.

[149] X. Bao, W. Adjardjah, A. Okine, W. Zhang and N. Bao, “Vertical handover scheme for enhancing the QoE in VLC heterogeneous networks,” in *Proc. IEEE Int. Conf. Commun. in China (ICCC)*, Beijing, China, 2018, pp. 437-442.

[150] S. Liang, H. Tian, B. Fan and R. Bai, “A novel vertical handover algorithm in a hybrid visible light communication and LTE system,” *IEEE Veh. Technol. Conf. (VTC)*, Boston, MA, 2015, pp. 1-5.

[151] X. Wu, M. Safari, and H. Haas, “Joint optimization of load balancing and handover for hybrid LiFi and WiFi networks,” *IEEE Wireless Commun. Netw. Conf. (WCNC)*, San Francisco, CA, 2017, pp.1-5.

[152] Y. Wang and H. Haas, “Dynamic Load balancing with handover in hybrid Li-Fi and Wi-Fi networks” *J. Lightw. Technol.*, vol. 33, no. 22,pp. 4671-4682, Nov. 2015.

[153] X. Wu and H. Haas,“Handover skipping for LiFi,” *IEEE Access*, vol. 7, pp.38369-38378, Mar. 2019.

[154] A. A. Purwita, M. D. Soltani, M. Safariand H. Haas, “Handover probability of hybrid LiFi/RF-based networks with randomly-oriented devices,” *IEEE Veh. Technol. Conf. (VTC)*, Porto, 2018, pp. 1-5.

[155] M. Kafafy, Y. Fahmy, M. Abdallah and M. Khairy, “Power efficient downlink resource allocation for hybrid RF/VLC wireless networks,” *IEEE Wireless Commun. Netw. Conf. (WCNC)*, San Francisco, CA, 2017, pp. 1-6.

[156] M. Kashef, M. Ismail, M. Abdallah, K. A. Qaraqe and E. Serpedin, “Energy efficient resource allocation for mixed RF/VLC heterogeneous Wireless Networks,” *IEEE J. Sel. Areas Commun.*, vol. 34,no. 4, pp. 883-893, April 2016.

[157] H. Zhang, N. Liu, K. Long, J. Cheng, V. C. M. Leung and L. Hanzo,“Energy efficient subchannel and power allocation for software-defined heterogeneous VLC and RF networks,” *IEEE J.Sel. Areas Commun.*, vol. 36, no. 3, pp. 658-670, Mar. 2018.

[158] A. Khreishah, S. Shao, A. Gharaibeh, M. Ayyash, H. Elgala and N. Ansari, “A hybrid RF-VLC system for energy efficient wireless access,” *IEEE Trans. Green Commun. Netw.*, vol. 2, no. 4, pp. 932-944, Dec. 2018.

[159] J. Kong, M. Ismail, E. Serpedin and K. A. Qaraqe, “Energy efficient optimization of base station intensities for hybrid RF/VLC networks,” to appear in *IEEE Trans. Wireless Commun.*,.

[160] Y. Hsiao, Y. Wu and C. Lin, "Energy-efficient beamforming design for MU-MISO mixed RF/VLC heterogeneous wireless networks," *IEEE Trans. Signal Process.*, vol. 67, no. 14, pp. 3770-3784, Jul. 2019.

[161] G. Pan, H. Lei, Z. Ding and Q. Ni, "On 3-D hybrid VLC-RF systems with light energy harvesting and OMA scheme over RF links," in *Proc. IEEE Global Commun. Conf. (GLOBECOM)*, Singapore, 2017, pp. 1-6.

[162] G. Pan, H. Lei, Z.Ding and Q. Ni, "3-D hybrid VLC-RF indoor IoT systems with light energy harvesting," to appear in *IEEE Trans. Green Commun.Netw.*.

[163] T. Rakia, H. Yang, F. Gebali and M.Alouini, "Optimal design of dual-hop VLC/RF communication system with energy harvesting," *IEEE Commun. Lett.*, vol. 20, no.10, pp. 1979-1982, Oct. 2016.

[164] M. R. Zenaidi, Z. Rezki, M. Abdallah, K. A. Qaraqe and M. Alouini, "Achievable rate-region of VLC/RF communications with an energy harvesting relay,," in *Proc. IEEE Global Commun. Conf. (GLOBECOM)*, Singapore, 2017, pp. 1-7.

[165] P. K. Sharma, Y. Jeong and J. H.Park, "EH-HL: effective communication model by integrated EH-WSN and hybrid LiFi/WiFi for IoT," *IEEE Internet of Things J.*, vol. 5, no. 3, pp. 1719-1726, Jun. 2018.

[166] J. Al-Khori, G. Nauryzbayev, M. M. Abdallah and M. Hamdi, "Joint beamforming design and power minimization for friendly jamming relaying hybrid/VLC systems," *IEEE Photon. J.*, vol. 11, no. 2, pp. 1-18, Apr. 2019.

[167] Z. Liao, L. Yang, J. Chen, H. Yang and M. Alouini, "Physical layer security for dual-hop VLC/RF communication systems," *IEEE Commun. Lett.*, vol. 22, no. 12, pp. 2603-2606, Dec. 2018.

[168] J. Al-Khori, G. Nauryzbayev, M. M. Abdallah and M. Hamdi, "Secrecy performance of decode-and-forward based hybrid RF/VLC relaying systems," *IEEE Access*, vol. 7, pp. 10844-10856, Jun. 2019.

[169] G. Pan, J. Ye and Z. Ding, "Secure hybrid VLC-RF systems with light energy harvesting," *IEEE Trans. Commun.*,vol. 65, no. 10,pp. 4348-4359, Oct. 2017.

[170] Harald Haas, "LiFi is a paradigm-shifting 5G technology," *Reviews in Physics*, Vol. 3, pp 26-31, Nov. 2018.

[171] Z. Dong et al., "An integrated transmitter for LED-based visible light communication and positioning system in a 180nm BCD technology," in *IEEE Bipolar/bicmos Circuits and Technology Meeting*, 2014, pp.84-87.

[172] J. Zhang et al., "Towards a visible light network architecture for continuous communication and localization," in *Proc. IEEE Workshop on Visible Light Commun. Syst.*, 2016, pp.1-9.

[173] I. C. Rust, and H.H. Asada, "A dual-use visible light approach to integrated communication and localization of underwater robots with application to non-destructive nuclear reactor inspection," in *IEEE Int. Conf. on Robotics and Automation*, 2012,pp.2445-2450.

[174] M. I. Aminikashani, W. Gu, and M. Kavehrad, "Indoor positioning with OFDM visible light communications," in IEEE *Consumer Commun. & Netw. Conf.*, 2016, pp.505-510.

[175] B. Lin, X. Tang, Z. Ghassemlooy, C. Lin, and Y. Li, "Experimental demonstration of an indoor VLC positioning system based on OFDMA," *IEEE Photon. J.*, vol. PP, no. 99, pp.1-10, Feb. 2017.

[176] Y. Xu, Z. Wang,P. Liu, J. Chen, S. Han, C. Yu, and J. Yu, "Accuracy analysis and improvement of visible light positioning based on VLC system using orthogonal frequency division multiple access," *Opt. Express*, vol. 26, no. 7, pp. 9230-9242, Apr. 2018.

[177] M. Bellanger *et al.*, "FBMC physical layer: A primer," *PHYDYAS Tech*. Rep., 2010.

[178] S. Y. Jung, S. M. Jung, and S. K. Han, "AMO-FBMC for asynchronous heterogeneous signal integrated optical transmission," *IEEE Photon. Technol. Lett.*, vol.27, no. 2, pp. 133-136, Jan. 2015.

[179] J. Zhang *et al.*, "Full-duplex quasi-gapless carrier-aggregation using FBMC in centralized radio-over-fiber heterogeneous networks," *J. Lightwave Technol.*, vol. 35, no. 4, pp. 989-996, Feb. 2017.

[180] M. Xu, J. Zhang, F. Lu, and J. Wang, "FBMC in next-generation mobile front haul networks with centralized pre-equalization," *IEEE Photon. Technol. Lett.*, vol. 28, no. 18, pp. 1912-1915, Sep. 2016.

[181] H. L. Yang, C. Chen, W.-D. Zhong, S. Zhang, and P. Du, "An integrated indoor visible light communication and positioning system based on FBMC-SCM," in *Proc. IEEE Phot. Conf. (IPC)*, 2017, pp. 129-130.

[182] H. Yang, C. Chen, W. Zhong, A. Alphones, S. Zhang, and P. Du, "Demonstration of a quasi-gapless integrated visible light communication and positioning system," *IEEE Photon. Technol. Lett.*, vol. 30, no. 23, pp. 2001-2004, Dec. 2018.

[183] H. L. Yang, W. D. Zhong, A. Alphones, C. Chen, S. Zhang and P. F. Du, "Coordinated resource allocation for multi-user multi-cell integrated visible light communication and positioning systems," Submitted to *IEEE Trans. Veh. Technol.*.

[184] L. Wu, Z. Zhang, J. Dang, and H. Liu, "Adaptive modulation schemes for visible light communications," J. Lightw. Technol., vol.33, no. 1, pp. 117-125, Jan. 2015.

[185] J. He, J. He, and J. Shi, "An enhanced adaptive scheme with pairwise coding for OFDM-VLC system," *IEEE Photon. Technol. Lett.*, vol. 30, no.13, pp. 1254-1257, Jul. 2018.

[186] X. Huang, *et al.*, "2.0-Gb visible light link based on adaptive bit allocation OFDM of a single phosphorescent white LED," *IEEE Photon. J.*, vol. 7, no. 5, pp. 1-8, Oct. 2015.

[187] G. Zhang, J. Zhang, X. Hong, and S. He, "Low-complexity frequency domain nonlinear compensation for OFDM based high-speed visible light communication systems with light emitting diodes," *Opt. Express*, vol. 25, no. 4, pp. 3780-3794, Feb. 2017.

[188] H. Chen, Z. Xu, Q. Gao and S. Li, "A 51.6 Mb/s experimental VLC system using a monochromic organic LED," *IEEE Photon. J.*, vol. 10, no. 2, pp. 1-12, Apr. 2018.

[189] Y. Hong, J. Xu, and L. Chen, "Experimental investigation of multi-band OCT precoding for OFDM-based visible light communications," *Opt. Express*, vol. 25, no. 17, pp. 12908-12914, May 2017.

[190] H. Yang, *et al.*, "Resource allocation for multi-user integrated visible light communication and positioning systems," in *Proc. IEEE Int. Conf. Commun. (ICC)*, China, 2019, pp. 1-6.

[191] B. G. Guzmn, A. A. Dowhuszko, V. P. Gil Jimnez, and A. I. PrezNeira, "Robust cooperative multicarrier transmission scheme for optical wireless cellular networks," IEEE Photon. Technol. Lett., vol. 30, no. 2, pp. 197-200, Jan. 2018.

[192] M. A. Dastgheib, H. Beyranvand, J. A. Salehi, and M. Maier, "Mobility aware resource allocation in VLC networks using T-step look-ahead policy," *J. Lightw. Technol.*, vol. 36, no. 23, pp. 5358-5370, Dec.2018.

[193] W. Wu, F. Zhou, and Q. Yang, "Adaptive network resource optimization for heterogeneous VLC/RF wireless networks," *IEEE Trans. Wireless Commun.*, vol. 66, no. 11, pp.5568-5581, Nov. 2018.

[194] S. Shao et al., "Poster abstract: optimizing handover parameters by Q-learning for heterogeneous RF-VLC networks," *IEEE INFOCOM*, Paris, France, 2019, pp. 1069-1070.

[195] H. L. Yang, P. F. Du, W. D. Zhong, C. Chen, A. Alphones, and S. Zhang, "Reinforcement learning based intelligent resource allocation for integrated VLCP systems," *IEEE Wireless Commun. Lett.*, vol. 8, no. 4, pp. 1204-1207, Aug. 2019.

[196] H. Yang, W. Zhong, C. Chen, A. Alphones and P. Du, "QoS-driven optimized design-based integrated visible light communication and positioning for indoor IoT networks," *IEEE Internet of Things J.*, vol. 7, no. 1, pp. 269-283, Jan. 2020.

[197] R. Mesleh, H. Elgala, and H. Haas, "On the performance of different OFDM based optical wireless communication systems," *IEEE/OSA J. Opt. Commun. Netw.*, vol. 3, no. 8, pp. 620-628,Aug. 2011.

[198] F. Alam, M. T. Chew, T. Wenge, et al., "An accurate visible light positioning system using regenerated fingerprint database based on calibrated propagation model," appear in *IEEE T. Instrum. Meas.*.

[199] A. Ahin, Y. S. Erolu, Gven, N.Pala, and M. Yksel, "Hybrid 3-D localization for visible light communication systems," *J. Lightw. Technol.*, vol. 33, no.22, pp. 4589-4599, Nov. 2015.

[200] M. F. Keskin and S. Gezici, "Comparative theoretical analysis of distance estimation invisible light positioning systems," *J. Lightw. Technol.*, vol. 34, no. 3, pp. 854-865, Feb. 2016.

[201] T. T. Son, H. Le-Minh, F. Mousa, Z. Ghassemlooy, and N. V. Tuan, "Adaptive correction model for indoor MIMO VLC using positioning technique with node knowledge," in *Proc. IEEE ComManTel*, DaNang,2015, pp. 94-98.

[202] A. R. Jimenez, F. Seco, C. Prieto, and J. Guevara, "A comparison of pedestrian dead-reckoning algorithms using a low-cost MEMS IMU," in *Proc. IEEE WISP*, Budapest, 2009, pp. 37-42.

[203] Q. Ye, B. Rong, Y. Chen, M. Al-Shalash, C. Caramanis, and J. G. Andrews, "User association for load balancing in heterogeneous cellular networks," *IEEE Trans. Wireless Commun.*, vol. 12, no. 6, pp. 2706- 2716, Jun.2013.

[204] T. Bu, L. Li, and R. Ramjee, "Generalized proportional fair scheduling in third generation wireless data networks," in *Proc. IEEE INFOCOM*, Apr. 2006, pp. 1-12。

[205] S. Boyd and L. Vandenberghe, Convex Optimization. Cambridge, U.K.: Cambridge Univ. Press, 2004.

[206] B. Li, J. Wang, R. Zhang, H. Shen, C. Zhao, and L. Hanzo, "Multiuser MISO transceiver design for indoor downlink visible light communication under per-LED optical power constraints," *IEEE Photon. J.*, vol. 7, no. 4, pp. 1-15, Aug. 2015.

[207] H. Shen, Y. Deng, W. Xu, and C. Zhao, "Rate maximization for downlink multi-user visible light communications," *IEEE Access*, vol. 4, no.1, pp. 6567-6573, Apr. 2016.

[208] Q. Wang, Z. Wang, and L. Dai, "Multiuser MIMO-OFDM for visible light communications," *IEEE Photon. J.*, vol. 7, no. 6, pp. 1-11, Dec. 2015.

[209] H. Marshoud, P. C. Sofotasios, S. Muhaidat, et al., "Optical adaptive precoding for visible light communications," *IEEE Access*, pp. 1-10, Feb. 2018.

[210] V. R. Cadambe, and S. A. Jafar, "Interference alignment and degrees of freedom of the K-user interference channel," *IEEE Trans. Inf. Theory*, vol. 54, no. 8, pp.3425-3441, Aug. 2008.

[211] A. Motahari, S. Oveis-Gharan, M.-A.Maddah-Ali, and A. Khandani, "Real interference alignment: exploiting the potential of single antenna systems," *IEEE Trans. Inf. Theory*, vol. 60, no. 8, pp. 4799-4810, Aug. 2014.

[212] S. M. Razavi, and T. Ratnarajah, "Adaptive LS- and MMSE-based beamformer design for multiuser MIMO interference channels," *IEEE Trans. Veh. Technol.*, vol. 65, no. 1, pp.132-144, Jan. 2016.

[213] X. Zhang, Q. Gao, and Z. Xu, "Optical interference alignment for an indoor visible light communication X-channel," in *IEEE GlobalSIP*, Orlando, FL, 2015, pp.1175-117.

[214] L. Wu, Z. Zhang, J. Dang, and H. Liu, "Blind interference alignment for multiuser MISO indoor visible light communications," *IEEE Commun. Lett.*, vol. 21, no. 5, pp.1039-1042, Jan. 2017.

[215] V. Dorpe, "Aligning the light without channel state information for visible light communications," *IEEE J. Sel. Areas Commmun.*, vol. 36, no.1, pp. 91-105, Jan. 2018.

[216] H. L. Yang, C. Chen, W. D. Zhong and A. Alphones, "Joint precoder and equalizer design for multi-user multi-cell MIMO VLC systems," *IEEE Trans. Veh. Technol.*, vol. 67, no. 12, pp. 11354-11364, Dec. 2018.

[217] R. Horn, and C. Johnson, Topics in Matrix Analysis. New York, NY, USA: Cambridge Univ. Press, 1991.

[218] CVX Research, Inc., "CVX: Matlab software for disciplined convex programming, version2.0 (beta), Jun. 2013.

[219] N. Jindal, "MIMO broadcast channels with finite-rate feedback," *IEEE Trans. Inf. Theory*, vol. 52, no. 1, pp. 5045-5060, Nov. 2006.

[220] Z.-Q. Luo, W.-K. Ma, A.-C. So, Y. Ye, and S. Zhang, "Semidefinite relaxation of quadratic optimization problems," *IEEE Signal Process. Mag.*, vol. 27, no. 3, pp. 20-34, May 2010.

[221] Y.-J. Lee et al., "Study of GaN-based light-emitting diodes grown on chemical wet-etching-patterned sapphire substrate with v-shaped pits roughening surfaces," *J. Lightw. Technol.*, vol. 26,no. 11, pp. 1455- 1463, Jun. 2008

[222] N. Saxena, A. Roy, B. J.R. Sahu, and H. Kim, "Efficient IoT gateway over 5G wireless: anew design with prototype and implementation results," *IEEE Commun. Mag.*, vol. 55, no. 2, pp. 97-105, Feb. 2017.

[223] B. Khalfi, B. Hamdaoui, and M. Guizani, "Extracting and exploiting inherent sparsity for efficient IoT support in 5G: challenges and potential solutions," *IEEE Wireless Commun.*, vol. 24, no.5, pp. 68-73, Oct. 2017.

[224] L. I. Albraheem, L. H.Alhudaithy, A. A. Aljaser, M. R. Aldhafian, and G. M. Bahliwah, "Toward designing a Li-Fi-based hierarchical IoT architecture," *IEEE Access*, vol. 6, pp. 40811-40825, May 2018.

[225] X. Liu, X. Wei, L. Guo, Y. Liu, Q. Song, and A. Jamalipour, "Turning the signal interference into benefits: towards indoor self-powered visible light communication for IoT devices in industrial radio-hostile environments," *IEEE Access*, vol. 7, pp.24978-24989, Nov. 2019.

[226] S. Shao, A. Khreishah, and H.Elgala, "Pixelated VLC-backscattering for self-charging indoor IoT devices," *IEEE Photon. Technol. Lett.*, vol. 29, no. 2, pp. 177-180, 15 Jan. 2017.

[227] D. A. Basnayaka and H. Haas, "Design and analysis of a hybrid radio frequency and visible light communication system," *IEEE Trans. Commun.*, vol. 65,no. 10, pp. 4334-4347, Oct. 2017.

[228] Y. Wang, D. A. Basnayaka, X. Wu, and H. Haas, "Optimization of load balancing in hybrid LiFi/RF networks," *IEEE Trans. Commun.*, vol. 65, no. 4, pp.1708-1720, Apr. 2017.

[229] X. Li, R. Zhang, and L. Hanzo, "Cooperative load balancing in hybrid visible light communications and WiFi," *IEEE Trans. Commun.*, vol. 63, no.4, pp. 13191329, Apr. 2015.

[230] S. Shao and A. Khreishah,"Delay analysis of unsaturated heterogeneous omnidirectional-directional small cell wireless networks: the case of RFVLC coexistence," *IEEE Trans. Wireless Commun.*, vol.15, no. 12, pp. 8406-8421, Dec. 2016.

[231] F. Jin, R. Zhang, and L. Hanzo, "Resource allocation under delay guarantee constraints for heterogeneous visible-light and RF femtocell," *IEEE Trans. Wireless Commun.*, vol. 14, no. 2, pp.1020-1034, Feb.2015.

[232] J. Wang, et al., "Learning-aided network association for hybrid indoor LiFi-WiFi systems," *IEEE Trans. Veh. Technol.*, vol. 67, no. 4, pp. 3561- 3574, Apr. 2018.

[233] Z. Du, C. Wang, Y. Sun, and G. Wu, "Context-aware indoor VLC/RF heterogeneous network selection: reinforcement learning with knowledge transfer," *IEEE Access*, vol. 6, pp.33275-33284, 2018.

[234] Y. C. Hsiao, C. M. Chen and C. Lin, "Energy efficiency maximization in multi-user miso Mixed RF/VLC heterogeneous cellular networks," in *Proc. IEEE Int. Conf. Commun. (ICC)*, Hong Kong, 2018, pp. 1-9.

[235] A. E. Kalor,R. Guillaume, J. J. Nielsen, A. Mueller, and P. Popovski,"Network slicing in Industry 4.0 applications: abstractionmethods and end-to-end analysis," *IEEE Trans. Ind. Informat.*, vol. 14, no. 12, pp. 5419-5427, Dec. 2018.

[236] J. Mei, K. Zheng, L. Zhao, Y. Teng, and X. Wang, "A latency and reliability guaranteed resource allocation scheme for LTE V2Vcommunication systems," *IEEE Trans. Wireless Commun.*, vol.17, no. 6, pp. 3850-3860, Jun. 2018.

[237] H. L. Yang, C. Chen and W. D. Zhong, "Cognitive multi-cell visible light communication with hybrid underlay/overlay resource allocation," *IEEE Photon. Technol. Lett.*, vol. 30, no. 12, pp. 1135-1138, Jun.2018.

[238] H. L. Yang, C. Chen, W. D. Zhong and A. Alphones, "Learning-based energy-efficient resource management by heterogeneous RF/VLC for ultra-reliable low-latency industrial IoT networks," Appear in *IEEE Trans. Ind. Informat.*.

[239] Q. Wang, D. Giustiniano and M. Zuniga, "In light and in darkness, in motion and in stillness: A reliable and adaptive receiver for the Internet of Lights," *IEEE J. Sel. Areas Commun.*, vol. 36, no. 1, pp. 149-161, Jan. 2018.

[240] IST-4-027756WINNER II D1.1.2 V1.2. (2008, Feb.). WINNER II Channel Models [Online]. Available: http://www.ist-winner.org.

[241] M. Wiering and M. Otterlo, Reinforcement learning: State of-the-art, Springer Publishing Company, Incorporated, 2014.

[242] N. Mastronarde and M. van der Schaar, "Joint physical-layer and system level power management for delay-sensitive wireless communications," *IEEE Trans. Mobile Comput.*, vol. 12, no. 4, pp. 694-709, Apr. 2013.

[243] M.Doudou, D. Djenouri, and N. Badache, "Survey on latency issues of asynchronous MAC protocols in delay-sensitive wireless sensor networks," *IEEE Commun. Surveys Tuts.*, vol. 15, no. 2, pp.528-550, Second 2013.

[244] Y. Wu, F. Hu, S. Kumar, J. D.Matyjas, Q. Sun, and Y. Zhu, "Apprenticeship learning based spectrum decision in multi-channel wireless mesh networks with multi-beam antennas," *IEEE Trans. Mobile Comput.*, vol. 17,no. 2, pp. 314-325, Feb. 2017.

[245] X. He, R. Jin, and H. Dai, "Deep PDS-learning for privacy-aware offloading in MEC-enabled IoT," *IEEE Internet of Things J.*, vol. 6, no. 3, pp.4547-4555, Jun. 2019.